

UNIVERSITA' DEGLI STUDI DI NAPOLI
"FEDERICO II"



DOTTORATO DI RICERCA IN INGEGNERIA
AEROSPAZIALE, NAVALE E DELLA QUALITA'

XXVI CICLO

*Vertical Motion Assessment for
Planing Hulls*

Supervisor
Prof. Ermina Begovic

Candidate
Silvia Pennino

Coordinator
Prof. Luigi de Luca

Submitted on March 2014

Acknowledgements

I wish to express sincere thanks to Professor Ermina Begovic for her invaluable support and help, for the enthusiasm and the positivity with which she encouraged me. She has always been present, in these years, not only as a professor but also as a friend, playing both roles in an extraordinary way.

Contents

List of figures	v
List of tables	x
Nomenclature	xi
1. INTRODUCTION	1
1.1. Background.....	1
1.2 Aims and Objectives of the Thesis	2
1.3 Contents of the Thesis	3
2. PLANING HULL HYDRODYNAMICS	5
2.1 Planing hulls in calm water.....	5
2.2 Planing hull seakeeping	11
3. MATHEMATICAL MODEL ACCORDING TO PAYNE	14
3.1 Introduction.....	14
3.2 Problem formulation.....	15
3.2.1 Hydrostatic force	17
3.2.2 Froude-Krilov force.....	18
3.2.3 Diffraction force	20
3.2.4 Hydrodynamic force.....	20
3.2.5 Velocity	22
3.2.6 Added mass determination	23
3.3 Motions equations.....	26

3.3.1	Force equilibrium in coordinate system G_{xyz}	26
3.3.2	Moment equilibrium in coordinate system G_{xyz}	31
3.4	The 2D nonlinear numerical code.....	34
3.5	Comparison of numerical and experimental data for monohedral hull ..	38
4.	MATHEMATICAL MODEL ACCORDING TO HICKS ET AL.	58
4.1	Introduction.....	58
4.2	Fully nonlinear mathematical model for planing hulls.....	58
4.3	Motions equations.....	65
4.3.1	Force equilibrium in coordinate system G_{xyz}	66
4.3.2	Moments equilibrium in coordinate system G_{xyz}	75
4.4	Fully non-linear 2D time domain code.....	86
4.5	Comparison of numerical and experimental data for monohedral and warped hull	90
4.6	Frequency domain analysis.....	118
5.	CONCLUSIONS	123
5.1	Final remarks	123
5.2	Conclusions and future work developments.....	131
	REFERENCES.....	134

List of figures

Figure 2.1. Forces acting on planing hull in calm water (from Savitsky 1964).....	6
Figure 2.2. Planing hull in calm water (cortesy of prof. Bertorello C.).....	7
Figure 2.3. Definition of wetted surface by Savitsky et al. (2006).....	8
Figure 2.4. Physics of planing – monohedral hull tested at DII at $F_{rv}=2.88$	9
Figure 2.5. Different phases of free falling wedge into a free surface of water.....	12
Figure 3.1. Reference systems definition.....	15
Figure 3.2. Acting forces at planing hull in waves and definition of motions.....	16
Figure 3.3. Change of wetted surface and hydrostatic force definition.....	18
Figure 3.4. View of planing hull from Earth Fixed Plane, definition of relative velocities	22
Figure 3.5. Effective penetration, two cases according to chine immersion.....	24
Figure 3.6. Flow separation for pile up consideration.....	25
Figure 3.7. Integration limits.....	29
Figure 3.8. Imported geometry.....	35
Figure 3.9. Incident wave and wetted sections properties.....	35
Figure 3.10. Intersection wave-section.....	36
Figure 3.11. Simulink model.....	37
Figure 3.12. Input wave (mm), calculated heave(mm) and pitch (deg).....	38
Figure 3.13. Monohedral hull geometry.....	39
Figure 3.14. Numerical vs. experimental heave, $v=3.4$ m/s and $f=0.9$ Hz.....	41
Figure 3.15. Numerical vs. experimental pitch, $v=3.4$ m/s and $f=0.9$ Hz.....	42
Figure 3.16. Numerical vs. experimental acceleration at CG, $v=3.4$ m/s and $f=0.9$ Hz ...	42
Figure 3.17. Numerical vs. experimental acceleration at bow, $v=3.4$ m/s and $f=0.9$ Hz..	42
Figure 3.18. Numerical vs. experimental heave, $v=3.4$ m/s and $f=0.65$ Hz.....	43
Figure 3.19. Numerical vs. experimental pitch, $v=3.4$ m/s and $f=0.65$ Hz.....	43
Figure 3.20. Numerical vs. experimental acceleration at CG, $v=3.4$ m/s and $f=0.65$ Hz .	43
Figure 3.21. Numerical vs. experimental acceleration at bow, $v=3.4$ m/s and $f=0.65$ Hz	44
Figure 3.22. Numerical vs. experimental heave, $v=3.4$ m/s and $f=0.45$ Hz.....	44
Figure 3.23. Numerical vs. experimental pitch, $v=3.4$ m/s and $f=0.45$ Hz.....	44
Figure 3.24. Numerical vs. experimental acceleration at CG, $v=3.4$ m/s and $f=0.45$ Hz .	45
Figure 3.25. Numerical vs. experimental acceleration at bow, $v=3.4$ m/s and $f=0.45$ Hz	45
Figure 3.26. Numerical vs. experimental heave, $v=4.6$ m/s and $f=0.9$ Hz.....	45
Figure 3.27. Numerical vs. experimental pitch, $v=4.6$ m/s and $f=0.9$ Hz.....	46
Figure 3.28. Numerical vs. experimental acceleration at CG, $v=4.6$ m/s and $f=0.9$ Hz ...	46
Figure 3.29. Numerical vs. experimental acceleration at bow, $v=4.6$ m/s and $f=0.9$ Hz..	46
Figure 3.30. Numerical vs. experimental heave, $v=4.6$ m/s and $f=0.65$ Hz.....	47
Figure 3.31. Numerical vs. experimental pitch, $v=4.6$ m/s and $f=0.65$ Hz.....	47
Figure 3.32. Numerical vs. experimental acceleration at CG, $v=4.6$ m/s and $f=0.65$ Hz .	47
Figure 3.33. Numerical vs. experimental acceleration at bow, $v=4.6$ m/s and $f=0.65$ Hz	48
Figure 3.34. Numerical vs. experimental heave, $v=4.6$ m/s and $f=0.45$ Hz.....	48
Figure 3.35. Numerical vs. experimental pitch, $v=4.6$ m/s and $f=0.45$ Hz.....	48

Figure 3.36. Numerical vs. experimental acceleration at CG, $v=4.6$ m/s and $f=0.45$ Hz .	49
Figure 3.37. Numerical vs. experimental acceleration at bow, $v=4.6$ m/s and $f=0.45$ Hz	49
Figure 3.38. Numerical vs. experimental heave, $v=5.75$ m/s and $f=0.9$ Hz.....	49
Figure 3.39. Numerical vs. experimental pitch, $v=5.75$ m/s and $f=0.9$ Hz.....	50
Figure 3.40. Numerical vs. experimental acceleration at CG, $v=5.75$ m/s and $f=0.9$ Hz .	50
Figure 3.41. Numerical vs. experimental acceleration at bow, $v=5.75$ m/s and $f=0.9$ Hz	50
Figure 3.42. Numerical vs. experimental heave, $v=5.75$ m/s and $f=0.65$ Hz.....	51
Figure 3.43. Numerical vs. experimental pitch, $v=5.75$ m/s and $f=0.65$ Hz.....	51
Figure 3.44. Numerical vs. experimental acceleration at CG, $v=5.75$ m/s and $f=0.65$ Hz	51
Figure 3.45. Numerical vs. experimental acceleration at bow, $v=5.75$ m/s and $f=0.65$ Hz	52
Figure 3.46. Numerical vs. experimental heave, $v=5.75$ m/s and $f=0.45$ Hz.....	52
Figure 3.47. Numerical vs. experimental pitch, $v=5.75$ m/s and $f=0.45$ Hz.....	52
Figure 3.48. Numerical vs. experimental acceleration at CG, $v=5.75$ m/s and $f=0.45$ Hz	53
Figure 3.49. Numerical vs. experimental acceleration at bow, $v=5.75$ m/s and $f=0.45$ Hz	53
Figure 3.50. FFT of heave, pitch and accelerations at $v=3.4$ m/s, $f = 0.65$ Hz.....	54
Figure 3.51. FFT of heave, pitch and accelerations at $v=4.6$ m/s, $f = 0.65$ Hz.....	54
Figure 3.52. FFT of heave, pitch and accelerations at $v=5.75$ m/s, $f = 0.65$ Hz.....	54
Figure 3.53. Numerical vs. experimental heave, 1 st model.....	55
Figure 3.54. Numerical vs. experimental pitch, 1 st model	55
Figure 4.1. Velocity components.....	59
Figure 4.2. Moments acting on planing hull in waves.....	75
Figure 4.3. Simulink model	87
Figure 4.4. Flow chart.....	89
Figure 4.5. Warped hull geometry	90
Figure 4.6. Numerical vs. experimental heave, $v=3.4$ m/s and $f=0.9$ Hz - MONO	92
Figure 4.7. Numerical vs. experimental pitch, $v=3.4$ m/s and $f=0.9$ Hz - MONO	92
Figure 4.8. Numerical vs. experimental acceleration at CG, $v=3.4$ m/s and $f=0.9$ Hz - MONO	92
Figure 4.9. Numerical vs. experimental acceleration at bow, $v=3.4$ m/s and $f=0.9$ Hz- MONO	93
Figure 4.10. Numerical vs. experimental heave, $v=3.4$ m/s and $f=0.65$ Hz - MONO	93
Figure 4.11. Numerical vs. experimental pitch, $v=3.4$ m/s and $f=0.65$ Hz - MONO	93
Figure 4.12. Numerical vs. experimental acceleration at CG, $v=3.4$ m/s and $f=0.65$ Hz - MONO	94
Figure 4.13. Numerical vs. experimental acceleration at bow, $v=3.4$ m/s and $f=0.65$ Hz - MONO	94
Figure 4.14. Numerical vs. experimental heave, $v=3.4$ m/s and $f=0.45$ Hz - MONO	94
Figure 4.15. Numerical vs. experimental pitch, $v=3.4$ m/s and $f=0.45$ Hz - MONO	95
Figure 4.16. Numerical vs. experimental acceleration at CG, $v=3.4$ m/s and $f=0.45$ Hz - MONO	95
Figure 4.17. Numerical vs. experimental acceleration at bow, $v=3.4$ m/s and $f=0.45$ Hz - MONO	95

Figure 4.18. Numerical vs. experimental heave, $v=4.6$ m/s and $f=0.9$ Hz - MONO	96
Figure 4.19. Numerical vs. experimental pitch, $v=4.6$ m/s and $f=0.9$ Hz - MONO	96
Figure 4.20. Numerical vs. experimental acceleration at CG, $v=4.6$ m/s and $f=0.9$ Hz - MONO	96
Figure 4.21. Numerical vs. experimental acceleration at bow, $v=4.6$ m/s and $f=0.9$ Hz - MONO	97
Figure 4.22. Numerical vs. experimental heave, $v=4.6$ m/s and $f=0.65$ Hz - MONO	97
Figure 4.23. Numerical vs. experimental pitch, $v=4.6$ m/s and $f=0.65$ Hz - MONO	97
Figure 4.24. Numerical vs. experimental acceleration at CG, $v=4.6$ m/s and $f=0.65$ Hz - MONO	98
Figure 4.25. Numerical vs. experimental acceleration at bow, $v=4.6$ m/s and $f=0.65$ Hz - MONO	98
Figure 4.26. Numerical vs. experimental heave, $v=4.6$ m/s and $f=0.45$ Hz - MONO	98
Figure 4.27. Numerical vs. experimental pitch, $v=4.6$ m/s and $f=0.45$ Hz - MONO	99
Figure 4.28. Numerical vs. experimental acceleration at CG, $v=4.6$ m/s and $f=0.45$ Hz - MONO	99
Figure 4.29. Numerical vs. experimental acceleration at bow, $v=4.6$ m/s and $f=0.45$ Hz - MONO	99
Figure 4.30. Numerical vs. experimental heave, $v=5.75$ m/s and $f=0.9$ Hz - MONO	100
Figure 4.31. Numerical vs. experimental pitch, $v=5.75$ m/s and $f=0.9$ Hz - MONO	100
Figure 4.32. Numerical vs. experimental acceleration at CG, $v=5.75$ m/s and $f=0.9$ Hz - MONO	100
Figure 4.33. Numerical vs. experimental acceleration at bow, $v=5.75$ m/s and $f=0.9$ Hz - MONO	101
Figure 4.34. Numerical vs. experimental heave, $v=5.75$ m/s and $f=0.65$ Hz - MONO ..	101
Figure 4.35. Numerical vs. experimental pitch, $v=5.75$ m/s and $f=0.65$ Hz - MONO ...	101
Figure 4.36. Numerical vs. experimental acceleration at CG, $v=5.75$ m/s and $f=0.65$ Hz - MONO	102
Figure 4.37. Numerical vs. experimental acceleration at bow, $v=5.75$ m/s and $f=0.65$ Hz - MONO	102
Figure 4.38. Numerical vs. experimental heave, $v=5.75$ m/s and $f=0.45$ Hz - MONO ..	102
Figure 4.39. Numerical vs. experimental pitch, $v=5.75$ m/s and $f=0.45$ Hz - MONO ...	103
Figure 4.40. Numerical vs. experimental acceleration at CG, $v=5.75$ m/s and $f=0.45$ Hz - MONO	103
Figure 4.41. Numerical vs. experimental acceleration at bow, $v=5.75$ m/s and $f=0.45$ Hz - MONO	103
Figure 4.42. Numerical vs. experimental heave, $v=3.4$ m/s and $f=0.9$ Hz - W2	104
Figure 4.43. Numerical vs. experimental pitch, $v=3.4$ m/s and $f=0.9$ Hz - W2.....	104
Figure 4.44. Numerical vs. experimental acceleration at CG, $v=3.4$ m/s and $f=0.9$ Hz - W2.....	104
Figure 4.45. Numerical vs. experimental acceleration at bow, $v=3.4$ m/s and $f=0.9$ Hz - W2.....	105
Figure 4.46. Numerical vs. experimental heave, $v=3.4$ m/s and $f=0.65$ Hz - W2	105
Figure 4.47. Numerical vs. experimental pitch, $v=3.4$ m/s and $f=0.65$ Hz - W2.....	105

Figure 4.48. Numerical vs. experimental acceleration at CG, $v=3.4$ m/s and $f=0.65$ Hz - W2.....	106
Figure 4.49. Numerical vs. experimental acceleration at bow, $v=3.4$ m/s and $f=0.65$ Hz - W2.....	106
Figure 4.50. Numerical vs. experimental heave, $v=3.4$ m/s and $f=0.45$ Hz - W2	106
Figure 4.51. Numerical vs. experimental pitch, $v=3.4$ m/s and $f=0.45$ Hz - W2.....	107
Figure 4.52. Numerical vs. experimental acceleration at CG, $v=3.4$ m/s and $f=0.45$ Hz - W2.....	107
Figure 4.53. Numerical vs. experimental acceleration at bow, $v=3.4$ m/s and $f=0.45$ Hz - W2.....	107
Figure 4.54. Numerical vs. experimental heave, $v=4.6$ m/s and $f=0.9$ Hz - W2	108
Figure 4.55. Numerical vs. experimental pitch, $v=4.6$ m/s and $f=0.9$ Hz - W2.....	108
Figure 4.56. Numerical vs. experimental acceleration at CG, $v=4.6$ m/s and $f=0.9$ Hz - W2.....	108
Figure 4.57. Numerical vs. experimental acceleration at bow, $v=4.6$ m/s and $f=0.9$ Hz - W2.....	109
Figure 4.58. Numerical vs. experimental heave, $v=4.6$ m/s and $f=0.65$ Hz - W2	109
Figure 4.59. Numerical vs. experimental pitch, $v=4.6$ m/s and $f=0.65$ Hz - W2.....	109
Figure 4.60. Numerical vs. experimental acceleration at CG, $v=4.6$ m/s and $f=0.65$ Hz - W2.....	110
Figure 4.61. Numerical vs. experimental acceleration at bow, $v=4.6$ m/s and $f=0.65$ Hz - W2.....	110
Figure 4.62. Numerical vs. experimental heave, $v=4.6$ m/s and $f=0.45$ Hz - W2	110
Figure 4.63. Numerical vs. experimental pitch, $v=4.6$ m/s and $f=0.45$ Hz - W2.....	111
Figure 4.64. Numerical vs. experimental acceleration at CG, $v=4.6$ m/s and $f=0.45$ Hz - W2.....	111
Figure 4.65. Numerical vs. experimental acceleration at bow, $v=4.6$ m/s and $f=0.45$ Hz - W2.....	111
Figure 4.66. Numerical vs. experimental heave, $v=5.75$ m/s and $f=0.9$ Hz - W2	112
Figure 4.67. Numerical vs. experimental pitch, $v=5.75$ m/s and $f=0.9$ Hz - W2.....	112
Figure 4.68. Numerical vs. experimental acceleration at CG, $v=5.75$ m/s and $f=0.9$ Hz - W2.....	112
Figure 4.69. Numerical vs. experimental acceleration at bow, $v=5.75$ m/s and $f=0.9$ Hz - W2.....	113
Figure 4.70. Numerical vs. experimental heave, $v=5.75$ m/s and $f=0.65$ Hz - W2	113
Figure 4.71. Numerical vs. experimental pitch, $v=5.75$ m/s and $f=0.65$ Hz - W2.....	113
Figure 4.72. Numerical vs. experimental acceleration at CG, $v=5.75$ m/s and $f=0.65$ Hz - W2.....	114
Figure 4.73. Numerical vs. experimental acceleration at bow, $v=5.75$ m/s and $f=0.65$ Hz - W2.....	114
Figure 4.74. Numerical vs. experimental heave, $v=5.75$ m/s and $f=0.45$ Hz - W2	114
Figure 4.75. Numerical vs. experimental pitch, $v=5.75$ m/s and $f=0.45$ Hz - W2.....	115
Figure 4.76. Numerical vs. experimental acceleration at CG, $v=5.75$ m/s and $f=0.45$ Hz - W2.....	115

Figure 4.77. Numerical vs. experimental acceleration at bow, $v=5.75$ m/s and $f=0.45$ Hz - W2.....	115
Figure 4.78. Numerical vs. experimental heave, monohedral hull, 2 nd model	116
Figure 4.79. Numerical vs. experimental pitch, monohedral hull, 2 nd model	117
Figure 4.80. Numerical vs. experimental heave, warped hull, 2 nd model	117
Figure 4.81. Numerical vs. experimental pitch, warped hull, 2 nd model.....	118
Figure 4.82. Accelerations FFT for monohedral hull at $v=3.4$ m/s, $f = 0.45$ Hz	119
Figure 4.83. Accelerations FFT for monohedral hull at $v=4.6$ m/s, $f = 0.45$ Hz	119
Figure 4.84 Accelerations FFT for monohedral hull at $v=5.75$ m/s, $f = 0.45$ Hz	120
Figure 4.85. FFT for monohedral hull	121
Figure 4.86. FFT for warped hull.....	122
Figure 4.87. Numerical vs. experimental acceleration at bow for monohedral and warped hull at $v=5.75$ m/s and $f=0.9$ Hz	122
Figure 5.1. Numerical vs. experimental heave, $v= 5.75$ m/s.....	125
Figure 5.2. Numerical vs. experimental pitch, $v= 5.75$ m/s.....	125
Figure 5.3. Numerical vs. experimental acceleration at CG (first and second harmonic), $v= 5.75$ m/s and $f=0.9$ Hz	126
Figure 5.4. Numerical vs. experimental acceleration at bow (first and second harmonic), $v= 5.75$ m/s and $f=0.9$ Hz	126
Figure 5.5. Numerical vs. experimental acceleration at CG (first and second harmonic), $v= 5.75$ m/s and $f=0.65$ Hz	127
Figure 5.6. Numerical vs. experimental acceleration at bow (first and second harmonic), $v= 5.75$ m/s and $f=0.65$ Hz	127
Figure 5.7. Numerical vs. experimental acceleration at CG (first and second harmonic), $v= 5.75$ m/s and $f=0.45$ Hz	128
Figure 5.8. Numerical vs. experimental acceleration at bow (first and second harmonic), $v= 5.75$ m/s and $f=0.45$ Hz	128
Figure 5.9. Numerical vs. experimental heave for warped hull, $v= 4.6$ m/s.....	129
Figure 5.10. Numerical vs. experimental pitch for warped hull, $v= 4.6$ m/s	129
Figure 5.11. Numerical vs. experimental acceleration at LCG for warped hull, $v= 4.6$ m/s	130
Figure 5.12. Numerical vs. experimental bow acceleration for warped hull, $v= 4.6$ m/s	130
Figure 5.13. Numerical vs. experimental acceleration at bow for warped hull, $v =5.75$ m/s and $f= 0.9$ Hz	131

List of tables

Table 1 – Monohedral model's principal characteristics	39
Table 2 – Seakeeping tests matrix	40
Table 3 – Calm water values – input for seakeeping calculations	40
Table 4 – First and second mathematical model	63
Table 5 – WARP 2 model's principal characteristics	90
Table 6 – Calm water values – input for seakeeping calculations	91

Nomenclature

A	: wave amplitude, mm
A_{ij}	: added mass coefficient
B	: beam, m
B_C	: beam at chine, m
B_{ij}	: damping coefficient
C_{ij}	: restoring coefficient
$C_{L\beta}$: lift coefficient relative to deadrise angle β
C_V	: Froude number based on beam, $C_V = \frac{v}{\sqrt{g \cdot B}}$
C_Δ	: load coefficient, $C_\Delta = \frac{\Delta}{\rho \cdot g \cdot B^3}$
D	: total drag, N
D_f	: friction drag force along the hull, N
DII	: Department of Industrial Engineering, University of Naples Federico II
f	: wave frequency, Hz
F_{FK}	: Froude-Krilov force, N
F_{HD}	: hydrodynamic force, N
F_{HS}	: hydrostatic force, N
F_r	: Froude number, $F_r = \frac{v}{\sqrt{g \cdot L_{WL}}}$
F_{rv}	: volumetric Froude number, $F_{rv} = \frac{v}{\sqrt{g \cdot \nabla^{1/3}}}$
F_{Z-HD}	: vertical component of hydrodynamic force, N
g	: acceleration of gravity, 9.80665 m/s ²
H	: wave height, m
HSC	: high speed craft
H/λ	: wave steepness – ratio between wave height and wave length
k	: wave number, rad/m, $k = \omega^2/g = 2\pi/\lambda$
k_{44}	: transversal radius of gyration, m
k_{55}	: longitudinal radius of gyration, m
L	: length, m
L/B	: length-beam ratio
L_{A-B}	: length of clear part of models, m
LCG	: longitudinal position of the centre of gravity from transom, m
L_{OA}	: length over all, m
L_{WL}	: length on waterline, m
m_A	: sectional added mass, kg/m
M_{FK}	: Froude-Krilov moment, Nm
M_{HD}	: hydrodynamic moment, Nm
M_{HS}	: hydrostatic moment, Nm

T	: thrust force, N
T_{AP}	: draught at aft perpendicular, m
U	: relative velocity in plane of the cross section parallel to the baseline, m/s
v	: boat speed, m/s
V	: relative velocity in plane of the cross section normal to the baseline, m/s
VCG	: vertical position of the centre of gravity, m
W	: weight force, N
w_z	: vertical component of the wave velocity, m/s
Z_V	: sinkage at measured position, m
β	: deadrise angle, deg
Δ	: displacement, N
ε	: wave phase, rad, deg
η	: wave elevation, m
η_1	: surge displacement, m
η_3	: heave displacement, m
η_5	: pitch displacement, deg
η_3 / A	: non dimensional heave response
η_5 / kA	: non dimensional pitch response
λ	: wave length, m
λ / L_{OA}	: wave length - length over all ratio
μ	: wave direction with respect to the bow, deg
τ	: running trim angle, deg
ω	: circular wave frequency, rad/s
ω_e	: encounter frequency, rad/s, $\omega_e = \omega - kv \cos \mu$

Chapter 1

1. INTRODUCTION

1.1. Background

The number of high-speed planing hulls has significantly increased in recent years owing to their speed and performance requested in military, recreational, racing, and transportation purposes. Planing vessels are characterised by relatively small dimensions ($L < 30$ m), hard chine along the hull, relatively low L/B ratio, relatively high Froude number together with significant running trim and reduced wetted surface in the planing condition.

Accurate analysis of the hull behaviour in motion plays an important role, mainly due to the significance of their optimum and reliable operation under a variety of sea conditions. The structural design of these hulls is also important as it has direct effects on their weight, hydrodynamic performances, cost and the load they can transport.

Seakeeping methods, based on linear and non-linear assumptions applicable on displacement ships, are not able to account for flow separation on hard chine and take into account dynamic lift therefore they will result in an not accurate evaluation of motions and loads in waves.

In order to apply nonlinear based methods in a design context of fast planing hull, it is necessary to develop a methodology able to take into account the principal nonlinearities associated with strong variation of wetted surface, hydrodynamic

lift and running trim and impulsive loads due to high forward speed, that is fast enough to be used in everyday ship design.

Nonlinear planing hulls seakeeping methods techniques have been developed for more than thirty years. Since first works in the field of planing hulls, in order to model properly the wave - body interaction problem, a time domain approach is chosen, as it allows to remove the assumption of harmonic responses. Both 2D and 3D panel methods have been developed with different level of nonlinearities included in mathematical models. Very often the validation of new methods is reported only with Fridsma's prismatic hull forms and therefore the real potential of methods is not known to research community.

1.2 Aims and Objectives of the Thesis

The aim of this thesis is to develop a mathematical model and associated computational tool able to predict correctly wave induced motions and loads for planing hulls sailing in rough seas. The proposed methodology should be able to take into account the principal nonlinear effects associated with hydrodynamics of planing regime.

The main objectives of the thesis are two:

- to model principal nonlinear effects associated with motion in planing condition in large amplitude waves;
- to ensure accurate, robust and low computational cost tool to be used in design context.

To these aims, two mathematical nonlinear models for analysis and simulation of nonlinear planing hull dynamics have been considered: first one following Payne (1994, 1995), Ruscelli (2009), Ghadimi et al. (2013) and second one after Zarnick (1978), Keuning (1994), Ackers et al. (1999, etc.), Hicks et al. (1994, 1995), van Deyzen (2008).

Both the mathematical models have been validated against experimental results in small and large amplitude waves at different speeds and in a wide range of wave frequencies. The systematic series of warped planing hull developed at Department of Industrial Engineering, University of Naples, is used as benchmark. Since the aim of this thesis is to apply the proposed methodology in a practical design problem, emphasis is given to vertical motions and accelerations prediction, with objective to understand the importance and feasibility of using a 2D+t nonlinear tool to assess wave induced motions and accelerations.

1.3 Contents of the Thesis

This thesis begins with a critical review that describes and comments on the previous works conducted in the subjected area. The development of nonlinear mathematical model required to review and study publications from different fields, therefore the first part of Chapter 2 recalls planing hull's hydrodynamics in calm water and introduces concept of planing hull behaviour in wave. The second part of Chapter 2 reviews seakeeping methodologies for planing hulls distinguishing them with respect to the mathematical model implied in.

The third Chapter describes in detail the first developed mathematical model, presents formulation of the motion equations, together with the numerical solution developed in Matlab-Simulink environment. The obtained numerical results are compared with experimental results for monohedral hull, presented in Begovic et al. (2012, 2014). The seakeeping tests were performed in the Tank of University of Naples Federico II reporting heave, pitch and accelerations at CG and at bow for three model speeds. The numerical and experimental motions and accelerations are analysed in time domain and in frequency domain. From the spectral analysis was possible to determine the magnitude of the higher order harmonics, which are negligible for motions and significant for accelerations. Small non-linearity in the motions, results in a significant contribution of the

higher order harmonics in accelerations. After validation of developed code, some critical issues have been identified resulting in not always satisfying pitch and bow acceleration prediction.

The difficulties related to the description of planing hulls seakeeping physics through a set of mathematical equations led to the development of the second mathematical model in which two simplifying hypothesis on small pitch angle and horizontal velocity equal to the advancing speed have been removed. The fourth Chapter describes in detail the second mathematical model. The validation of this fully non-linear mathematical model in regular waves with the experimental results, is done not only for monohedral hull but also for the most innovative warped hull form with variable angle of the bottom, representative of current trends.

Chapter 5 gives the comparison of two developed models, describes the achievements, contains some concluding remarks as well as suggestions for further work.

Chapter 2

2. PLANING HULL HYDRODYNAMICS

2.1 Planing hulls in calm water

Planing vessel embodies simultaneously concept of high relative speed together with flow separation on chine and dynamic trim as result of hydrodynamic lift. Planing hulls have characteristics that distinguish them from other types of hulls. Understanding the characteristics of the hull is important in making an accurate prediction of the behaviour of the planing hull under various operating conditions.

It is possible to distinguish three conventional modes of motion: displacement, semi-planing (transition), and planing. During the displacement mode the Fr number is less than ~ 0.5 . Once Fr exceeds 0.85, boat shifts to the planing mode. In the semi-planing mode, one part of hull weight is supported by hydrodynamic force and the Froude number stays less than ~ 0.85 . Similar to the displacement mode, the trim of the hull, wetted surface area, and drag all increase in this case. To achieve the planing mode, the hull has to overcome a so-called resistance barrier, which requires a relatively high power. The practical upper limit for the semi-displacement mode occurs when Fr reaches ~ 0.85 . As the Froude number increases, the trim of the hull gradually decreases and tends to a constant value.

High relative speed itself (even at $Fr > 0.85$) does not mean the hull will be planing. To obtain the hydrodynamic support is necessary that the hull has some geometric characteristics:

As it can be seen from Figure 2.2 and Figure 2.3 the flow around the hull is characterised by pressure area, whisker spray area and spray.



Figure 2.2. Planing hull in calm water (cortesy of prof. Bertorello C.)

The shape of planing hull wetted surface can be divided into two parts. The first described as “pressure area” is limited by wetted chine length, wetted keel length and stagnation line and it is the part of hull for which all hydrodynamic equations for lift, drag and centre of pressure are applicable. The second, smaller, called “spray area” is forward of stagnation line, Savitsky (1964), as shown in Figure 2.3. Savitsky et al. (2006), renames the spray area as “whisker spray area”. This area is the part of the hull bottom still in contact with water delimited by the stagnation line and the spray edge. The spray visible on the sides is not of hydrodynamic interest.

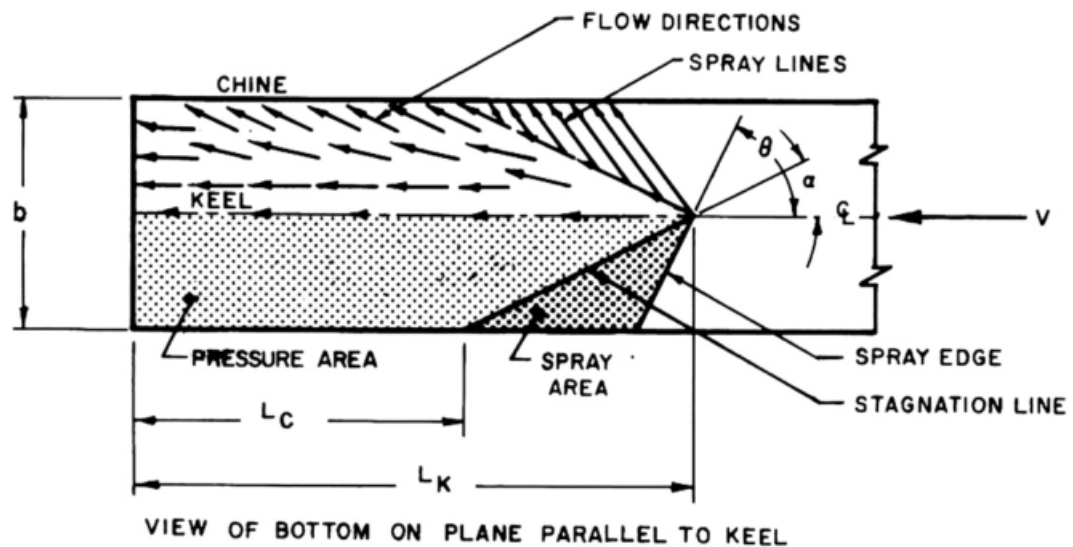


Figure 2.3. Definition of wetted surface by Savitsky et al. (2006)

To assess the hydrodynamic resistance of high speed planing hulls experimental, empirical and numerical approaches are used. The most used method to assess the prismatic hull resistance in total hydrodynamic lift was proposed by Savitsky (1964). The original Savitsky method is based on regression analysis of extensive experimental data on prismatic planing hulls, giving formulas for lift, drag and centre of pressure coefficients and determines the equilibrium conditions at speed evaluating: trim, draft, wetted keel and chine lengths and finally hydrodynamic resistance. In Savitsky et al. (2006). suggested the improvement of the original work by Savitsky (Oct. 1964) including whisker spray drag and aerodynamic drag. Original ‘‘Savitsky’’ method includes only drag due to the viscosity and pressure but it does not consider the so called ‘‘whisker spray’’ area forward of the stagnation line. It is shown that the magnitude of this resistance component is dependent upon the running trim and hull deadrise and it is largest for high deadrise hulls operating at relatively low trim angles what is typical for very high-speed hulls. Savitsky et al. (2006) indicated that whisker spray resistance component could be up to 15% of total resistance highlighting the necessity to include this component when estimating the total resistance of planing monohulls. As regard warped hull it is not possible to apply simple projection of wetted area

or length as in Savitsky (1964, 2006) procedures. In Begovig and Bertorello (2012) these parameters are determined in their effective values taking into account the effect of the bottom warping. The wetted surface and whisker spray area are evaluated thanks to the transparent bottom of the models presented in Begovig and Bertorello (2012). Clear bottoms allowed visual inspection and recording of the wetted areas limited by stagnation line, chine and keel wetted lengths and spray edge as shown in Figure 2.4. After a detailed analysis of the obtained photos, the wetted surface was drawn on 3D models drawings and four principal unknowns of planing and preplaning hydrodynamic regime: mean wetted length, wetted surface of pressure area, mean wetted length of whisker spray and wetted surface of whisker spray, are identified.

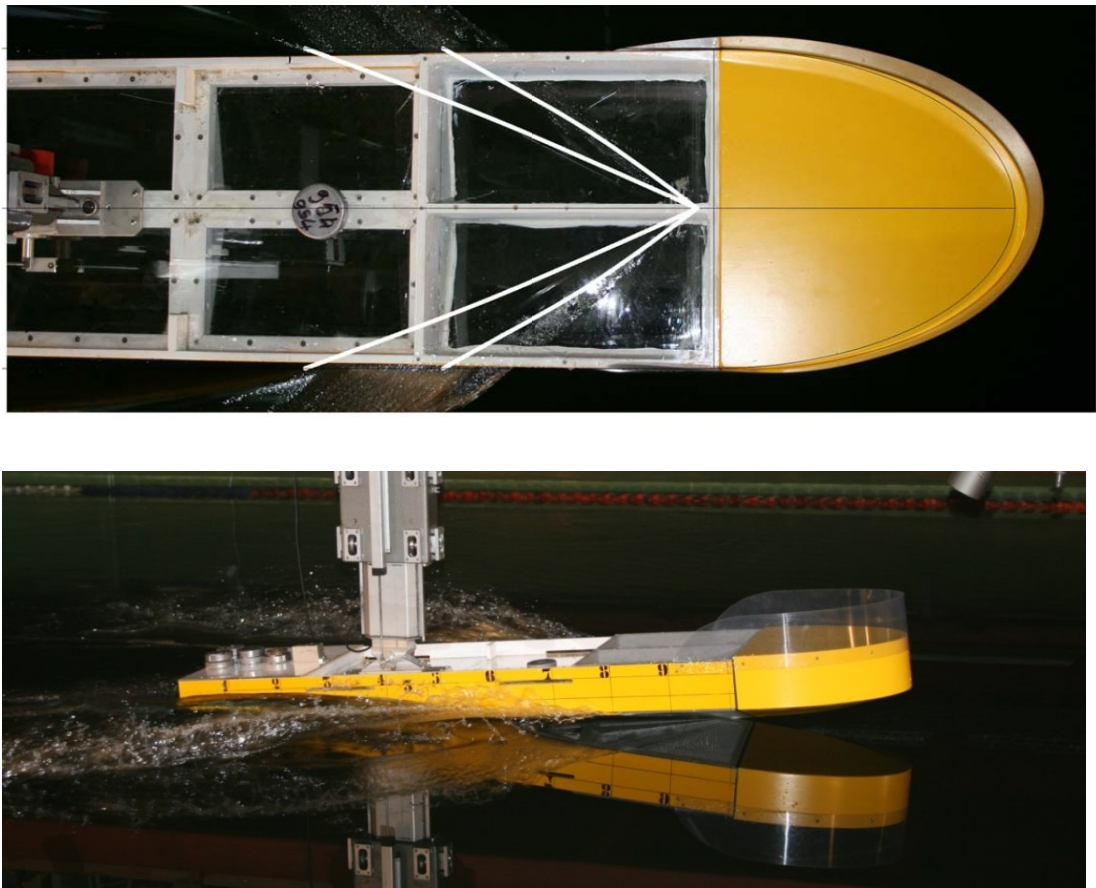


Figure 2.4. Physics of planing – monohedral hull tested at DII at $F_{rv} = 2.88$

Although experimental tests are the most reliable way for modelling these flows, relatively limited number of systematic research is presented in scientific community generally considering so called “prismatic hulls” or monohedral hulls. Monohedral hull form is characterised by constant deadrise angle (angle between the bottom of the hull with the base line) along the hull. Prismatic hull moreover is mathematical form with the chine line parallel to base line. The monohedral hullform with V bottom and constant deadrise angle has been most common and widely used to achieve high relative speed by hydrodynamic lift since early sixties. This is due to good performances as well as to its intrinsic simplicity, leading to easy design and simple construction. Finally a sound method for resistance assessment and a small number of geometric and dynamic factors influencing the hydrodynamic performances have contributed to monohedral hullform success and diffusion.

At early stage of planing craft development low values of deadrise angle from 7 to 14 degrees to get adequate hydrodynamic lift by high $C_{L\beta}$ values were used. Since early eighties more advanced construction techniques and lighter and powerful engines become available and higher values up to 25 degrees were commonly used to improve seakeeping behaviour in rough sea, although experiencing higher still water resistance. Within this frame the deadrise angle has been identified and it is still considered a very important geometrical factor influencing both resistance and seakeeping in a counteracting way. In the last decade the fuel cost increase and the enhanced consideration of comfort and safety in rough sea have strongly influenced the HSC monohull design. The standard monohedral hull form has been modified into warped hull form to get both reduced horsepower and adequate seakeeping. The forward and central parts of the hull present very high deadrise angles for best seakeeping while the after flat bottom provides the necessary hydrodynamic lift. Hull bottom is warped to fit the requested deadrise angles. This solution can be used successfully only if the flat after part remains always below the free surface.

In this case the widely used tools for monohedral hullform hydrodynamic behaviour assessment cannot be considered reliable. The variation of deadrise angles complicates the wetted surface assessment and influences running trim.

2.2 Planing hull seakeeping

Since first works on planing craft performances in rough water, experimental and semi-empirical methods took place over complicated mathematical modelling of planing hull seakeeping. Fridsma's experimental work and regression formulas developed by Fridsma (1969, 1971), reviewed in Savitsky and Brown (1976) and Savitsky and Koelbel (1993) are still the milestones for assessment of added resistance and accelerations values at CG and bow, at different speed regimes of monohedral planing hulls. Recently some new systematic series of planing hulls hydrodynamic properties in calm water are published by Taunton et al. (2010), Metcalf (2005) and Begovic et al. (2012). Important new contributions for planing hull behaviour in rough sea are reported in Taunton (2011) suggesting Gamma distribution for acceleration prediction instead of Rayleigh distribution as found from Fridsma's work. Soletic (2010) analysed longitudinal distribution of accelerations and compared his experimental results with those from regression formulas indicating the discrepancies in widely used predictions. In Begovic et al. (2014) effect of deadrise variation along the hull on heave, pitch and acceleration at CG and bow is analysed for small systematic series of three warped hulls in regular waves forming a possible benchmark for software testing.

As regard numerical predictions for planing hulls seakeeping, a fundamental step in forming the mathematical model of planing hull seakeeping is transformation of complex 3D problem into 2D wedge impacting on the water surface.

As reported by Wang (2013) the problem of a free falling wedge entering into a free surface of water, can be described by four successive phases: impact, flow

separation from the knuckles, creation and pinch-off of the cavity above the body, and oscillation of the cavity after the pinch-off, schematised in Figure 2.5.

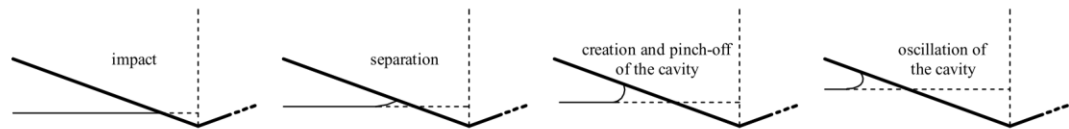


Figure 2.5. Different phases of free falling wedge into a free surface of water

During the impact before the water reaches the knuckle of the wedge and flow separation occurs, impulse loads occur. After the rising water reaches the knuckles of the wedge, separation occurs and the hydrodynamic force on the wedge will drop dramatically. The water is displaced outwards by the wedge. In planing hull hydrodynamics, first two phases are of particular interest, and as the compressibility and air-cushion effects are of short duration and they were neglected in almost all studies, leading to a potential theory. First works on slamming phase are from von Karman (1929) and Wagner (1932), who studied the impact of the floats of landing seaplanes on the water surface.

Several authors from Troesch (1992), Royce (2001), Sun (2007, 2011), Troesch (2010) developed potential flow methods solving two-dimensional impact of a wedge with varying degrees of complexity. General approach is to find pressure distribution over an immersing wedge and subsequently to find pressure distribution and loads on planing hull.

Another approach following the work of Martin and Zarnick is based on strip theory approach where the normal hydrodynamic force per unit length acting at each section is assumed equal to the rate of change of momentum and cross flow drag components. The most important works based on this approach are: Martin (1976), Zarnick (1978), Keuning (1994), Hicks (1995), Ackers (1999), van Deyzen (2008). Martin (1976) developed a linear semi-empirical strip theory for

constant deadrise prisms in regular waves. In this method no free surface deformations are taken into account except for a correction for pile-up, leading to very simple analytical formulations for the added mass coefficients and a very efficient method. Later Zarnick (1978) extended the method to a non-linear time domain strip theory for planing constant deadrise prisms. Keuning (1994) further extended the basic model of Zarnick (1978) to variable deadrise hulls and added empirical formulations for the trim and sinkage based on model tests, in this way stretching the applicability of the method into a wider speed range. Hicks (1995) presented non-linear model without simplification of small trim angle. This model leads to second order members in forces equilibrium equations. Van Deyzen (2008) extended Keuning's model to three degrees of freedom: surge, heave and pitch motion can be simulated and in particular the simulations can be carried out for a planing boat sailing in regular head seas, using either a constant forward speed or constant thrust.

Ackers (1999) extended the two-dimensional method proposed by Zarnick (1978), to calculate the pressure on panels along the hull and particular emphasis was on the added mass coefficient determination for different deadrise angles.

Garne (2005) used a combination of the semi-empirical non-linear strip theory of Zarnick and Keuning, combined with precomputed sectional hydrodynamic coefficients based on Tulin (1957) for planing craft in waves. Sebastiani et al. (2008) presented 2D nonlinear theory based on Zarnick theory using Payne (1994, 1995) approach for added mass. Ruscelli (2009) and Ghadimi et al. (2013) developed the final extension of Sebastiani's methodology to the three coupled degrees of freedom (heave, roll and pitch). The presented validation are for Fridsma's prismatic hulls and proper roll validation is missing due to the lack of data.

In the last decades there is an increased interest in CFD simulations of planing hulls but still planing hull behavior modelling for RANSE methods is complicated, requiring advanced users, enormous computational time and obtained results have precision in the order of simplified theories.

Chapter 3

3. MATHEMATICAL MODEL ACCORDING TO PAYNE

3.1 Introduction

For analysis and simulation of nonlinear planing hull dynamics a mathematical model, following Payne (1994, 1995), Ruscelli (2009) and Ghadimi et al. (2013), is developed. The complete theoretical model "non-linear time domain simulation" was subsequently implemented in a numerical code. Nonlinear time domain simulations were performed using 2D+t theory. At each time step, the total force and moment on the hull is obtained by using the sectional forces calculated in those 2D planes at exact wetted surface. Validation of developed code is performed for monohedral hull with 16.7 degrees deadrise at three velocities. Time series of experimental data concerning vertical motions and accelerations at two longitudinal positions at wide range of wave frequencies and at three model speeds have assured very good benchmarking for developed code validation. Original part of work is detailed analysis of numerical and experimental acceleration data in frequency and time domain identifying the level of nonlinearities in motions and acceleration responses.

3.2 Problem formulation

Planing hull is advancing with constant speed v . For the definition of the mathematical model is necessary to define three reference systems as shown in Figure 3.1.

- 1) $G\xi\psi\zeta$ is the local coordinates system, reference system moving with the boat, with origin on the boat centre of gravity G ; ξ axis is parallel to the inclined base line, positive forward; ζ axis perpendicular to base line, positive downwards; ψ axis perpendicular to plan $\xi\zeta$, positive rightwards;
- 2) $OXYZ$ is the mobile reference system, in the case of constant speed it is an inertial reference system. This reference system moving with the same boat speed v , with origin O on the projection of the centre of gravity on the undisturbed free surface of water at the initial instant; x axis along waterline direction, positive forward; z axis perpendicular to waterline, positive downwards; y axis perpendicular to the initial boat symmetry plan, positive rightwards, is adopted for the description of the wave elevation;
- 3) $Gxyz$ with origin located at the boat's centre of gravity, the x axis is aligned along the calm water free-surface, positive in the direction of boat travel and the z axis positive downward. In this reference system the equilibrium equations are solved.

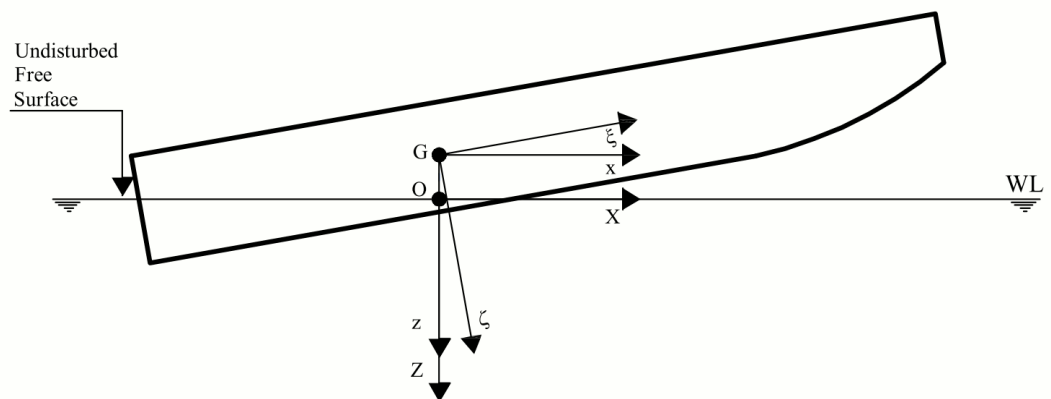


Figure 3.1. Reference systems definition

The forces acting on a planing hull in calm sea conditions are: weight force W , shaft thrust T , drag D , hydrodynamic force F_{HD} and hydrostatic component F_{HS} as schematized in Figure 3.2. When the wave invests the hull the modification of hull volume changes the vertical forces balance. If compared to the planing hull in calm sea, there are exciting force due to the wave and different hydrostatic forces due to the modified immersed hull form and volume.

The final equilibrium for seakeeping problem is given by: weight force, hydrostatic force, exciting force and hydrodynamic force. Shaft thrust and drag are neglected, as their horizontal components, that are predominant, are assumed constant over time and thus in stationary equilibrium.

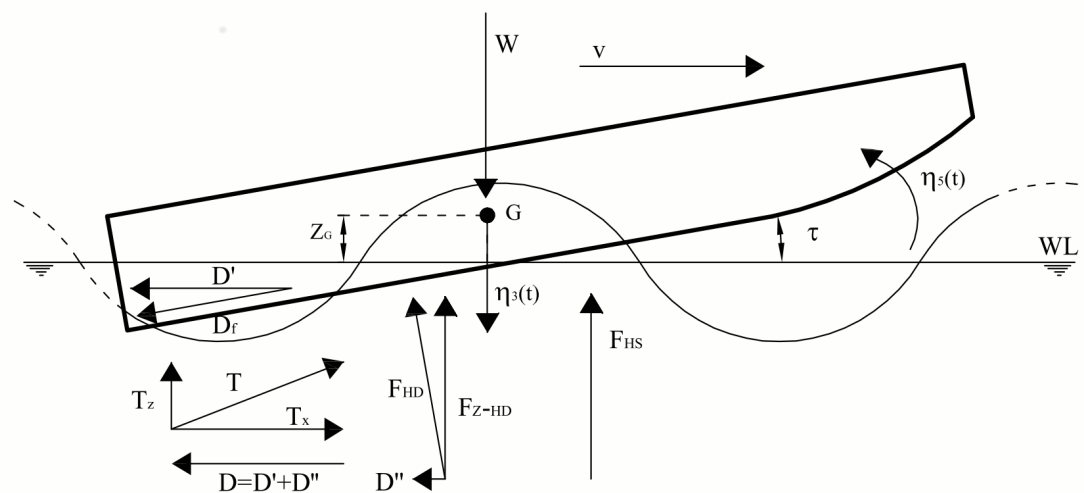


Figure 3.2. Acting forces at planing hull in waves and definition of motions

Forces acting on a planing hull in waves are considered independent and further defined as:

- hydrostatic force;
- hydrodynamic force (lift);

- Froude-Krylov hydrodynamic force (pressures generated by the undisturbed incident wave);
- diffraction hydrodynamic force (fluid pressure due to the hull motion).

Froude-Krilov forces and diffraction are the exciting forces. In mathematical model for planing hull, diffraction force is assumed zero.

The considered vertical motions of the hull are characterized by heave η_3 (positive downward) and pitch η_5 (positive bow up). All other motions are neglected. The initial heave is corrected with sinkage, i.e. vertical rise of centre of gravity, while the initial pitch is equal to τ , running trim at considered speed.

3.2.1 Hydrostatic force

In the planing mode the hydrostatic force is negligible, is the hydrodynamic lift that support the weight, when the wave passes through the hull the wetted surface changes (Figure 3.3) and the hydrostatic component may become no longer negligible.

The sectional static component is calculated as:

$$f_{HS}(\xi, t) = \rho \cdot g \cdot A(\xi, t)$$

where $A(\xi, t)$ is the cross sectional area, ρ is the water density and g the gravitational acceleration. Global hydrostatic force acting on hull is defined as:

$$F_{HS}(t) = \int_{L(t)} f_{HS}(\xi, t) d\xi$$

Leading to final expression for hydrostatic forces:

$$F_{HS} = \int_{L(t)} \rho \cdot g \cdot A(\xi, t) d\xi$$

$$M_{HS} = \int_{L(t)} \rho \cdot g \cdot A(\xi, t) \cdot \xi \cdot \cos \theta d\xi$$

where $L(t)$ is the wetted length.

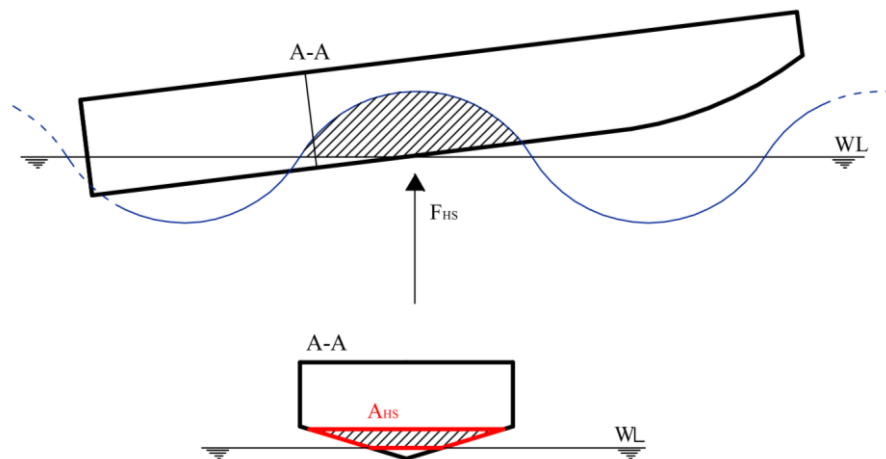


Figure 3.3. Change of wetted surface and hydrostatic force definition

3.2.2 Froude-Krilov force

Following the Airy theory; applied in a non-linear form which accounts for the effective draught of each section, the sectional Froude Krilov force is calculated as the integral on the wetted perimeter of the dynamic component of pressure. The regular waves are described in the reference system OXYZ by:

$$\eta(X, Y, t) = A \cos(kX \cos(\mu) + kY \sin(\mu) - \omega_e t + \varepsilon)$$

where:

A: wave amplitude (m);

k: wave number ($k = \omega^2/g = 2\pi/\lambda$);

μ : wave direction (rad) with respect to bow ($0^\circ =$ following sea, $180^\circ =$ head sea);

ω : wave frequency (rad/s);

ω_e : encounter frequency ($\omega_e = \omega - kv \cos \mu$);

ε : wave phase (rad) between 0 and 2π .

With this definition at initial time, the regular wave has its crest in correspondence with the boat centre of gravity.

The pressures on the hull are calculated as shown in equation:

$$p_{FK} = \rho g(z - Z_G) - Z_W e^{-k(z - Z_G)}$$

The total pressure is the sum of two components: hydrostatic and dynamic. In this formulation is necessary to consider only the dynamic component.

$$p_{FK} = Z_W e^{-k(z - Z_G)}$$

where:

Z_W : wave elevation;

z : actual vertical position of intersection of wave and hull section in Gxyz reference system;

Z_G : the distance between the centre of gravity and the still water line.

The sectional force is given by:

$$f_{FK}(\xi, t) = \int_{S(\xi, t)} p_{FK}(\psi, \zeta; t) \cdot n \, dS$$

where S is the wetted perimeter of each section.

The integration along the hull length of the sectional forces gives the total wave forces.

$$F_{FK} = \int_{L(t)} f_{FK}(\xi, t) \, d\xi$$

$$M_{FK} = \int_{L(t)} f_{FK}(\xi, t) \cdot \xi \cdot \cos \theta \, d\xi$$

3.2.3 Diffraction force

The hydrodynamic diffraction forces are assumed zero. The amplitude of the diffracted waves is proportional to the hull volume, which is, in planing conditions, small and therefore also the damping forces, related to the diffraction of wave, are negligible compared to the other forces. This implicates that the developed model has a range of validity limited only to planing regime.

3.2.4 Hydrodynamic force

The sectional dynamic component $f_{HD}(\xi, t)$ is calculated considering that the force exerted by a fluid on the hull is equal to the variation of the momentum associated to the fluid mass moved by the boat with speed equal to the relative vertical velocity between the boat and the undisturbed fluid.

$$f_{HD}(\xi, t) = \frac{D}{Dt}(m_A(\xi, t) \cdot V(\xi, t))$$

where:

V: relative velocity in plane of the cross section normal to the baseline, as defined in Figure 3.4;

m_A : added mass associated with the section form.

Material derivate of hydrodynamic force can be further written as:

$$\frac{D}{Dt}(m_A(\xi, t) \cdot V(\xi, t)) = \dot{m}_A(\xi, t) \cdot V(\xi, t) + m_A(\xi, t) \cdot \dot{V}(\xi, t) - U \frac{\partial(m_A(\xi, t) \cdot V(\xi, t))}{\partial \xi}$$

The horizontal velocity U is approximated to the advance velocity v.

The vertical component of the hydrodynamic force is the lift, as defined in Figure 3.2. The three terms of the sectional lift force can be seen as:

- contribution of added mass due to the changing of immersed volume;
- inertial contribution due to the relative velocity between water and boat;
- forward velocity contribution.

The global lift force is reported in the following equations:

$$F_{Z-HD} = F_{HD} \cdot \cos \theta = \int_{L(t)} m_A(\xi, t) \cdot \dot{V}(\xi, t) \cdot \cos \theta(t) d\xi$$

$$+ \int_{L(t)} \dot{m}_A(\xi, t) \cdot V(\xi, t) \cdot \cos \theta(t) d\xi - \int_{L(t)} U \cdot \frac{\partial(m_A(\xi, t) \cdot V(\xi, t))}{\partial \xi} \cdot \cos \theta(t) d\xi$$

$$F_{Z-HD} = F_{Z-HD}^I + F_{Z-HD}^{II} - F_{Z-HD}^{III}$$

$$F_{Z-HD}^I = \int_{L(t)} m_A(\xi, t) \cdot \dot{V}(\xi, t) \cdot \cos \theta(t) d\xi$$

$$F_{Z-HD}^{II} = \int_{L(t)} \dot{m}_A(\xi, t) \cdot V(\xi, t) \cdot \cos \theta(t) d\xi$$

$$F_{Z-HD}^{III} = \int_{L(t)} U \cdot \frac{\partial(m_A(\xi, t) \cdot V(\xi, t))}{\partial \xi} \cdot \cos \theta(t) d\xi$$

Similarly, the global hydrodynamic component of the pitch moment is obtained by the sum of three contributions.

$$M_{HD} = \int_{L(t)} m_A(\xi, t) \cdot \dot{V}(\xi, t) \cdot \xi d\xi + \int_{L(t)} \dot{m}_A(\xi, t) \cdot V(\xi, t) \cdot \xi d\xi - \int_{L(t)} U \cdot \frac{\partial(m_A(\xi, t) \cdot V(\xi, t))}{\partial \xi} \cdot \xi d\xi$$

$$M_{HD} = M_{HD}^I + M_{HD}^{II} - M_{HD}^{III}$$

$$M_{HD}^I = \int_{L(t)} m_A(\xi, t) \cdot \dot{V}(\xi, t) \cdot \xi d\xi$$

$$M_{HD}^{II} = \int_{L(t)} \dot{m}_A(\xi, t) \cdot V(\xi, t) \cdot \xi d\xi$$

$$M_{HD}^{III} = \int_{L(t)} U \cdot \frac{\partial(m_A(\xi, t) \cdot V(\xi, t))}{\partial \xi} \cdot \xi d\xi$$

3.2.5 Velocity

The relative speed of the boat is the sum of two components:

- a component due to the advanced velocity and to the keel inclination angle with respect to the horizontal (stationary component);
- a component resulting from the relative movement between the section and the water free surface in the concerned section (dynamic component).

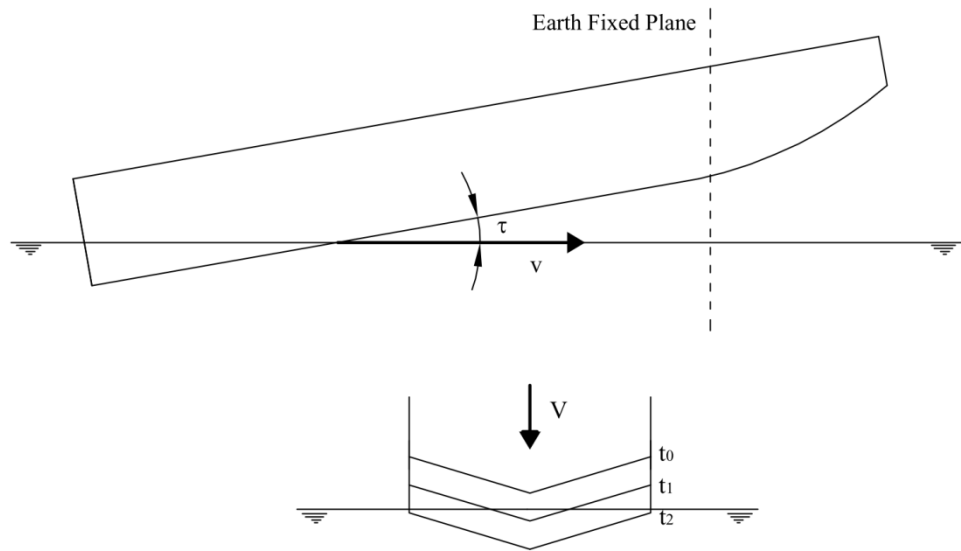


Figure 3.4. View of planing hull from Earth Fixed Plane, definition of relative velocities

$$V(\xi, t) = \dot{\eta}_1 \sin \theta + (\dot{\eta}_3 - w_z) \cos \theta - \dot{\eta}_5 \cdot \xi$$

$$\dot{\eta}_1 = \text{const} = v$$

The vertical component of the wave velocity is calculated by:

$$w_z = A\omega \sin(kX \cos(\mu) + kY \sin(\mu) - \omega_e t + \varepsilon) \cdot e^{-k(z-Z_G)}$$

Considering that for small angles $\sin \theta \approx \theta$ and $\cos \theta \approx 1$ the relative velocity becomes defined as:

$$V(\xi, t) = v\theta + \dot{\eta}_3 - \dot{\eta}_5 \cdot \xi - w_z$$

3.2.6 Added mass determination

Since von Karman and Wagner works on impacting wedge, added mass determination was reviewed by many authors. In von Karman's impact model (1929), the water surface elevation and gravity are neglected and the added mass of the cylinder is approximated as one half the added mass of a flat plate of length equal to the cylinder and width equal to the that of the cylinder in the plane of the undisturbed free surface. This assumption is incorrect for bodies with deadrise angles below 45 degrees. Wagner (1932) further developed Von Karman's theory by accounting for the local uprise of the water and he included the effects of the wave that was generated by the impacting body in the added mass calculation. The asymptotic assumptions advanced by Wagner are included in most current hydrodynamics impact models. Wagner arrived at “ $\pi/2$ wetting (wave rise) factor” results from retaining the first order term of the contour expansion and integrating the velocity ratio in time. Pierson(1948) proposed linear variation of splash up coefficient between two limit solutions given by Wagner and von Karman. Mei (1999) presented generalized Wagner's method using conformal mapping of ships-like sections aimed to practical use for slamming assessment. He reviewed solutions from von Karman, Wagner and Pierson for splashing up coefficient and for slamming force prediction. Important conclusions are that Pierson's hypothesis considerably underestimates the splash-up coefficient between two limits. Pile up coefficient is a function of deadrise and the asymptotic theory of von Karman underestimates the slamming force, while Wagner's overestimates it. Although Pierson hypothesis underestimates splash up coefficient, the Payne's theory based on this assumption agrees well with experimental results for slamming force.

In developed numerical code, the Payne's approach has been used, as follows:

The 2D sectional added mass m_A is expressed by:

$$m_A = \frac{\pi}{2} C_m \rho \left(\frac{d_{eff}}{\tan \beta} \right)^2$$

Where:

C_m : non-dimensional sectional added mass coefficient, Payne (1989, 1994, 1995);

d_{eff} : ‘effective penetration’ of generic section inside water including pile-up, as defined in Figure 3.5;

β : deadrise angle (deg);

ρ : water density (kg/m^3).

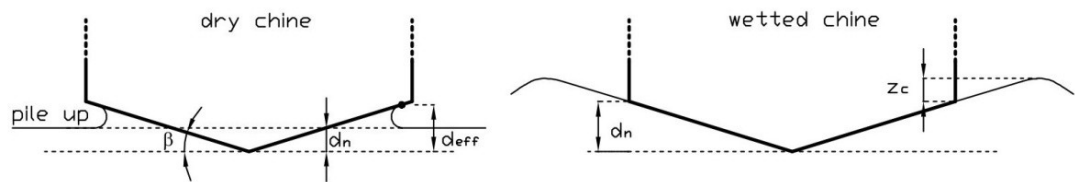


Figure 3.5. Effective penetration, two cases according to chine immersion

$$d_{eff} = d_n \cdot (1 + k_p)$$

$$1 + k_p = \frac{\pi}{2} - \beta \left(1 - \frac{2}{\pi} \right)$$

The non-dimensional added mass coefficient C_m is calculated as:

$$C_m = C_{m0} + \Delta C_m$$

Where:

C_{m0} : basic two-dimensional flow added mass coefficient, $C_{m0} = \left(1 - \frac{\beta}{2\pi} \right)^2$;

ΔC_m : coefficient of the incremental added mass due to chine immersion

$$\Delta C_m = C_{m0} K \frac{z_c}{b};$$

K : experimental coefficient, it varies with the deadrise angle, for $0 < \beta < 40$ its value is ≈ 2 ;

$$K = 2.05 \left[1 - \left(\frac{2}{\pi} \beta \right)^{\frac{9}{2}} \right]$$

z_c : water elevation above chine, as defined in Figure 3.5;

b : local section chine's beam.



Figure 3.6. Flow separation for pile up consideration

It should be noted that Zarnick (1978), Ackers (1999) and Singleton (2004) for case of immersed chine assumed added mass constant, i.e. there is no longer splash up or increasing wetted beam. This is physically more correct, as it is shown in the Figure 3.6.

Nevertheless very good results based on Payne's theory as reported by Mei, and reasonably accurate results reported by Sebastiani, Ruscelli and Ghadimi for vertical motions encouraged to follow Payne's approach completely.

3.3 Motions equations

The boat, under the action of the waves, will move according to the motion classical Newton laws.

In the case of two degrees of freedom:

$$\begin{cases} m \cdot \ddot{\eta}_3 = \sum F_Z(t) \\ I_{55} \cdot \ddot{\eta}_5 = \sum M_Y(t) \end{cases}$$

$$m \cdot \ddot{\eta}_3 = -F_{HD} \cos \theta - F_{HS} - F_{FK} + W$$

$$I_{55} \cdot \ddot{\eta}_5 = M_{HD} + M_{HS} + M_{FK}$$

where:

- m : boat mass;
- I_{55} : mass moment of with respect to y axis;
- θ : pitch angle;
- F_{HD} : hydrodynamic force;
- F_{HS} : hydrostatic force;
- F_{FK} : Froude-Krilov force;
- W : weight of boat;
- M_{HD} : hydrodynamic moment;
- M_{HS} : hydrostatic moment;
- M_{FK} : Froude-Krilov moment.

3.3.1 Force equilibrium in coordinate system Gxyz

It's necessary to develop the terms of the equation of force equilibrium.

$$m \cdot \ddot{\eta}_3 = -F_{HD} \cos \theta - F_{HS} - F_{FK} + W$$

first:

$$F_3 = -F_{HS} - F_{FK} + W$$

$$m \cdot \ddot{\eta}_3 = -F_{HD} \cos \theta + F_3$$

Considering:

$$V(\xi, t) = v\eta_5 + \dot{\eta}_3 - \dot{\eta}_5 \cdot \xi - w_Z$$

$$\dot{V}(\xi, t) = v\dot{\eta}_5 + \ddot{\eta}_3 - \ddot{\eta}_5 \cdot \xi - \dot{w}_Z$$

In Gxyz reference system vertical component of dynamic hydrodynamic force F_{Z-HD} is given by:

$$F_{Z-HD} = F_{HD} \cdot \cos \theta = \int_{L(t)} m_A(\xi, t) \cdot \dot{V}(\xi, t) \cdot \cos \theta(t) d\xi + \int_{L(t)} \dot{m}_A(\xi, t) \cdot V(\xi, t) \cdot \cos \theta(t) d\xi - \int_{L(t)} U \cdot \frac{\partial(m_A(\xi, t) \cdot V(\xi, t))}{\partial \xi} \cdot \cos \theta(t) d\xi$$

It can be written $F_{Z-HD} = F_{Z-HD}^I + F_{Z-HD}^{II} - F_{Z-HD}^{III}$, with following definitions:

$$F_{Z-HD}^I = \int_{L(t)} m_A(\xi, t) \cdot \dot{V}(\xi, t) \cdot \cos \theta(t) d\xi$$

$$F_{Z-HD}^{II} = \int_{L(t)} \dot{m}_A(\xi, t) \cdot V(\xi, t) \cdot \cos \theta(t) d\xi$$

$$F_{Z-HD}^{III} = \int_{L(t)} U \cdot \frac{\partial(m_A(\xi, t) \cdot V(\xi, t))}{\partial \xi} \cdot \cos \theta(t) d\xi$$

Developing one by one component of hydrodynamic force we have:

$$F_{Z-HD}^I = \int_{L(t)} m_A \cdot \cos \theta \cdot \dot{V} d\xi = v \int_{L(t)} m_A \cdot \dot{\eta}_5 \cdot \cos \theta d\xi + \int_{L(t)} m_A \cdot \dot{\eta}_3 \cdot \cos \theta d\xi - \int_{L(t)} \xi \cdot m_A \cdot \dot{\eta}_5 \cdot \cos \theta d\xi - \int_{L(t)} m_A \cdot \dot{w}_Z \cdot \cos \theta d\xi$$

It can written:

$$A_{33}^I = \int_{L(t)} m_A \cdot \cos \theta d\xi$$

$$A_{35}^I = - \int_{L(t)} \xi \cdot m_A \cdot \cos \theta d\xi$$

$$B_{35}^I = v \int_{L(t)} m_A \cdot \cos \theta \, d\xi$$

$$F_{W3}^I = - \int_{L(t)} m_A \cdot \dot{w}_Z \cdot \cos \theta \, d\xi$$

$$\boxed{F_{Z-HD}^I = A_{33}^I \cdot \ddot{\eta}_3 + A_{35}^I \cdot \ddot{\eta}_5 + B_{35}^I \cdot \dot{\eta}_5 + F_{W3}^I}$$

$$\begin{aligned} F_{Z-HD}^{II} &= \int_{L(t)} \dot{m}_A \cdot V \cdot \cos \theta \, d\xi \\ &= \int_{L(t)} \dot{m}_A \cdot v \cdot \cos \theta \cdot \eta_5 \, d\xi + \int_{L(t)} \dot{m}_A \cdot \dot{\eta}_3 \cdot \cos \theta \, d\xi - \int_{L(t)} \dot{m}_A \cdot \dot{\eta}_5 \cdot \xi \cdot \cos \theta \, d\xi \\ &- \int_{L(t)} \dot{m}_A \cdot w_Z \cdot \cos \theta \, d\xi \end{aligned}$$

$$B_{33}^{II} = \int_{L(t)} \dot{m}_A \cdot \cos \theta \, d\xi$$

$$B_{35}^{II} = - \int_{L(t)} \dot{m}_A \cdot \xi \cdot \cos \theta \, d\xi$$

$$C_{35}^{II} = \int_{L(t)} \dot{m}_A \cdot v \cdot \cos \theta \cdot d\xi$$

$$F_{W3}^{II} = - \int_{L(t)} \dot{m}_A \cdot w_Z \cdot \cos \theta \, d\xi$$

$$\boxed{F_{Z-HD}^{II} = B_{33}^{II} \cdot \dot{\eta}_3 + B_{35}^{II} \cdot \dot{\eta}_5 + C_{35}^{II} \cdot \eta_5 + F_{W3}^{II}}$$

$$F_{Z-HD}^{III} = \int_{L(t)} v \cdot \frac{\partial(m_A(\xi, t) \cdot V(\xi, t))}{\partial \xi} \cdot \cos \theta(t) \, d\xi$$

It can be noted that

$$\int_{L(t)} \frac{\partial(m_A \cdot V)}{\partial \xi} \, d\xi = V \cdot m_A \Big|_{stern}^{bow}$$

Before continuing with the development of the mathematical model is needed to specify the meaning of "stern" (later denoted by s) and "bow" (later denoted by b). Considering the wetted length $L(t)$ (Figure 3.7), for ease of viewing in calm water, "bow" and "stern" will be the limits of integration, in other words the bow limit

and the stern limit of the wetted length. The "bow section" is the last wetted section, its wetted height is zero this implies a zero value also for the added mass associated with the section. The integral is reduced to the value of the integrated function only on the "stern section".

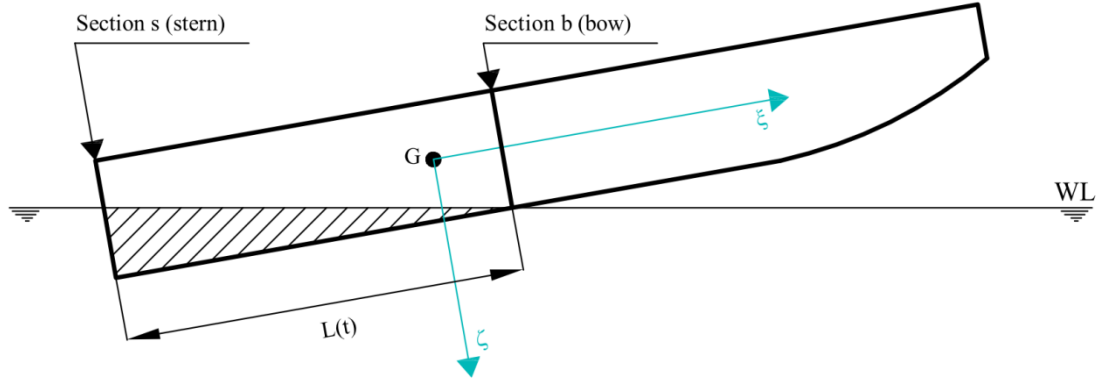


Figure 3.7. Integration limits

Therefore F_{Z-HD}^{III} becomes:

$$F_{Z-HD}^{III} = v \cdot \cos \theta \cdot [(m_A \cdot V)_{BOW} - (m_A \cdot V)_{STERN}]$$

Substituting the expressions for V it follows:

$$F_{Z-HD}^{III} = v^2 \cdot \cos \theta (m_{Ab} - m_{As}) \eta_5 + v \cdot \cos \theta (m_{Ab} - m_{As}) \dot{\eta}_3 - v \cdot \cos \theta (m_{Ab} \xi_b - m_{As} \xi_s) \dot{\eta}_5 - v \cdot \cos \theta (m_{Ab} w_{Zb} - m_{As} w_{Zs})$$

$$C_{35}^{III} = v^2 \cdot \cos \theta (m_{Ab} - m_{As})$$

$$B_{33}^{III} = v \cdot \cos \theta (m_{Ab} - m_{As})$$

$$B_{35}^{III} = -v \cdot \cos \theta (m_{Ab} \xi_b - m_{As} \xi_s)$$

$$F_{W3}^{III} = -v \cdot \cos \theta (m_{Ab} w_{Zb} - m_{As} w_{Zs})$$

Finally we have:

$$F_{Z-HD}^{III} = B_{33}^{III} \cdot \dot{\eta}_3 + B_{35}^{III} \cdot \dot{\eta}_5 + C_{35}^{III} \eta_5 + F_{W3}^{III}$$

Finally hydrodynamic force in Gxyz reference system is given as:

$$F_{Z-HD} = F_{Z-HD}^I + F_{Z-HD}^{II} - F_{Z-HD}^{III}$$

And consequently the coefficients are given as:

$$A_{33} = A_{33}^I = \int_{L(t)} m_A \cdot \cos \theta \, d\xi$$

$$A_{35} = A_{35}^I = - \int_{L(t)} \xi \cdot m_A \cdot \cos \theta \, d\xi$$

$$B_{33} = B_{33}^{II} - B_{33}^{III} = \int_{L(t)} \dot{m}_A \cdot \cos \theta \, d\xi - v \cdot \cos \theta (m_{Ab} - m_{As})$$

$$B_{35} = B_{35}^I + B_{35}^{II} - B_{35}^{III} \\ = v \int_{L(t)} m_A \cdot \cos \theta \, d\xi - \int_{L(t)} \dot{m}_A \cdot \xi \cdot \cos \theta \, d\xi + v \cdot \cos \theta (m_{Ab} \xi_b - m_{As} \xi_s)$$

$$C_{35} = C_{35}^{II} - C_{35}^{III} = \int_{L(t)} \dot{m}_A \cdot v \cdot \cos \theta \cdot d\xi - v^2 \cdot \cos \theta (m_{Ab} - m_{As})$$

$$F_{3-W} = F_{W3}^I + F_{W3}^{II} - F_{W3}^{III} \\ = - \int_{L(t)} m_A \cdot \dot{w}_Z \cdot \cos \theta \, d\xi - \int_{L(t)} \dot{m}_A \cdot w_Z \cdot \cos \theta \, d\xi + v \cdot \cos \theta (m_{Ab} w_{Zb} - m_{As} w_{Zs})$$

$$F_{Z-HD} = A_{33} \cdot \ddot{\eta}_3 + A_{35} \cdot \ddot{\eta}_5 + B_{33} \cdot \dot{\eta}_3 + B_{35} \cdot \dot{\eta}_5 + C_{35} \cdot \eta_5 + F_{3-W}$$

Finally forces equilibrium can be rewritten in form:

$$m \cdot \ddot{\eta}_3 = -F_{Z-HD} + F_3$$

$$m \cdot \ddot{\eta}_3 = -(A_{33} \cdot \ddot{\eta}_3 + A_{35} \cdot \ddot{\eta}_5 + B_{33} \cdot \dot{\eta}_3 + B_{35} \cdot \dot{\eta}_5 + C_{35} \cdot \eta_5 + F_{3-W}) + F_3$$

$$(m + A_{33}) \cdot \ddot{\eta}_3 + A_{35} \cdot \ddot{\eta}_5 + B_{33} \cdot \dot{\eta}_3 + B_{35} \cdot \dot{\eta}_5 + C_{35} \cdot \eta_5 = F_3 - F_{3-W}$$

3.3.2 Moment equilibrium in coordinate system Gxyz

Moments equilibrium with respect to the y axis is given by:

$$I_{55} \cdot \ddot{\eta}_5 = M_{HD} + M_{HS} + M_{FK}$$

$$F_5 = M_{HS} + M_{FK}$$

$$I_{55} \cdot \ddot{\eta}_5 = M_{HD} + F_5$$

M_{HD} is given by:

$$M_{HD} = \int_{L(t)} m_A(\xi, t) \cdot \dot{V}(\xi, t) \cdot \xi d\xi + \int_{L(t)} \dot{m}_A(\xi, t) \cdot V(\xi, t) \cdot \xi d\xi - \int_{L(t)} U \cdot \frac{\partial(m_A(\xi, t) \cdot V(\xi, t))}{\partial \xi} \cdot \xi d\xi$$

$$M_{HD} = M_{HD}^I + M_{HD}^{II} - M_{HD}^{III}$$

Developing each term

$$M_{HD}^I = \int_{L(t)} m_A \cdot \xi \cdot v \cdot \dot{\eta}_5 d\xi + \int_{L(t)} m_A \cdot \xi \cdot \dot{\eta}_3 d\xi - \int_{L(t)} m_A \cdot \xi^2 \cdot \ddot{\eta}_5 d\xi - \int_{L(t)} m_A \cdot \xi \cdot \dot{w}_Z d\xi$$

It can be written:

$$A_{55}^I = - \int_{L(t)} m_A \cdot \xi^2 d\xi$$

$$A_{53}^I = \int_{L(t)} m_A \cdot \xi d\xi$$

$$B_{55}^I = \int_{L(t)} m_A \cdot \xi \cdot v d\xi$$

$$F_{W5}^I = - \int_{L(t)} m_A \cdot \xi \cdot \dot{w}_Z d\xi$$

$$\boxed{M_{HD}^I = A_{55}^I \cdot \ddot{\eta}_5 + A_{53}^I \cdot \ddot{\eta}_3 + B_{55}^I \cdot \dot{\eta}_5 + F_{W5}^I}$$

$$M_{HD}^{II} = \int_{L(t)} \dot{m}_A v \cdot \xi \cdot \eta_5 d\xi + \int_{L(t)} \dot{m}_A \cdot \dot{\eta}_3 \cdot \xi d\xi - \int_{L(t)} \dot{m}_A \cdot \xi^2 \cdot \dot{\eta}_5 d\xi - \int_{L(t)} \dot{m}_A \cdot \xi \cdot w_Z d\xi$$

It can be written:

$$B_{53}^{II} = \int_{L(t)} \dot{m}_A \cdot \xi d\xi$$

$$B_{55}^{II} = - \int_{L(t)} \dot{m}_A \cdot \xi^2 d\xi$$

$$C_{55}^{II} = \int_{L(t)} \dot{m}_A v \cdot \xi d\xi$$

$$F_{W5}^{II} = - \int_{L(t)} \dot{m}_A \cdot \xi \cdot w_Z d\xi$$

$$\boxed{M_{HD}^{II} = B_{53}^{II} \cdot \dot{\eta}_3 + B_{55}^{II} \cdot \dot{\eta}_5 + C_{55}^{II} \cdot \eta_5 + F_{W5}^{II}}$$

$$M_{HD}^{III} = \int_{L(t)} U \cdot \frac{\partial(m_A(\xi, t) \cdot V(\xi, t))}{\partial \xi} \cdot \xi d\xi$$

It can be noted that:

$$\int_{L(t)} \xi \frac{\partial(m_A \cdot V)}{\partial \xi} d\xi = \xi \cdot V \cdot m_A \Big|_{stern}^{bow} - \int_{L(t)} m_A \cdot V d\xi$$

$$\begin{aligned} M_{HD}^{III} &= v^2 \cdot (m_{Ab} \cdot \xi_b - m_{As} \cdot \xi_s) \cdot \eta_5 - \int_{L(t)} v^2 \cdot m_A \cdot \eta_5 d\xi \\ &\quad + v \cdot (m_{Ab} \cdot \xi_b - m_{As} \cdot \xi_s) \cdot \dot{\eta}_3 - \int_{L(t)} v \cdot m_A \cdot \dot{\eta}_3 d\xi \\ &\quad - v \cdot (m_{Ab} \cdot \xi_b^2 - m_{As} \cdot \xi_s^2) \cdot \dot{\eta}_5 + \int_{L(t)} v \cdot m_A \cdot \xi \cdot \dot{\eta}_5 d\xi \\ &\quad - v \cdot (m_{Ab} \cdot \xi_b \cdot w_{Zb} - m_{As} \cdot \xi_s \cdot w_{Zs}) + \int_{L(t)} v \cdot m_A \cdot w_Z d\xi \end{aligned}$$

$$B_{55}^{III} = -v \cdot (m_{Ab} \xi_b^2 - m_{As} \xi_s^2) + \int_{L(t)} v \cdot m_A \cdot \xi d\xi$$

$$B_{53}^{III} = v \cdot (m_{Ab} \xi_b - m_{As} \xi_s) - \int_{L(t)} v \cdot m_A \cdot d\xi$$

$$C_{55}^{III} = v^2 \cdot (m_{Ab} \xi_b - m_{As} \xi_s) - \int_{L(t)} v^2 \cdot m_A d\xi$$

$$F_{W-5}^{III} = -v \cdot (m_{Ab} \cdot w_{Zb} \cdot \xi_b - m_{As} \cdot w_{Zs} \cdot \xi_s) + \int_{L(t)} v \cdot m_A \cdot w_Z d\xi$$

$$\boxed{M_{Z-HD}^{III} = B_{55}^{III} \cdot \dot{\eta}_5 + B_{53}^{III} \cdot \dot{\eta}_3 + C_{55}^{III} \cdot \eta_5 + F_{W5}^{III}}$$

Finally it can be written:

$$A_{55} = A_{55}^I = - \int_{L(t)} m_A \cdot \xi^2 d\xi$$

$$A_{53} = A_{53}^I = \int_{L(t)} m_A \cdot \xi d\xi$$

$$B_{53} = B_{53}^II - B_{53}^{III} = \int_{L(t)} \dot{m}_A \cdot \xi d\xi - v \cdot (m_{Ab} \xi_b - m_{As} \xi_s) + \int_{L(t)} v \cdot m_A \cdot d\xi$$

$$\begin{aligned} B_{55} &= B_{55}^I + B_{55}^{II} - B_{55}^{III} = \\ &\int_{L(t)} m_A \cdot \xi \cdot v d\xi - \int_{L(t)} \dot{m}_A \cdot \xi^2 d\xi + v \cdot (m_{Ab} \xi_b^2 - m_{As} \xi_s^2) - \int_{L(t)} v \cdot m_A \cdot \xi d\xi = \\ &- \int_{L(t)} \dot{m}_A \cdot \xi^2 d\xi + v \cdot (m_{Ab} \xi_b^2 - m_{As} \xi_s^2) \end{aligned}$$

$$C_{53} = C_{53}^{II} - C_{53}^{III} = \int_{L(t)} \dot{m}_A v \cdot \xi d\xi - v^2 \cdot (m_{Ab} \xi_b - m_{As} \xi_s) + \int_{L(t)} v^2 \cdot m_A d\xi$$

$$\begin{aligned} F_{5-W} &= F_{W5}^I + F_{W5}^{II} - F_{W5}^{III} = \\ &- \int_{L(t)} m_A \cdot \xi \cdot \dot{w}_Z d\xi - \int_{L(t)} \dot{m}_A \cdot \xi \cdot w_Z d\xi \\ &+ v \cdot (m_{Ab} \cdot w_{Zb} \cdot \xi_b - m_{As} \cdot w_{Zs} \cdot \xi_s) - \int_{L(t)} v \cdot m_A \cdot w_Z d\xi \end{aligned}$$

Finally to compose the motion equation the hydrodynamic coefficients must be multiplied by -1 and the final expressions are:

$$A_{55} = -A_{55} = \int_{L(t)} m_A \cdot \xi^2 d\xi$$

$$A_{53} = -A_{53} = - \int_{L(t)} m_A \cdot \xi d\xi$$

$$B_{53} = -B_{53} = - \int_{L(t)} \dot{m}_A \cdot \xi d\xi + v \cdot (m_{Ab} \xi_b - m_{As} \xi_s) - \int_{L(t)} v \cdot m_A \cdot d\xi$$

$$B_{55} = -B_{55} = \int_{L(t)} \dot{m}_A \cdot \xi^2 d\xi - v \cdot (m_{Ab} \xi_b^2 - m_{As} \xi_s^2)$$

$$C_{53} = -C_{53} = - \int_{L(t)} \dot{m}_A v \cdot \xi d\xi + v^2 \cdot (m_{Ab} \xi_b - m_{As} \xi_s) - \int_{L(t)} v^2 \cdot m_A d\xi$$

$$-M_{HD} = A_{55} \cdot \ddot{\eta}_5 + A_{53} \cdot \ddot{\eta}_3 + B_{55} \cdot \dot{\eta}_5 + B_{53} \cdot \dot{\eta}_3 + C_{55} \cdot \eta_5 - F_{5-W}$$

Finally momentum equilibrium can be rewritten in form:

$$I_{55} \cdot \dot{\eta}_5 = M_{HD} + F_5$$

$$I_{55} \cdot \ddot{\eta}_5 = -A_{55} \cdot \ddot{\eta}_5 - A_{53} \cdot \ddot{\eta}_3 - B_{55} \cdot \dot{\eta}_5 - B_{53} \cdot \dot{\eta}_3 - C_{55} \cdot \eta_5 + F_{5-W} + F_5$$

$$(I_{55} + A_{55}) \cdot \ddot{\eta}_5 + A_{53} \cdot \ddot{\eta}_3 + B_{55} \cdot \dot{\eta}_5 + B_{53} \cdot \dot{\eta}_3 + C_{55} \cdot \eta_5 = F_{5-W} + F_5$$

3.4 The 2D nonlinear numerical code

The code is developed for hard-chine hulls with variable deadrise and beam along boat length. The mathematical model is implemented using the ‘‘Strip Theory’’, considering the hull as made of 2D ‘strips’, and evaluating the total 3D forces as the resultants of sectional forces which act separately on each section without interactions.

The geometry is imported from a 3D CAD modellers, the ship half-section points are organized into a three-dimensional array (Figure 3.8). The developed code consists of two parts. The first part allows the calculation of forces and motions coefficients depending on the effective wetted surface in incident wave. After defining the incident wave, as shown in Figure 3.9, the most important task of the code is the calculation of the ship-wave intersections as shown in Figure 3.10. After the definition of these intersections the code evaluates forces, moments and coefficients involved in the equations of equilibrium.

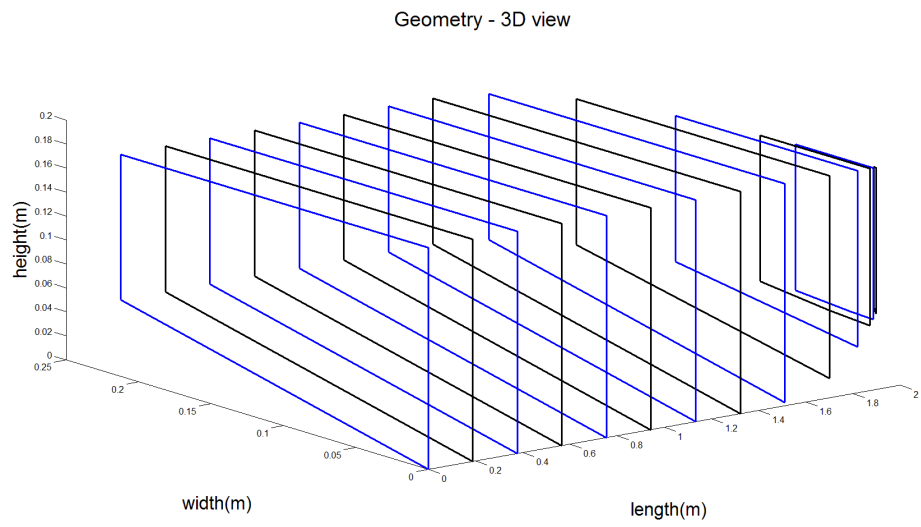


Figure 3.8. Imported geometry

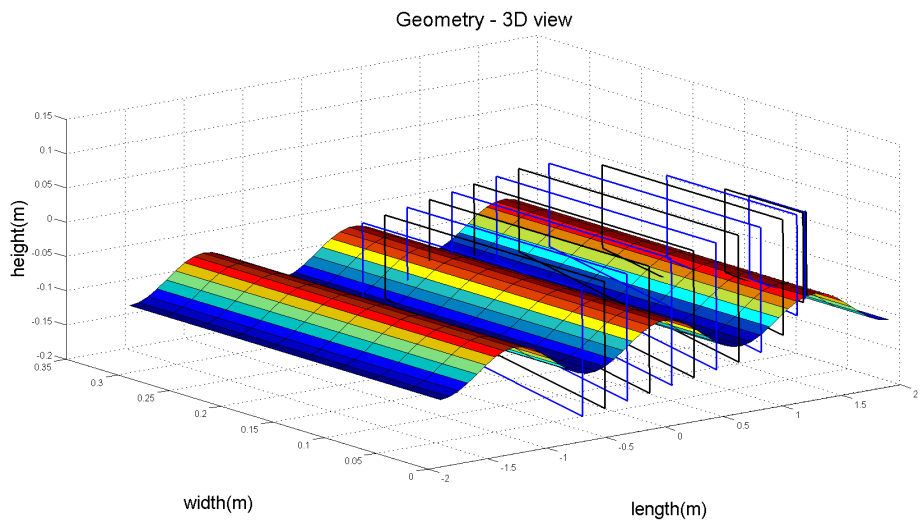


Figure 3.9. Incident wave and wetted sections properties

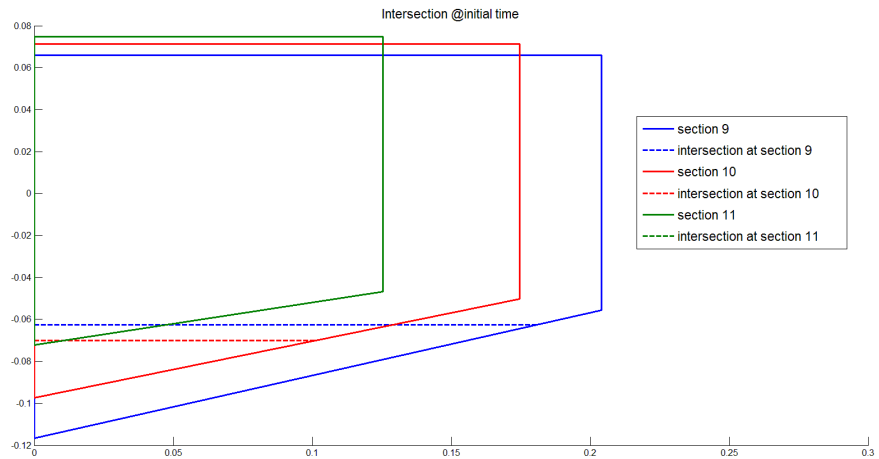


Figure 3.10. Intersection wave-section

The system of equations is solved instant by instant using the numerical integration algorithm of 4th order Runge-Kutta adding the initial conditions relative to the undisturbed steady equilibrium position at the specified speed. The ship velocity, running trim and sinkage are input parameters and heave and pitch motions are computed as a variation in time around this position.

Developed Simulink code scheme is shown in Figure 3.11.

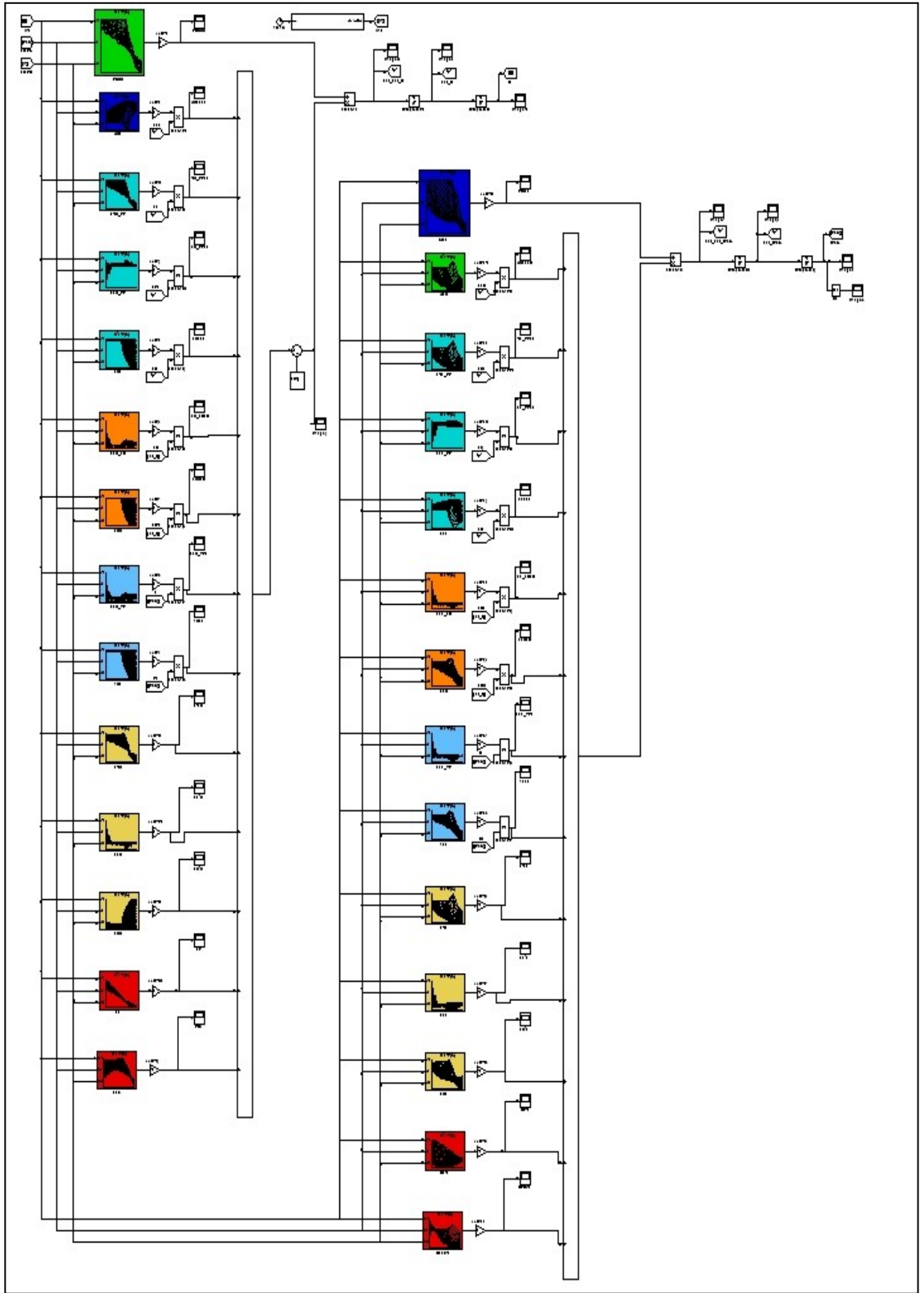


Figure 3.11. Simulink model

For incident wave given by wave amplitude and frequency the example of calculated heave and pitch during the chosen simulation time is shown in Figure 3.12.

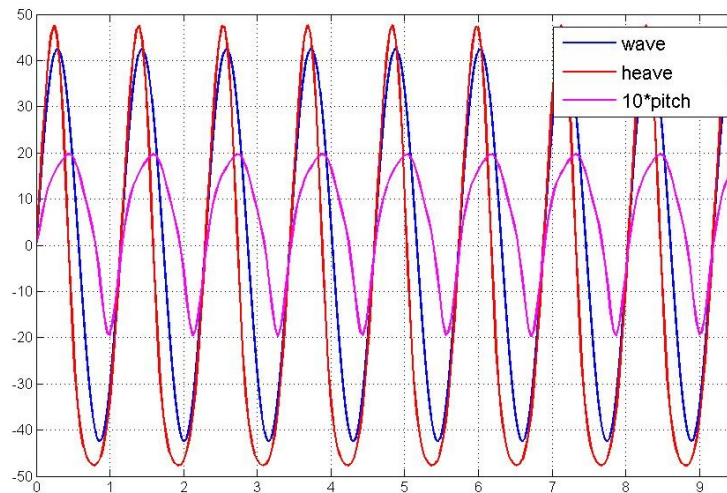


Figure 3.12. Input wave (mm), calculated heave(mm) and pitch (deg)

3.5 Comparison of numerical and experimental data for monohedral hull

To validate the developed code experimental data set performed in the Tank of University of Naples Federico II, is used. The measurements of resistance, dynamic sinkage and trim were performed in calm water and these results are presented in Begovic and Bertorello (2012). From the calm water tests speeds of interest were identified: 3.4, 4.6 and 5.75 m/s, it was seen that:

- at speed 4.6 model has perfect flow separation;
- maximum realistic speed for testing in waves is 5.75;
- the speed of 3.4 is the speed where the planing begins.

Seakeeping results for monohedral hull, with deadrise angle 16.7 degrees, shown in Figure 3.13, presented in Begovic et al. (2014), contain heave, pitch and

accelerations at CG and at bow for three model speeds corresponding to $F_{rv} = 1.92, 2.60$ and 3.25 . Model main dimensions and inertial properties are given in Table 1.

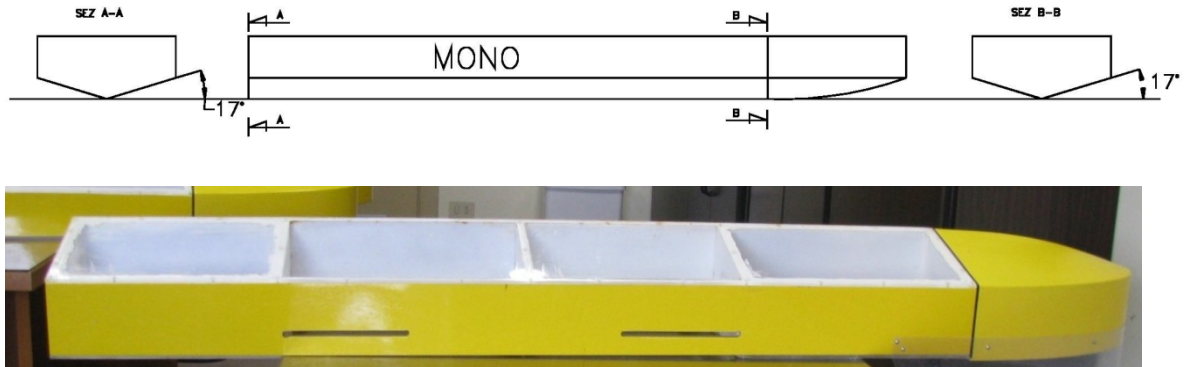


Figure 3.13. Monohedral hull geometry

Table 1 – Monohedral model's principal characteristics

L_{OA}	L_{A-B}	B	T_{AP}	Δ	β	LCG	VCG	k_{44}	k_{55}
(m)	(m)	(m)	(m)	(N)	(deg)	(m)	(m)	(m)	(m)
1.9	1.5	0.424	0.096	319.7	16.7	0.697	0.143	0.1281	0.5833

The LCG position is set from tests in calm water with aim to assure the trim of about four degrees at speed, leading to 1.66 degree astern as static trim.

Four degrees running trim represents a realistic scenario for a planing hull in service. Seakeeping tests were performed at constant speed with models restrained to sway, roll and yaw. Model speed, heave, pitch, added resistance were measured at the point of 53.5 cm from the stern, while accelerations are measured at 0.72m and at 1.62m from stern. Measured heave is recalculated to the longitudinal centre of gravity LCG position reported in Table 1. Wave frequencies and encounter waves amplitudes are given in Table 2. All data are sampled at 500 Hz.

Table 2 – Seakeeping tests matrix

f	ω	k	λ	λ/L_{OA}	A	H/λ
(Hz)	(rad/s)	(rad/m)	(m)		(mm)	
1.00	6.283	4.026	1.561	0.821	16	0.020
0.90	5.655	3.261	1.927	1.014	20	0.021
0.80	5.027	2.576	2.439	1.284	20	0.016
0.70	4.398	1.973	3.185	1.676	20	0.013
0.65	4.084	1.701	3.694	1.944	32	0.017
0.60	3.770	1.449	4.335	2.282	32	0.015
0.55	3.456	1.218	5.160	2.716	35	0.014
0.50	3.142	1.006	6.243	3.286	35	0.011
0.45	2.827	0.815	7.708	4.057	45	0.012
0.40	2.513	0.644	9.755	5.134	45	0.009

Once the code has been validated, calculations are performed for wave amplitudes measured in seakeeping tests, reported in Table 2 and for input condition summarized in Table 3.

Table 3 – Calm water values – input for seakeeping calculations

v (m/s)	3.40	4.60	5.75
Sinkage (mm)	3.65	9.75	17.42

Running trim (deg)	3.97	4.17	4.02
--------------------	------	------	------

Calculations are performed with a time step 0.002 s, the same as the sampling frequency in performed experiments. Simulation time of 50 seconds in model scale was considered, although from model tests maximum time history is about 15 s. Examples of calculated vs. measured responses are given from Figure 3.14 to Figure 3.49, for three speeds of 3.4 m/s, 4.6 m/s and 5.75 m/s corresponding respectively to $F_{rv} = 1.92$, 2.60 and 3.25 and for three wave's frequencies of 0.9, 0.65 and 0.45 Hz.

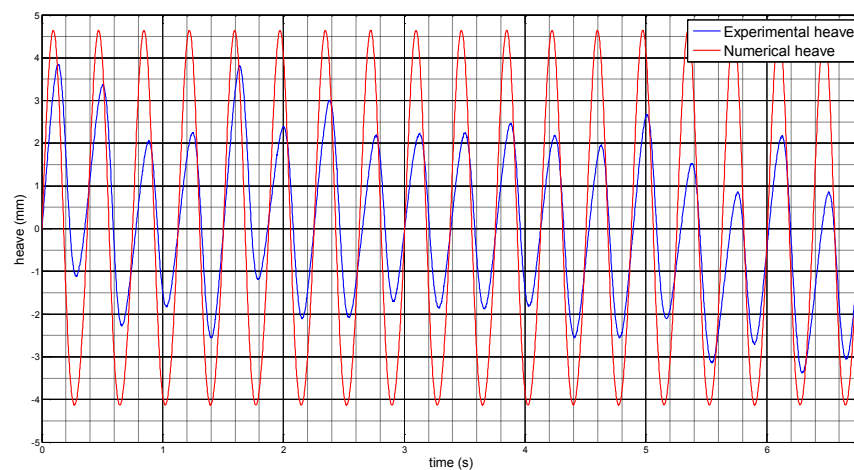


Figure 3.14. Numerical vs. experimental heave, $v=3.4$ m/s and $f=0.9$ Hz

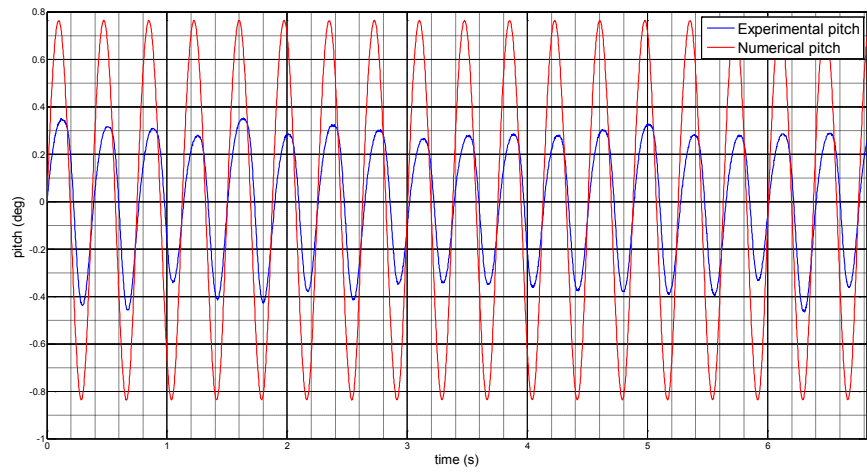


Figure 3.15. Numerical vs. experimental pitch, $v=3.4$ m/s and $f=0.9$ Hz

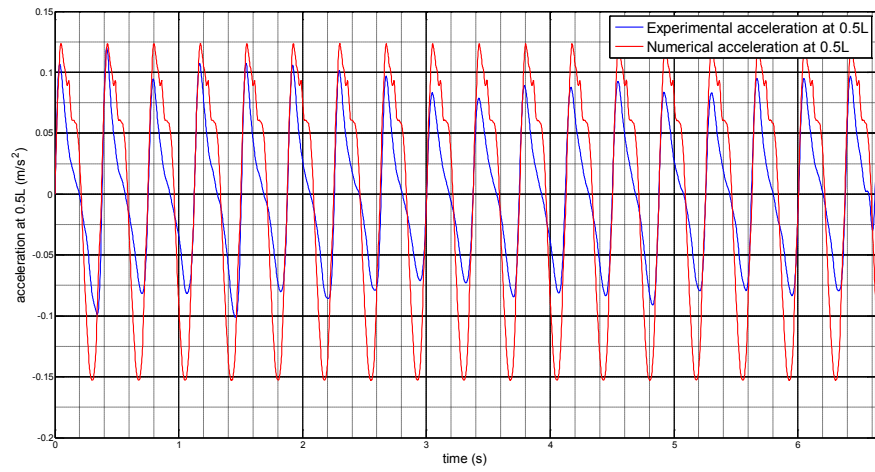


Figure 3.16. Numerical vs. experimental acceleration at CG, $v=3.4$ m/s and $f=0.9$ Hz

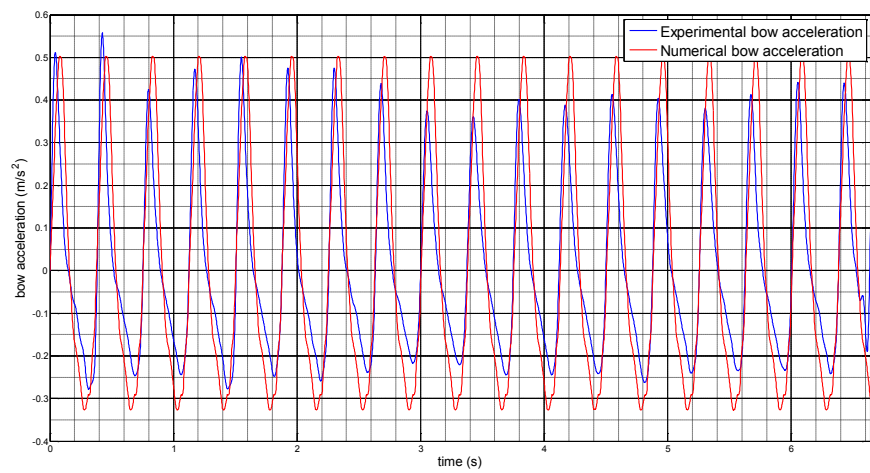


Figure 3.17. Numerical vs. experimental acceleration at bow, $v=3.4$ m/s and $f=0.9$ Hz

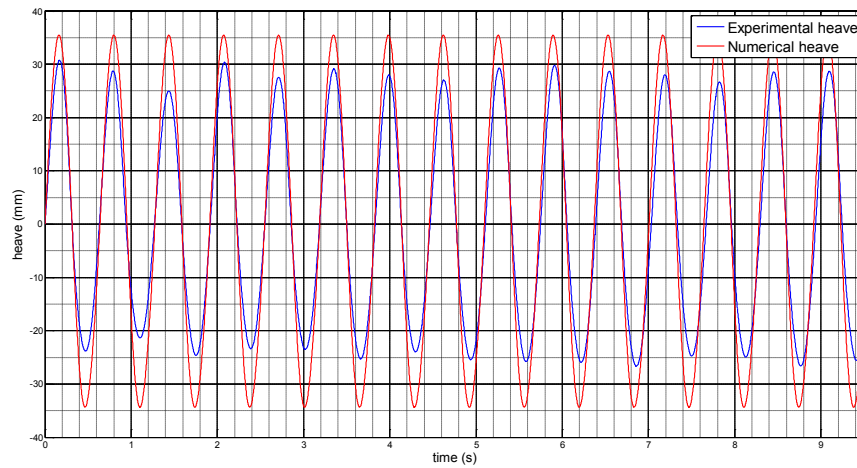


Figure 3.18. Numerical vs. experimental heave, $v=3.4$ m/s and $f=0.65$ Hz

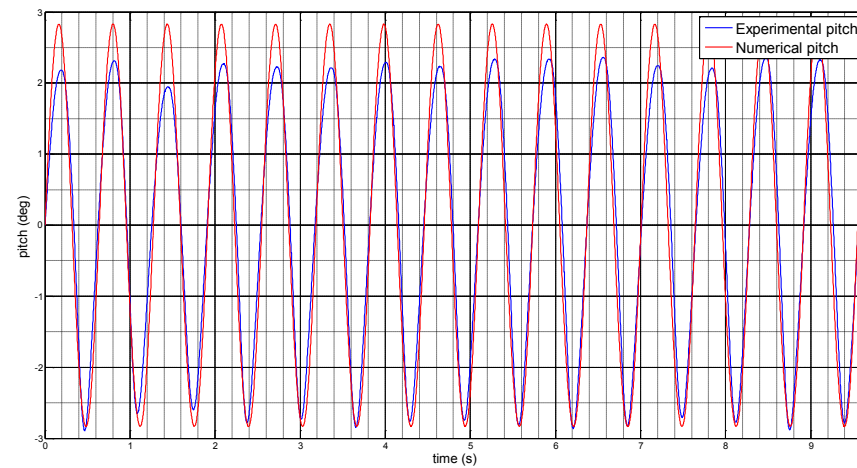


Figure 3.19. Numerical vs. experimental pitch, $v=3.4$ m/s and $f=0.65$ Hz

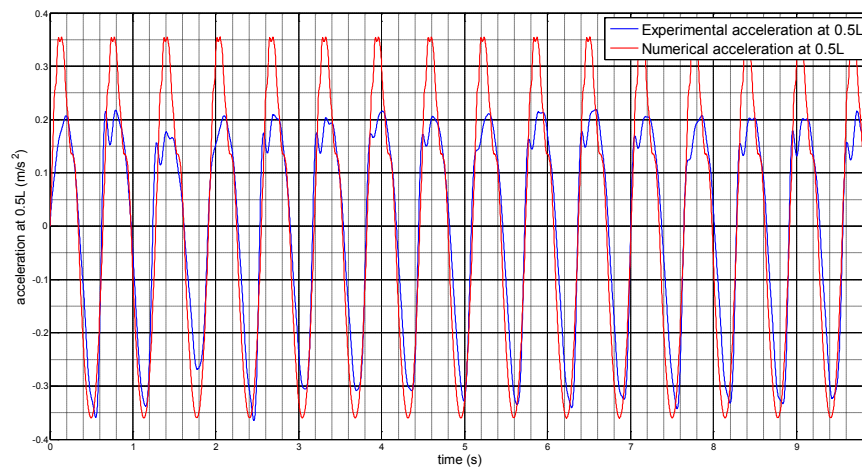


Figure 3.20. Numerical vs. experimental acceleration at CG, $v=3.4$ m/s and $f=0.65$ Hz

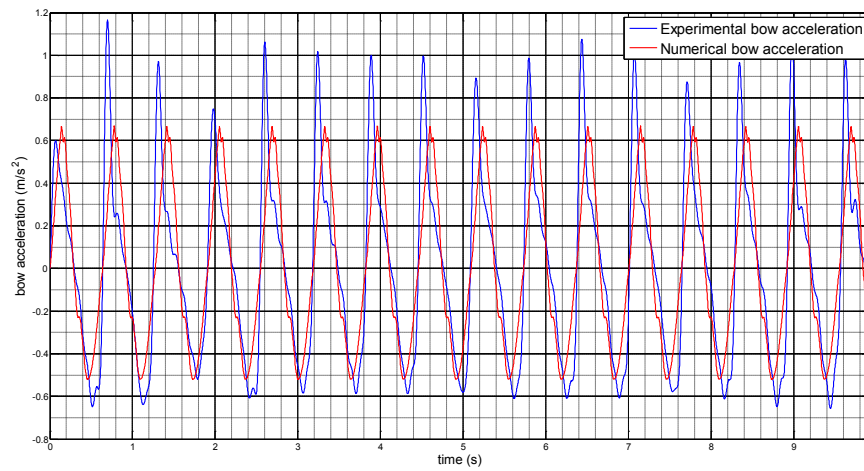


Figure 3.21. Numerical vs. experimental acceleration at bow, $v=3.4 \text{ m/s}$ and $f=0.65 \text{ Hz}$

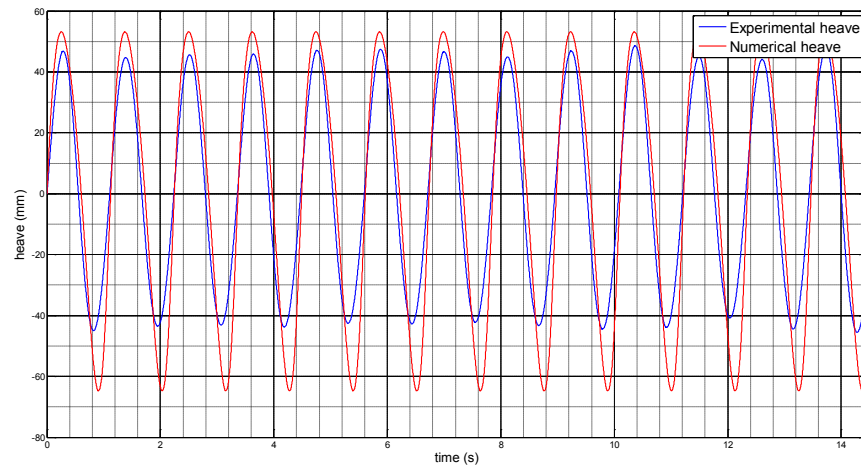


Figure 3.22. Numerical vs. experimental heave, $v=3.4 \text{ m/s}$ and $f=0.45 \text{ Hz}$

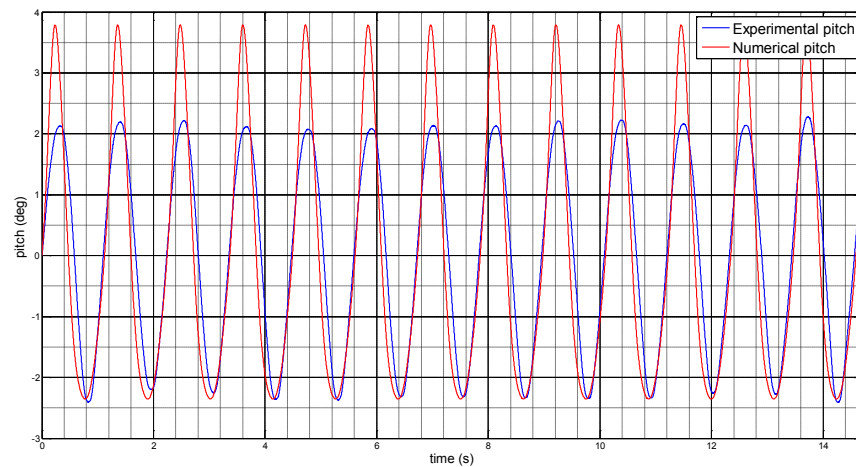


Figure 3.23. Numerical vs. experimental pitch, $v=3.4 \text{ m/s}$ and $f=0.45 \text{ Hz}$

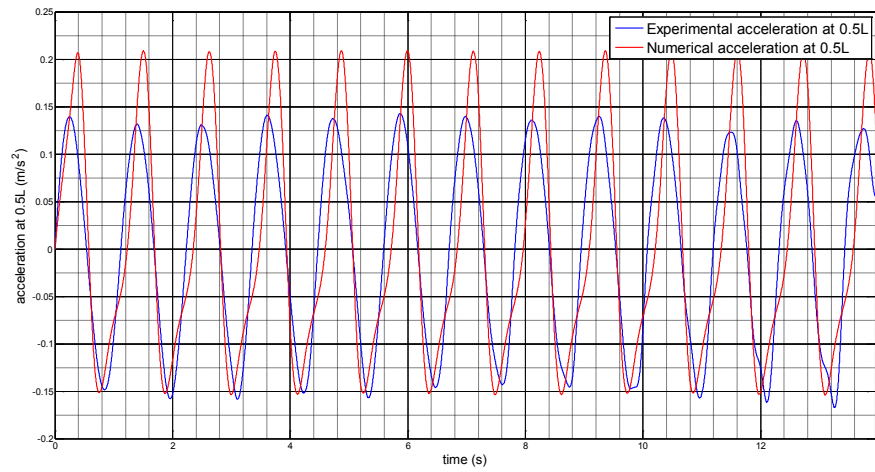


Figure 3.24. Numerical vs. experimental acceleration at CG, $v=3.4$ m/s and $f=0.45$ Hz

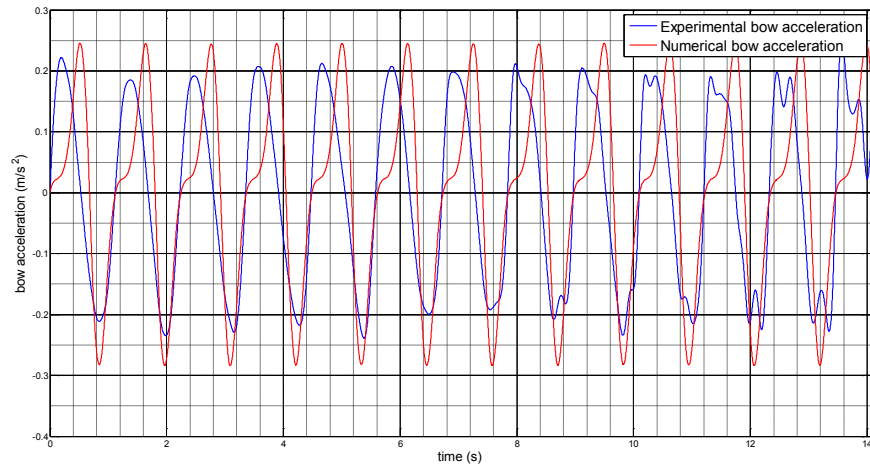


Figure 3.25. Numerical vs. experimental acceleration at bow, $v=3.4$ m/s and $f=0.45$ Hz

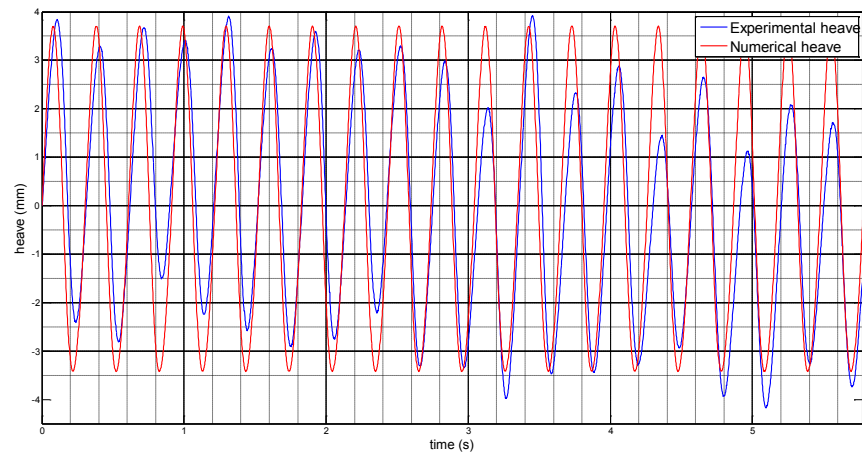


Figure 3.26. Numerical vs. experimental heave, $v=4.6$ m/s and $f=0.9$ Hz

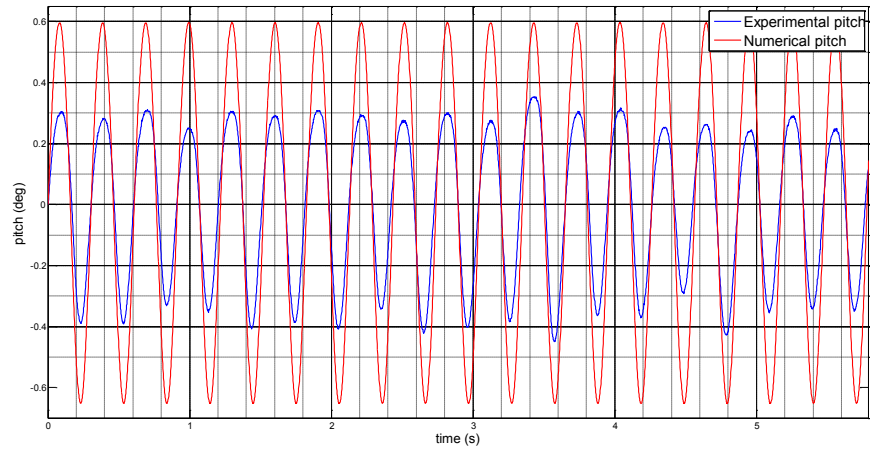


Figure 3.27. Numerical vs. experimental pitch, $v=4.6$ m/s and $f=0.9$ Hz

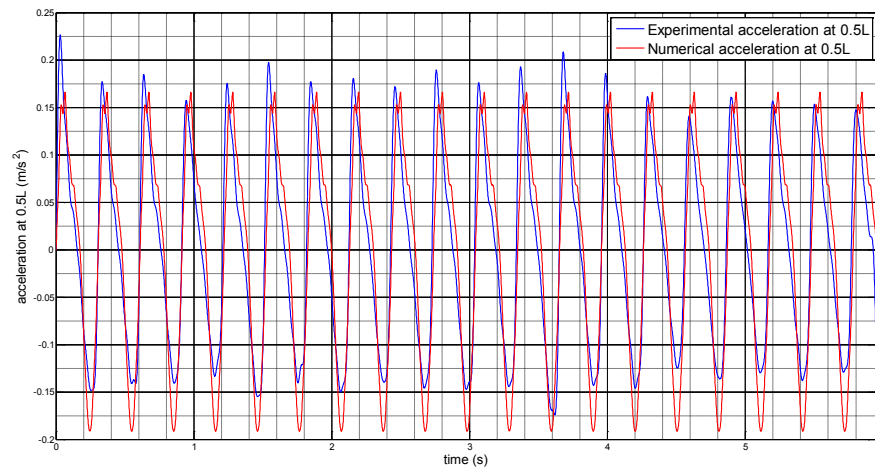


Figure 3.28. Numerical vs. experimental acceleration at CG, $v=4.6$ m/s and $f=0.9$ Hz

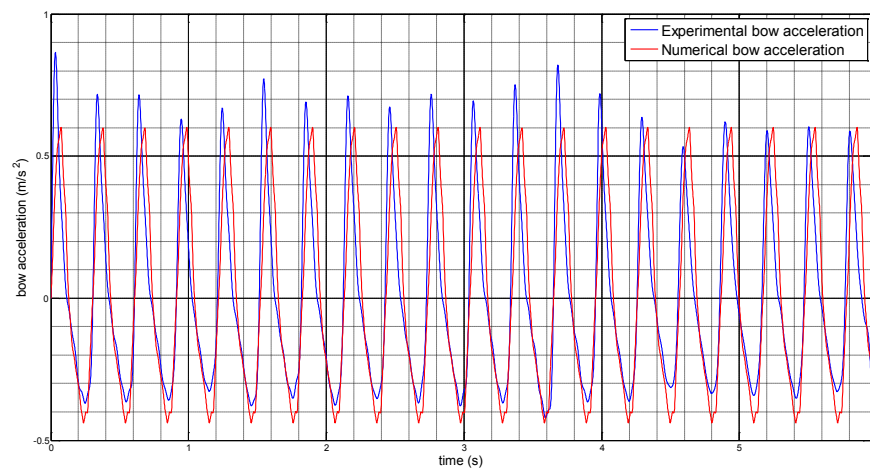


Figure 3.29. Numerical vs. experimental acceleration at bow, $v=4.6$ m/s and $f=0.9$ Hz

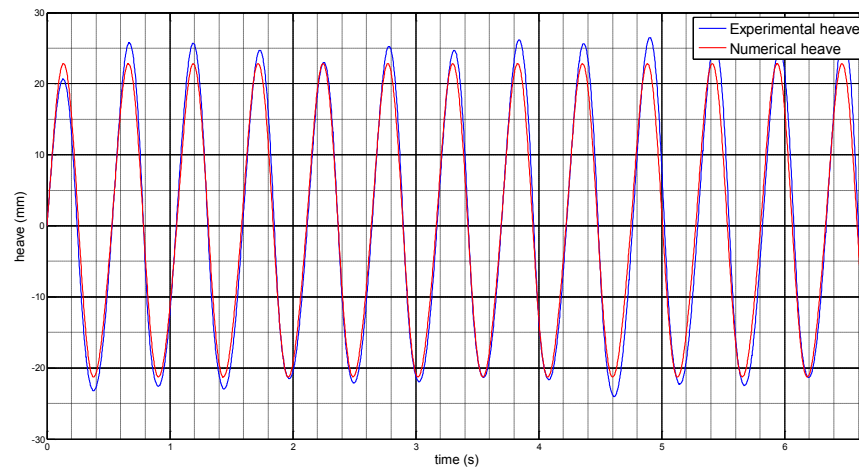


Figure 3.30. Numerical vs. experimental heave, $v=4.6$ m/s and $f=0.65$ Hz

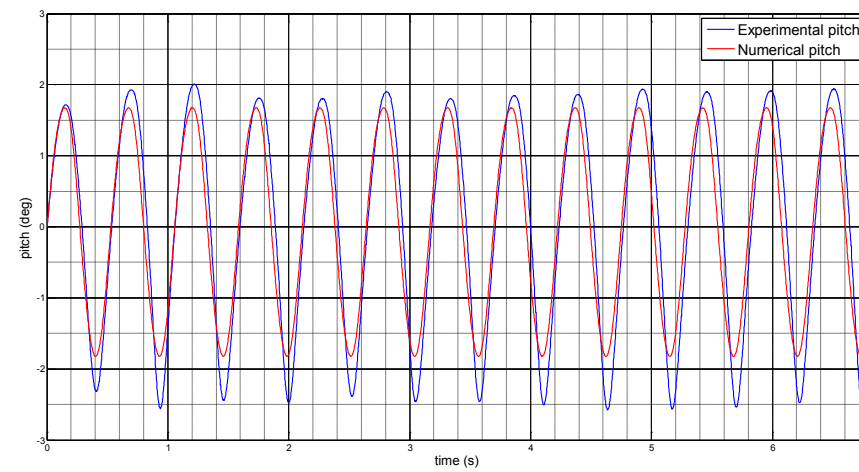


Figure 3.31. Numerical vs. experimental pitch, $v=4.6$ m/s and $f=0.65$ Hz

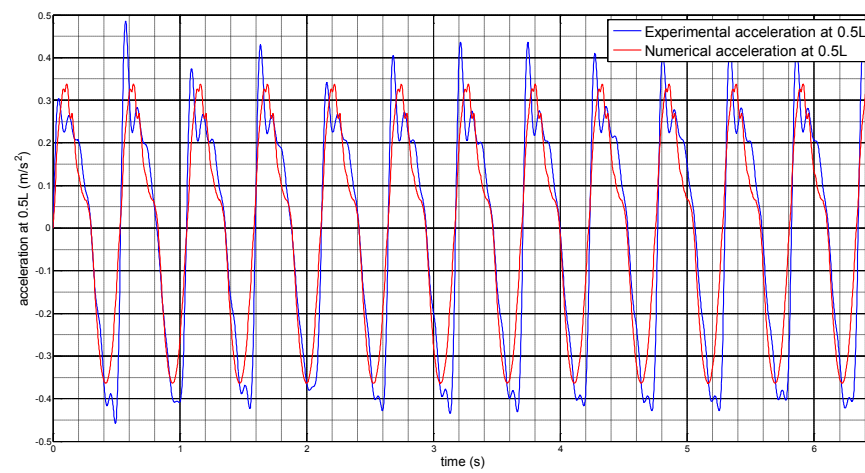


Figure 3.32. Numerical vs. experimental acceleration at CG, $v=4.6$ m/s and $f=0.65$ Hz

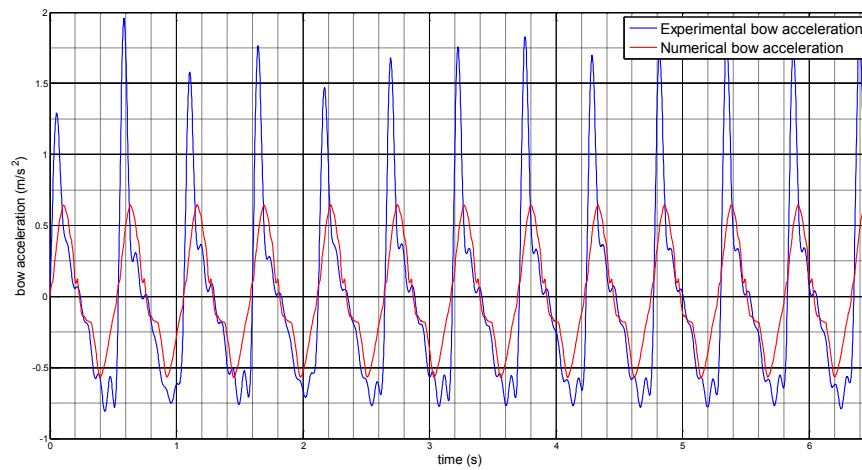


Figure 3.33. Numerical vs. experimental acceleration at bow, $v=4.6 \text{ m/s}$ and $f=0.65 \text{ Hz}$

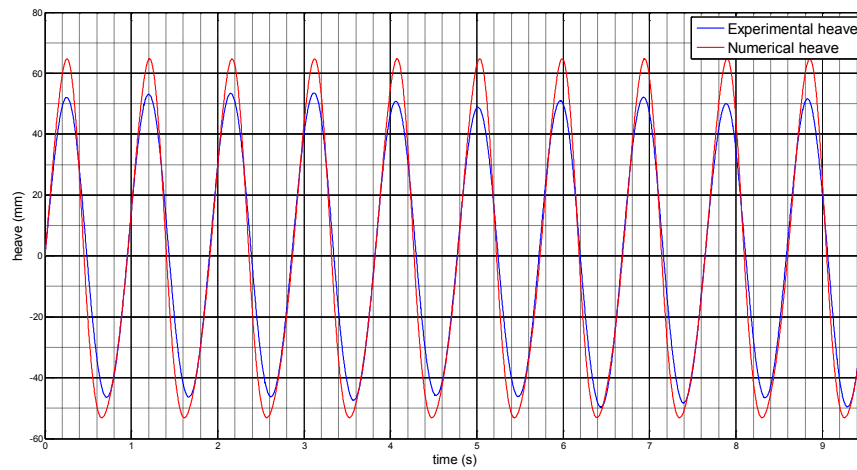


Figure 3.34. Numerical vs. experimental heave, $v=4.6 \text{ m/s}$ and $f=0.45 \text{ Hz}$

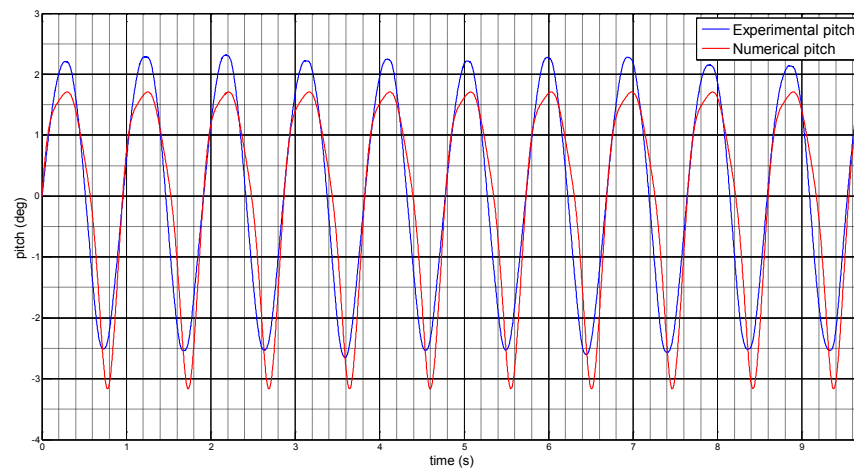


Figure 3.35. Numerical vs. experimental pitch, $v=4.6 \text{ m/s}$ and $f=0.45 \text{ Hz}$

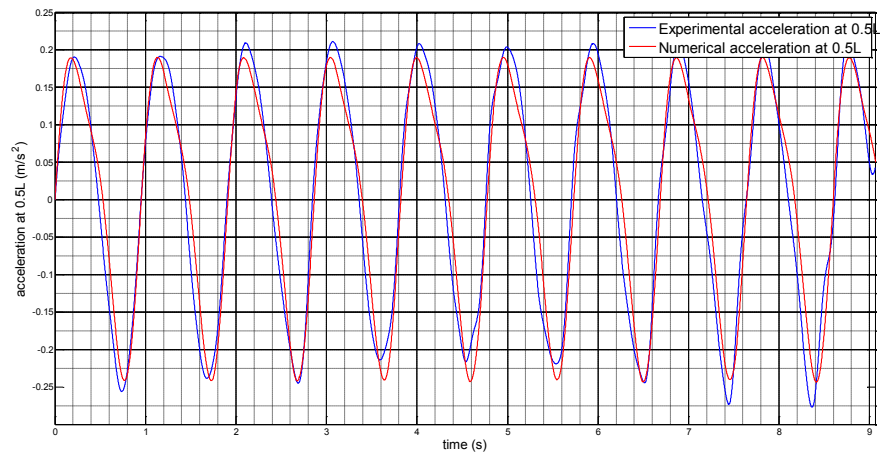


Figure 3.36. Numerical vs. experimental acceleration at CG, $v=4.6$ m/s and $f=0.45$ Hz

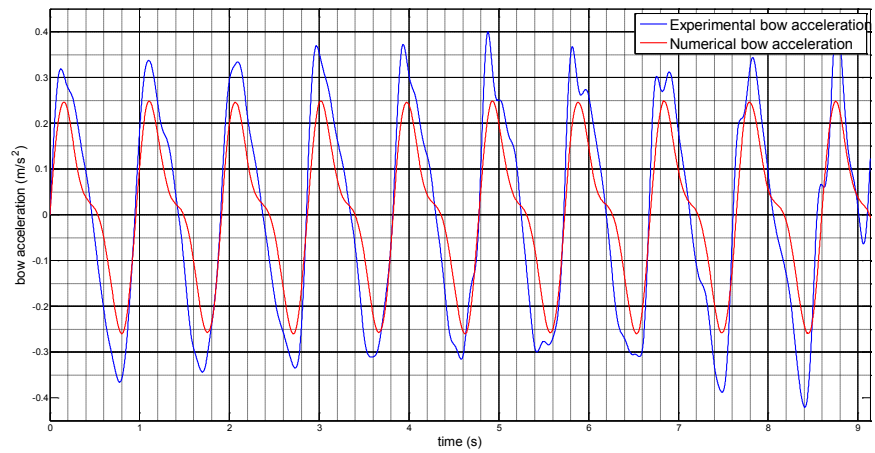


Figure 3.37. Numerical vs. experimental acceleration at bow, $v=4.6$ m/s and $f=0.45$ Hz

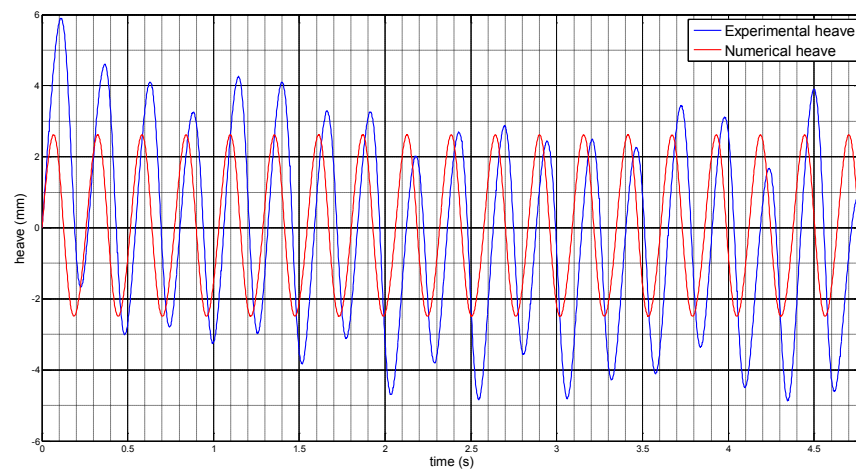


Figure 3.38. Numerical vs. experimental heave, $v=5.75$ m/s and $f=0.9$ Hz

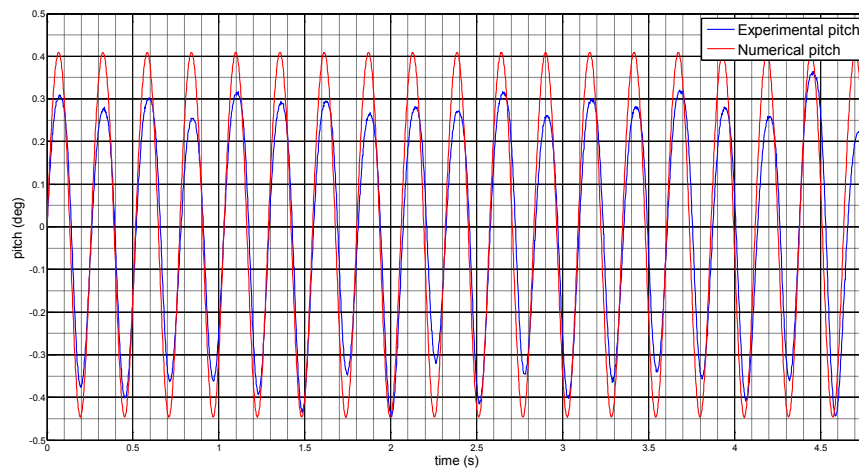


Figure 3.39. Numerical vs. experimental pitch, $v=5.75$ m/s and $f=0.9$ Hz

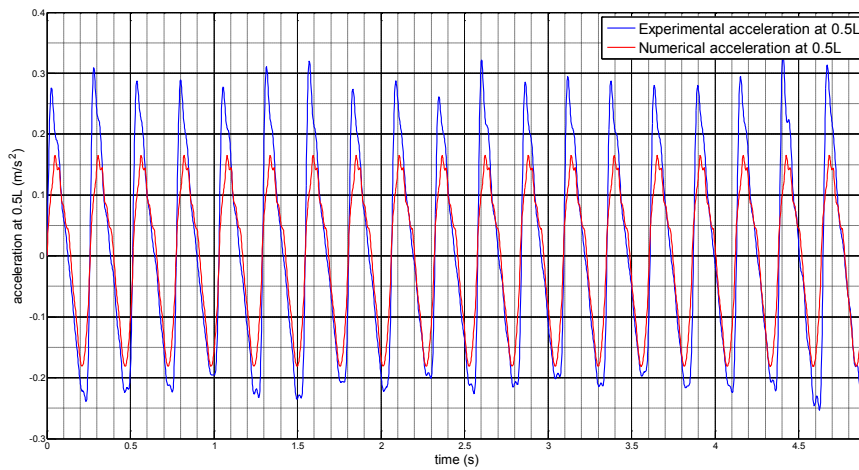


Figure 3.40. Numerical vs. experimental acceleration at CG, $v=5.75$ m/s and $f=0.9$ Hz

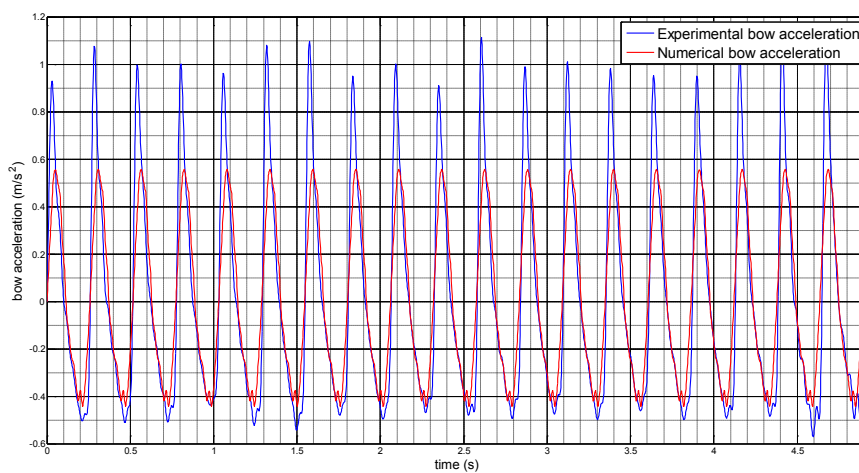


Figure 3.41. Numerical vs. experimental acceleration at bow, $v=5.75$ m/s and $f=0.9$ Hz

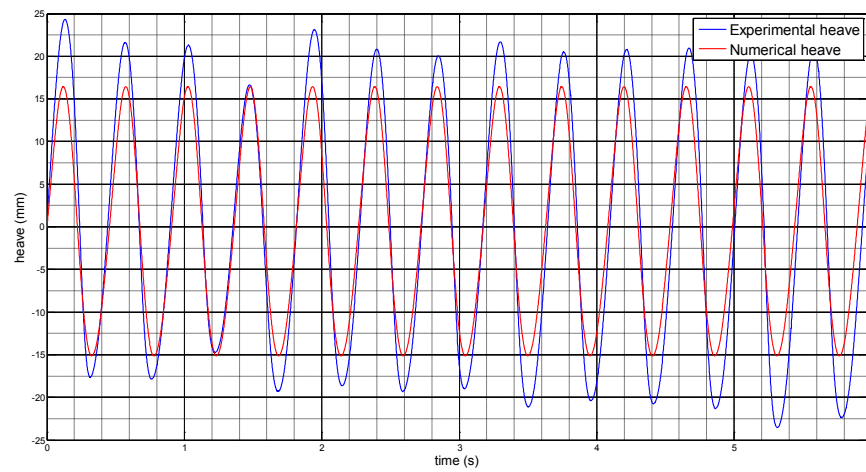


Figure 3.42. Numerical vs. experimental heave, $v=5.75$ m/s and $f=0.65$ Hz

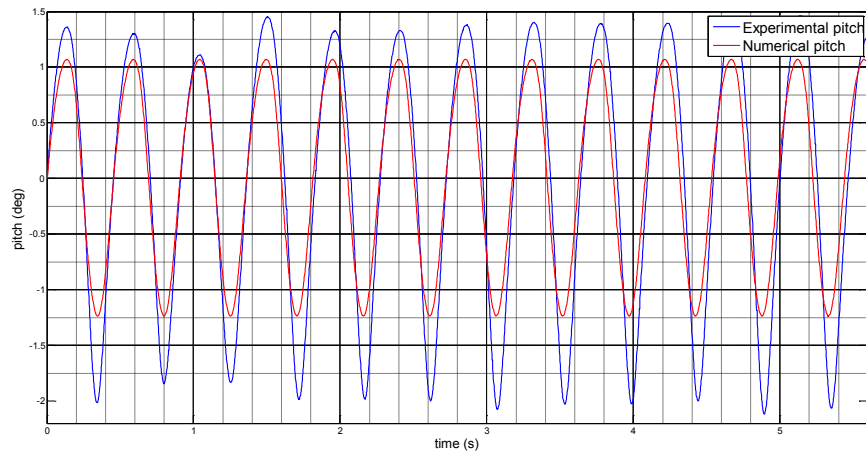


Figure 3.43. Numerical vs. experimental pitch, $v=5.75$ m/s and $f=0.65$ Hz

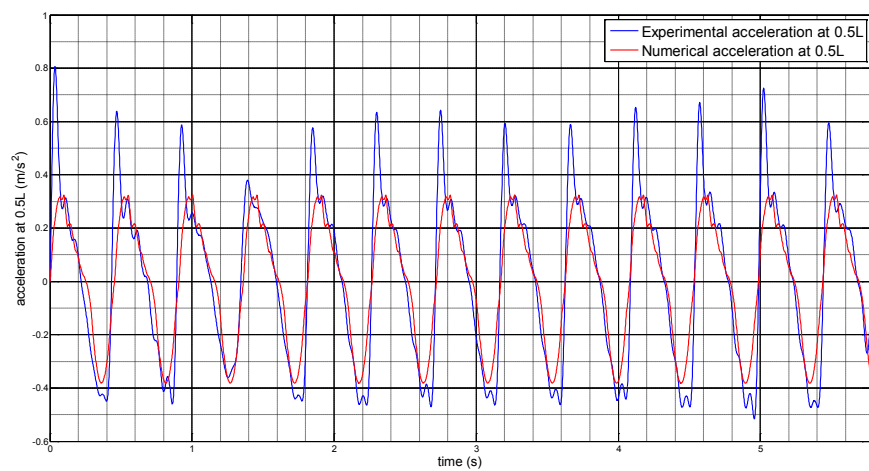


Figure 3.44. Numerical vs. experimental acceleration at CG, $v=5.75$ m/s and $f=0.65$ Hz

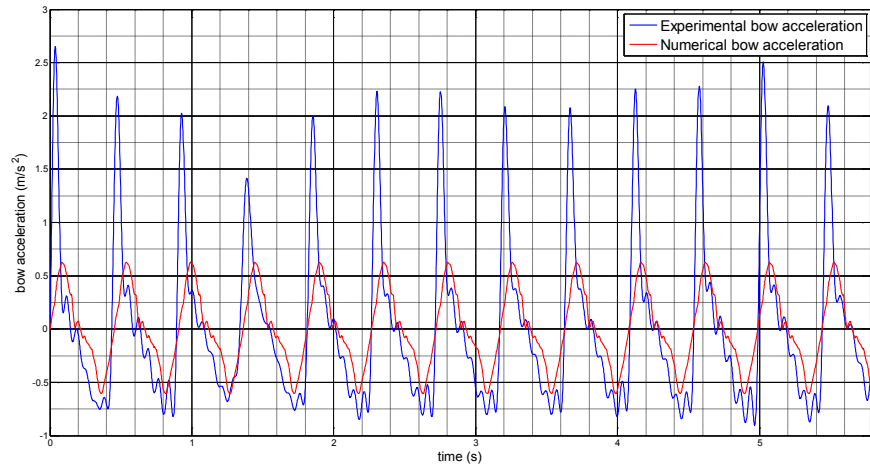


Figure 3.45. Numerical vs. experimental acceleration at bow, $v=5.75$ m/s and $f=0.65$ Hz

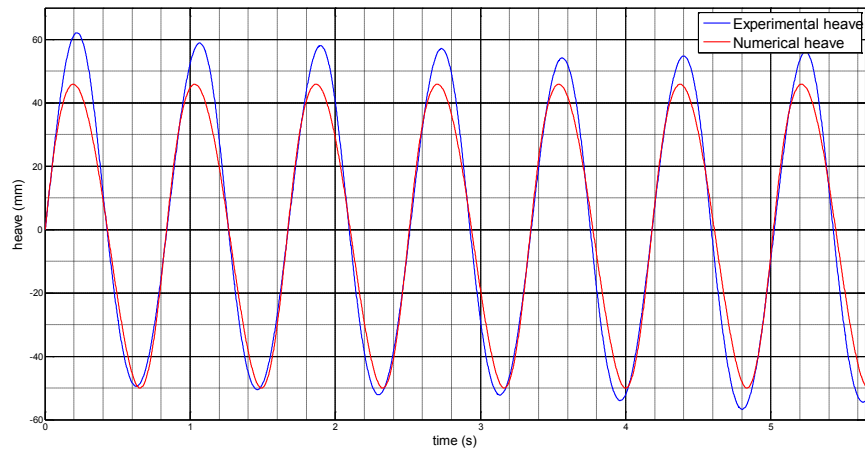


Figure 3.46. Numerical vs. experimental heave, $v=5.75$ m/s and $f=0.45$ Hz

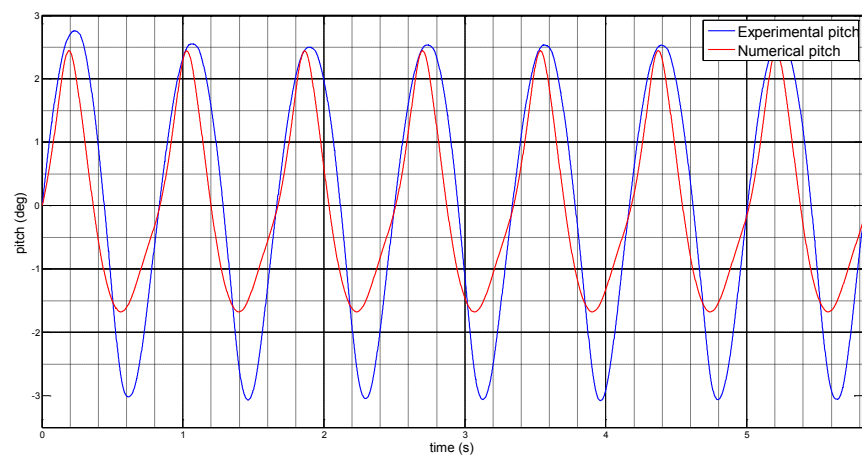


Figure 3.47. Numerical vs. experimental pitch, $v=5.75$ m/s and $f=0.45$ Hz

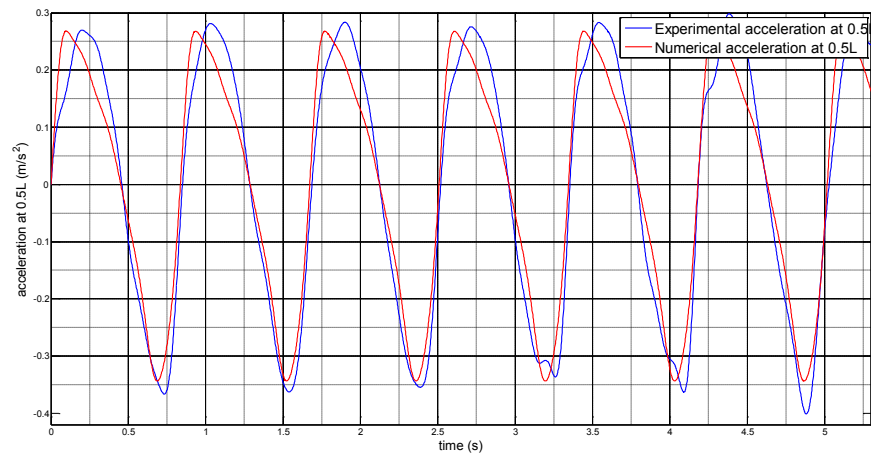


Figure 3.48. Numerical vs. experimental acceleration at CG, $v=5.75$ m/s and $f=0.45$ Hz

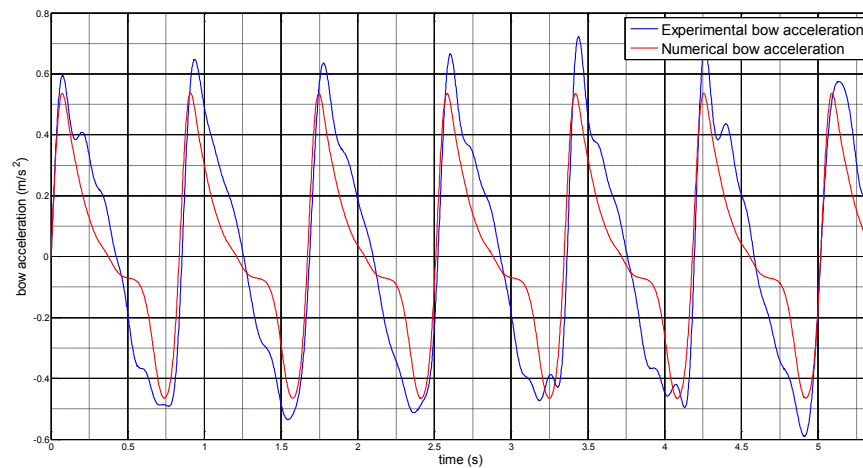


Figure 3.49. Numerical vs. experimental acceleration at bow, $v=5.75$ m/s and $f=0.45$ Hz

It has to be noted that pitch curve presents different shape of crests and troughs, indicating nonlinear form. Furthermore, it is evident, even at first sight, that accelerations, both at CG and at bow, are composed from a few harmonic components. Before any further data analysis, FFT has been performed, and it was shown that very small second order harmonic in heave and small second order harmonic in pitch will result in very pronounced higher order harmonics in accelerations, as can be observed in Figure 3.50, Figure 3.51 and Figure 3.52.

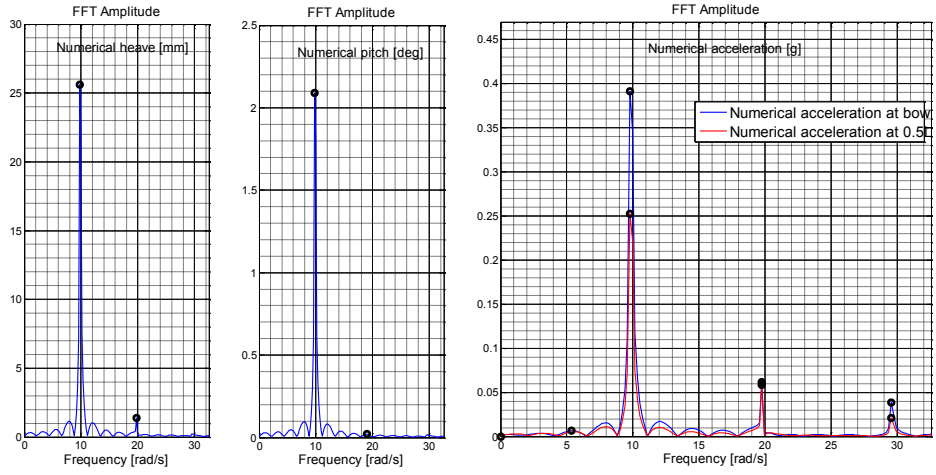


Figure 3.50. FFT of heave, pitch and accelerations at $v=3.4\text{m/s}$, $f = 0.65\text{Hz}$

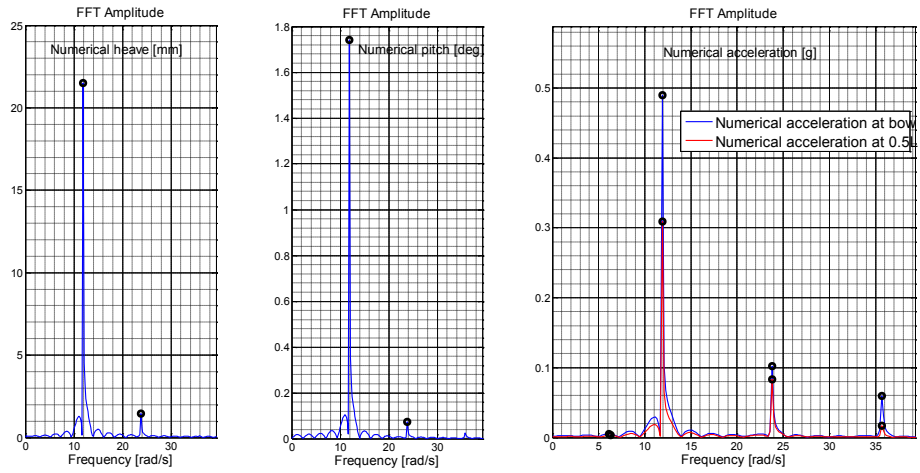


Figure 3.51. FFT of heave, pitch and accelerations at $v=4.6\text{m/s}$, $f = 0.65\text{Hz}$

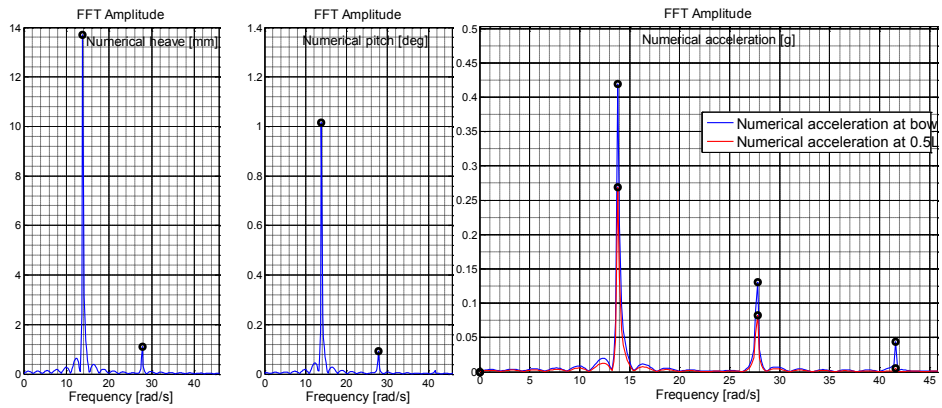


Figure 3.52. FFT of heave, pitch and accelerations at $v=5.75\text{m/s}$, $f = 0.65\text{Hz}$

The Figure 3.53 and Figure 3.54 summarize the results obtained for three speeds at three wave's frequencies for heave and pitch for both models.

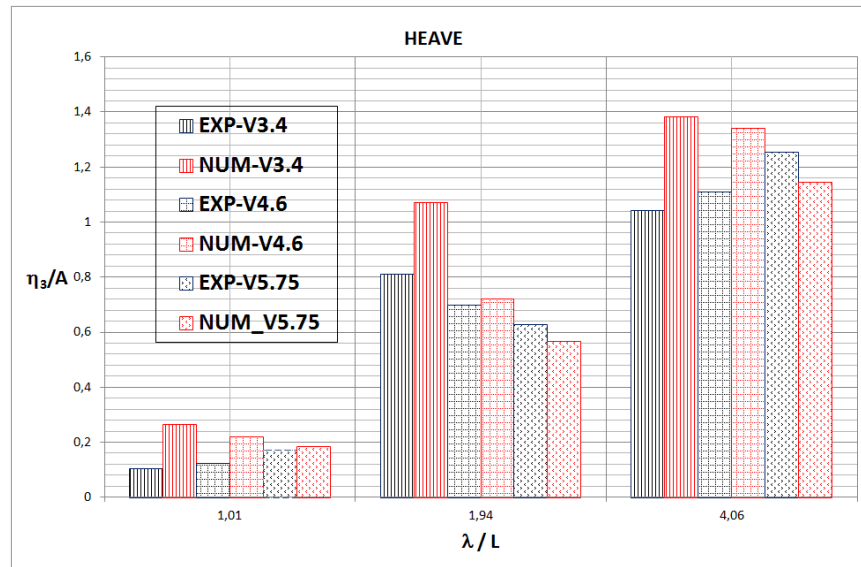


Figure 3.53. Numerical vs. experimental heave, 1st model

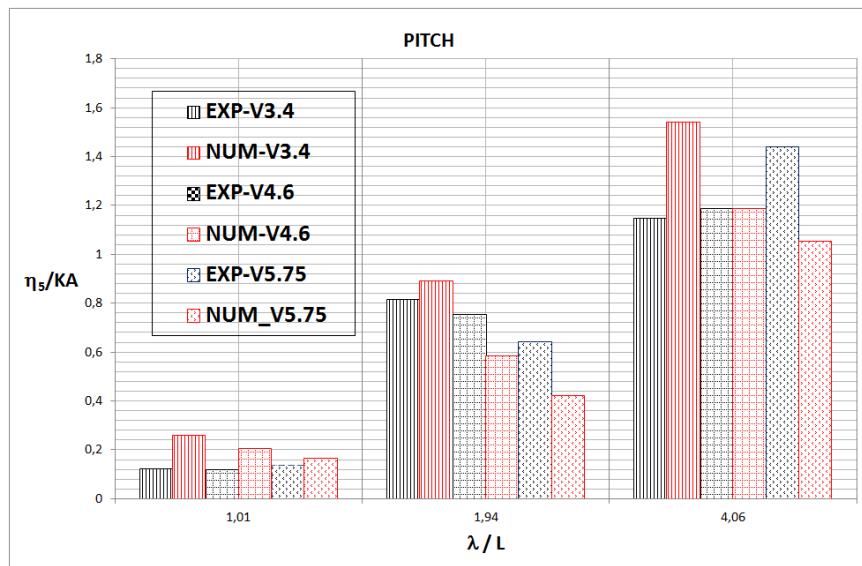


Figure 3.54. Numerical vs. experimental pitch, 1st model

From the comparisons with experimental data it was possible to observe that heave motion is generally well predicted for the two higher speeds. Heave prediction is in the worst case within 20%, except for short wave at speed of 4.6 m/s. At the lowest speed, heave is always overestimated, difference is about 20% at intermediate frequencies ($\lambda/L \sim 2$), higher for shorter wave ($\lambda/L < 2$) and longer wave ($\lambda/L \sim 4$). The same trend, at the lowest speed, is observed for pitch, at longer waves is significantly overestimated, the differences between experimental and numerical values are within 35%. At model speed of 4.6 m/s, pitch is very fairly predicted but underestimated for all the wave with λ/L greater than 1.3. At the highest speed pitch is underestimated for almost all wave frequencies. The biggest difference between numerical and experimental is approximately 50%.

Once the motions are calculated in centre of gravity, for any other position vertical displacement can be obtained by the composition of the elementary motions. Furthermore having time series of experimental data, numerically obtained vertical motion is derived twice to obtain accelerations at LCG and at bow. As it was commented for Figure 3.50, Figure 3.51 and Figure 3.52, and previously analysed extensively in Begovic et al. (2014), accelerations, especially at bow have more harmonics in response and this is only due to a motions composition. To validate accelerations calculations, comparison of experimental and numerical values are reported for time series in Figure 3.16, Figure 3.17, Figure 3.20, Figure 3.21, Figure 3.24, Figure 3.25, Figure 3.28, Figure 3.29, Figure 3.32, Figure 3.33, Figure 3.36, Figure 3.37, Figure 3.40, Figure 3.41, Figure 3.44, Figure 3.45, Figure 3.48 and Figure 3.49. What can be noted that accelerations at LCG are reasonably well predicted for all speeds, only at the highest speed the differences in resonance region are of about 50%. As regard bow accelerations can be seen that as speed increases, the bow acceleration prediction underestimation increases. This is mainly due to the pitch underestimation at the highest speed, playing important role in motion composition. Comparison of all data at all tested wave frequencies and speeds is presented in Begovic et al. (2014), submitted to Applied Ocean Research.

Generally two trends can be observed: one regarding advancing speed and one regarding wave lengths. At lowest speed, predicted values are higher than experimental, medium speed are very well predicted and at the highest speed predicted values are lower than experimental. It is the same trend as for pitch.

As regard wave length, it can be seen from the values predicted for longer waves that the model can be considered representative only for λ/L up to approximately 3. This suggests to consider the different behaviour that a planing boat has when encountering waves of length very close or much longer than its length. In fact, when the waves are very long, the planing hull tends to ride over the wave profile and not to pass through as it happens with short waves. From a practical point of view the most interesting are the lower λ/L ratios. In fact to deal with planing boats means that small craft and high relative speed regime will practically limit operability to small sea states and maximum significant wave heights of about 2 meters and wave period of about 6 seconds, leading to wave length of approximately 60 meters and it is of about 3-4 times typical planing boat length.

Chapter 4

4. MATHEMATICAL MODEL ACCORDING TO HICKS ET AL.

4.1 Introduction

The numerical code developed on the basis of mathematical model described in Chapter 3, is robust and fast; it is accurate especially in the prediction of heave and acceleration at CG. Assumptions of small trim angle and horizontal velocity identical to forward speed lead to great simplification of mathematical model but pitch prediction is not always satisfying, especially at very high speed and longer waves. In addition, developed code gives very good results for monohedral hull, but not for innovative warped hull where in particular pitch motion has been significantly underestimated. Reasons why obtained numerical results for warped hull are so different from experimental have been attributed to mathematical model assumptions. To improve the numerical results for warped hull forms mathematical model has been reviewed from the beginning.

4.2 Fully nonlinear mathematical model for planing hulls

Starting from analysis of forces acting on a planing hull as defined by Zarnick, Keuning, Hicks, Van Deyzen, etc, the second mathematical model has been

formulated. Following the work of Hicks, where fully non-linear formulation has been established, two assumptions: small pitch angle and horizontal velocity equal to advancing speed, have been removed. Furthermore since Zarnick and Martin works, vertical force is composed by hydrodynamic force and cross flow drag force. As van Deyzen (2008) noted, the cross flow drag is of minor order of magnitude with respect to the other forces and after first mathematical model results, it was considered that cross flow drag can be neglected in force equilibrium.

The hydrodynamic force formulation is evaluated according to 3.2.4 without approximation in the expression of V and considering U as a function of the coordinate ξ and time, considering all its component (Figure 4.1).

$$\frac{D}{Dt}(m_A(\xi,t) \cdot V(\xi,t)) = \dot{m}_A(\xi,t) \cdot V(\xi,t) + m_A(\xi,t) \cdot \dot{V}(\xi,t) - U(\xi,t) \frac{\partial(m_A(\xi,t) \cdot V(\xi,t))}{\partial t}$$

where U is the relative velocity in plane of the cross section parallel to the baseline.

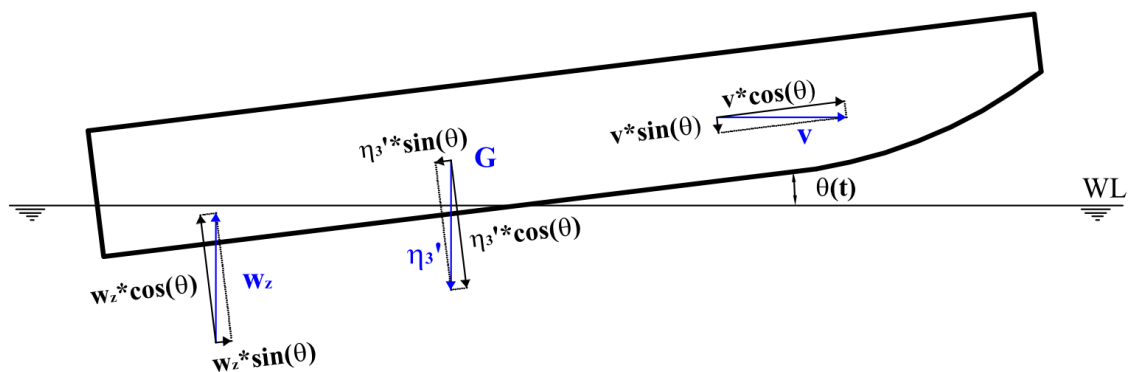


Figure 4.1. Velocity components

The velocity components as shown in Figure 4.1 in the body coordinate system along the hull can be represented as functions for the craft's forward speed, pitch,

heave and wave orbital velocities. The horizontal component of the wave orbital velocity is small when compared to the steady forward speed v , and is therefore neglected. The velocity expressions are:

$$U(\xi, t) = \dot{\eta}_1 \cos \theta - (\dot{\eta}_3 - w_z) \sin \theta$$

$$V(\xi, t) = \dot{\eta}_1 \sin \theta + (\dot{\eta}_3 - w_z) \cos \theta - \dot{\eta}_5 \cdot \xi$$

$$\begin{aligned} \dot{V}(\xi, t) = & \ddot{\eta}_1 \sin \theta - \ddot{\eta}_5 \cdot \xi + (\ddot{\eta}_3 - \dot{w}_z) \cos \theta \\ & + (\dot{\eta}_1 \cdot \cos \theta - \dot{\eta}_3 \cdot \sin \theta + w_z \cdot \sin \theta) \dot{\eta}_5 \end{aligned}$$

There is no surge, so the η_1 is a stationary component due to the advanced velocity and to the keel inclination angle with respect to the horizontal.

With: $\dot{\eta}_1 = const = v$ and $\ddot{\eta}_1 = 0$, velocity components are:

$$U(\xi, t) = v \cos \theta - (\dot{\eta}_3 - w_z) \sin \theta$$

$$V(\xi, t) = v \sin \theta + (\dot{\eta}_3 - w_z) \cos \theta - \dot{\eta}_5 \cdot \xi$$

Applying $\frac{dw_z}{dt} = \dot{w}_z - U \frac{\partial w_z}{\partial \xi}$ we have:

$$\begin{aligned} \dot{V}(\xi, t) = & -\ddot{\eta}_5 \cdot \xi + \ddot{\eta}_3 \cos \theta - \dot{w}_z \cos \theta + U \frac{\partial w_z}{\partial \xi} \cos \theta \\ & + (v \cdot \cos \theta - \dot{\eta}_3 \cdot \sin \theta + w_z \cdot \sin \theta) \dot{\eta}_5 \end{aligned}$$

The more rigorous mathematical treatment involves the presence in the final equations of equilibrium of some terms of the second order (B_{33_2nd} , A_{35_2nd} , B_{53_2nd} , A_{53_2nd}) and also involves significant changes in the expression of factors included in the final equations, an example is shown in Table 4 (B_{33}).

Exciting forces are obtained by assuming that the wave excitation is caused both by the geometrical properties of the wave, altering the wetted length and draft of the craft, and by the vertical component of the wave orbital velocity at the surface w_z , altering the normal velocity V . The diffraction forces are assumed zero as the amplitude of the diffracted waves is proportional to the hull volume, which is, in

case of planing, small and therefore also the damping forces, related to the diffraction of wave, are negligible compared to the other forces.

The buoyancy force on a segment is assumed to act vertically and to be equal to the equivalent static buoyancy of the section multiplied with a correction factor a_{bf} :

$$f_{HS} = a_{bf} \cdot \rho \cdot g \cdot A$$

The full amount of static buoyancy is never realized, because at the high speeds under consideration the flow separates from the chines and the stern, reducing the pressures at these locations to the atmospheric pressure. Therefore the total pressure distribution deviates considerably from the hydrostatic pressure distribution when applying Archimedes Law and the coefficient a_{bf} has a value between 0 and 1. When the moment of this force is determined another correction factor, namely a_{bm} , is used.

Originally, Zarnick used constant values for C_m , a_{bf} and a_{bm} . He assumed that the added mass coefficient C_m was equal to 1 and that the buoyancy correction a_{bf} was equal to 1/2 and that a_{bm} , the correction for the longitudinal distribution of the hydrostatic force, was equal to 1/2 a_{bf} . He used a pile-up factor independent of deadrise, equal to $\pi/2$. Keuning showed that Zarnick's method is only applicable to very high speeds, because of the constant values he used for the hydromechanics coefficients. Keuning, together with Kant (1989), approximated the trim angle and sinkage of the craft under consideration using polynomial expressions derived from the results of systematic model tests, the Delft Systematic Deadrise Series (DSDS) (1982, 1993). The solution of the equations of motion, describing the steady state planing in calm water, is known, because of these polynomial expressions. Substituting these values for sinkage and trim in the equations of motion results in a system of two equations and three unknowns. Keuning and Kant assumed that there is no additional factor for the correction of the longitudinal distribution of the hydrostatic lift and therefore a_{bm} is equal to 1. Subsequently the values of C_m and a_{bf} are determined. Van Deyzen reported that

determining the hydromechanics coefficients in this way, the hydrodynamic lift is brought into the computational model with a higher level of accuracy than in the original Zarnick model.

In both mathematical models, developed in this thesis, for the calculation of the added mass coefficient Payne's theory is applied. According to 3.2.6 the added mass coefficient is a function of the deadrise angle but also of the instantaneous immersion. In fact, as in the first mathematical model, two cases were distinguished: dry chine and wet chine. When the chine is dry, there is a superlevation of free surface and this is valid in both mathematical models. When the chine is wet in the first model the wetted height d_{eff} is considered as defined in 3.2.6. In the second model, when the chine is wet, the immersion d_n is equal to d_{eff} and they are equal to the chine height to consider the separation of the flow at the chine. Superlevation of free surface is considered only in ΔC_m – coefficient of incremental added mass.

To calculate the coefficients a_{bf} and a_{bm} a system of two equations in two unknowns considering the vertical force and moment equilibrium in calm water are solved.

Considering the expression of the hydrodynamic force, the last term takes into account the variation of the section added mass along the hull. This contribution can be visualized by considering the 2-D flow plane as a substantive surface moving past the body with velocity $U = -d\xi/dt$ tangent to the baseline. As the surface moves past the body, the section geometry in the moving surface may change with a resultant change in added mass. This term exists even in steady-state conditions and is the lift-producing factor in low-aspect ratio theory.

A planing vessel, sailing in calm water with a constant speed, is sailing in stationary condition. Sinkage and trim are constant in time. If only steady state planing is considered the following simplifications may be introduced in the equations:

$$\ddot{\eta}_1 = \ddot{\eta}_3 = \ddot{\eta}_5 = 0$$

$$U = v \cos \theta$$

$$V = v \sin \theta$$

$$F_{HD-HS} + W = 0$$

$$M_{HD-HS} = 0$$

where:

$$F_{HD-HS} = \int_{L(t)} U \cdot \frac{\partial(m_A \cdot V)}{\partial \xi} \cdot \cos \theta d\xi - \int_{L(t)} a_{bf} \cdot \rho \cdot g \cdot A d\xi$$

$$M_{HD-HS} = - \int_{L(t)} U \cdot \frac{\partial(m_A \cdot V)}{\partial \xi} \cdot \xi d\xi + \int_{L(t)} a_{bm} \cdot \rho \cdot g \cdot A \cdot \xi \cdot \cos \theta d\xi$$

Finally the main characteristics of two mathematical models are summarized in Table 4, where the differences are highlighted in coloured cells.

Table 4 – First and second mathematical model

First Model	Second Model
Hydrodynamic force associated with change of fluid momentum	Hydrodynamic force associated with change of fluid momentum
Shaft thrust and Drag are neglected	Shaft thrust and Drag are neglected
$F_{HS} = \int_{L(t)} \rho \cdot g \cdot A(\xi, t) d\xi$ $M_{HS} = \int_{L(t)} \rho \cdot g \cdot A(\xi, t) \cdot \xi \cdot \cos \theta d\xi$	$F_{HS} = \int_{L(t)} a_{bf} \cdot \rho \cdot g \cdot A(\xi, t) d\xi$ $M_{HS} = \int_{L(t)} a_{bm} \cdot \rho \cdot g \cdot A(\xi, t) \cdot \xi \cdot \cos \theta d\xi$

<p>Exciting forces:</p> <ul style="list-style-type: none"> • Diffraction force is neglected • no Froude-Krylov in horizontal direction • only Froude-Krylov force in vertical direction 	<p>Exciting forces:</p> <ul style="list-style-type: none"> • Diffraction force is neglected • no Froude-Krylov in horizontal direction • only Froude-Krylov force in vertical direction
<p>The sectional Froude Krilov force:</p> <ul style="list-style-type: none"> • calculated as the integral on the wetted perimeter of the dynamic component of pressure 	<p>Wave excitation is caused by:</p> <ul style="list-style-type: none"> ❖ changes in the underwater hull geometry ❖ vertical orbital velocity
<ul style="list-style-type: none"> • U is approximated to the advance velocity v • small angles assumption → no second order terms 	<ul style="list-style-type: none"> • U is NOT approximated to the advance velocity v • NO small angles assumption → second order terms
$B_{33} = B_{33}^{II} - B_{33}^{III}$ $= \int_{L(t)} \dot{m}_A \cdot \cos \theta d\xi - v \cdot \cos \theta (m_{Ab} - m_{As})$	$B_{33} = B_{33}^I + B_{33}^{II} - B_{33}^{III} =$ $- \cos^2 \theta \cdot \sin \theta \cdot (m_{Ab} w_{Zb} - m_{As} w_{Zs})$ $+ \int_{L(t)} \dot{m}_A \cdot w_Z \cdot \cos^2 \theta \cdot \sin \theta d\xi$ $+ \int_{L(t)} \dot{m}_A \cdot \cos^2 \theta d\xi - v \cdot \cos^3 \theta \cdot (m_{Ab} - m_{As})$ $+ \cos \theta \cdot \sin \theta \cdot (m_{Ab} \cdot (v \sin \theta - w_{Zb} \cos \theta)$ $- m_{As} \cdot (v \sin \theta - w_{Zs} \cos \theta))$ $- \int_{L(t)} \dot{m}_A \cdot w_Z \cos^2 \theta \cdot \sin \theta d\xi$

4.3 Motions equations

Planing hull is advancing with constant speed v . Reference systems are the same as defined in Figure 3.1 and vertical force equilibrium is identical to those in Figure 3.2.

If the motions of the craft are restricted to pitch, heave and surge the equation of motions, according to the classical Newton laws, can be written as:

$$\begin{cases} m \cdot \ddot{\eta}_1 = \sum F_x(t) \\ m \cdot \ddot{\eta}_3 = \sum F_z(t) \\ I_{55} \cdot \ddot{\eta}_5 = \sum M_y(t) \end{cases}$$

$$m \cdot \ddot{\eta}_1 = T_x - F_{HD} \sin \theta - D_f \cos \theta$$

$$m \cdot \ddot{\eta}_3 = T_z - F_{HD} \cos \theta + D_f \sin \theta + W - F_{HS}$$

$$I_{55} \cdot \ddot{\eta}_5 = F_{HD} \cdot x_C + F_{HS} \cdot x_{HS} - D_f \cdot x_D + T \cdot x_P$$

where:

- m : boat mass;
- I_{55} : mass moment of with respect to y axis;
- θ : pitch angle;
- F_{HD} : hydrodynamic force;
- F_{HS} : hydrostatic force;
- D_f : friction drag force;
- W : weight of boat;
- T_x : thrust component in x direction, $T_x = T \cos(\theta + \alpha)$;
- T_z : thrust component in z direction, $T_z = -T \sin(\theta + \alpha)$;
- α : propeller shaft angle;
- x_C : distance from centre of gravity (CG) to centre of pressure for normal force;
- x_D : is distance from CG to centre of action for friction drag force;

- x_{HS} : distance from centre of gravity (CG) to centre of resultant hydrostatic force;
- x_p : moment arm of thrust about CG.

Assuming that the perturbation velocities in the forward direction are small in comparison to the speed of the craft, the equations of motion may be further simplified by neglecting the perturbations and setting the forward velocity equal to a constant.

$$\dot{\eta}_1 = const; \ddot{\eta}_1 = 0$$

If it is also assumed that shaft thrust and drag are neglected, as assumed constant over time and thus in stationary equilibrium, the equations of motion may be written as:

$$m \cdot \ddot{\eta}_3 = -F_{HD} \cos \theta - F_{HS} + W$$

$$I_{55} \cdot \ddot{\eta}_5 = F_{HD} \cdot x_C + F_{HS} \cdot x_{HS}$$

Calculation of forces equilibrium is based on linearity assumption of superposition of linear effects, i.e. each force is independent and calculated separately. The mathematical model is implemented using the ‘‘Strip Theory concept’’, considering the hull as made of 2D ‘strips’, and evaluating the total 3D forces as the resultants of sectional forces which act separately on each section without interactions.

4.3.1 Force equilibrium in coordinate system Gxyz

In Gxyz reference system vertical component of dynamic hydrodynamic force $F_{Z_{HD}}$ is given by:

$$\begin{aligned}
F_{Z-HD} = F_{HD} \cdot \cos \theta = & \int_{L(t)} m_A(\xi, t) \cdot \dot{V}(\xi, t) \cdot \cos \theta(t) d\xi \\
& + \int_{L(t)} \dot{m}_A(\xi, t) \cdot V(\xi, t) \cdot \cos \theta(t) d\xi \\
& - \int_{L(t)} U(\xi, t) \cdot \frac{\partial(m_A(\xi, t) \cdot V(\xi, t))}{\partial \xi} \cdot \cos \theta(t) d\xi
\end{aligned}$$

It can be written $F_{Z-HD} = F_{Z-HD}^I + F_{Z-HD}^{II} - F_{Z-HD}^{III}$, with following definitions:

$$F_{Z-HD}^I = \int_{L(t)} m_A(\xi, t) \cdot \dot{V}(\xi, t) \cdot \cos \theta(t) d\xi$$

$$F_{Z-HD}^{II} = \int_{L(t)} \dot{m}_A(\xi, t) \cdot V(\xi, t) \cdot \cos \theta(t) d\xi$$

$$F_{Z-HD}^{III} = \int_{L(t)} U(\xi, t) \cdot \frac{\partial(m_A(\xi, t) \cdot V(\xi, t))}{\partial \xi} \cdot \cos \theta(t) d\xi$$

Developing one by one component of hydrodynamic force we have:

$$\begin{aligned}
F_{Z-HD}^I = & \int_{L(t)} m_A \cdot \cos \theta \cdot \dot{V} d\xi = \\
& - \int_{L(t)} m_A \cdot \dot{\eta}_5 \cdot \xi \cdot \cos \theta d\xi + \int_{L(t)} m_A \cdot \dot{\eta}_3 \cdot \cos^2 \theta d\xi \\
& - \int_{L(t)} m_A \cdot \dot{w}_Z \cdot \cos^2 \theta d\xi + \int_{L(t)} m_A \cdot U \cdot \frac{\partial w_Z}{\partial \xi} \cdot \cos^2 \theta d\xi + v \int_{L(t)} m_A \cdot \dot{\eta}_5 \cdot \cos^2 \theta d\xi \\
& - \int_{L(t)} m_A \cdot \dot{\eta}_3 \cdot \dot{\eta}_5 \cdot \cos \theta \cdot \sin \theta d\xi + \int_{L(t)} m_A \cdot \dot{\eta}_5 \cdot w_Z \cdot \cos \theta \cdot \sin \theta d\xi
\end{aligned}$$

Developing further we have:

$$\begin{aligned}
\int_{L(t)} m_A \cdot U \cdot \frac{\partial w_Z}{\partial \xi} \cdot \cos^2 \theta d\xi = & \int_{L(t)} v \cdot m_A \cdot \frac{\partial w_Z}{\partial \xi} \cdot \cos^3 \theta d\xi \\
& - \int_{L(t)} m_A \cdot \dot{\eta}_3 \cdot \frac{\partial w_Z}{\partial \xi} \cdot \cos^2 \theta \cdot \sin \theta d\xi \\
& + \int_{L(t)} m_A \cdot w_Z \cdot \frac{\partial w_Z}{\partial \xi} \cdot \cos^2 \theta \cdot \sin \theta d\xi
\end{aligned}$$

$$\begin{aligned}
F_{Z-HD}^I &= \int_{L(t)} m_A \cdot \ddot{\eta}_3 \cdot \cos^2 \theta \, d\xi - \int_{L(t)} m_A \cdot \ddot{\eta}_5 \cdot \xi \cdot \cos \theta \, d\xi \\
&\quad - \int_{L(t)} m_A \cdot \dot{\eta}_3 \cdot \dot{\eta}_5 \cdot \cos \theta \cdot \sin \theta \, d\xi - \int_{L(t)} m_A \cdot \dot{\eta}_3 \cdot \frac{\partial w_Z}{\partial \xi} \cdot \cos^2 \theta \cdot \sin \theta \, d\xi \\
&\quad + v \int_{L(t)} m_A \cdot \dot{\eta}_5 \cdot \cos^2 \theta \, d\xi + \int_{L(t)} m_A \cdot \dot{\eta}_5 \cdot w_Z \cdot \cos \theta \cdot \sin \theta \, d\xi \\
&\quad - \int_{L(t)} m_A \cdot \dot{w}_Z \cdot \cos^2 \theta \, d\xi + \int_{L(t)} v \cdot m_A \cdot \frac{\partial w_Z}{\partial \xi} \cdot \cos^3 \theta \, d\xi \\
&\quad + \int_{L(t)} m_A \cdot w_Z \cdot \frac{\partial w_Z}{\partial \xi} \cdot \cos^2 \theta \cdot \sin \theta \, d\xi
\end{aligned}$$

It can written:

$$A_{33}^I = \int_{L(t)} m_A \cdot \cos^2 \theta \, d\xi$$

$$A_{35}^I = - \int_{L(t)} m_A \cdot \xi \cdot \cos \theta \, d\xi$$

$$\begin{aligned}
B_{33}^I &= - \int_{L(t)} m_A \cdot \frac{\partial w_Z}{\partial \xi} \cdot \cos^2 \theta \cdot \sin \theta \, d\xi = \\
&\quad - \cos^2 \theta \cdot \sin \theta \cdot (m_{Ab} w_{Zb} - m_{As} w_{Zs}) + \int_{L(t)} \dot{m}_A \cdot w_Z \cdot \cos^2 \theta \cdot \sin \theta \, d\xi
\end{aligned}$$

$$B_{35}^I = v \int_{L(t)} m_A \cdot \cos^2 \theta \, d\xi + \int_{L(t)} m_A \cdot w_Z \cdot \cos \theta \cdot \sin \theta \, d\xi$$

$$A_{35-2nd}^I = - \int_{L(t)} m_A \cdot \cos \theta \cdot \sin \theta \, d\xi$$

$$\begin{aligned}
F_{W3}^I &= - \int_{L(t)} m_A \cdot \dot{w}_Z \cdot \cos^2 \theta \, d\xi + \int_{L(t)} v \cdot m_A \cdot \frac{\partial w_Z}{\partial \xi} \cdot \cos^3 \theta \, d\xi \\
&\quad + \int_{L(t)} m_A \cdot w_Z \cdot \frac{\partial w_Z}{\partial \xi} \cdot \cos^2 \theta \cdot \sin \theta \, d\xi = \\
&\quad - \int_{L(t)} m_A \cdot \dot{w}_Z \cdot \cos^2 \theta \, d\xi \\
&\quad + v \cdot \cos^3 \theta \cdot (m_{Ab} w_{Zb} - m_{As} w_{Zs}) - \int_{L(t)} v \cdot \dot{m}_A \cdot w_Z \cdot \cos^3 \theta \, d\xi \\
&\quad + \frac{1}{2} \cos^2 \theta \cdot \sin \theta \cdot (m_{Ab} w_{Zb}^2 - m_{As} w_{Zs}^2) - \frac{1}{2} \int_{L(t)} \dot{m}_A \cdot w_Z^2 \cdot \cos^2 \theta \cdot \sin \theta \, d\xi
\end{aligned}$$

$$F_{Z-HD}^I = A_{33}^I \cdot \dot{\eta}_3 + A_{35}^I \cdot \dot{\eta}_5 + B_{33}^I \cdot \dot{\eta}_3 + B_{35}^I \cdot \dot{\eta}_5 + A_{35-2nd}^I \cdot \dot{\eta}_3 \cdot \dot{\eta}_5 + F_{W3}^I$$

$$\begin{aligned} F_{Z-HD}^{II} &= \int_{L(t)} \dot{m}_A \cdot V \cdot \cos \theta \, d\xi \\ &= \int_{L(t)} \dot{m}_A \cdot v \cdot \cos \theta \cdot \sin \theta \, d\xi + \int_{L(t)} \dot{m}_A \cdot \dot{\eta}_3 \cdot \cos^2 \theta \, d\xi - \int_{L(t)} \dot{m}_A \cdot w_Z \cdot \cos^2 \theta \, d\xi \\ &\quad - \int_{L(t)} \dot{m}_A \cdot \dot{\eta}_5 \cdot \xi \cdot \cos \theta \, d\xi \end{aligned}$$

$$B_{33}^{II} = \int_{L(t)} \dot{m}_A \cdot \cos^2 \theta \, d\xi$$

$$B_{35}^{II} = - \int_{L(t)} \dot{m}_A \cdot \xi \cdot \cos \theta \, d\xi$$

$$F_{W3}^{II} = \int_{L(t)} \dot{m}_A \cdot v \cdot \cos \theta \cdot \sin \theta \, d\xi - \int_{L(t)} \dot{m}_A \cdot w_Z \cdot \cos^2 \theta \, d\xi$$

$$F_{Z-HD}^{II} = B_{33}^{II} \cdot \dot{\eta}_3 + B_{35}^{II} \cdot \dot{\eta}_5 + F_{W3}^{II}$$

$$F_{Z-HD}^{III} = \int_{L(t)} U(\xi, t) \cdot \frac{\partial(m_A(\xi, t) \cdot V(\xi, t))}{\partial \xi} \cdot \cos \theta(t) \, d\xi$$

Substituting the expression for U we have:

$$\begin{aligned} F_{Z-HD}^{III} &= \int_{L(t)} v \cdot \frac{\partial(m_A \cdot V)}{\partial \xi} \cdot \cos^2 \theta \, d\xi - \int_{L(t)} \dot{\eta}_3 \cdot \frac{\partial(m_A \cdot V)}{\partial \xi} \cdot \cos \theta \cdot \sin \theta \, d\xi \\ &\quad + \int_{L(t)} w_Z \cdot \frac{\partial(m_A \cdot V)}{\partial \xi} \cdot \cos \theta \cdot \sin \theta \, d\xi \end{aligned}$$

It can be noted that

$$\int_{L(t)} w_Z \frac{\partial(m_A \cdot V)}{\partial \xi} \, d\xi = w_Z \cdot V \cdot m_A|_{stern}^{bow} - \int_{L(t)} m_A \cdot V \cdot \frac{\partial w_Z}{\partial \xi} \, d\xi$$

The meaning of "stern" (later denoted by s) and "bow" (later denoted by b) is the same specified in 3.3.1 (Figure 3.7).

Therefore F_{Z-HD}^{III} becomes:

$$\begin{aligned}
F_{Z-HD}^{III} = & v \cdot \cos^2 \theta \cdot [(m_A \cdot V)_{BOW} - (m_A \cdot V)_{STERN}] \\
& - \cos \theta \cdot \sin \theta \cdot [(m_A \cdot V)_{BOW} - (m_A \cdot V)_{STERN}] \cdot \dot{\eta}_3 \\
& + \left\{ \begin{aligned} & \cos \theta \cdot \sin \theta \cdot [(m_A \cdot V \cdot w_Z)_{BOW} - (m_A \cdot V \cdot w_Z)_{STERN}] \\ & - \int_{L(t)} m_A \cdot V \cdot \frac{\partial(w_Z)}{\partial \xi} \cdot \cos \theta \cdot \sin \theta d\xi \end{aligned} \right\}
\end{aligned}$$

Substituting the expressions for V it follows:

$$\begin{aligned}
F_{Z-HD}^{III} = & v \cdot \cos^2 \theta \cdot \left[\begin{aligned} & m_{Ab} \cdot (v \sin \theta + (\dot{\eta}_3 - w_Z) \cos \theta - \dot{\eta}_5 \cdot \xi)_B \\ & - m_{As} \cdot (v \sin \theta + (\dot{\eta}_3 - w_Z) \cos \theta - \dot{\eta}_5 \cdot \xi)_S \end{aligned} \right] \\
& - \cos \theta \cdot \sin \theta \cdot \left[\begin{aligned} & m_{Ab} \cdot (v \sin \theta + (\dot{\eta}_3 - w_Z) \cos \theta - \dot{\eta}_5 \cdot \xi)_B \\ & - m_{As} \cdot (v \sin \theta + (\dot{\eta}_3 - w_Z) \cos \theta - \dot{\eta}_5 \cdot \xi)_S \end{aligned} \right] \cdot \dot{\eta}_3 \\
& + \cos \theta \cdot \sin \theta \cdot [m_{Ab} \cdot (v \sin \theta + (\dot{\eta}_3 - w_Z) \cos \theta - \dot{\eta}_5 \cdot \xi)_B \cdot w_{Zb} \\
& \quad - m_{As} \cdot (v \sin \theta + (\dot{\eta}_3 - w_Z) \cos \theta - \dot{\eta}_5 \cdot \xi)_S \cdot w_{Zs}] \\
& - \int_{L(t)} m_A \cdot (v \sin \theta + (\dot{\eta}_3 - w_Z) \cos \theta - \dot{\eta}_5 \cdot \xi) \cdot \frac{\partial w_Z}{\partial \xi} \cdot \cos \theta \cdot \sin \theta d\xi
\end{aligned}$$

$$\begin{aligned}
F_{Z-HD}^{III} = & v \cdot \cos^2 \theta \cdot (m_{Ab} \cdot v \sin \theta - m_{As} \cdot v \sin \theta) \\
& + v \cdot \cos^2 \theta \cdot \dot{\eta}_3 \cos \theta \cdot (m_{Ab} - m_{As}) \\
& - v \cdot \cos^2 \theta \cdot \cos \theta \cdot (m_{Ab} \cdot w_{Zb} - m_{As} \cdot w_{Zs}) \\
& - v \cdot \cos^2 \theta \cdot \dot{\eta}_5 \cdot (m_{Ab} \xi_b - m_{As} \xi_s) \\
& - \cos \theta \cdot \sin \theta \cdot (m_{Ab} \cdot v \sin \theta - m_{As} \cdot v \sin \theta) \cdot \dot{\eta}_3 \\
& - \cos^2 \theta \cdot \sin \theta \cdot (m_{Ab} - m_{As}) \cdot \dot{\eta}_3^2 \\
& + \cos \theta \cdot \sin \theta \cdot \cos \theta \cdot (m_{Ab} \cdot w_{Zb} - m_{As} \cdot w_{Zs}) \cdot \dot{\eta}_3 \\
& + \cos \theta \cdot \sin \theta \cdot (m_{Ab} \xi_b - m_{As} \xi_s) \cdot \dot{\eta}_3 \cdot \dot{\eta}_5 \\
& + \cos \theta \cdot \sin \theta \cdot (m_{Ab} \cdot w_{Zb} \cdot v \sin \theta - m_{As} \cdot w_{Zs} v \sin \theta) \\
& + \cos \theta \cdot \sin \theta \cdot \dot{\eta}_3 \cdot \cos \theta (m_{Ab} \cdot w_{Zb} - m_{As} \cdot w_{Zs}) \\
& - \cos \theta \cdot \sin \theta \cdot \cos \theta (m_{Ab} w_{Zb}^2 - m_{As} w_{Zs}^2) \\
& - \cos \theta \cdot \sin \theta \cdot \dot{\eta}_5 \cdot (m_{Ab} \xi_b \cdot w_{Zb} - m_{As} \xi_s \cdot w_{Zs}) \\
& - \int_{L(t)} m_A \cdot v \sin \theta \cdot \frac{\partial(w_Z)}{\partial \xi} \cdot \cos \theta \cdot \sin \theta d\xi \\
& - \int_{L(t)} m_A \cdot \dot{\eta}_3 \cdot \cos \theta \cdot \frac{\partial(w_Z)}{\partial \xi} \cdot \cos \theta \cdot \sin \theta d\xi \\
& + \int_{L(t)} m_A \cdot w_Z \cos \theta \cdot \frac{\partial(w_Z)}{\partial \xi} \cdot \cos \theta \cdot \sin \theta d\xi \\
& + \int_{L(t)} m_A \cdot \dot{\eta}_5 \cdot \xi \cdot \frac{\partial(w_Z)}{\partial \xi} \cdot \cos \theta \cdot \sin \theta d\xi
\end{aligned}$$

$$\begin{aligned}
B_{33}^{III} &= v \cdot \cos^2 \theta \cdot \cos \theta \cdot (m_{Ab} - m_{As}) \\
&\quad - \cos \theta \cdot \sin \theta \cdot (m_{Ab} \cdot v \sin \theta - m_{As} \cdot v \sin \theta) \\
&\quad + \cos \theta \cdot \sin \theta \cdot \cos \theta \cdot (m_{Ab} w_{Zb} - m_{As} w_{Zs}) \\
&\quad + \cos \theta \cdot \sin \theta \cdot \cos \theta (m_{Ab} \cdot w_{Zb} - m_{As} \cdot w_{Zs}) \\
&\quad - \int_{L(t)} m_A \cdot \cos \theta \cdot \frac{\partial(w_Z)}{\partial \xi} \cdot \cos \theta \cdot \sin \theta d\xi
\end{aligned}$$

With:

$$\begin{aligned}
\int_{L(t)} m_A \cdot \cos \theta \cdot \frac{\partial(w_Z)}{\partial \xi} \cdot \cos \theta \cdot \sin \theta d\xi &= (m_{Ab} \cdot w_{Zb} - m_{As} \cdot w_{Zs}) \cdot \cos^2 \theta \cdot \sin \theta \\
&\quad - \int_{L(t)} \dot{m}_A \cdot w_Z \cdot \cos^2 \theta \cdot \sin \theta d\xi
\end{aligned}$$

$$\begin{aligned}
B_{33}^{III} &= v \cdot \cos^3 \theta \cdot (m_{Ab} - m_{As}) \\
&\quad - \cos \theta \cdot \sin \theta \cdot (m_{Ab} \cdot v \sin \theta - m_{As} \cdot v \sin \theta) \\
&\quad + \cos \theta \cdot \sin \theta \cdot \cos \theta \cdot (m_{Ab} \cdot w_{Zb} - m_{As} \cdot w_{Zs}) \\
&\quad + \cos \theta \cdot \sin \theta \cdot \cos \theta (m_{Ab} \cdot w_{Zb} - m_{As} \cdot w_{Zs}) \\
&\quad - \cos^2 \theta \cdot \sin \theta \cdot (m_{Ab} \cdot w_{Zb} - m_{As} \cdot w_{Zs}) + \int_{L(t)} \dot{m}_A \cdot w_Z \cos^2 \theta \cdot \sin \theta d\xi
\end{aligned}$$

Finally:

$$\begin{aligned}
B_{33}^{III} &= v \cdot \cos^3 \theta \cdot (m_{Ab} - m_{As}) \\
&\quad - \cos \theta \cdot \sin \theta \cdot (m_{Ab} \cdot (v \sin \theta - w_{Zb} \cos \theta) - m_{As} \cdot (v \sin \theta - w_{Zs} \cos \theta)) \\
&\quad + \int_{L(t)} \dot{m}_A \cdot w_Z \cos^2 \theta \cdot \sin \theta d\xi
\end{aligned}$$

$$\begin{aligned}
B_{35}^{III} &= -v \cdot \cos^2 \theta \cdot (m_{Ab} \xi_b - m_{As} \xi_s) \\
&\quad - \cos \theta \cdot \sin \theta \cdot (m_{Ab} \xi_b \cdot w_{Zb} - m_{As} \xi_s \cdot w_{Zs}) \\
&\quad + \int_{L(t)} m_A \cdot \xi \cdot \frac{\partial(w_Z)}{\partial \xi} \cdot \cos \theta \cdot \sin \theta d\xi
\end{aligned}$$

Considering:

$$\begin{aligned}
\int_{L(t)} m_A \cdot \xi \cdot \frac{\partial(w_Z)}{\partial \xi} \cdot \cos \theta \cdot \sin \theta d\xi &= \cos \theta \cdot \sin \theta \cdot (m_{Ab} \xi_b \cdot w_{Zb} - m_{As} \xi_s \cdot w_{Zs}) \\
&\quad - \int_{L(t)} \dot{m}_A \cdot w_Z \cdot \xi \cdot \cos \theta \cdot \sin \theta d\xi - \int_{L(t)} m_A \cdot w_Z \cdot \cos \theta \cdot \sin \theta d\xi
\end{aligned}$$

$$\begin{aligned}
B_{35}^{III} &= -v \cdot \cos^2 \theta \cdot (m_{Ab} \xi_b - m_{As} \xi_s) \\
&\quad - \cos \theta \cdot \sin \theta \cdot (m_{Ab} \xi_b \cdot w_{Zb} - m_{As} \xi_s \cdot w_{Zs}) \\
&\quad + \cos \theta \cdot \sin \theta \cdot (m_{Ab} \xi_b \cdot w_{Zb} - m_{As} \xi_s \cdot w_{Zs}) - \int_{L(t)} \dot{m}_A \cdot w_Z \cdot \xi \cdot \cos \theta \cdot \sin \theta d\xi \\
&\quad - \int_{L(t)} m_A \cdot w_Z \cdot \cos \theta \cdot \sin \theta d\xi \\
&= -v \cdot \cos^2 \theta \cdot (m_{Ab} \xi_b - m_{As} \xi_s) - \int_{L(t)} \dot{m}_A \cdot w_Z \cdot \xi \cdot \cos \theta \cdot \sin \theta d\xi \\
&\quad - \int_{L(t)} m_A \cdot w_Z \cdot \cos \theta \cdot \sin \theta d\xi
\end{aligned}$$

$$A_{35-2nd}^{III} = \cos \theta \cdot \sin \theta \cdot (m_{Ab} \xi_b - m_{As} \xi_s)$$

$$B_{33-2nd}^{III} = -\cos^2 \theta \cdot \sin \theta \cdot (m_{Ab} - m_{As})$$

$$\begin{aligned}
F_{W3}^{III} &= v \cdot \cos^2 \theta \cdot (m_{Ab} \cdot v \sin \theta - m_{As} \cdot v \sin \theta) \\
&\quad - v \cdot \cos^2 \theta \cdot \cos \theta \cdot (m_{Ab} \cdot w_{Zb} - m_{As} \cdot w_{Zs}) \\
&\quad + \cos \theta \cdot \sin \theta \cdot (m_{Ab} \cdot w_{Zb} \cdot v \sin \theta - m_{As} \cdot w_{Zs} v \sin \theta) \\
&\quad - \cos \theta \cdot \sin \theta \cdot \cos \theta (m_{Ab} w_{Zb}^2 - m_{As} w_{Zs}^2) \\
&\quad - \int_{L(t)} m_A \cdot v \sin \theta \cdot \frac{\partial(w_Z)}{\partial \xi} \cdot \cos \theta \cdot \sin \theta d\xi \\
&\quad + \int_{L(t)} m_A \cdot w_Z \cos \theta \cdot \frac{\partial(w_Z)}{\partial \xi} \cdot \cos \theta \cdot \sin \theta d\xi
\end{aligned}$$

$$\begin{aligned}
F_{W3}^{III} &= v \cdot \cos^2 \theta \cdot (m_{Ab} \cdot (v \sin \theta - w_{Zb} \cos \theta) - m_{As} \cdot (v \sin \theta - w_{Zs} \cos \theta)) \\
&\quad + \cos \theta \cdot \sin \theta \cdot (m_{Ab} \cdot w_{Zb} \cdot v \sin \theta - m_{As} \cdot w_{Zs} v \sin \theta) \\
&\quad - \cos^2 \theta \cdot \sin \theta (m_{Ab} w_{Zb}^2 - m_{As} w_{Zs}^2) \\
&\quad - v \sin^2 \theta \cdot \cos \theta \cdot (m_{Ab} \cdot w_{Zb} - m_{As} \cdot w_{Zs}) + \int_{L(t)} \dot{m}_A \cdot w_Z \cdot v \sin^2 \theta \cdot \cos \theta d\xi \\
&\quad + \frac{1}{2} \cos^2 \theta \cdot \sin \theta (m_{Ab} w_{Zb}^2 - m_{As} w_{Zs}^2) - \frac{1}{2} \int_{L(t)} \dot{m}_A \cdot w_Z^2 \cdot \cos^2 \theta \cdot \sin \theta d\xi
\end{aligned}$$

Finally we have:

$$\begin{aligned}
F_{W3}^{III} &= v \cdot \cos^2 \theta \cdot (m_{Ab} \cdot (v \sin \theta - w_{Zb} \cos \theta) - m_{As} \cdot (v \sin \theta - w_{Zs} \cos \theta)) \\
&\quad - \frac{1}{2} \cos^2 \theta \cdot \sin \theta (m_{Ab} w_{Zb}^2 - m_{As} w_{Zs}^2) \\
&\quad + \int_{L(t)} \dot{m}_A \cdot w_Z \cdot v \sin^2 \theta \cdot \cos \theta d\xi - \frac{1}{2} \int_{L(t)} \dot{m}_A \cdot w_Z^2 \cdot \cos^2 \theta \cdot \sin \theta d\xi
\end{aligned}$$

$$\boxed{F_{Z-HD}^{III} = B_{33}^{III} \cdot \dot{\eta}_3 + B_{35}^{III} \cdot \dot{\eta}_5 + A_{35-2nd}^{III} \cdot \dot{\eta}_3 \cdot \dot{\eta}_5 + B_{33-2nd}^{III} \cdot \dot{\eta}_3^2 + F_{W3}^{III}}$$

Finally hydrodynamic force in Gxyz reference system is given as:

$$F_{Z-HD} = F_{Z-HD}^I + F_{Z-HD}^{II} - F_{Z-HD}^{III}$$

And consequently the coefficients are given as:

$$A_{33} = A_{33}^I = \int_{L(t)} m_A \cdot \cos^2 \theta d\xi$$

$$A_{35} = A_{35}^I = - \int_{L(t)} m_A \cdot \xi \cdot \cos \theta d\xi$$

$$\begin{aligned}
A_{35-2nd} &= A_{35-2nd}^I - A_{35-2nd}^{III} \\
&= - \int_{L(t)} m_A \cdot \cos \theta \cdot \sin \theta d\xi - \cos \theta \cdot \sin \theta \cdot (m_{Ab} \xi_b - m_{As} \xi_s)
\end{aligned}$$

$$\begin{aligned}
B_{33} &= B_{33}^I + B_{33}^{II} - B_{33}^{III} = \\
&\quad - \cos^2 \theta \cdot \sin \theta \cdot (m_{Ab} w_{Zb} - m_{As} w_{Zs}) + \int_{L(t)} \dot{m}_A \cdot w_Z \cdot \cos^2 \theta \cdot \sin \theta d\xi \\
&\quad + \int_{L(t)} \dot{m}_A \cdot \cos^2 \theta d\xi \\
&\quad - v \cdot \cos^3 \theta \cdot (m_{Ab} - m_{As}) \\
&\quad + \cos \theta \cdot \sin \theta \cdot (m_{Ab} \cdot (v \sin \theta - w_{Zb} \cos \theta) - m_{As} \cdot (v \sin \theta - w_{Zs} \cos \theta)) \\
&\quad - \int_{L(t)} \dot{m}_A \cdot w_Z \cos^2 \theta \cdot \sin \theta d\xi
\end{aligned}$$

$$\begin{aligned}
B_{35} &= B_{35}^I + B_{35}^{II} - B_{35}^{III} = \\
&v \int_{L(t)} m_A \cdot \cos^2 \theta \, d\xi + \int_{L(t)} m_A \cdot w_Z \cdot \cos \theta \cdot \sin \theta \, d\xi \\
&- \int_{L(t)} \dot{m}_A \cdot \xi \cdot \cos \theta \, d\xi \\
&+ v \cdot \cos^2 \theta \cdot (m_{Ab} \xi_b - m_{As} \xi_s) + \int_{L(t)} \dot{m}_A \cdot w_Z \cdot \xi \cdot \cos \theta \cdot \sin \theta \, d\xi \\
&+ \int_{L(t)} m_A \cdot w_Z \cdot \cos \theta \cdot \sin \theta \, d\xi
\end{aligned}$$

$$B_{33-2nd} = -B_{33-2nd}^{III} = \cos^2 \theta \cdot \sin \theta \cdot (m_{Ab} - m_{As})$$

$$\begin{aligned}
F_{W3} &= F_{W3}^I + F_{W3}^{II} - F_{W3}^{III} = \\
&- \int_{L(t)} m_A \cdot \dot{w}_Z \cdot \cos^2 \theta \, d\xi \\
&+ v \cdot \cos^3 \theta \cdot (m_{Ab} w_{Zb} - m_{As} w_{Zs}) - \int_{L(t)} v \cdot \dot{m}_A \cdot w_Z \cdot \cos^3 \theta \, d\xi \\
&+ \frac{1}{2} \cos^2 \theta \cdot \sin \theta \cdot (m_{Ab} w_{Zb}^2 - m_{As} w_{Zs}^2) - \frac{1}{2} \int_{L(t)} \dot{m}_A \cdot w_Z^2 \cdot \cos^2 \theta \cdot \sin \theta \, d\xi \\
&\quad + \int_{L(t)} \dot{m}_A \cdot v \cdot \cos \theta \cdot \sin \theta \, d\xi - \int_{L(t)} \dot{m}_A \cdot w_Z \cdot \cos^2 \theta \, d\xi \\
&- v \cdot \cos^2 \theta \cdot (m_{Ab} \cdot (v \sin \theta - w_{Zb} \cos \theta) - m_{As} \cdot (v \sin \theta - w_{Zs} \cos \theta)) \\
&+ \frac{1}{2} \cos^2 \theta \cdot \sin \theta (m_{Ab} w_{Zb}^2 - m_{As} w_{Zs}^2) \\
&- \int_{L(t)} \dot{m}_A \cdot w_Z \cdot v \sin^2 \theta \cdot \cos \theta \, d\xi + \frac{1}{2} \int_{L(t)} \dot{m}_A \cdot w_Z^2 \cdot \cos^2 \theta \cdot \sin \theta \, d\xi
\end{aligned}$$

$$\begin{aligned}
F_{W3} &= F_{W3}^I + F_{W3}^{II} - F_{W3}^{III} = \\
&- \int_{L(t)} m_A \cdot \dot{w}_Z \cdot \cos^2 \theta \, d\xi + v \cdot \cos^3 \theta \cdot (m_{Ab} w_{Zb} - m_{As} w_{Zs}) \\
&+ \int_{L(t)} \dot{m}_A \cdot v \cdot \cos \theta \cdot \sin \theta \, d\xi - \int_{L(t)} \dot{m}_A \cdot w_Z \cdot \cos^2 \theta \, d\xi \\
&- v \cdot \cos^2 \theta \cdot (m_{Ab} \cdot (v \sin \theta - w_{Zb} \cos \theta) - m_{As} \cdot (v \sin \theta - w_{Zs} \cos \theta)) \\
&+ \cos^2 \theta \cdot \sin \theta (m_{Ab} w_{Zb}^2 - m_{As} w_{Zs}^2) \\
&- \int_{L(t)} \dot{m}_A \cdot w_Z \cdot v \cdot \cos \theta \, d\xi
\end{aligned}$$

$$\begin{aligned}
F_{Z-HD} &= A_{33} \cdot \ddot{\eta}_3 + A_{35} \cdot \ddot{\eta}_5 + A_{35-2nd} \cdot \dot{\eta}_3 \cdot \dot{\eta}_5 \\
&+ B_{33} \cdot \dot{\eta}_3 + B_{35} \cdot \dot{\eta}_5 + B_{33-2nd} \cdot \dot{\eta}_3^2 \\
&+ F_{3-W}
\end{aligned}$$

Hydrostatic component:

$$F_{HS} = \int_{L(t)} a_{bf} \cdot \rho \cdot g \cdot A(\xi, t) d\xi$$

Finally forces equilibrium can be rewritten in form:

$$m \cdot \ddot{\eta}_3 = -F_{Z-HD} - F_{HS} + W$$

$$\begin{aligned}
m \cdot \ddot{\eta}_3 &= -(A_{33} \cdot \ddot{\eta}_3 + A_{35} \cdot \ddot{\eta}_5 + B_{33-2nd} \cdot \dot{\eta}_3^2 + A_{35-2nd} \cdot \dot{\eta}_3 \cdot \dot{\eta}_5 + B_{33} \cdot \dot{\eta}_3 + B_{35} \cdot \dot{\eta}_5 + F_{3-W}) \\
&- F_{HS} + W
\end{aligned}$$

$$(m + A_{33}) \cdot \ddot{\eta}_3 + A_{35} \cdot \ddot{\eta}_5 + B_{33-2nd} \cdot \dot{\eta}_3^2 + A_{35-2nd} \cdot \dot{\eta}_3 \cdot \dot{\eta}_5 + B_{33} \cdot \dot{\eta}_3 + B_{35} \cdot \dot{\eta}_5 = W - F_{3-W} - F_{HS}$$

4.3.2 Moments equilibrium in coordinate system Gxyz

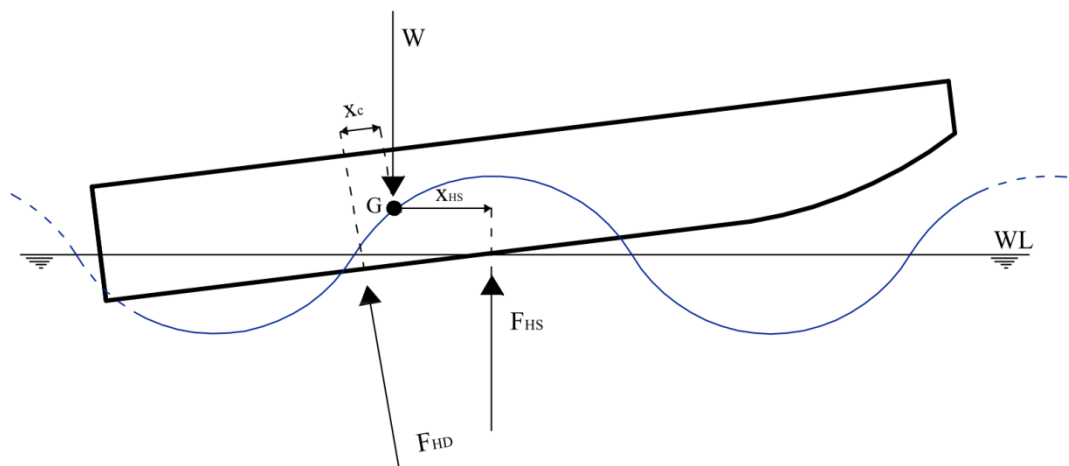


Figure 4.2. Moments acting on planing hull in waves

Moments equilibrium with respect to the y axis is given by:

$$I_{55} \cdot \ddot{\eta}_5 = M_{HD} + M_{HS} = F_{HD} \cdot x_C + F_{HS} \cdot x_{HS}$$

$$F_{HS} = \int_{L(t)} a_{bf} \cdot \rho \cdot g \cdot A(\xi, t) d\xi$$

$$M_{HS} = \int_{L(t)} a_{bm} \cdot \rho \cdot g \cdot A(\xi, t) \cdot \xi \cdot \cos \theta d\xi$$

Hydrodynamic force F_{HD} is given by:

$$F_{HD} = \int_{L(t)} m_A(\xi, t) \cdot \dot{V}(\xi, t) d\xi + \int_{L(t)} \dot{m}_A(\xi, t) \cdot V(\xi, t) d\xi - \int_{L(t)} U(\xi, t) \cdot \frac{\partial(m_A(\xi, t) \cdot V(\xi, t))}{\partial \xi} \cdot d\xi$$

And M_{HD} is given by:

$$M_{HD} = \int_{L(t)} m_A(\xi, t) \cdot \dot{V}(\xi, t) \cdot \xi d\xi + \int_{L(t)} \dot{m}_A(\xi, t) \cdot V(\xi, t) \cdot \xi d\xi - \int_{L(t)} U(\xi, t) \cdot \frac{\partial(m_A(\xi, t) \cdot V(\xi, t))}{\partial \xi} \cdot \xi d\xi$$

$$M_{HD} = M_{HD}^I + M_{HD}^{II} - M_{HD}^{III}$$

Developing each term

$$\begin{aligned} M_{HD}^I &= \int_{L(t)} m_A \cdot \dot{V} \cdot \xi d\xi \\ &= \int_{L(t)} m_A \cdot \xi \cdot [-\ddot{\eta}_5 \cdot \xi + \ddot{\eta}_3 \cos \theta - \dot{w}_Z \cos \theta + U \frac{\partial w_Z}{\partial \xi} \cos \theta \\ &\quad + (v \cdot \cos \theta - \dot{\eta}_3 \cdot \sin \theta + w_Z \cdot \sin \theta) \dot{\eta}_5] d\xi \end{aligned}$$

$$\begin{aligned} M_{HD}^{II} &= \int_{L(t)} m_A \cdot \xi^2 \cdot (-\ddot{\eta}_5) d\xi + \int_{L(t)} m_A \cdot \xi \cdot \ddot{\eta}_3 \cos \theta d\xi - \int_{L(t)} m_A \cdot \xi \cdot \dot{w}_Z \cos \theta d\xi \\ &\quad + \int_{L(t)} m_A \cdot \xi \cdot U \frac{\partial w_Z}{\partial \xi} \cos \theta d\xi + \int_{L(t)} m_A \cdot \xi \cdot v \cdot \dot{\eta}_5 \cos \theta d\xi \\ &\quad - \int_{L(t)} m_A \cdot \xi \cdot \dot{\eta}_3 \cdot \sin \theta \cdot \dot{\eta}_5 d\xi + \int_{L(t)} m_A \cdot \xi \cdot w_Z \sin \theta \cdot \dot{\eta}_5 d\xi \end{aligned}$$

Substituting expression for U, M_{HD}^I is given by:

$$\begin{aligned}
M_{HD}^I &= \int_{L(t)} m_A \cdot \xi^2 \cdot (-\ddot{\eta}_5) d\xi + \int_{L(t)} m_A \cdot \xi \cdot \ddot{\eta}_3 \cos \theta d\xi - \int_{L(t)} m_A \cdot \xi \cdot \dot{w}_Z \cos \theta d\xi \\
&+ \int_{L(t)} m_A \cdot \xi \cdot \frac{\partial w_Z}{\partial \xi} \cdot v \cdot \cos^2 \theta d\xi - \int_{L(t)} m_A \cdot \xi \cdot \frac{\partial w_Z}{\partial \xi} \cdot \cos \theta \cdot \dot{\eta}_3 \cdot \sin \theta d\xi \\
&+ \int_{L(t)} m_A \cdot \xi \cdot \frac{\partial w_Z}{\partial \xi} \cdot \cos \theta \cdot w_Z \cdot \sin \theta d\xi \\
&+ \int_{L(t)} m_A \cdot \xi \cdot v \cdot \dot{\eta}_5 \cdot \cos \theta d\xi - \int_{L(t)} m_A \cdot \xi \cdot \dot{\eta}_3 \cdot \sin \theta \cdot \dot{\eta}_5 d\xi \\
&+ \int_{L(t)} m_A \cdot \xi \cdot w_Z \cdot \sin \theta \cdot \dot{\eta}_5 d\xi
\end{aligned}$$

It can be written:

$$A_{55}^I = - \int_{L(t)} m_A \cdot \xi^2 d\xi$$

$$A_{53}^I = \int_{L(t)} m_A \cdot \xi \cdot \cos \theta d\xi$$

$$\begin{aligned}
B_{53}^I &= - \int_{L(t)} m_A \cdot \xi \cdot \frac{\partial w_Z}{\partial \xi} \cdot \cos \theta \cdot \sin \theta d\xi \\
&= - \sin \theta \cdot \cos \theta \cdot (m_{Ab} \xi_b w_{Zb} - m_{As} \xi_s w_{Zs}) \\
&+ \int_{L(t)} \dot{m}_A \cdot w_Z \cdot \xi \cdot \sin \theta \cdot \cos \theta d\xi + \int_{L(t)} m_A \cdot w_Z \cdot \sin \theta \cdot \cos \theta d\xi
\end{aligned}$$

$$B_{55}^I = \int_{L(t)} m_A \cdot \xi \cdot v \cdot \cos \theta d\xi + \int_{L(t)} m_A \cdot \xi \cdot w_Z \sin \theta d\xi$$

$$A_{53-2nd}^I = - \int_{L(t)} m_A \cdot \xi \sin \theta d\xi$$

$$\begin{aligned}
F_{W5}^I &= - \int_{L(t)} m_A \cdot \xi \cdot \dot{w}_Z \cos \theta d\xi + \int_{L(t)} m_A \cdot \xi \cdot \frac{\partial w_Z}{\partial \xi} v \cdot \cos^2 \theta d\xi \\
&+ \int_{L(t)} m_A \cdot \xi \cdot \frac{\partial w_Z}{\partial \xi} \cdot w_Z \cdot \sin \theta \cdot \cos \theta d\xi = \\
&- \int_{L(t)} m_A \cdot \xi \cdot \dot{w}_Z \cdot \cos \theta d\xi \\
&+ v \cos^2 \theta \cdot (m_{Ab} \xi_b w_{Zb} - m_{As} \xi_s w_{Zs}) - \int_{L(t)} \dot{m}_A \cdot w_Z \cdot \xi \cdot v \cdot \cos^2 \theta d\xi \\
&- \int_{L(t)} m_A \cdot w_Z \cdot v \cdot \cos^2 \theta d\xi \\
&+ \frac{1}{2} \sin \theta \cdot \cos \theta \cdot (m_{Ab} \xi_b w_{Zb}^2 - m_{As} \xi_s w_{Zs}^2) - \frac{1}{2} \int_{L(t)} \dot{m}_A \cdot w_Z^2 \cdot \xi \cdot \sin \theta \cdot \cos \theta d\xi \\
&- \frac{1}{2} \int_{L(t)} m_A \cdot w_Z^2 \cdot \sin \theta \cdot \cos \theta d\xi
\end{aligned}$$

$$\boxed{M_{HD}^I = A_{55}^I \cdot \ddot{\eta}_5 + A_{53}^I \cdot \ddot{\eta}_3 + B_{55}^I \cdot \dot{\eta}_5 + B_{53}^I \cdot \dot{\eta}_3 + A_{53-2nd}^I \cdot \dot{\eta}_3 \cdot \dot{\eta}_5 + F_{W5}^I}$$

$$\begin{aligned}
M_{HD}^{II} &= \int_{L(t)} \dot{m}_A(\xi, t) \cdot V(\xi, t) \cdot \xi d\xi \\
&= \int_{L(t)} \dot{m}_A \cdot (v \sin \theta + (\dot{\eta}_3 - w_Z) \cos \theta - \dot{\eta}_5 \cdot \xi) \cdot \xi d\xi
\end{aligned}$$

$$\begin{aligned}
M_{HD}^{II} &= \int_{L(t)} \dot{m}_A \cdot v \cdot \sin \theta \cdot \xi d\xi + \int_{L(t)} \dot{m}_A \cdot \dot{\eta}_3 \cdot \cos \theta \cdot \xi d\xi \\
&- \int_{L(t)} \dot{m}_A \cdot w_Z \cdot \cos \theta \cdot \xi d\xi - \int_{L(t)} \dot{m}_A \cdot \dot{\eta}_5 \cdot \xi \cdot \xi d\xi
\end{aligned}$$

It can be written:

$$B_{53}^{II} = \int_{L(t)} \dot{m}_A \cos \theta \cdot \xi d\xi$$

$$B_{55}^{II} = - \int_{L(t)} \dot{m}_A \cdot \xi^2 d\xi$$

$$F_{W5}^{II} = \int_{L(t)} \dot{m}_A (v \sin \theta - w_Z \cos \theta) \cdot \xi d\xi$$

$$\boxed{M_{HD}^{II} = B_{53}^{II} \cdot \dot{\eta}_3 + B_{55}^{II} \cdot \dot{\eta}_5 + F_{W5}^{II}}$$

$$M_{HD}^{III} = \int_{L(t)} U(\xi, t) \cdot \frac{\partial(m_A(\xi, t) \cdot V(\xi, t))}{\partial \xi} \cdot \xi d\xi$$

$$M_{HD}^{III} = \int_{L(t)} v \cdot \cos \theta \cdot \frac{\partial(m_A V)}{\partial \xi} \cdot \xi d\xi - \int_{L(t)} \dot{\eta}_3 \cdot \sin \theta \cdot \frac{\partial(m_A V)}{\partial \xi} \cdot \xi d\xi \\ + \int_{L(t)} w_Z \cdot \sin \theta \cdot \frac{\partial(m_A V)}{\partial \xi} \cdot \xi d\xi$$

$$M_{HD}^{III} = v \cos \theta \cdot [(m_A \cdot V \cdot \xi)_b - (m_A \cdot V \cdot \xi)_s] - \int_{L(t)} v \cdot \cos \theta \cdot m_A \cdot V d\xi \\ - \dot{\eta}_3 \sin \theta \cdot [(m_A \cdot V \cdot \xi)_b - (m_A \cdot V \cdot \xi)_s] + \int_{L(t)} \dot{\eta}_3 \cdot \sin \theta \cdot m_A \cdot V d\xi \\ + \sin \theta \cdot [(m_A \cdot V \cdot \xi \cdot w_Z)_b - (m_A \cdot V \cdot \xi \cdot w_Z)_s] - \int_{L(t)} \frac{\partial w_Z}{\partial \xi} \cdot \sin \theta \cdot m_A \cdot V \cdot \xi d\xi \\ - \int_{L(t)} w_Z \cdot \sin \theta \cdot m_A \cdot V d\xi$$

Substituting V into the expression for

$$M_{HD}^{III} = v \cos \theta \cdot [(m_A \cdot (v \sin \theta + (\dot{\eta}_3 - w_Z) \cos \theta - \dot{\eta}_5 \cdot \xi) \cdot \xi)_b \\ - (m_A \cdot (v \sin \theta + (\dot{\eta}_3 - w_Z) \cos \theta - \dot{\eta}_5 \cdot \xi) \cdot \xi)_s] \\ - \int_{L(t)} v \cos \theta \cdot m_A \cdot (v \sin \theta + (\dot{\eta}_3 - w_Z) \cos \theta - \dot{\eta}_5 \cdot \xi) d\xi \\ - \dot{\eta}_3 \sin \theta \cdot [(m_A \cdot (v \sin \theta + (\dot{\eta}_3 - w_Z) \cos \theta - \dot{\eta}_5 \cdot \xi) \cdot \xi)_b \\ - (m_A \cdot (v \sin \theta + (\dot{\eta}_3 - w_Z) \cos \theta - \dot{\eta}_5 \cdot \xi) \cdot \xi)_s] \\ + \int_{L(t)} \dot{\eta}_3 \sin \theta \cdot m_A \cdot (v \sin \theta + (\dot{\eta}_3 - w_Z) \cos \theta - \dot{\eta}_5 \cdot \xi) d\xi \\ + \sin \theta \cdot [(w_Z \cdot m_A \cdot (v \sin \theta + (\dot{\eta}_3 - w_Z) \cos \theta - \dot{\eta}_5 \cdot \xi) \cdot \xi)_b \\ - (w_Z \cdot m_A \cdot (v \sin \theta + (\dot{\eta}_3 - w_Z) \cos \theta - \dot{\eta}_5 \cdot \xi) \cdot \xi)_s] \\ - \int_{L(t)} \frac{\partial w_Z}{\partial \xi} \sin \theta \cdot m_A \cdot (v \sin \theta + (\dot{\eta}_3 - w_Z) \cos \theta - \dot{\eta}_5 \cdot \xi) \cdot \xi d\xi \\ - \int_{L(t)} w_Z \sin \theta \cdot m_A \cdot (v \sin \theta + (\dot{\eta}_3 - w_Z) \cos \theta - \dot{\eta}_5 \cdot \xi) d\xi$$

$$\begin{aligned}
M_{HD}^{III} = & v \cos \theta \cdot (m_{Ab} v \sin \theta \xi_b - m_{As} v \sin \theta \xi_s) - \int_{L(t)} v^2 \cos \theta \sin \theta \cdot m_A d\xi \\
& + v \cos \theta \cdot (m_{Ab} \dot{\eta}_3 \cos \theta \xi_b - m_{As} \dot{\eta}_3 \cos \theta \xi_s) - \int_{L(t)} v \cos^2 \theta \cdot m_A \dot{\eta}_3 d\xi \\
& - v \cos \theta \cdot (m_{Ab} w_{Zb} \cos \theta \xi_b - m_{As} w_{Zs} \cos \theta \xi_s) + \int_{L(t)} v \cos^2 \theta \cdot m_A w_Z d\xi \\
& - v \cos \theta \cdot (m_{Ab} \dot{\eta}_5 \xi_b^2 - m_{As} \dot{\eta}_5 \xi_s^2) + \int_{L(t)} v \cos \theta \cdot m_A \dot{\eta}_5 \cdot \xi d\xi \\
& - \dot{\eta}_3 \sin \theta \cdot (m_{Ab} v \sin \theta \xi_b - m_{As} v \sin \theta \xi_s) + \int_{L(t)} v \sin^2 \theta \cdot m_A \dot{\eta}_3 d\xi \\
& - \dot{\eta}_3 \sin \theta \cdot (m_{Ab} \dot{\eta}_3 \cos \theta \xi_b - m_{As} \dot{\eta}_3 \cos \theta \xi_s) + \int_{L(t)} \dot{\eta}_3^2 \sin \theta \cdot \cos \theta \cdot m_A d\xi \\
& + \dot{\eta}_3 \sin \theta \cdot (m_{Ab} w_{Zb} \cos \theta \xi_b - m_{As} w_{Zs} \cos \theta \xi_s) - \int_{L(t)} \dot{\eta}_3 \sin \theta \cdot \cos \theta \cdot w_Z m_A d\xi \\
& + \dot{\eta}_3 \sin \theta \cdot (m_{Ab} \dot{\eta}_5 \xi_b^2 - m_{As} \dot{\eta}_5 \xi_s^2) - \int_{L(t)} \dot{\eta}_3 \sin \theta \cdot m_A \dot{\eta}_5 \xi d\xi \\
& + \sin \theta \cdot (m_{Ab} \cdot w_{Zb} \cdot v \cdot \sin \theta \cdot \xi_b - m_{As} \cdot w_{Zs} \cdot v \cdot \sin \theta \cdot \xi_s) \\
& - \int_{L(t)} v \sin^2 \theta \cdot m_A \frac{\partial w_Z}{\partial \xi} \xi d\xi - \int_{L(t)} v \sin^2 \theta \cdot m_A w_Z d\xi \\
& + \sin \theta \cdot (m_{Ab} \cdot w_{Zb} \cdot \dot{\eta}_3 \cdot \cos \theta \cdot \xi_b - m_{As} \cdot w_{Zs} \cdot \dot{\eta}_3 \cdot \cos \theta \cdot \xi_s) \\
& - \int_{L(t)} \dot{\eta}_3 \sin \theta \cos \theta \cdot m_A \frac{\partial w_Z}{\partial \xi} \xi d\xi - \int_{L(t)} \dot{\eta}_3 \sin \theta \cdot \cos \theta m_A w_Z d\xi \\
& - \sin \theta \cdot (m_{Ab} \cdot w_{Zb}^2 \cdot \cos \theta \cdot \xi_b - m_{As} \cdot w_{Zs}^2 \cdot \cos \theta \cdot \xi_s) \\
& + \int_{L(t)} w_Z \sin \theta \cos \theta \cdot m_A \frac{\partial w_Z}{\partial \xi} \xi d\xi + \int_{L(t)} w_Z^2 \sin \theta \cdot \cos \theta m_A d\xi \\
& - \sin \theta \cdot (m_{Ab} \cdot w_{Zb} \cdot \dot{\eta}_5 \cdot \xi_b^2 - m_{As} \cdot w_{Zs} \cdot \dot{\eta}_5 \cdot \xi_s^2) \\
& + \int_{L(t)} \dot{\eta}_5 \sin \theta \cdot m_A \frac{\partial w_Z}{\partial \xi} \xi^2 d\xi + \int_{L(t)} \dot{\eta}_5 \sin \theta \cdot \xi m_A w_Z d\xi
\end{aligned}$$

$$\begin{aligned}
B_{55}^{III} = & -v \cos \theta \cdot (m_{Ab} \cdot \xi_b^2 - m_{As} \cdot \xi_s^2) + \int_{L(t)} v \cdot \cos \theta \cdot m_A \cdot \xi d\xi \\
& - \sin \theta \cdot (m_{Ab} \cdot w_{Zb} \cdot \xi_b^2 - m_{As} \cdot w_{Zs} \cdot \xi_s^2) \\
& + \int_{L(t)} \sin \theta \cdot m_A \cdot \frac{\partial w_Z}{\partial \xi} \cdot \xi^2 d\xi + \int_{L(t)} \sin \theta \cdot \xi \cdot m_A \cdot w_Z d\xi = \\
& -v \cos \theta \cdot (m_{Ab} \cdot \xi_b^2 - m_{As} \cdot \xi_s^2) + \int_{L(t)} v \cdot \cos \theta \cdot m_A \cdot \xi d\xi \\
& - \sin \theta \cdot (m_{Ab} \cdot w_{Zb} \cdot \xi_b^2 - m_{As} \cdot w_{Zs} \cdot \xi_s^2) \\
& + \sin \theta \cdot (m_{Ab} \cdot w_{Zb} \cdot \xi_b^2 - m_{As} \cdot w_{Zs} \cdot \xi_s^2) - \int_{L(t)} \sin \theta \cdot w_Z \cdot \dot{m}_A \cdot \xi^2 d\xi \\
& - \int_{L(t)} \sin \theta \cdot w_Z \cdot m_A \cdot 2\xi d\xi + \int_{L(t)} \sin \theta \cdot \xi m_A \cdot w_Z d\xi = \\
& -v \cos \theta \cdot (m_{Ab} \cdot \xi_b^2 - m_{As} \cdot \xi_s^2) + \int_{L(t)} v \cdot \cos \theta \cdot m_A \cdot \xi d\xi \\
& - \int_{L(t)} \sin \theta \cdot w_Z \cdot \dot{m}_A \cdot \xi^2 d\xi - \int_{L(t)} \sin \theta \cdot w_Z \cdot m_A \cdot \xi d\xi
\end{aligned}$$

$$\begin{aligned}
B_{53}^{III} = & v \cos \theta \cdot (m_{Ab} \cos \theta \xi_b - m_{As} \cos \theta \xi_s) - \int_{L(t)} v \cos^2 \theta \cdot m_A d\xi \\
& - \sin \theta \cdot (m_{Ab} v \sin \theta \xi_b - m_{As} v \sin \theta \xi_s) + \int_{L(t)} v \sin^2 \theta \cdot m_A d\xi \\
& + \sin \theta \cdot (m_{Ab} w_{Zb} \cos \theta \xi_b - m_{As} w_{Zs} \cos \theta \xi_s) - \int_{L(t)} \sin \theta \cdot \cos \theta \cdot w_Z m_A d\xi \\
& + \sin \theta \cdot (m_{Ab} w_{Zb} \cos \theta \xi_b - m_{As} w_{Zs} \cos \theta \xi_s) - \int_{L(t)} \sin \theta \cos \theta \cdot m_A \frac{\partial w_Z}{\partial \xi} \xi d\xi \\
& - \int_{L(t)} \sin \theta \cdot \cos \theta m_A w_Z d\xi = \\
& v(\cos^2 \theta - \sin^2 \theta) \cdot (m_{Ab} \xi_b - m_{As} \xi_s) + v(\sin^2 \theta - \cos^2 \theta) \int_{L(t)} m_A d\xi \\
& + \sin \theta \cdot (m_{Ab} w_{Zb} \cos \theta \xi_b - m_{As} w_{Zs} \cos \theta \xi_s) - \int_{L(t)} \sin \theta \cdot \cos \theta \cdot w_Z m_A d\xi \\
& + \sin \theta \cdot (m_{Ab} w_{Zb} \cos \theta \xi_b - m_{As} w_{Zs} \cos \theta \xi_s) \\
& - \sin \theta \cdot (m_{Ab} w_{Zb} \cos \theta \xi_b - m_{As} w_{Zs} \cos \theta \xi_s) \\
& + \int_{L(t)} \sin \theta \cdot \cos \theta \cdot \dot{m}_A \cdot w_Z \cdot \xi d\xi + \int_{L(t)} \sin \theta \cdot \cos \theta m_A w_Z d\xi \\
& - \int_{L(t)} \sin \theta \cdot \cos \theta m_A w_Z d\xi
\end{aligned}$$

$$\begin{aligned}
B_{53}^{III} &= v(\cos^2 \theta - \sin^2 \theta) \cdot (m_{Ab} \xi_b - m_{As} \xi_s) + v(\sin^2 \theta - \cos^2 \theta) \int_{L(t)} m_A d\xi \\
&+ \sin \theta \cdot (m_{Ab} w_{Zb} \cos \theta \xi_b - m_{As} w_{Zs} \cos \theta \xi_s) - \int_{L(t)} \sin \theta \cdot \cos \theta \cdot w_Z m_A d\xi \\
&+ \int_{L(t)} \sin \theta \cdot \cos \theta \cdot \dot{m}_A \cdot w_Z \cdot \xi d\xi
\end{aligned}$$

$$A_{53-2nd}^{III} = \sin \theta \cdot (m_{Ab} \xi_b^2 - m_{As} \xi_s^2) - \int_{L(t)} \sin \theta \cdot m_A \xi d\xi$$

$$B_{53-2nd}^{III} = -\sin \theta \cdot (m_{Ab} \cos \theta \xi_b - m_{As} \cos \theta \xi_s) + \int_{L(t)} \cos \theta \sin \theta \cdot m_A d\xi$$

$$\begin{aligned}
F_{W-5}^{III} &= v \cos \theta \cdot (m_{Ab} v \sin \theta \xi_b - m_{As} v \sin \theta \xi_s) - \int_{L(t)} v^2 \cos \theta \sin \theta \cdot m_A d\xi \\
&- v \cos \theta \cdot (m_{Ab} w_{Zb} \cos \theta \xi_b - m_{As} w_{Zs} \cos \theta \xi_s) + \int_{L(t)} v \cos^2 \theta \cdot m_A w_Z d\xi \\
&+ \sin \theta \cdot (m_{Ab} w_{Zb} v \sin \theta \xi_b - m_{As} w_{Zs} v \sin \theta \xi_s) - \int_{L(t)} v \sin^2 \theta \cdot m_A \frac{\partial w_Z}{\partial \xi} \xi d\xi \\
&- \int_{L(t)} v \sin^2 \theta \cdot m_A w_Z d\xi \\
&- \sin \theta \cdot (m_{Ab} w_{Zb}^2 \cos \theta \xi_b - m_{As} w_{Zs}^2 \cos \theta \xi_s) + \int_{L(t)} w_Z \sin \theta \cos \theta \cdot m_A \frac{\partial w_Z}{\partial \xi} \xi d\xi \\
&+ \int_{L(t)} w_Z^2 \sin \theta \cdot \cos \theta m_A d\xi \\
&= v \cos \theta \cdot (m_{Ab} v \sin \theta \xi_b - m_{As} v \sin \theta \xi_s) - \int_{L(t)} v^2 \cos \theta \sin \theta \cdot m_A d\xi \\
&- v \cos \theta \cdot (m_{Ab} w_{Zb} \cos \theta \xi_b - m_{As} w_{Zs} \cos \theta \xi_s) + \int_{L(t)} v \cos^2 \theta \cdot m_A w_Z d\xi \\
&+ \sin \theta \cdot (m_{Ab} w_{Zb} v \sin \theta \xi_b - m_{As} w_{Zs} v \sin \theta \xi_s) \\
&- \sin \theta \cdot (m_{Ab} w_{Zb} v \sin \theta \xi_b - m_{As} w_{Zs} v \sin \theta \xi_s) + \int_{L(t)} v \sin^2 \theta \cdot \dot{m}_A \cdot w_Z \cdot \xi d\xi \\
&+ \int_{L(t)} v \sin^2 \theta \cdot m_A \cdot w_Z d\xi - \int_{L(t)} v \sin^2 \theta \cdot m_A \cdot w_Z d\xi \\
&- \sin \theta \cdot (m_{Ab} w_{Zb}^2 \cos \theta \xi_b - m_{As} w_{Zs}^2 \cos \theta \xi_s) \\
&+ \frac{1}{2} \sin \theta \cos \theta \cdot (m_{Ab} w_{Zb}^2 \xi_b - m_{As} w_{Zs}^2 \xi_s) - \frac{1}{2} \int_{L(t)} \sin \theta \cos \theta \cdot \dot{m}_A \cdot w_Z^2 \cdot \xi d\xi \\
&- \frac{1}{2} \int_{L(t)} \sin \theta \cos \theta \cdot m_A \cdot w_Z^2 d\xi + \int_{L(t)} w_Z^2 \sin \theta \cdot \cos \theta m_A d\xi
\end{aligned}$$

$$\begin{aligned}
F_{W-5}^{III} &= v \cos \theta \cdot (m_{Ab} v \sin \theta \xi_b - m_{As} v \sin \theta \xi_s) - \int_{L(t)} v^2 \cos \theta \sin \theta \cdot m_A d\xi \\
&\quad - v \cos \theta \cdot (m_{Ab} w_{zb} \cos \theta \xi_b - m_{As} w_{zs} \cos \theta \xi_s) + \int_{L(t)} v \cos^2 \theta \cdot m_A w_Z d\xi \\
&\quad + \int_{L(t)} v \sin^2 \theta \cdot \dot{m}_A \cdot w_Z \cdot \xi d\xi - \sin \theta \cdot (m_{Ab} w_{zb}^2 \cos \theta \xi_b - m_{As} w_{zs}^2 \cos \theta \xi_s) \\
&\quad + \frac{1}{2} \sin \theta \cos \theta \cdot (m_{Ab} w_{zb}^2 \xi_b - m_{As} w_{zs}^2 \xi_s) - \frac{1}{2} \int_{L(t)} \sin \theta \cos \theta \cdot \dot{m}_A \cdot w_Z^2 \cdot \xi d\xi \\
&\quad - \frac{1}{2} \int_{L(t)} \sin \theta \cos \theta \cdot m_A \cdot w_Z^2 d\xi \\
&\quad + \int_{L(t)} w_Z^2 \sin \theta \cdot \cos \theta m_A d\xi
\end{aligned}$$

$$M_{Z-HD}^{III} = B_{55}^{III} \cdot \dot{\eta}_5 + B_{53}^{III} \cdot \dot{\eta}_3 + A_{53-2nd}^{III} \cdot \dot{\eta}_3 \cdot \dot{\eta}_5 + B_{53-2nd}^{III} \cdot \dot{\eta}_3^2 + F_{W5}^{III}$$

Finally it can be written:

$$A_{55} = A_{55}^I = - \int_{L(t)} m_A \cdot \xi^2 d\xi$$

$$A_{53} = A_{53}^I = \int_{L(t)} m_A \cdot \xi \cdot \cos \theta d\xi$$

$$\begin{aligned}
A_{53-2nd} &= A_{53-2nd}^I - A_{53-2nd}^{III} = - \int_{L(t)} m_A \cdot \xi \sin \theta d\xi \\
&\quad - \sin \theta \cdot (m_{Ab} \xi_b^2 - m_{As} \xi_s^2) + \int_{L(t)} \sin \theta \cdot m_A \xi d\xi
\end{aligned}$$

$$\begin{aligned}
B_{53} &= B_{53}^I + B_{53}^{II} - B_{53}^{III} = \\
&\quad - \sin \theta \cdot \cos \theta \cdot (m_{Ab} \xi_b w_{zb} - m_{As} \xi_s w_{zs}) \\
&\quad + \int_{L(t)} \dot{m}_A \cdot w_Z \cdot \xi \cdot \sin \theta \cdot \cos \theta d\xi + \int_{L(t)} m_A \cdot w_Z \cdot \sin \theta \cdot \cos \theta d\xi \\
&\quad + \int_{L(t)} \dot{m}_A \cos \theta \cdot \xi d\xi \\
&\quad - v(\cos^2 \theta - \sin^2 \theta) \cdot (m_{Ab} \xi_b - m_{As} \xi_s) - v(\sin^2 \theta - \cos^2 \theta) \int_{L(t)} m_A d\xi \\
&\quad - \sin \theta \cdot (m_{Ab} w_{zb} \cos \theta \xi_b - m_{As} w_{zs} \cos \theta \xi_s) + \int_{L(t)} \sin \theta \cdot \cos \theta \cdot w_Z m_A d\xi \\
&\quad - \int_{L(t)} \sin \theta \cdot \cos \theta \cdot \dot{m}_A \cdot w_Z \cdot \xi d\xi
\end{aligned}$$

$$\begin{aligned}
B_{55} &= B_{55}^I + B_{55}^{II} - B_{55}^{III} = \\
&\int_{L(t)} m_A \cdot \xi \cdot v \cdot \cos \theta \, d\xi + \int_{L(t)} m_A \cdot \xi \cdot w_Z \sin \theta \, d\xi \\
&- \int_{L(t)} \dot{m}_A \cdot \xi^2 \, d\xi \\
&+ v \cos \theta \cdot (m_{Ab} \cdot \xi_b^2 - m_{As} \cdot \xi_s^2) - \int_{L(t)} v \cos \theta \cdot m_A \cdot \xi \, d\xi \\
&+ \int_{L(t)} \sin \theta \cdot w_Z \cdot \dot{m}_A \cdot \xi^2 \, d\xi + \int_{L(t)} \sin \theta \cdot w_Z \cdot m_A \cdot \xi \, d\xi \\
B_{53-2nd} &= -B_{53-2nd}^{III} = \sin \theta \cdot (m_{Ab} \cos \theta \xi_b - m_{As} \cos \theta \xi_s) - \int_{L(t)} \cos \theta \sin \theta \cdot m_A \, d\xi
\end{aligned}$$

$$\begin{aligned}
F_{W5} &= F_{W5}^I + F_{W5}^{II} - F_{W5}^{III} = \\
&- \int_{L(t)} m_A \cdot \xi \cdot \dot{w}_Z \cos \theta \, d\xi \\
&+ v \cos^2 \theta \cdot (m_{Ab} \xi_b w_{Zb} - m_{As} \xi_s w_{Zs}) - \int_{L(t)} \dot{m}_A \cdot w_Z \cdot \xi \cdot v \cos^2 \theta \, d\xi \\
&- \int_{L(t)} m_A \cdot w_Z \cdot v \cos^2 \theta \, d\xi \\
&+ \frac{1}{2} \sin \theta \cdot \cos \theta \cdot (m_{Ab} \xi_b w_{Zb}^2 - m_{As} \xi_s w_{Zs}^2) - \frac{1}{2} \int_{L(t)} \dot{m}_A \cdot w_Z^2 \cdot \xi \cdot \sin \theta \cdot \cos \theta \, d\xi \\
&- \frac{1}{2} \int_{L(t)} m_A \cdot w_Z^2 \cdot \sin \theta \cdot \cos \theta \, d\xi \\
&+ \int_{L(t)} \dot{m}_A (v \sin \theta - w_Z \cos \theta) \cdot \xi \, d\xi \\
&- v \cos \theta \cdot (m_{Ab} v \sin \theta \xi_b - m_{As} v \sin \theta \xi_s) + \int_{L(t)} v^2 \cos \theta \sin \theta \cdot m_A \, d\xi \\
&+ v \cos \theta \cdot (m_{Ab} w_{zb} \cos \theta \xi_b - m_{As} w_{zs} \cos \theta \xi_s) - \int_{L(t)} v \cos^2 \theta \cdot m_A w_Z \, d\xi \\
&- \int_{L(t)} v \sin^2 \theta \cdot \dot{m}_A \cdot w_Z \cdot \xi \, d\xi \\
&+ \sin \theta \cdot (m_{Ab} w_{Zb}^2 \cos \theta \xi_b - m_{As} w_{Zs}^2 \cos \theta \xi_s) \\
&- \frac{1}{2} \sin \theta \cos \theta \cdot (m_{Ab} w_{Zb}^2 \xi_b - m_{As} w_{Zs}^2 \xi_s) + \frac{1}{2} \int_{L(t)} \sin \theta \cos \theta \cdot \dot{m}_A \cdot w_Z^2 \cdot \xi \, d\xi \\
&+ \frac{1}{2} \int_{L(t)} \sin \theta \cos \theta \cdot m_A \cdot w_Z^2 \, d\xi - \int_{L(t)} w_Z^2 \sin \theta \cdot \cos \theta \cdot m_A \, d\xi
\end{aligned}$$

$$\begin{aligned}
F_{W5} = & - \int_{L(t)} m_A \cdot \xi \cdot \dot{w}_Z \cos \theta d\xi \\
& + 2 \cdot v \cdot \cos^2 \theta \cdot (m_{Ab} \xi_b w_{Zb} - m_{As} \xi_s w_{Zs}) - \int_{L(t)} \dot{m}_A \cdot w_Z \cdot \xi d\xi \\
& - 2 \cdot \int_{L(t)} m_A \cdot w_Z \cdot v \cos^2 \theta d\xi \\
& + \int_{L(t)} \dot{m}_A \cdot (v \cdot \sin \theta - w_Z \cdot \cos \theta) \cdot \xi d\xi \\
& - v \cos \theta \cdot (m_{Ab} v \sin \theta \xi_b - m_{As} v \sin \theta \xi_s) + \int_{L(t)} v^2 \cdot \cos \theta \cdot \sin \theta \cdot m_A d\xi \\
& + \sin \theta \cdot (m_{Ab} w_{Zb}^2 \cos \theta \xi_b - m_{As} w_{Zs}^2 \cos \theta \xi_s) \\
& - \int_{L(t)} w_Z^2 \cdot \sin \theta \cdot \cos \theta \cdot m_A d\xi
\end{aligned}$$

Finally to compose the motion equation the hydrodynamic coefficients must be multiplied by -1 and the final expressions are:

$$A_{55} = -A_{55} = \int_{L(t)} m_A \cdot \xi^2 d\xi$$

$$A_{53} = -A_{53} = - \int_{L(t)} m_A \cdot \xi \cdot \cos \theta d\xi$$

$$\begin{aligned}
A_{53-2nd} = -A_{53-2nd} = & \int_{L(t)} m_A \cdot \xi \sin \theta d\xi \\
& + \sin \theta \cdot (m_{Ab} \xi_b^2 - m_{As} \xi_s^2) - \int_{L(t)} \sin \theta \cdot m_A \xi d\xi
\end{aligned}$$

$$\begin{aligned}
B_{53} = -B_{53} = & \\
& + \sin \theta \cdot \cos \theta \cdot (m_{Ab} \xi_b w_{Zb} - m_{As} \xi_s w_{Zs}) \\
& - \int_{L(t)} \dot{m}_A \cdot w_Z \cdot \xi \cdot \sin \theta \cdot \cos \theta d\xi - \int_{L(t)} m_A \cdot w_Z \cdot \sin \theta \cdot \cos \theta d\xi \\
& - \int_{L(t)} \dot{m}_A \cos \theta \cdot \xi d\xi \\
& + v(\cos^2 \theta - \sin^2 \theta) \cdot (m_{Ab} \xi_b - m_{As} \xi_s) + v(\sin^2 \theta - \cos^2 \theta) \int_{L(t)} m_A d\xi \\
& + \sin \theta \cdot (m_{Ab} w_{Zb} \cos \theta \xi_b - m_{As} w_{Zs} \cos \theta \xi_s) - \int_{L(t)} \sin \theta \cdot \cos \theta \cdot w_Z m_A d\xi \\
& + \int_{L(t)} \sin \theta \cdot \cos \theta \cdot \dot{m}_A \cdot w_Z \cdot \xi d\xi
\end{aligned}$$

$$\begin{aligned}
B_{55} = -B_{55} = & - \int_{L(t)} m_A \cdot \xi \cdot v \cdot \cos \theta \, d\xi - \int_{L(t)} m_A \cdot \xi \cdot w_Z \sin \theta \, d\xi \\
& + \int_{L(t)} \dot{m}_A \cdot \xi^2 \, d\xi \\
& - v \cos \theta \cdot (m_{Ab} \cdot \xi_b^2 - m_{As} \cdot \xi_s^2) + \int_{L(t)} v \cos \theta \cdot m_A \cdot \xi \, d\xi \\
& - \int_{L(t)} \sin \theta \cdot w_Z \cdot \dot{m}_A \cdot \xi^2 \, d\xi - \int_{L(t)} \sin \theta \cdot w_Z \cdot m_A \cdot \xi \, d\xi
\end{aligned}$$

$$B_{53-2nd} = -B_{53-2nd} = -\sin \theta \cdot (m_{Ab} \cos \theta \xi_b - m_{As} \cos \theta \xi_s) + \int_{L(t)} \cos \theta \sin \theta \cdot m_A \, d\xi$$

$$\begin{aligned}
-M_{HD} = & A_{55} \cdot \ddot{\eta}_5 + A_{53} \cdot \ddot{\eta}_3 + B_{53-2nd} \cdot \dot{\eta}_3^2 + A_{53-2nd} \cdot \dot{\eta}_3 \cdot \dot{\eta}_5 \\
& + B_{55} \cdot \dot{\eta}_5 + B_{53} \cdot \dot{\eta}_3 - F_{5-W} - F_{5-W}
\end{aligned}$$

Finally momentum equilibrium can be rewritten in form:

$$I_{55} \cdot \ddot{\eta}_5 = M_{HD} + M_{HS}$$

$$\begin{aligned}
I_{55} \cdot \ddot{\eta}_5 = & -A_{55} \cdot \ddot{\eta}_5 - A_{53} \cdot \ddot{\eta}_3 - B_{53-2nd} \cdot \dot{\eta}_3^2 - A_{53-2nd} \cdot \dot{\eta}_3 \cdot \dot{\eta}_5 \\
& - B_{55} \cdot \dot{\eta}_5 - B_{53} \cdot \dot{\eta}_3 + F_{5-W} + F_{HS}
\end{aligned}$$

$$(I_{55} + A_{55}) \cdot \ddot{\eta}_5 + A_{53} \cdot \ddot{\eta}_3 + B_{53-2nd} \cdot \dot{\eta}_3^2 + A_{53-2nd} \cdot \dot{\eta}_3 \cdot \dot{\eta}_5 + B_{55} \cdot \dot{\eta}_5 + B_{53} \cdot \dot{\eta}_3 = F_{5-W} + F_{HS}$$

4.4 Fully non-linear 2D time domain code

The structure of the code is the same explained in 3.4, making the appropriate changes to the functions, for the calculation of forces and motion coefficients depending on the effective wetted surface, and to the Simulink model, according with the new developed mathematical model. Developed Simulink code scheme is shown in Figure 4.3.

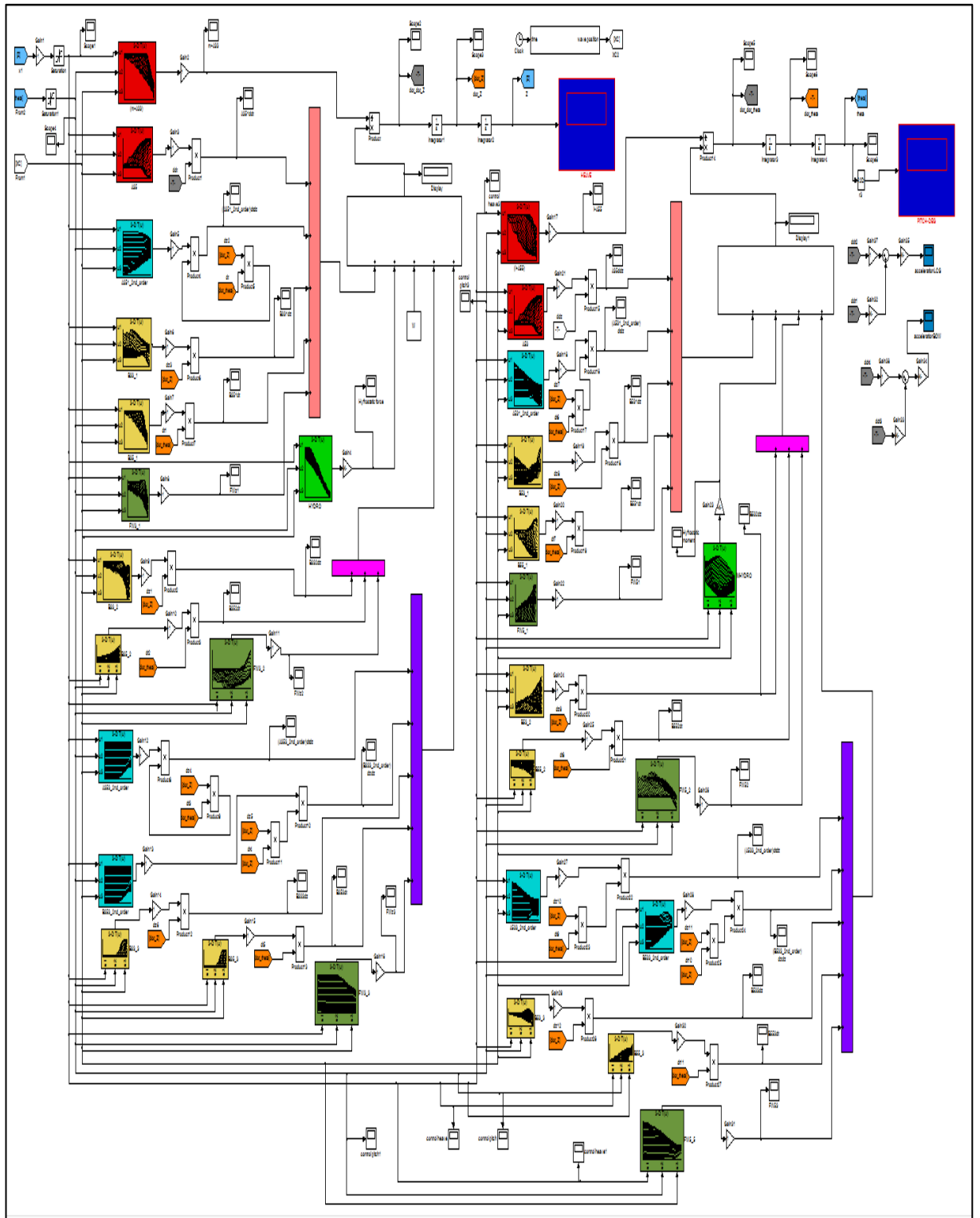


Figure 4.3. Simulink model

The flow chart in Figure 4.4 summarizes the developed code. The Matlab main script, launched for the simulation, calls different functions, previously created. It requires the file that defines the geometry and some input parameters. The first step is to solve the balance in calm sea condition. After the introduction of the wave intersections are calculated, and then: the immersed surface, the added mass and all the forces and factors that enter in the simulation. The same main script calls the Simulink model for the simulation in time. The results, automatically saved, are analysed in time and frequency domain. After calculations, the script asks for the experimental tests file and analyses them in the same manner as numerical. In this way is possible to get comparisons of time series and FFT analysis for numerical against experimental results.

The time step used in simulations is 0.002s the same as the sampling frequency of the experimental tests. This time step can lead to some numerical problems. For the calculation of the accelerations, as in the first model, we proceed to the composition of the motions and the double derivation of the obtained displacement. In some cases, especially for long wave, this samples is too thick causing numerical errors in the calculation of the derivatives and the amplitudes of the higher order harmonics result too high. In these cases it is necessary to reduce the sampling for derivatives, leaving unchanged the simulation step size. For additional control the accelerations are evaluated, also, during the simulation in Simulink. The developed code gives also the partial results as added mass, damping coefficients and forces components acting during the range of simulation chosen.

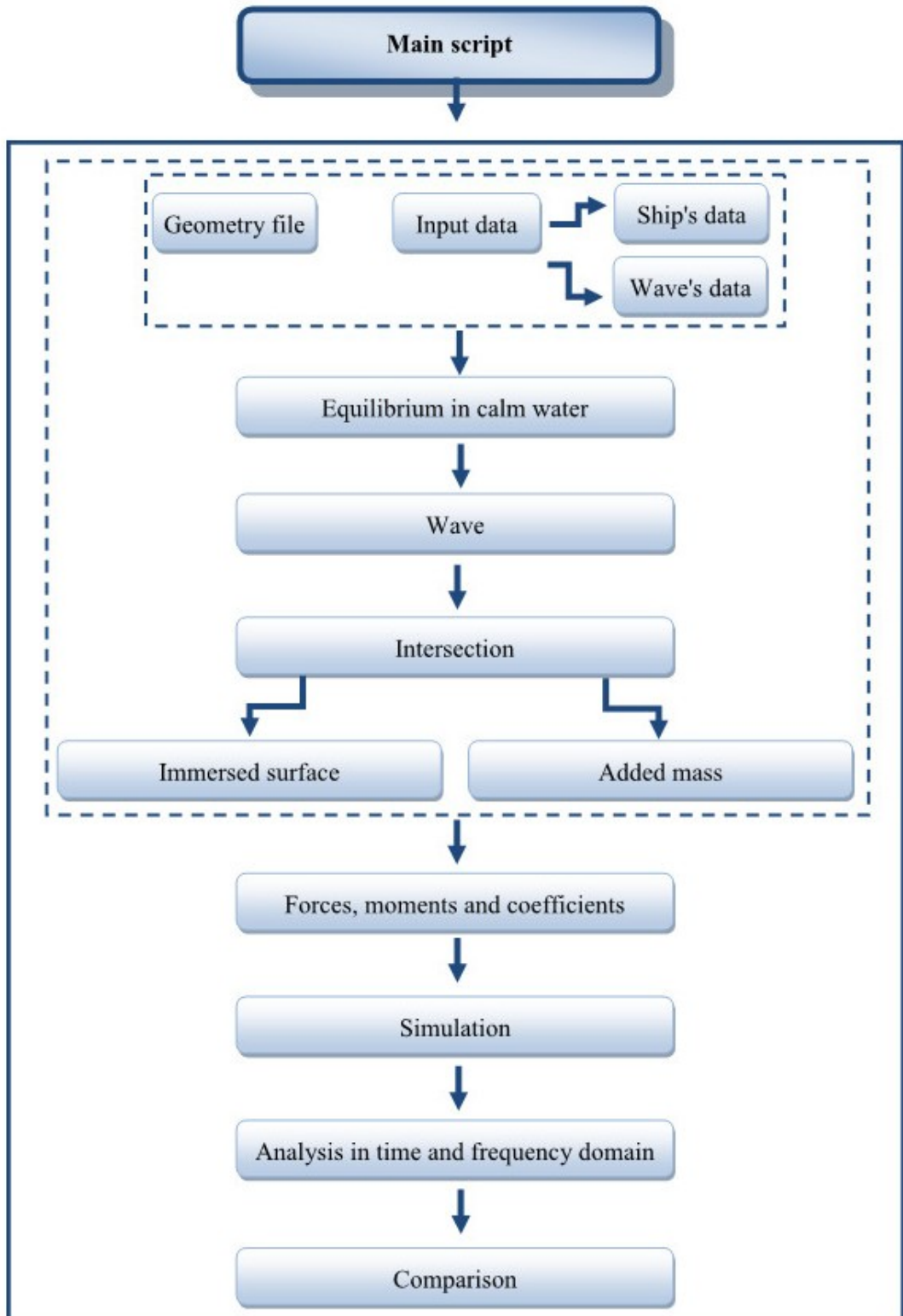


Figure 4.4. Flow chart

4.5 Comparison of numerical and experimental data for monohedral and warped hull

The idea of developing the second fully non-linear code was born after the validation of the first one against warped hull form, as it was expected, the fully nonlinear model could improve the prediction of motions for warped hulls. Therefore the validation of developed model is performed for both models: monohedral hull, shown in Figure 3.13, and for warped hull (WARP 2), shown in Figure 4.5. Principal characteristics of model WARP 2 are given in Table 5, while for monohedral hull are already presented in Table 1.

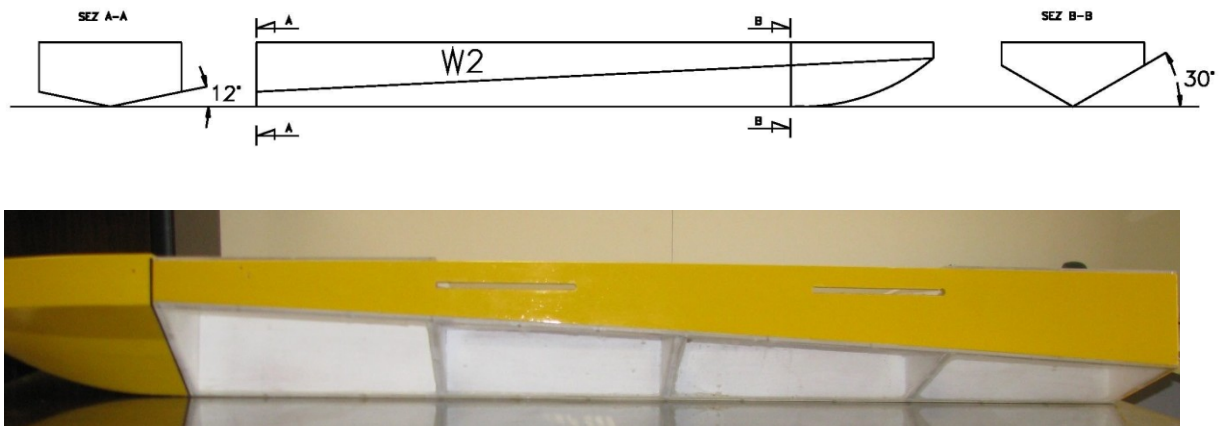


Figure 4.5. Warped hull geometry

Table 5 – WARP 2 model's principal characteristics

WARP 2									
LOA	L _{A-B}	B	T _{AP}	Δ	β	L _{CG}	V _{CG}	k ₄₄	k ₅₅
(m)	(m)	(m)	(m)	(N)	(deg)	(m)	(m)	(m)	(m)
1.9	1.5	0.424	0.110	319.7	11.6 – 30.1	0.609	0.155	0.1286	0.5491

As explained in 3.5 the static trim for monohedral and warped hull is of 1.66 degree astern to assure a realistic running trim of about four degree in both cases. Again all the details about seakeeping tests of WARP 2 can be found in Begovic et al. (2014).

Numerical calculations are performed for wave amplitudes measured in seakeeping tests, reported in Table 2 and for input condition summarized in Table 6.

Table 6 – Calm water values – input for seakeeping calculations

v (m/s)		MONO	WARP 2
3.4	Running trim (deg)	3.972	4.179
	Sinkage (mm)	-3.648	4.965
4.6	Running trim (deg)	4.174	4.145
	Sinkage (mm)	9.705	22.50
5.75	Running trim (deg)	4.024	3.221
	Sinkage (mm)	17.425	29.601

Examples of calculated vs. measured responses are given from Figure 4.6 to Figure 4.41 for monohedral hull and from Figure 4.42 to for warped hull, for three speeds of 3.4 m/s, 4.6 m/s and 5.75 m/s, corresponding respectively to $F_{rv} = 1.92$, 2.60 and 3.25, end for three wave's frequencies of 0.9, 0.65 and 0.45 Hz.

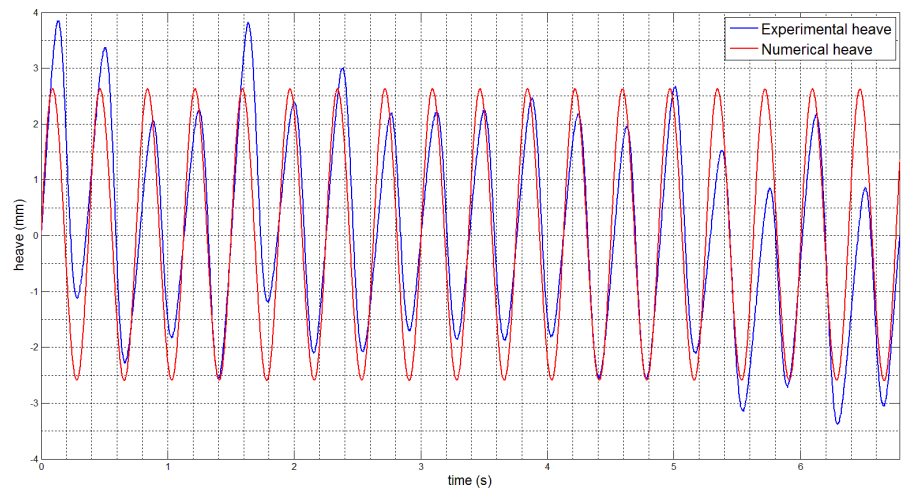


Figure 4.6. Numerical vs. experimental heave, $v=3.4$ m/s and $f=0.9$ Hz - MONO

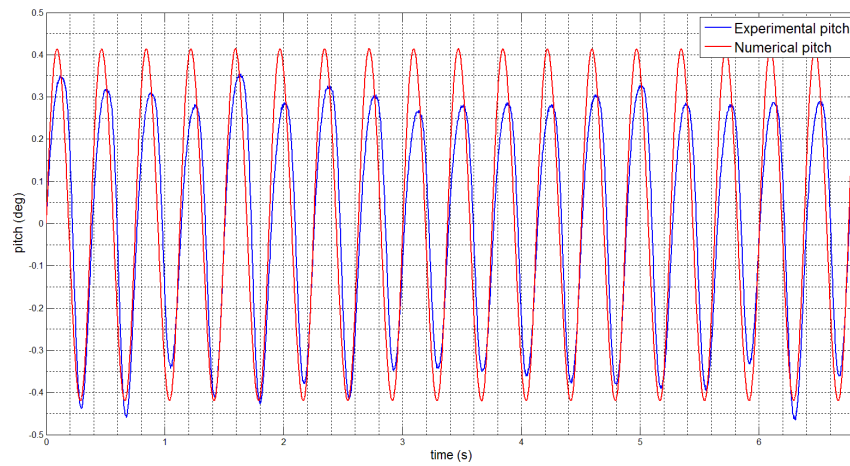


Figure 4.7. Numerical vs. experimental pitch, $v=3.4$ m/s and $f=0.9$ Hz - MONO

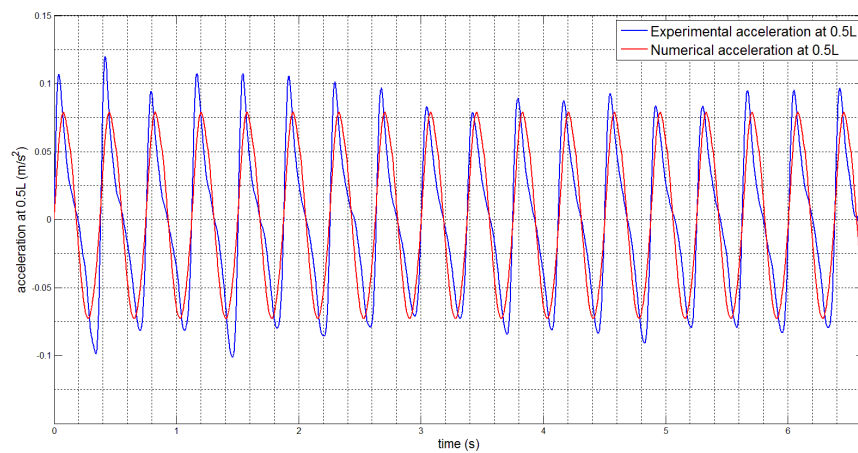


Figure 4.8. Numerical vs. experimental acceleration at CG, $v=3.4$ m/s and $f=0.9$ Hz - MONO

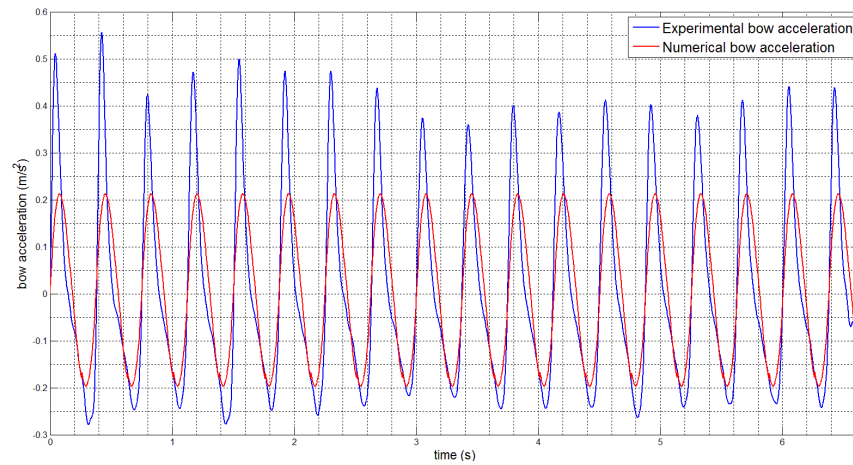


Figure 4.9. Numerical vs. experimental acceleration at bow, $v=3.4$ m/s and $f=0.9$ Hz- MONO

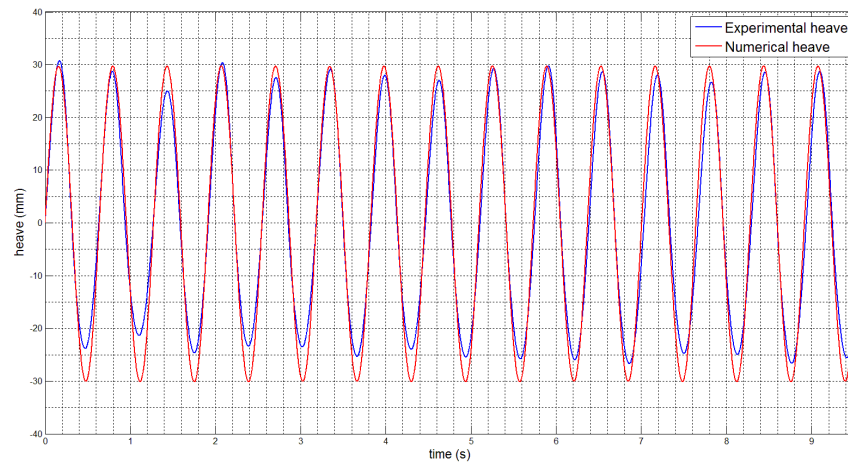


Figure 4.10. Numerical vs. experimental heave, $v=3.4$ m/s and $f=0.65$ Hz - MONO

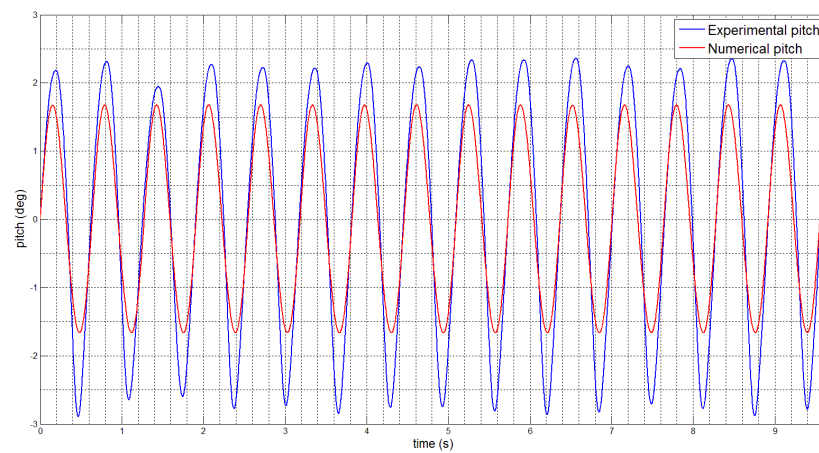


Figure 4.11. Numerical vs. experimental pitch, $v=3.4$ m/s and $f=0.65$ Hz - MONO

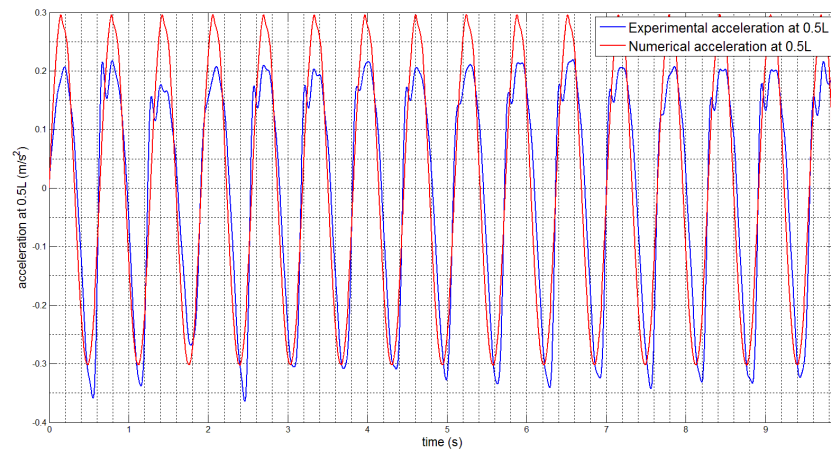


Figure 4.12. Numerical vs. experimental acceleration at CG, $v=3.4$ m/s and $f=0.65$ Hz - MONO

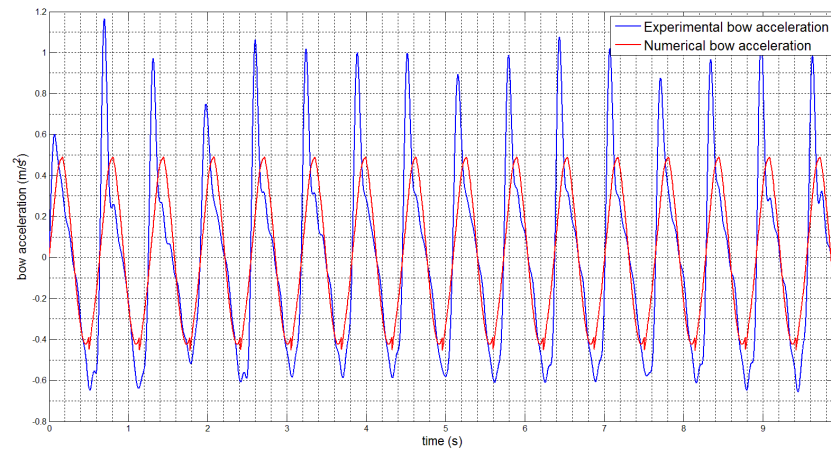


Figure 4.13. Numerical vs. experimental acceleration at bow, $v=3.4$ m/s and $f=0.65$ Hz - MONO

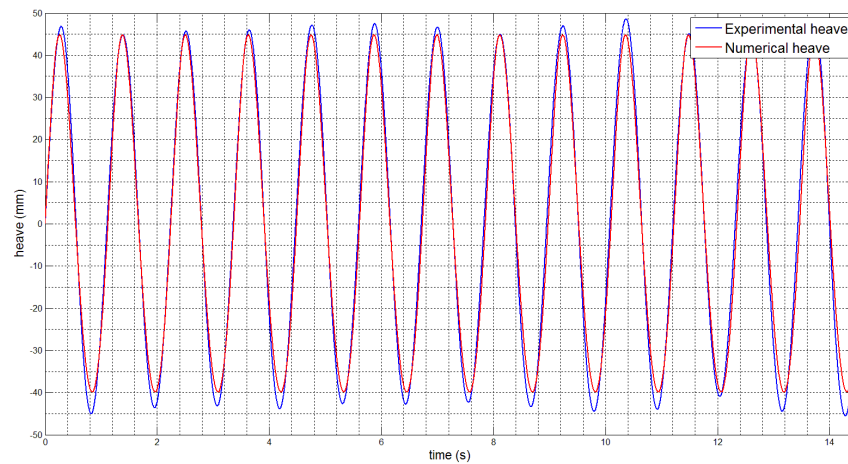


Figure 4.14. Numerical vs. experimental heave, $v=3.4$ m/s and $f=0.45$ Hz - MONO

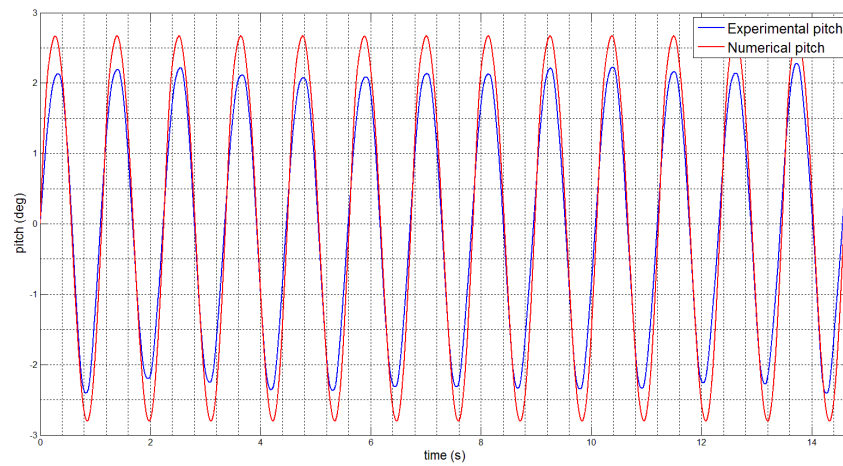


Figure 4.15. Numerical vs. experimental pitch, $v=3.4$ m/s and $f=0.45$ Hz - MONO

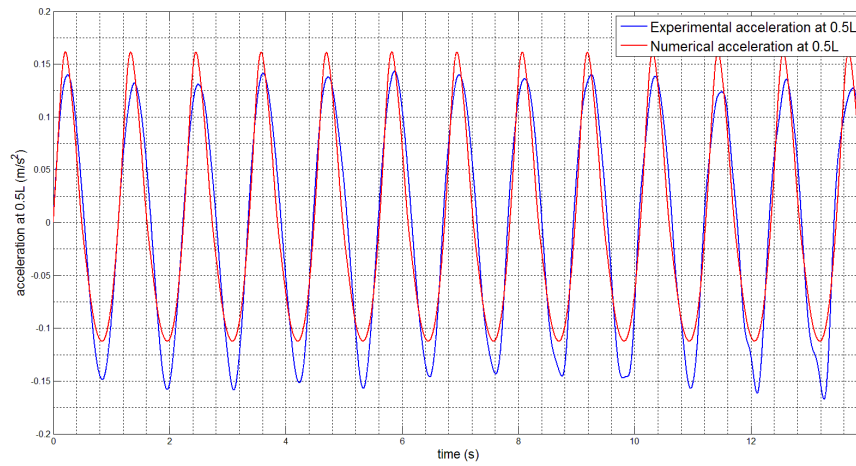


Figure 4.16. Numerical vs. experimental acceleration at CG, $v=3.4$ m/s and $f=0.45$ Hz - MONO

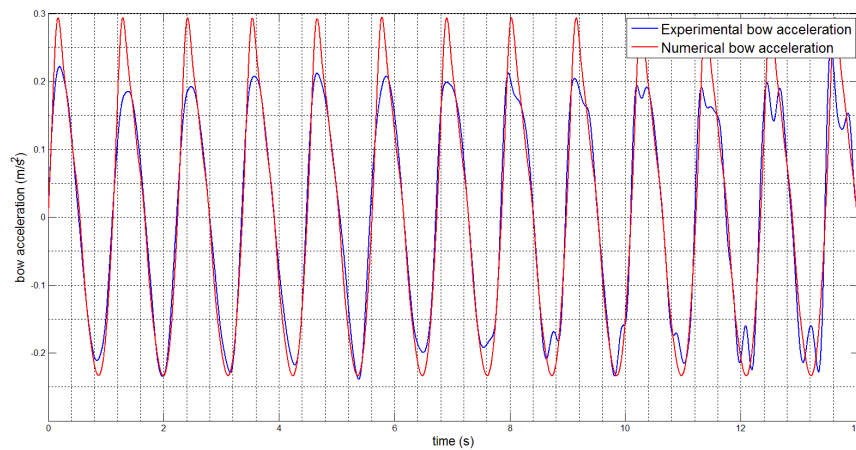


Figure 4.17. Numerical vs. experimental acceleration at bow, $v=3.4$ m/s and $f=0.45$ Hz - MONO

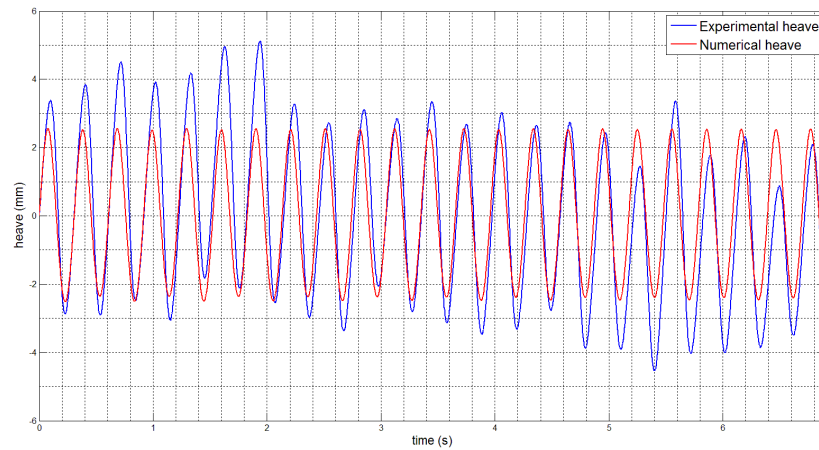


Figure 4.18. Numerical vs. experimental heave, $v=4.6$ m/s and $f=0.9$ Hz - MONO

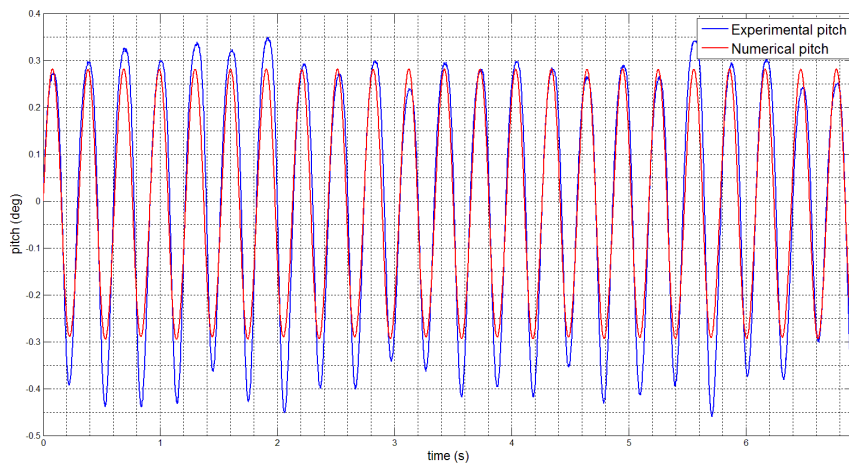


Figure 4.19. Numerical vs. experimental pitch, $v=4.6$ m/s and $f=0.9$ Hz - MONO

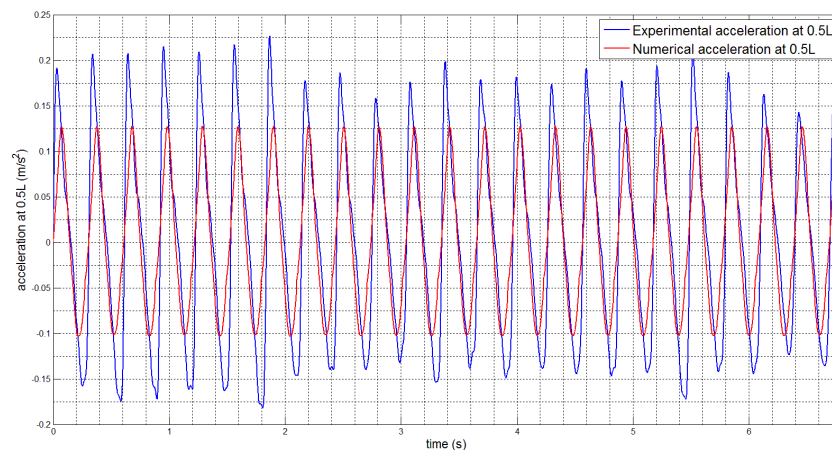


Figure 4.20. Numerical vs. experimental acceleration at CG, $v=4.6$ m/s and $f=0.9$ Hz - MONO

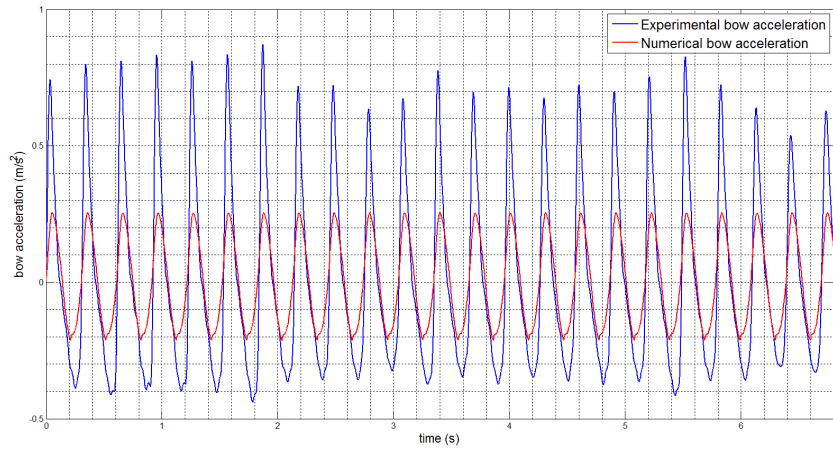


Figure 4.21. Numerical vs. experimental acceleration at bow, $v=4.6$ m/s and $f=0.9$ Hz - MONO

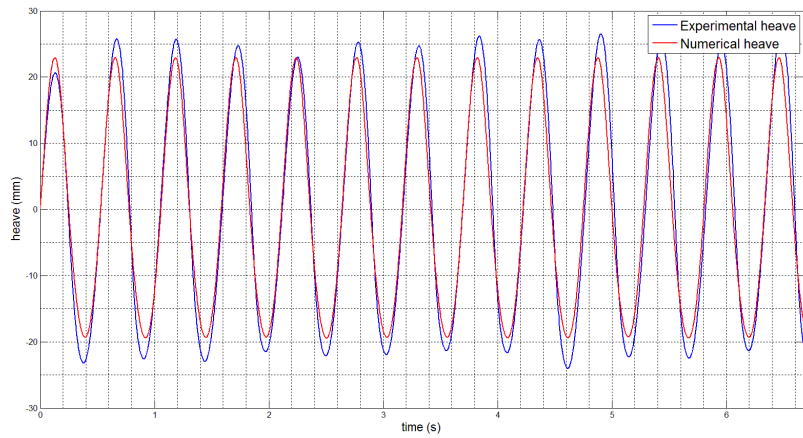


Figure 4.22. Numerical vs. experimental heave, $v=4.6$ m/s and $f=0.65$ Hz - MONO

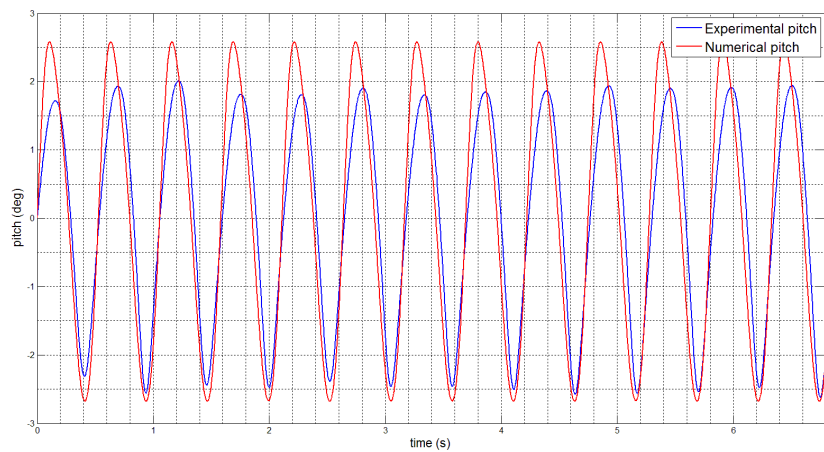


Figure 4.23. Numerical vs. experimental pitch, $v=4.6$ m/s and $f=0.65$ Hz - MONO

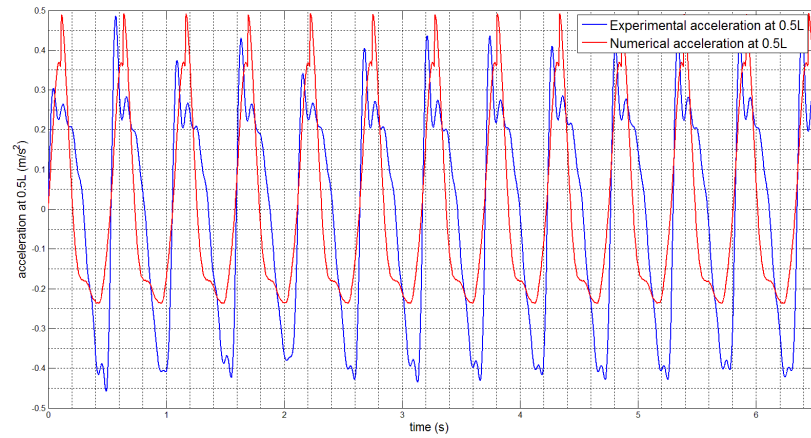


Figure 4.24. Numerical vs. experimental acceleration at CG, $v=4.6$ m/s and $f=0.65$ Hz - MONO

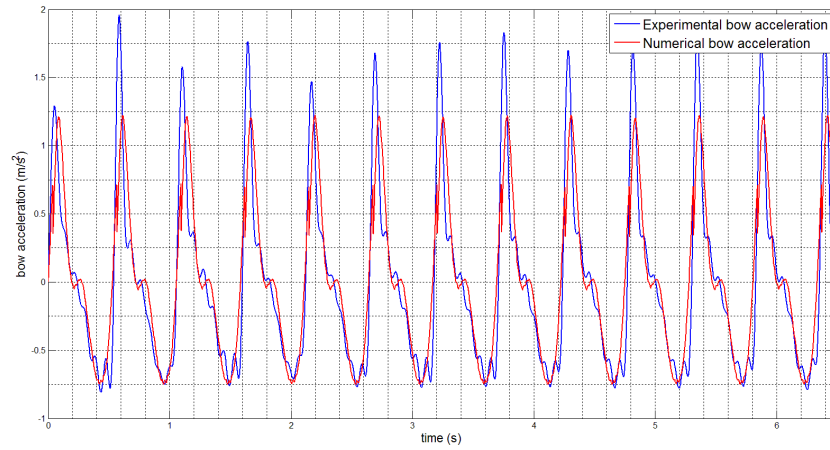


Figure 4.25. Numerical vs. experimental acceleration at bow, $v=4.6$ m/s and $f=0.65$ Hz - MONO

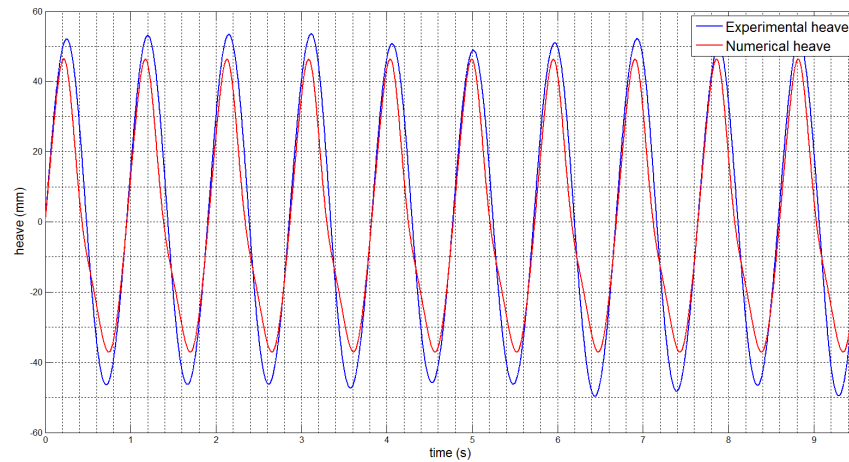


Figure 4.26. Numerical vs. experimental heave, $v=4.6$ m/s and $f=0.45$ Hz - MONO

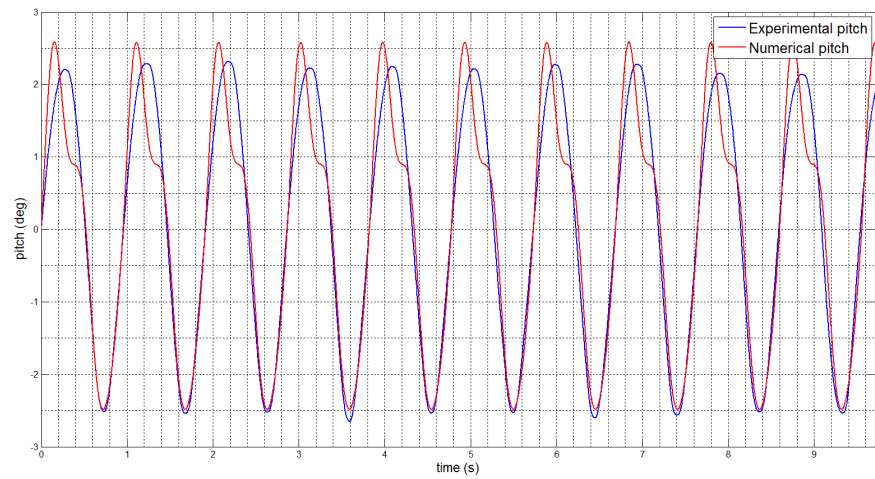


Figure 4.27. Numerical vs. experimental pitch, $v=4.6$ m/s and $f=0.45$ Hz - MONO

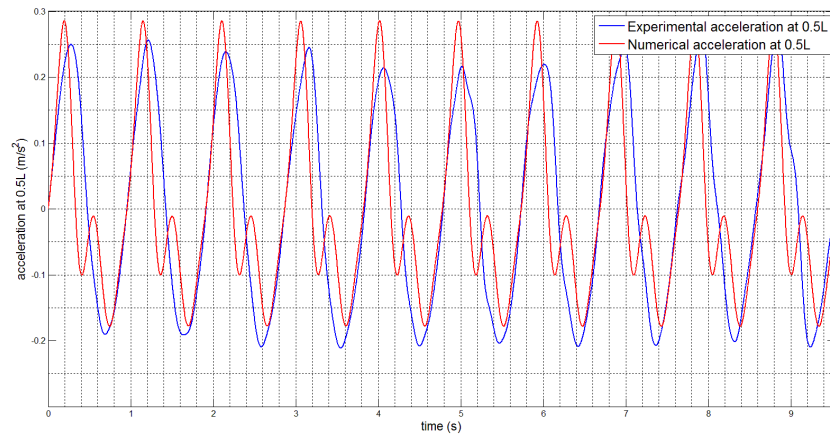


Figure 4.28. Numerical vs. experimental acceleration at CG, $v=4.6$ m/s and $f=0.45$ Hz - MONO

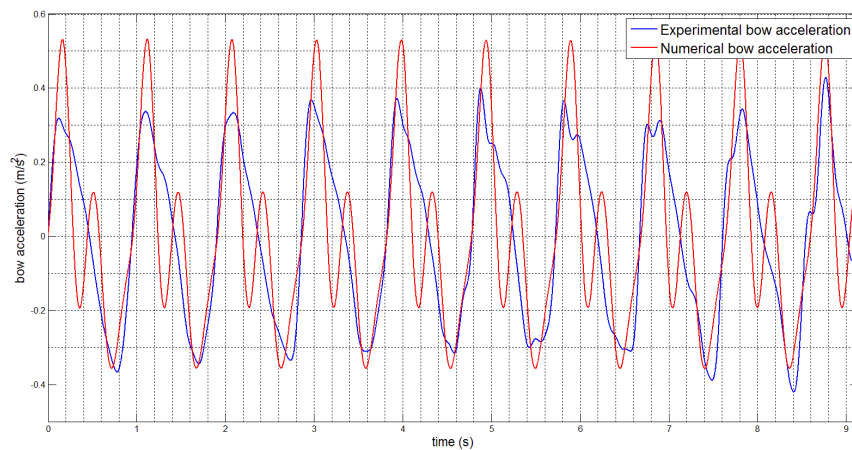


Figure 4.29. Numerical vs. experimental acceleration at bow, $v=4.6$ m/s and $f=0.45$ Hz - MONO

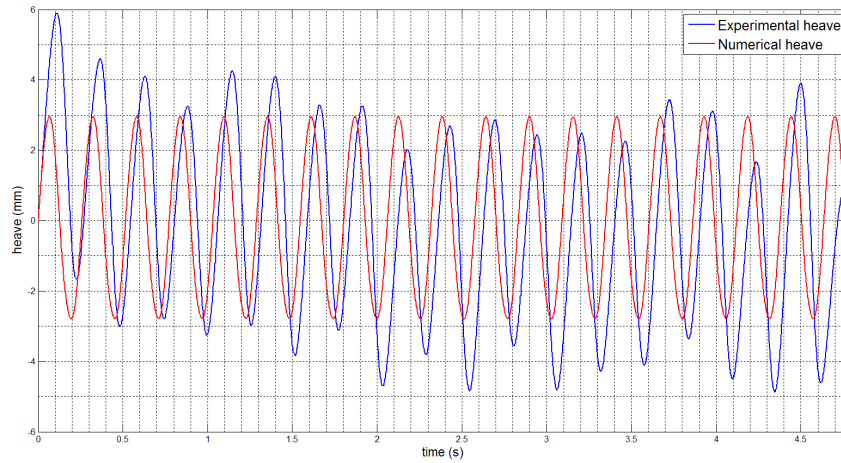


Figure 4.30. Numerical vs. experimental heave, $v=5.75$ m/s and $f=0.9$ Hz - MONO

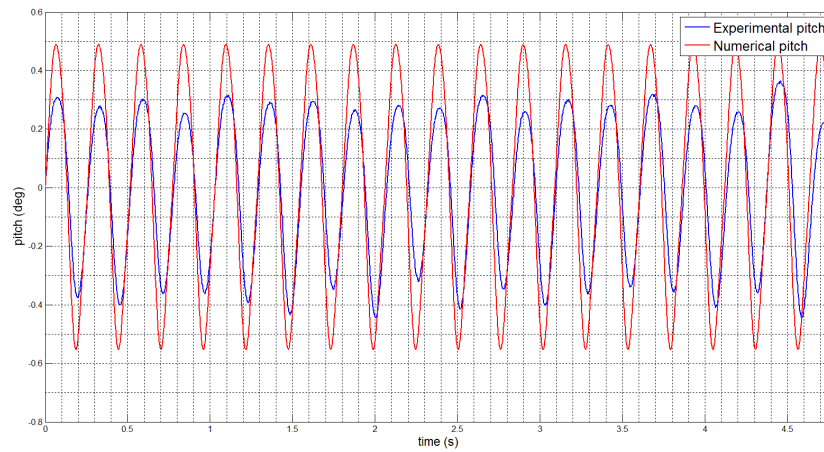


Figure 4.31. Numerical vs. experimental pitch, $v=5.75$ m/s and $f=0.9$ Hz - MONO

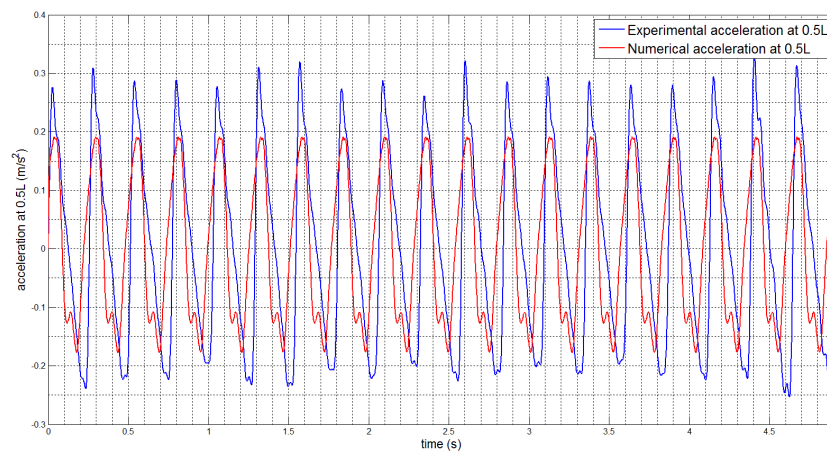


Figure 4.32. Numerical vs. experimental acceleration at CG, $v=5.75$ m/s and $f=0.9$ Hz - MONO

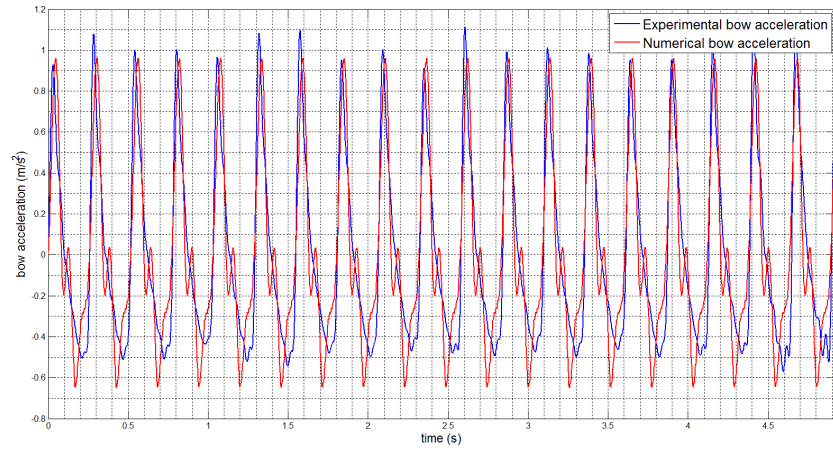


Figure 4.33. Numerical vs. experimental acceleration at bow, $v=5.75 \text{ m/s}$ and $f=0.9 \text{ Hz}$ - MONO

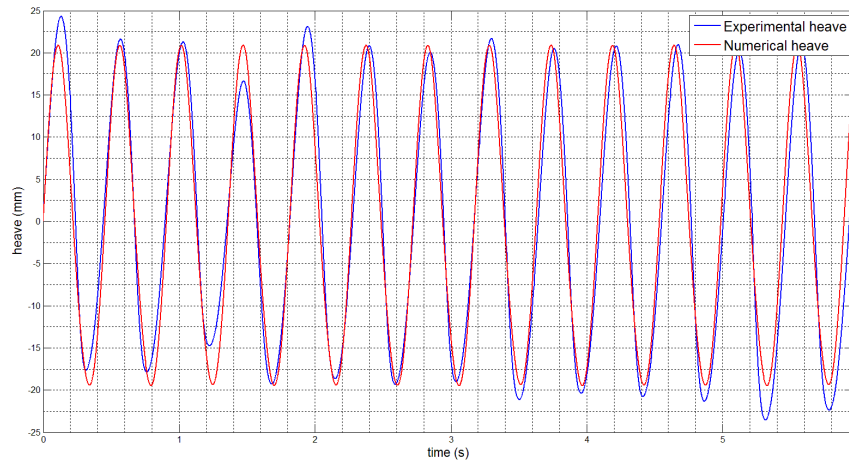


Figure 4.34. Numerical vs. experimental heave, $v=5.75 \text{ m/s}$ and $f=0.65 \text{ Hz}$ - MONO

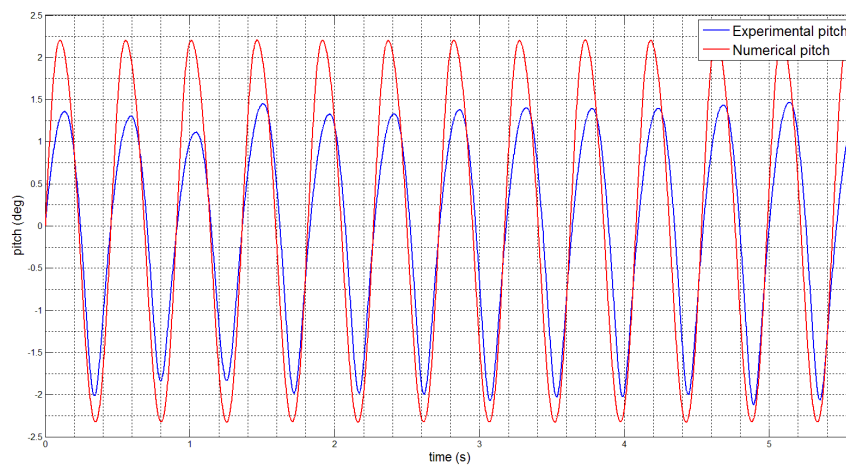


Figure 4.35. Numerical vs. experimental pitch, $v=5.75 \text{ m/s}$ and $f=0.65 \text{ Hz}$ - MONO

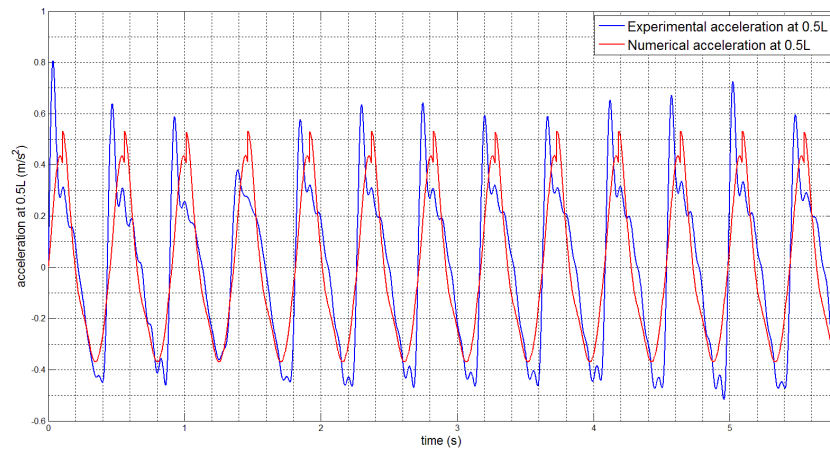


Figure 4.36. Numerical vs. experimental acceleration at CG, $v=5.75$ m/s and $f=0.65$ Hz - MONO

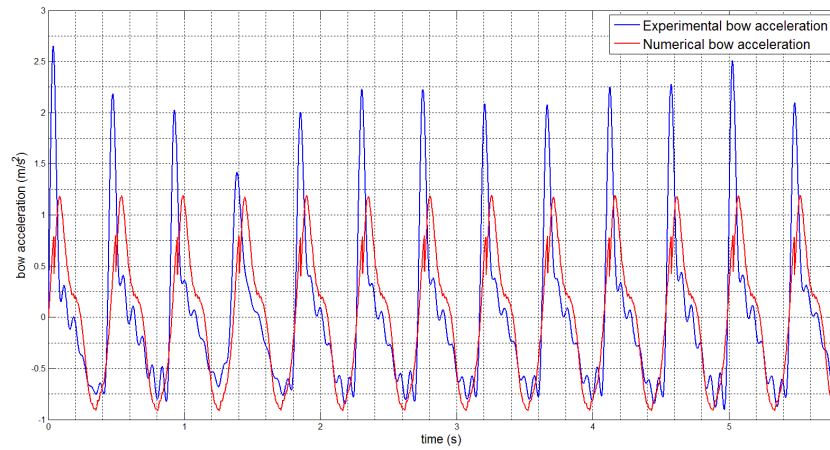


Figure 4.37. Numerical vs. experimental acceleration at bow, $v=5.75$ m/s and $f=0.65$ Hz - MONO

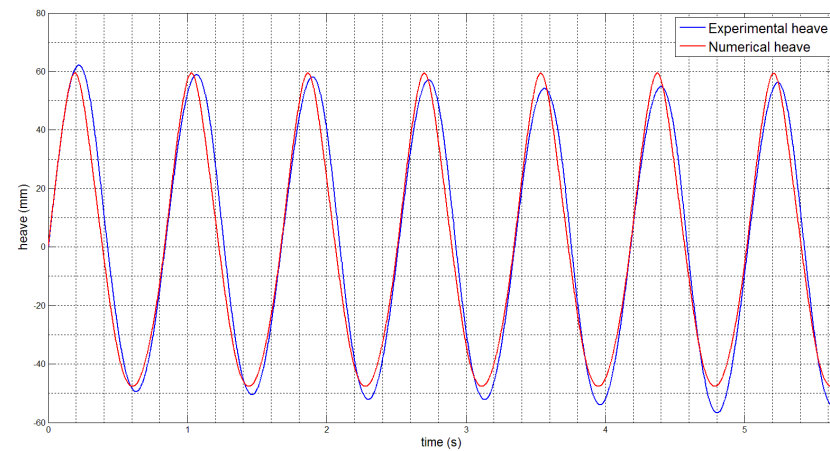


Figure 4.38. Numerical vs. experimental heave, $v=5.75$ m/s and $f=0.45$ Hz - MONO

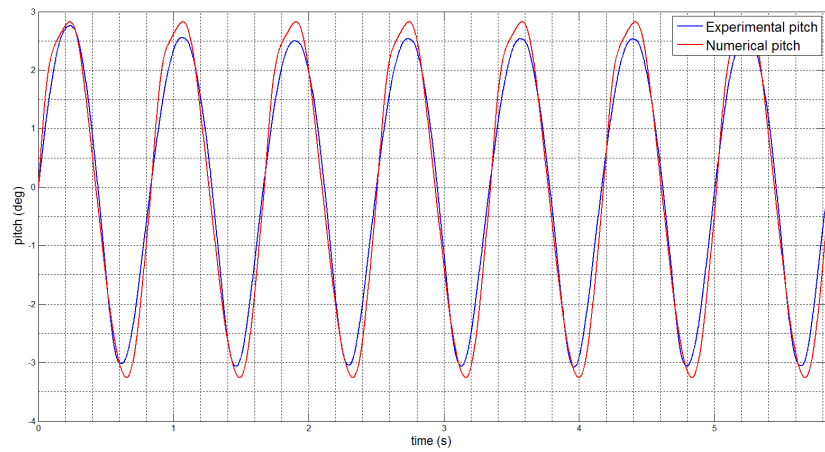


Figure 4.39. Numerical vs. experimental pitch, $v=5.75$ m/s and $f=0.45$ Hz - MONO

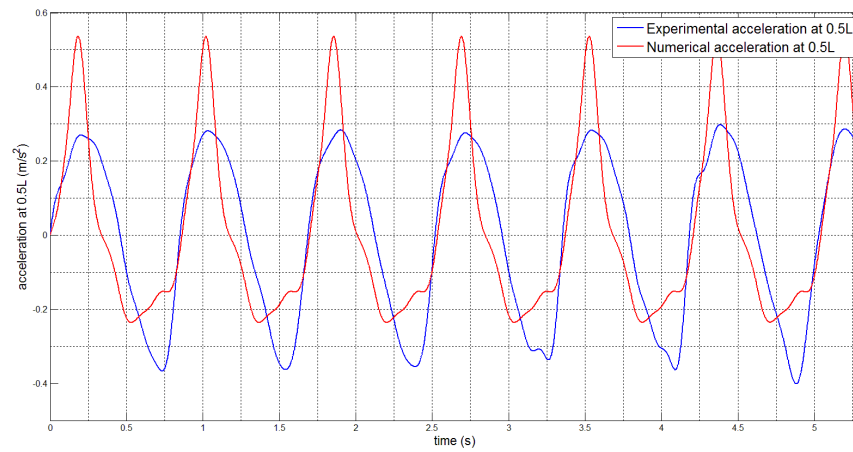


Figure 4.40. Numerical vs. experimental acceleration at CG, $v=5.75$ m/s and $f=0.45$ Hz - MONO

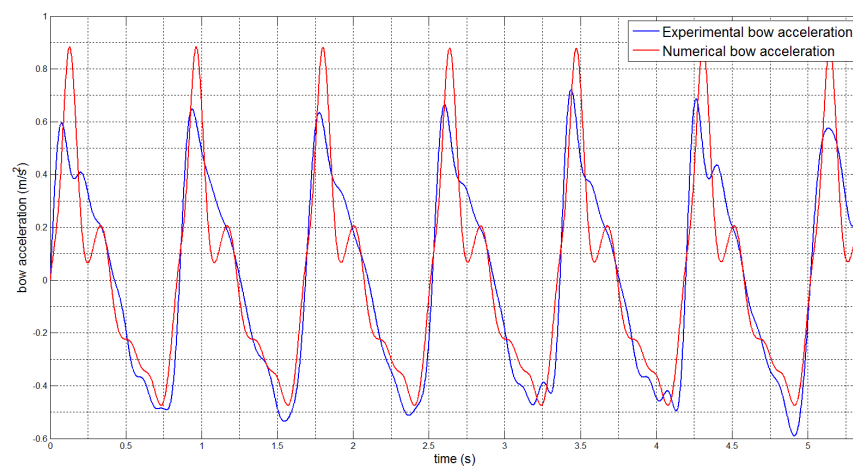


Figure 4.41. Numerical vs. experimental acceleration at bow, $v=5.75$ m/s and $f=0.45$ Hz - MONO

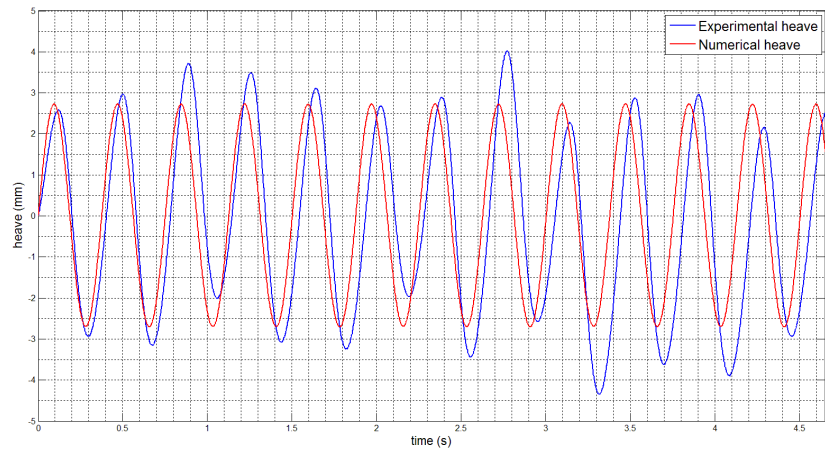


Figure 4.42. Numerical vs. experimental heave, $v=3.4$ m/s and $f=0.9$ Hz - W2

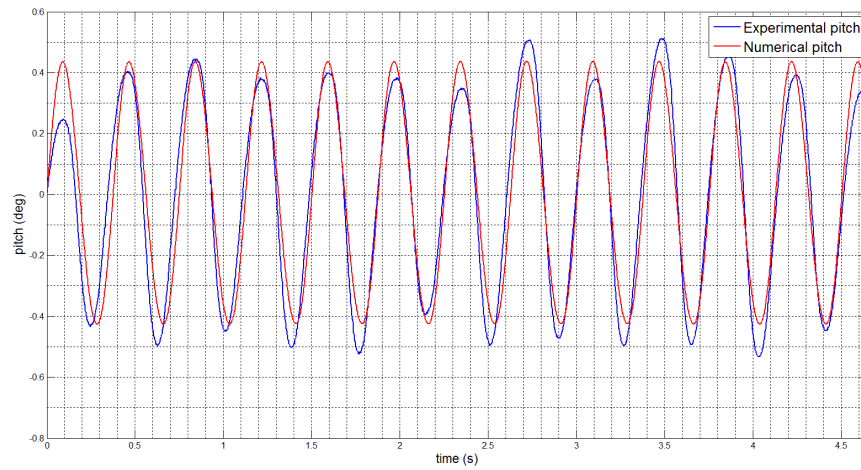


Figure 4.43. Numerical vs. experimental pitch, $v=3.4$ m/s and $f=0.9$ Hz - W2

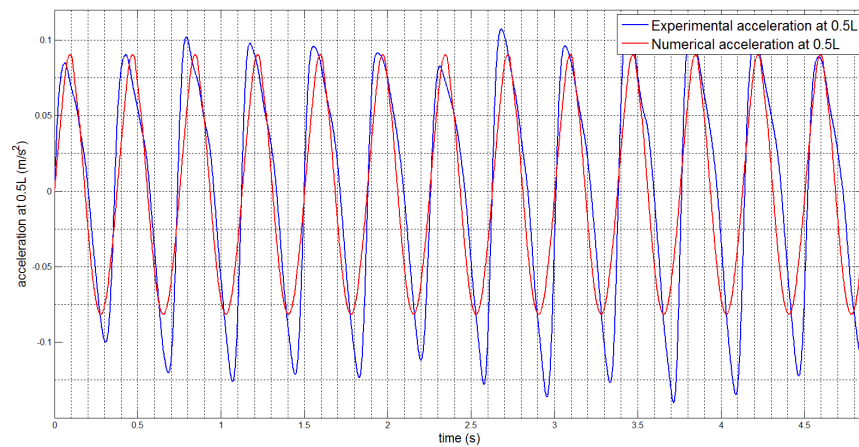


Figure 4.44. Numerical vs. experimental acceleration at CG, $v=3.4$ m/s and $f=0.9$ Hz - W2

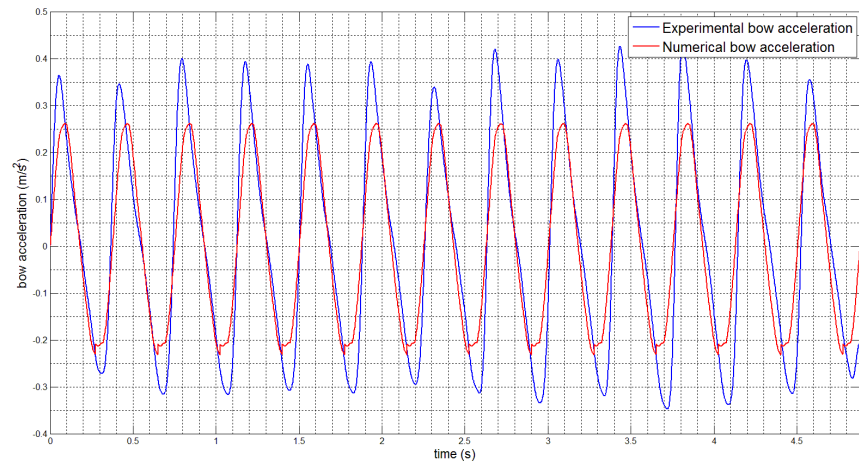


Figure 4.45. Numerical vs. experimental acceleration at bow, $v=3.4$ m/s and $f=0.9$ Hz - $W2$

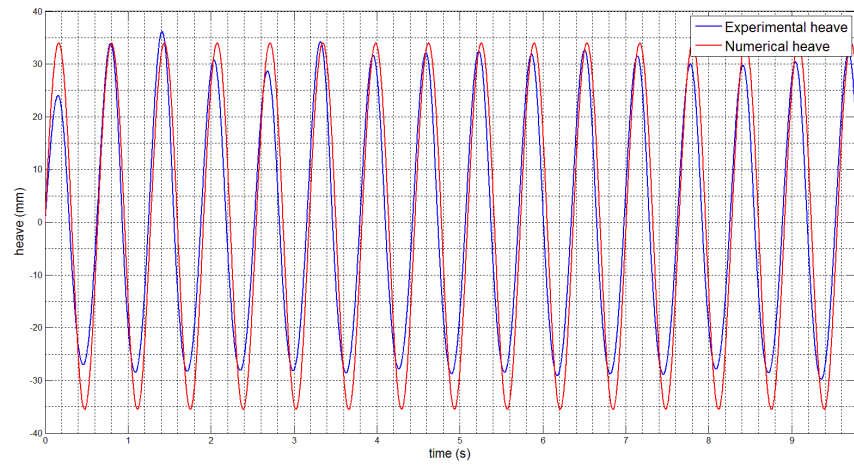


Figure 4.46. Numerical vs. experimental heave, $v=3.4$ m/s and $f=0.65$ Hz - $W2$

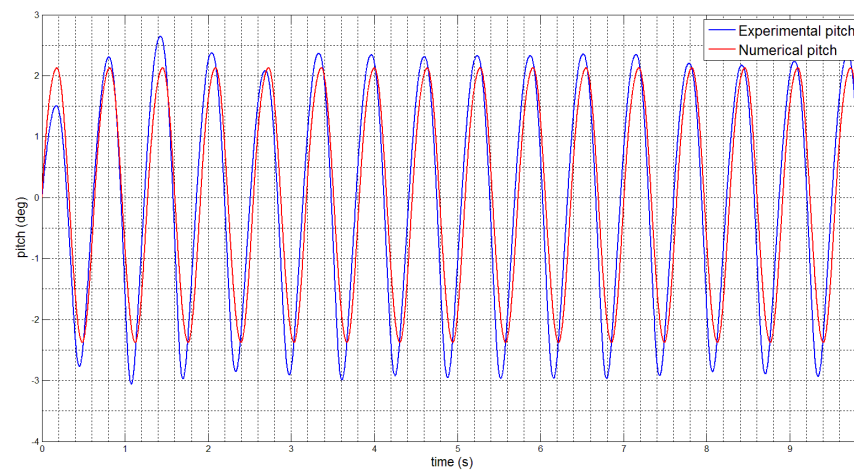


Figure 4.47. Numerical vs. experimental pitch, $v=3.4$ m/s and $f=0.65$ Hz - $W2$

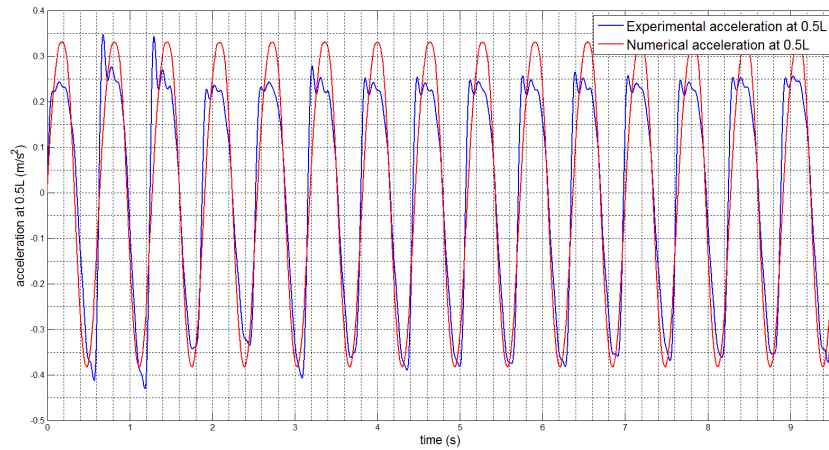


Figure 4.48. Numerical vs. experimental acceleration at CG, $v=3.4$ m/s and $f=0.65$ Hz - $W2$

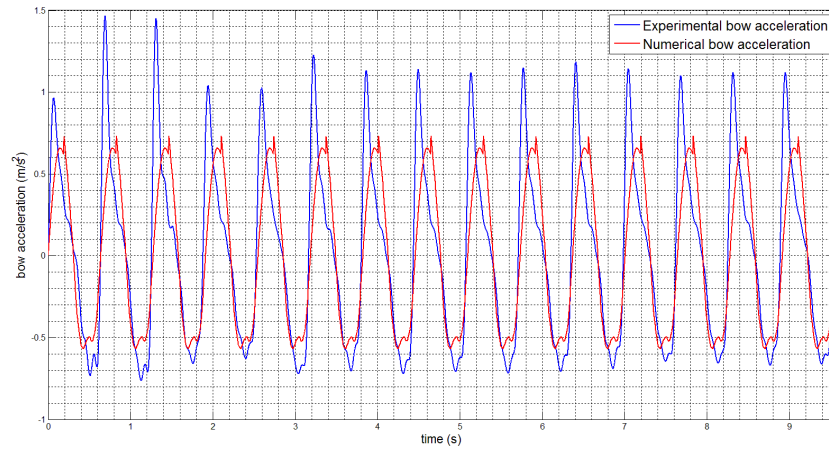


Figure 4.49. Numerical vs. experimental acceleration at bow, $v=3.4$ m/s and $f=0.65$ Hz - $W2$

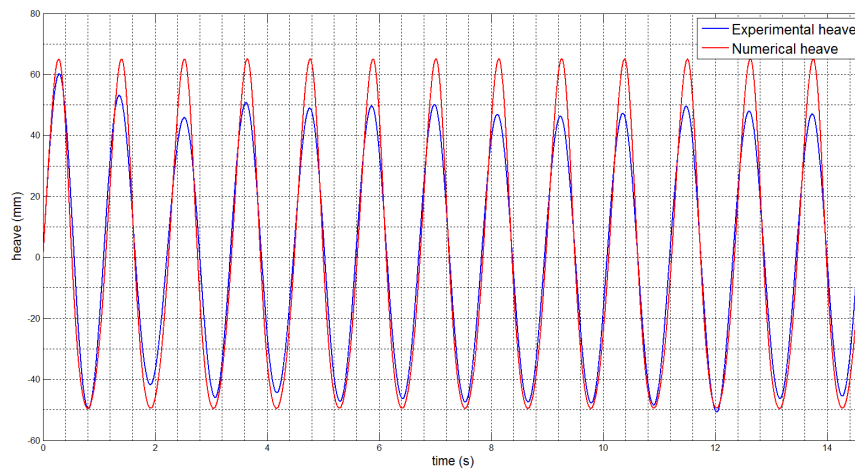


Figure 4.50. Numerical vs. experimental heave, $v=3.4$ m/s and $f=0.45$ Hz - $W2$

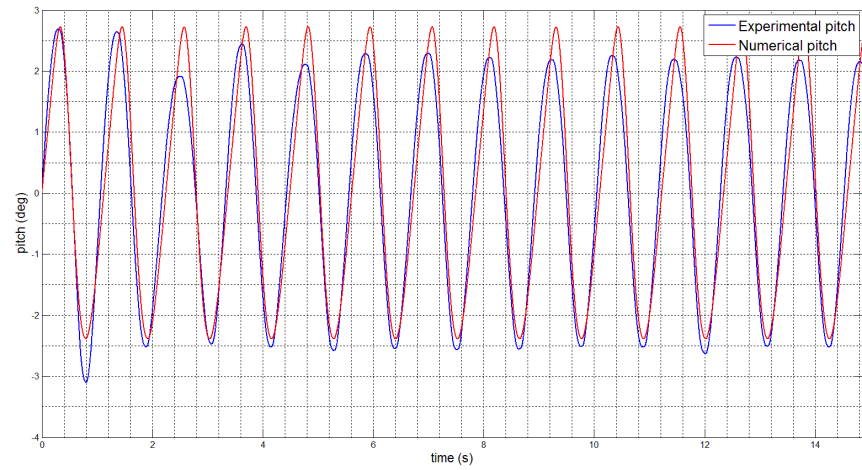


Figure 4.51. Numerical vs. experimental pitch, $v=3.4$ m/s and $f=0.45$ Hz - $W2$

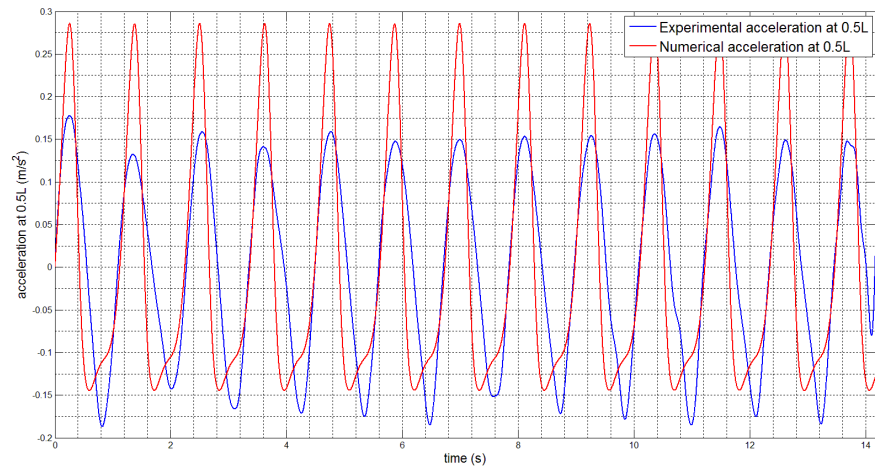


Figure 4.52. Numerical vs. experimental acceleration at CG, $v=3.4$ m/s and $f=0.45$ Hz - $W2$

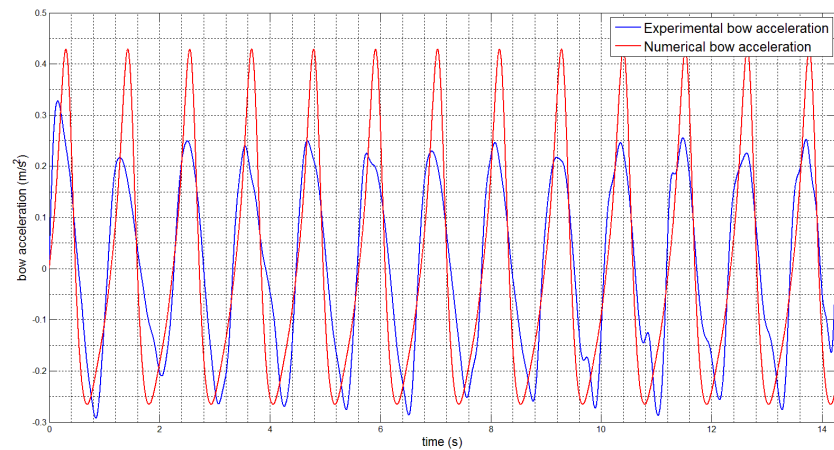


Figure 4.53. Numerical vs. experimental acceleration at bow, $v=3.4$ m/s and $f=0.45$ Hz - $W2$

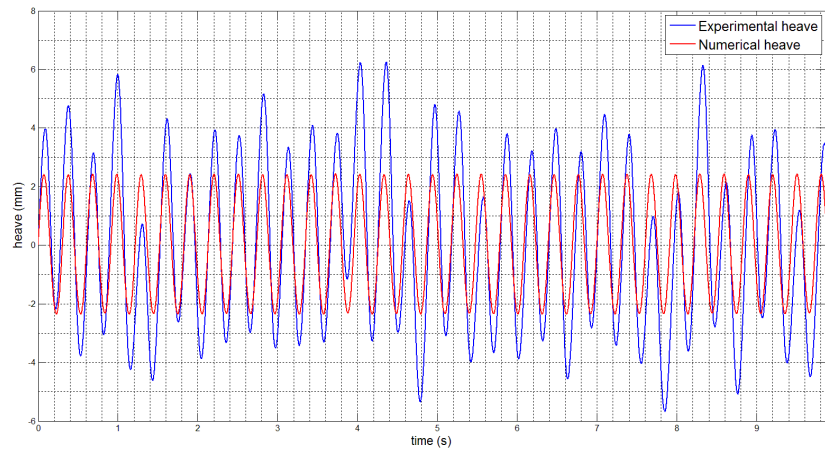


Figure 4.54. Numerical vs. experimental heave, $v=4.6$ m/s and $f=0.9$ Hz - $W2$

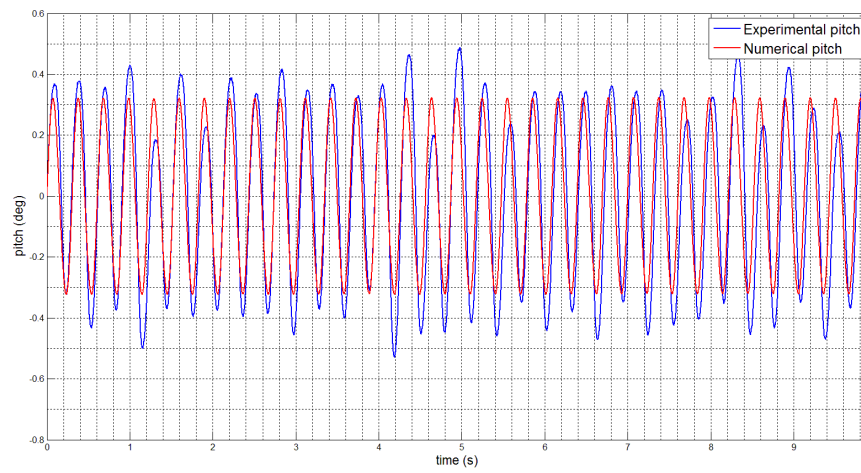


Figure 4.55. Numerical vs. experimental pitch, $v=4.6$ m/s and $f=0.9$ Hz - $W2$

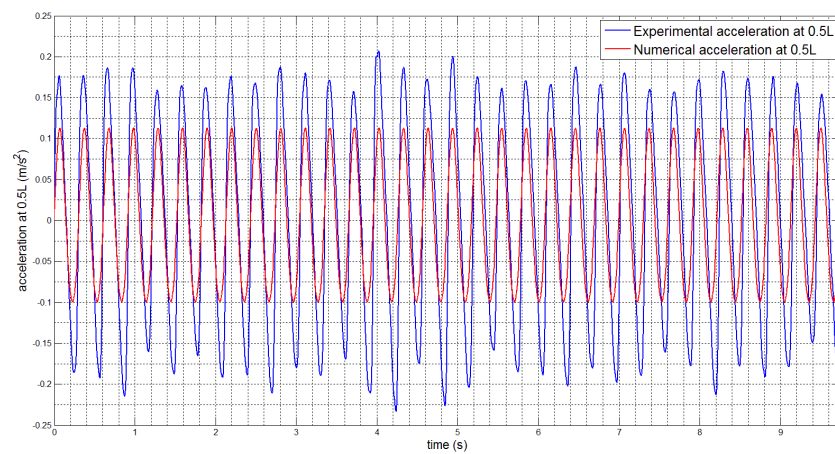


Figure 4.56. Numerical vs. experimental acceleration at CG, $v=4.6$ m/s and $f=0.9$ Hz - $W2$

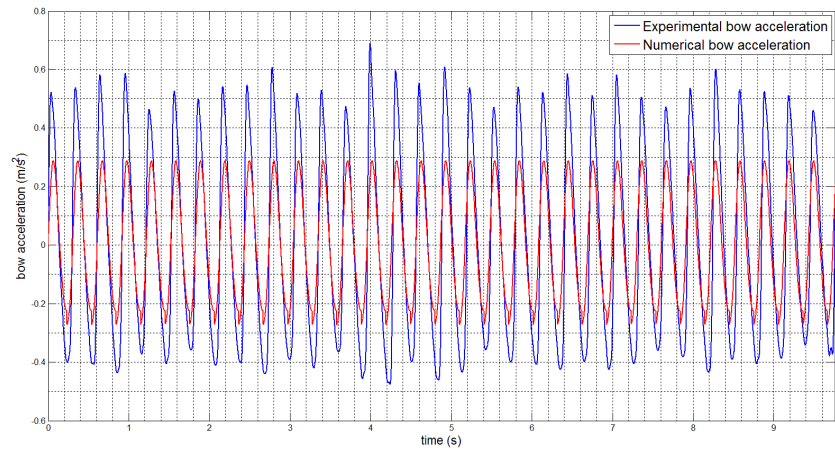


Figure 4.57. Numerical vs. experimental acceleration at bow, $v=4.6$ m/s and $f=0.9$ Hz - W2

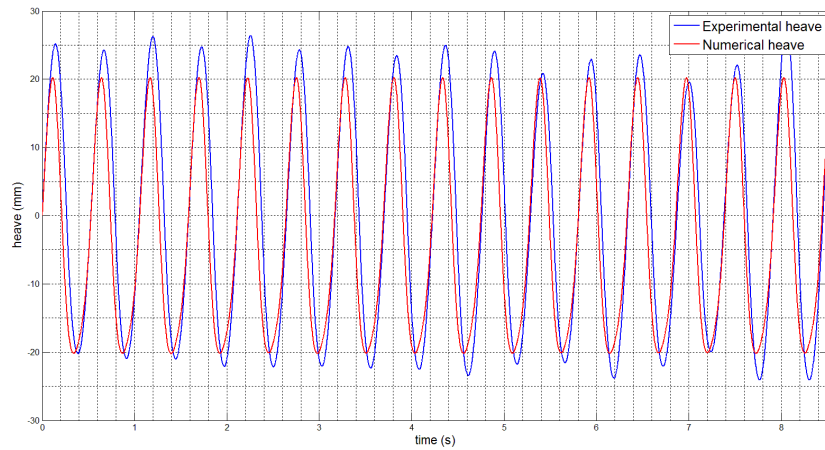


Figure 4.58. Numerical vs. experimental heave, $v=4.6$ m/s and $f=0.65$ Hz - W2

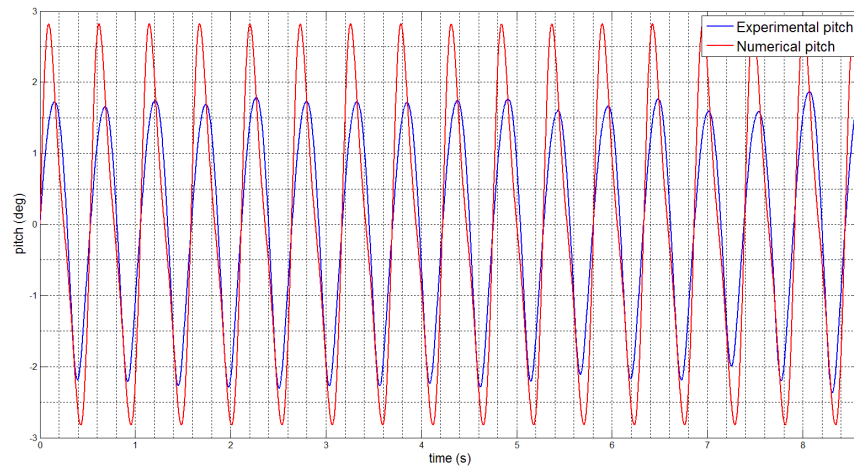


Figure 4.59. Numerical vs. experimental pitch, $v=4.6$ m/s and $f=0.65$ Hz - W2

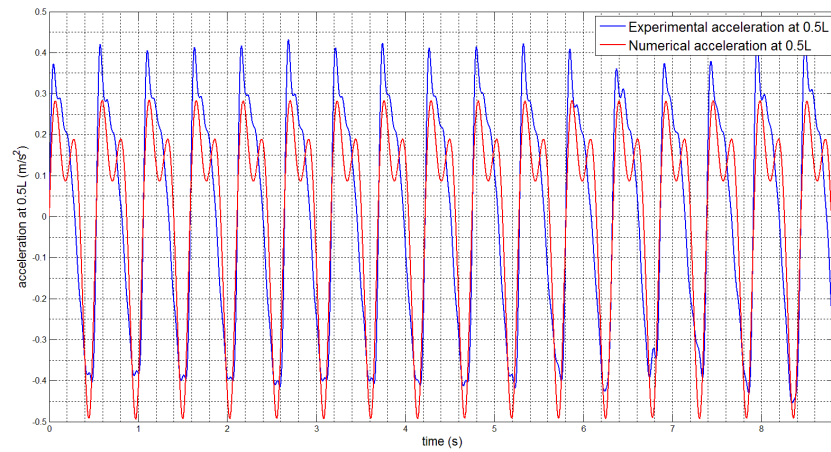


Figure 4.60. Numerical vs. experimental acceleration at CG, $v=4.6$ m/s and $f=0.65$ Hz - $W2$

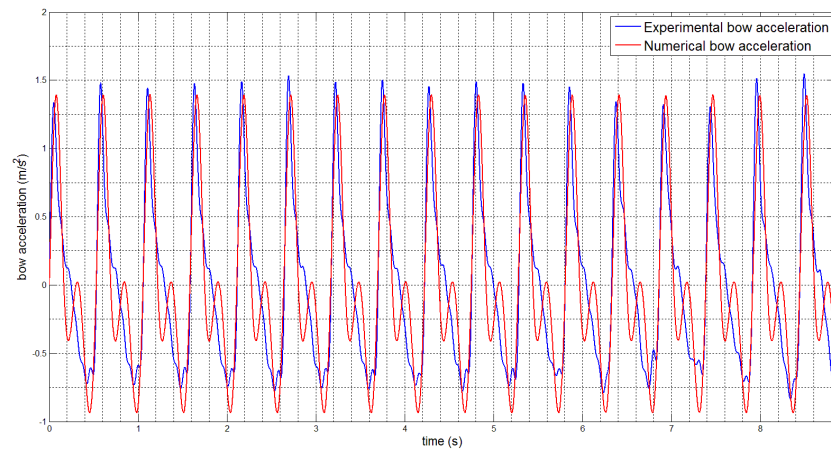


Figure 4.61. Numerical vs. experimental acceleration at bow, $v=4.6$ m/s and $f=0.65$ Hz - $W2$

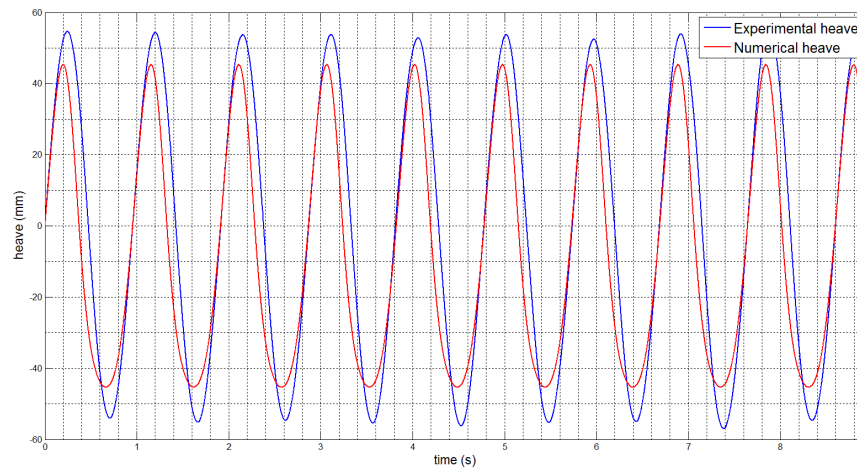


Figure 4.62. Numerical vs. experimental heave, $v=4.6$ m/s and $f=0.45$ Hz - $W2$

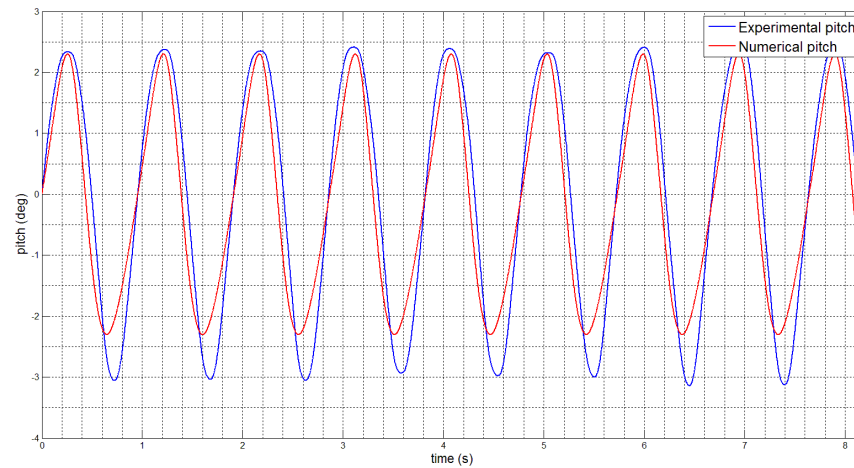


Figure 4.63. Numerical vs. experimental pitch, $v=4.6$ m/s and $f=0.45$ Hz - $W2$

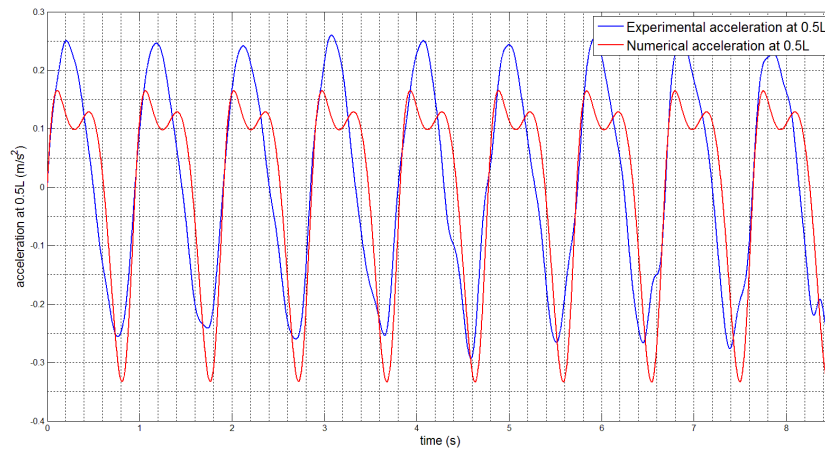


Figure 4.64. Numerical vs. experimental acceleration at CG, $v=4.6$ m/s and $f=0.45$ Hz - $W2$

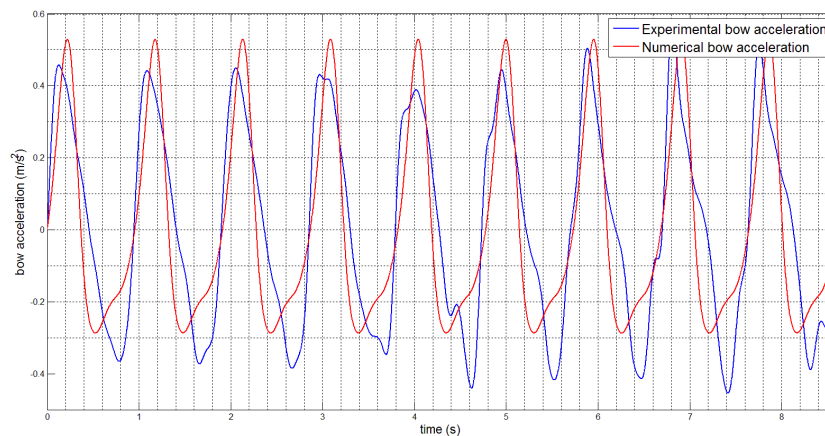


Figure 4.65. Numerical vs. experimental acceleration at bow, $v=4.6$ m/s and $f=0.45$ Hz - $W2$

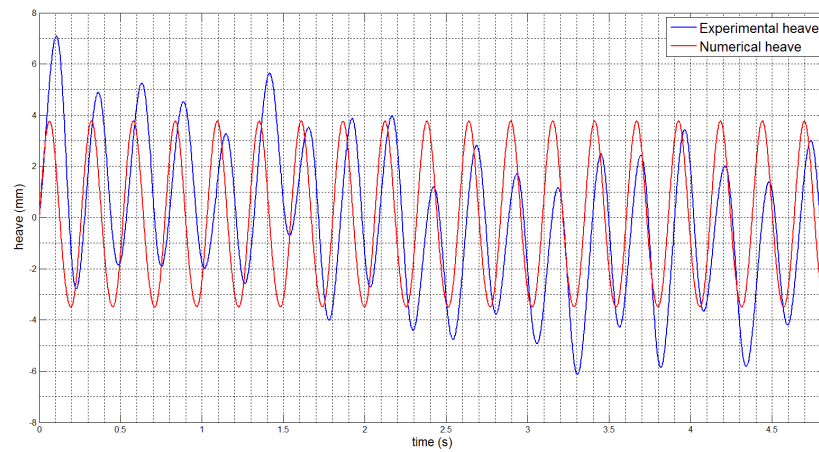


Figure 4.66. Numerical vs. experimental heave, $v=5.75$ m/s and $f=0.9$ Hz - W2

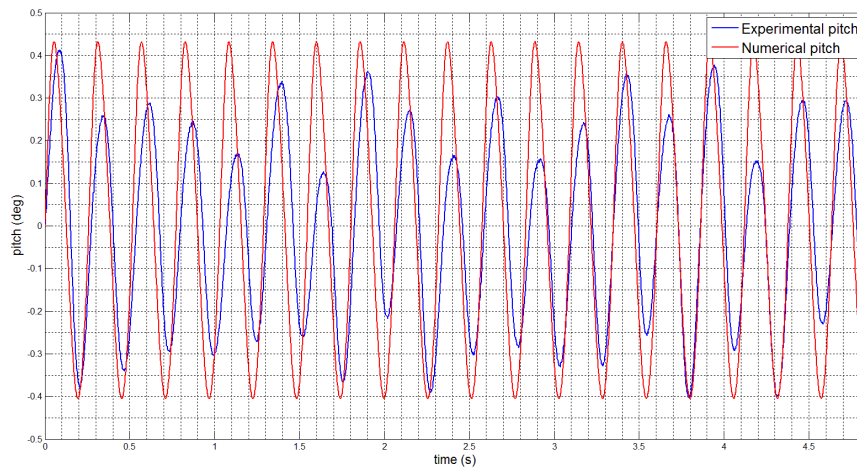


Figure 4.67. Numerical vs. experimental pitch, $v=5.75$ m/s and $f=0.9$ Hz - W2

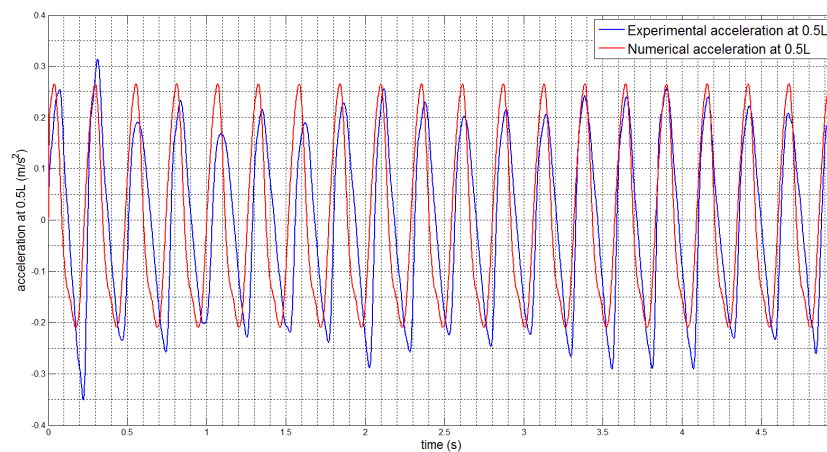


Figure 4.68. Numerical vs. experimental acceleration at CG, $v=5.75$ m/s and $f=0.9$ Hz - W2

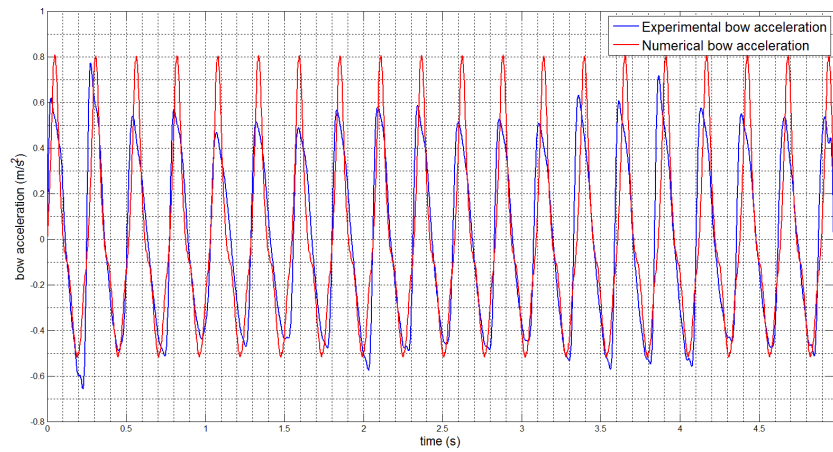


Figure 4.69. Numerical vs. experimental acceleration at bow, $v=5.75$ m/s and $f=0.9$ Hz - W2

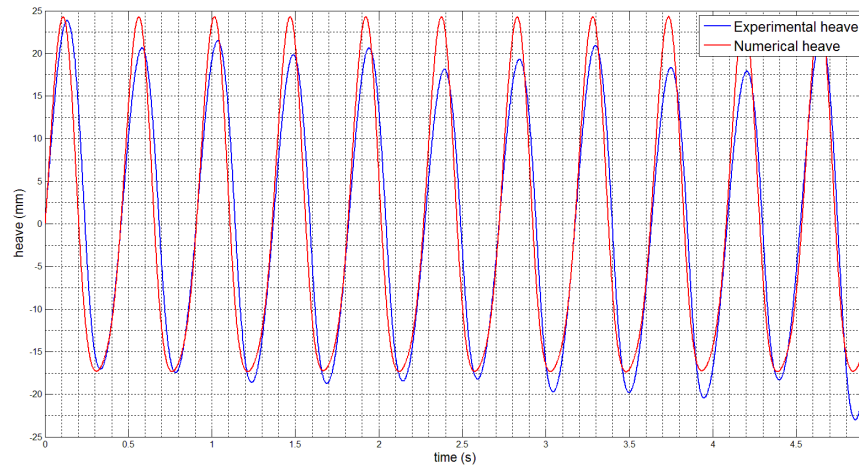


Figure 4.70. Numerical vs. experimental heave, $v=5.75$ m/s and $f=0.65$ Hz - W2

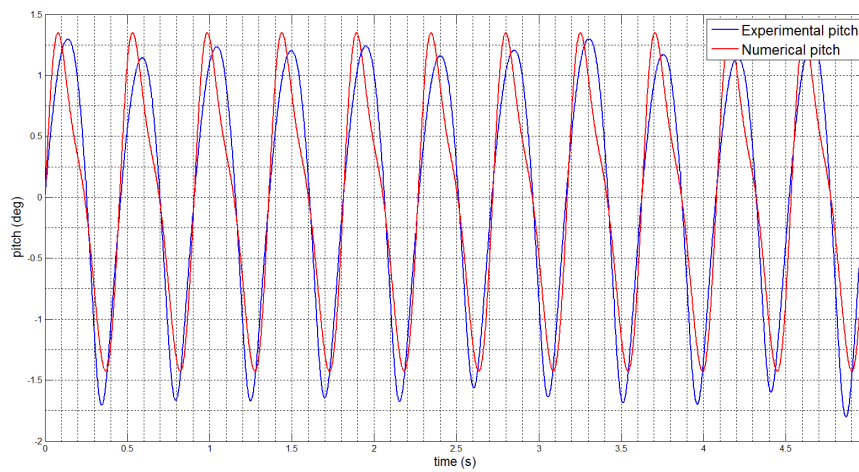


Figure 4.71. Numerical vs. experimental pitch, $v=5.75$ m/s and $f=0.65$ Hz - W2

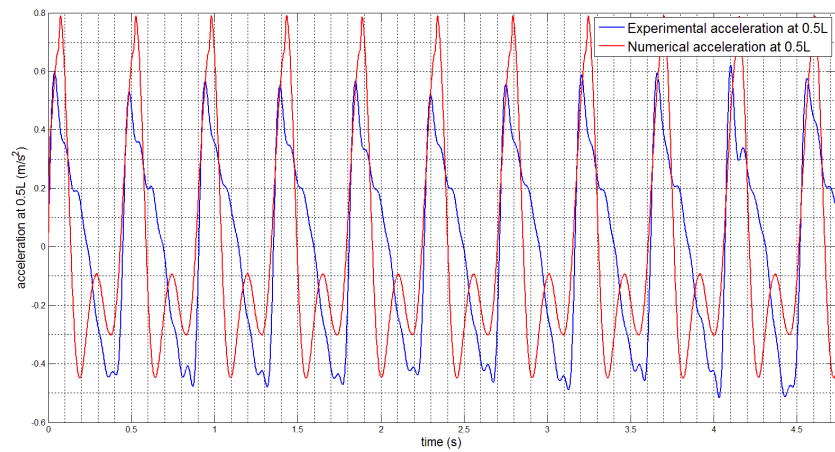


Figure 4.72. Numerical vs. experimental acceleration at CG, $v=5.75$ m/s and $f=0.65$ Hz - W2

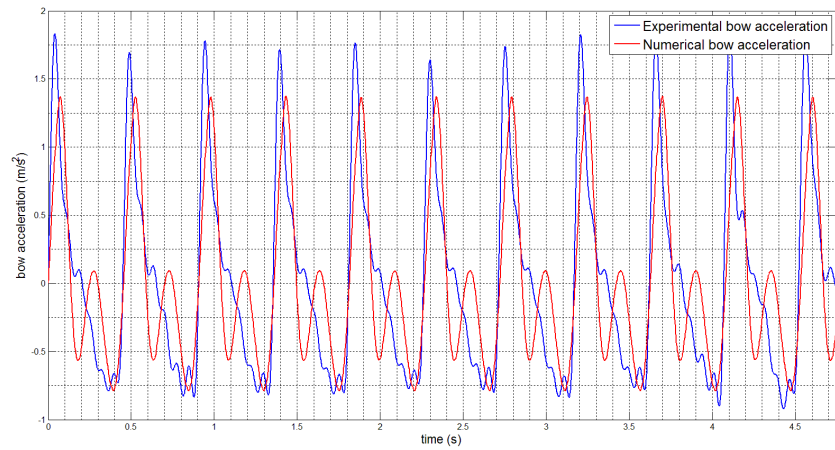


Figure 4.73. Numerical vs. experimental acceleration at bow, $v=5.75$ m/s and $f=0.65$ Hz - W2

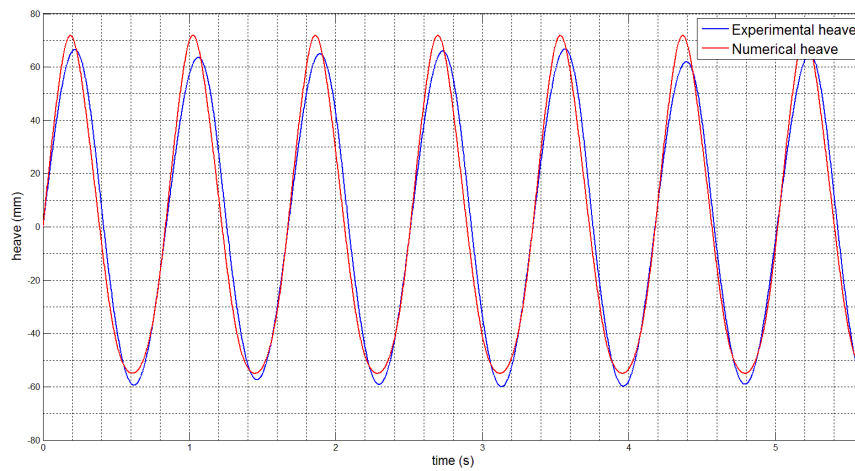


Figure 4.74. Numerical vs. experimental heave, $v=5.75$ m/s and $f=0.45$ Hz - W2

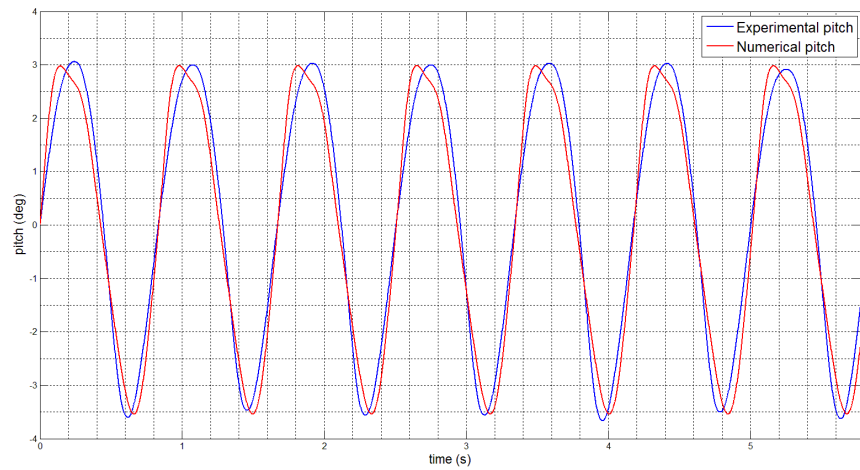


Figure 4.75. Numerical vs. experimental pitch, $v=5.75$ m/s and $f=0.45$ Hz - W2

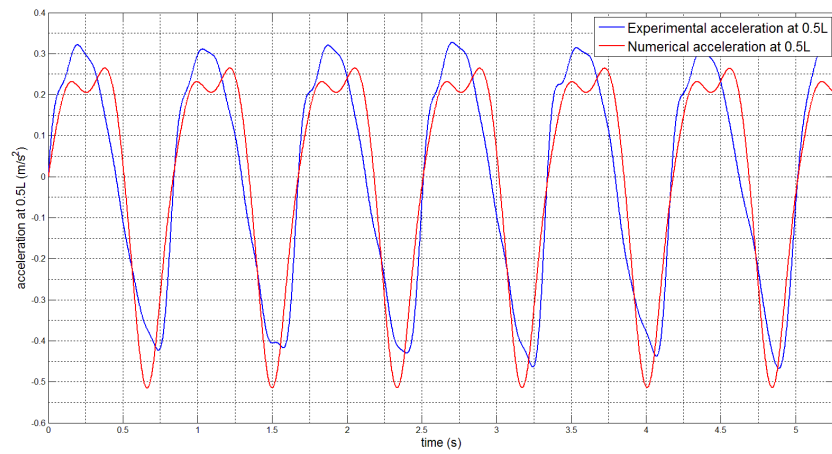


Figure 4.76. Numerical vs. experimental acceleration at CG, $v=5.75$ m/s and $f=0.45$ Hz - W2

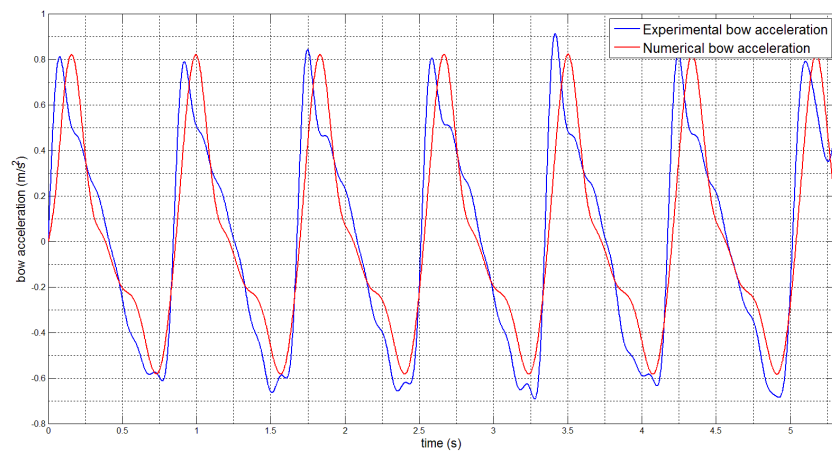


Figure 4.77. Numerical vs. experimental acceleration at bow, $v=5.75$ m/s and $f=0.45$ Hz - W2

The Figure 4.78, Figure 4.79, Figure 4.80 and Figure 4.81 summarize the results obtained for three speeds at three wave's frequencies for heave and pitch for both models. It can be noted very good prediction at all speeds and all considered frequencies for both models. From the comparison between Figure 3.53 and Figure 4.78 it is possible to note an improvement in the heave prediction for speed of 3.4 m/s at all the wave frequencies and for all speeds at short wave. While, comparing Figure 3.54 and Figure 4.79 it is evident the improvement in the pitch prediction especially for the higher speed.

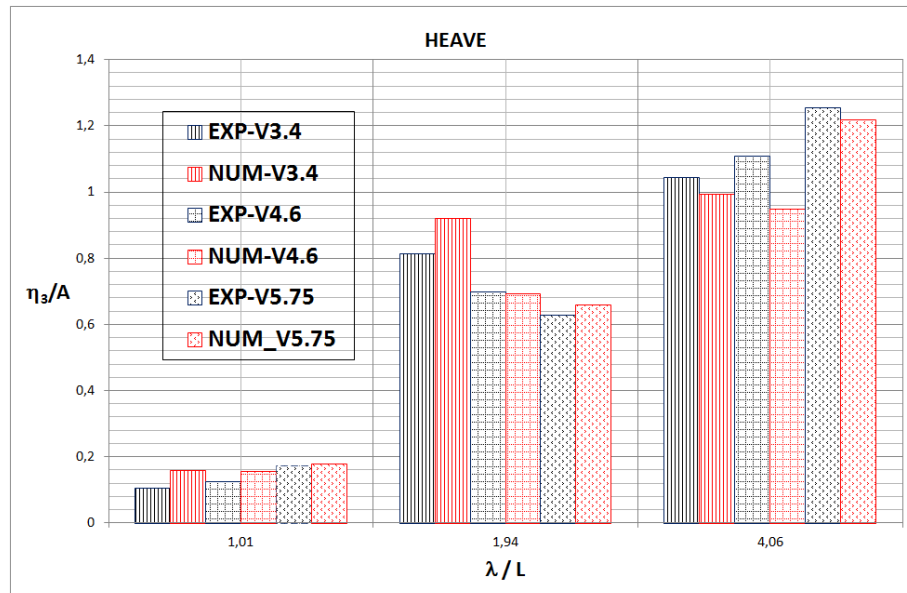


Figure 4.78. Numerical vs. experimental heave, monohedral hull, 2nd model

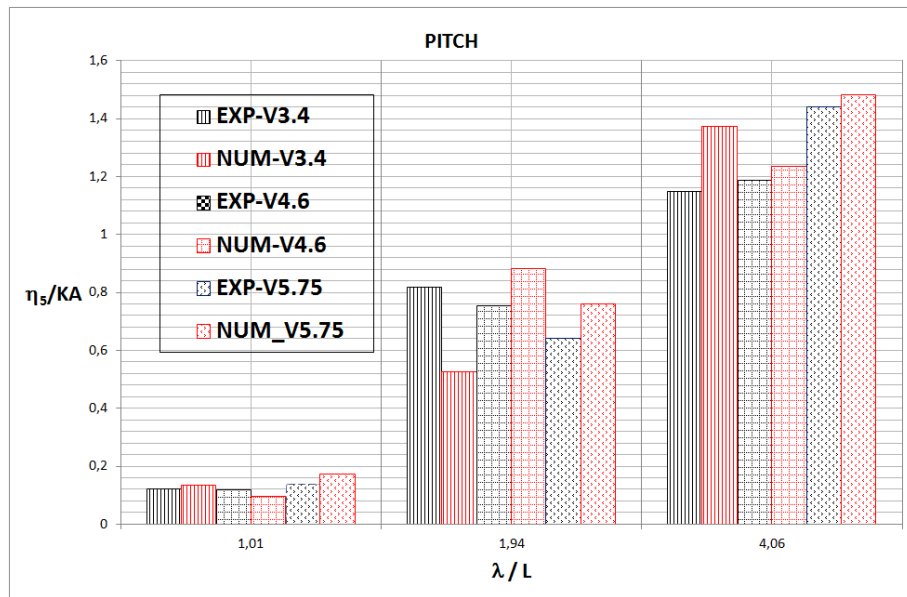


Figure 4.79. Numerical vs. experimental pitch, monohedral hull, 2nd model

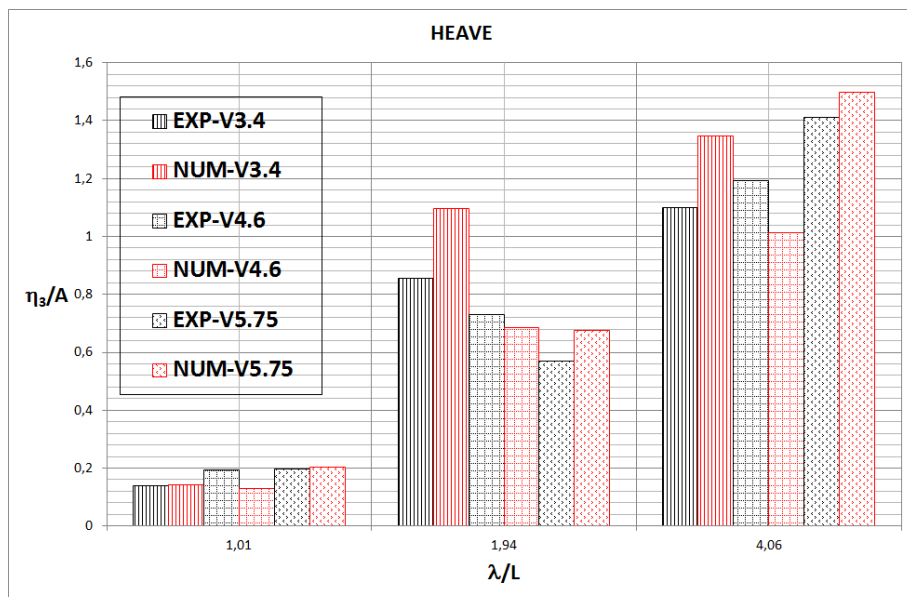


Figure 4.80. Numerical vs. experimental heave, warped hull, 2nd model

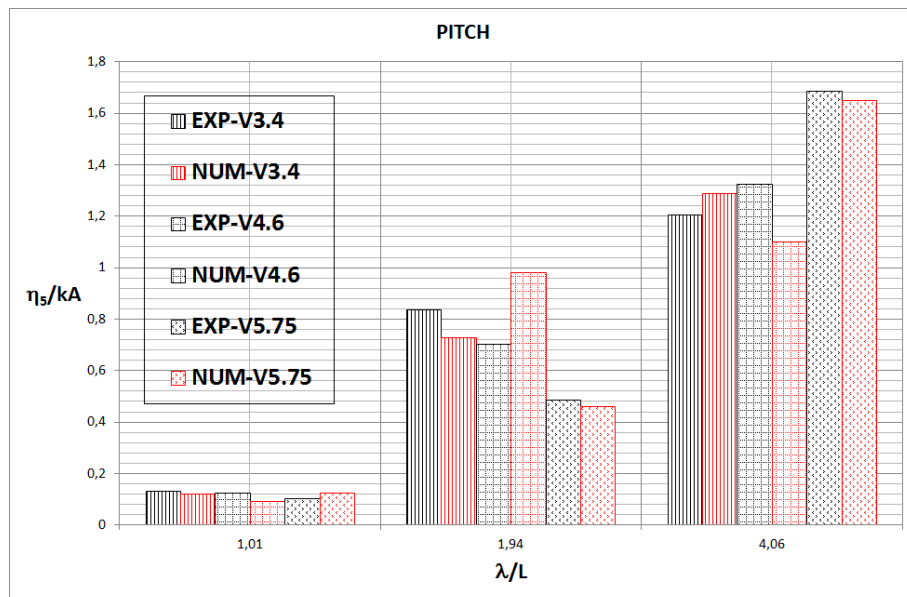


Figure 4.81. Numerical vs. experimental pitch, warped hull, 2nd model

4.6 Frequency domain analysis

For both models frequency domain analysis of measured and calculated data are performed. Frequency domain analysis is performed taking into consideration first and second harmonic. After careful consideration of spectral analysis for motions, it was seen, in according with experimental results, that the contribution of second harmonic is not more than 5% at highest speed and in resonance frequencies. Therefore the results given for heave and pitch at different velocities, in diagrams Figure 4.78 - Figure 4.81 are based on time domain analysis only.

From the experimental test was noted, and confirmed by numerical assessment, the importance of the higher order harmonics as the speed increases. An example of the numerical results for monohedral hull at different speeds and the wave frequency of 0.45Hz is shown in Figure 4.82, Figure 4.83 and Figure 4.84.

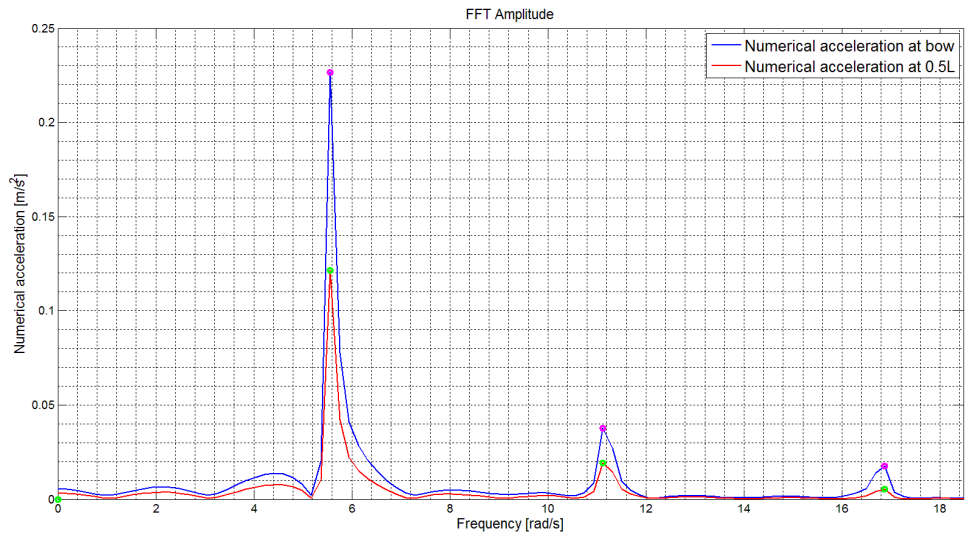


Figure 4.82. Accelerations FFT for monohedral hull at $v=3.4\text{m/s}$, $f = 0.45\text{Hz}$

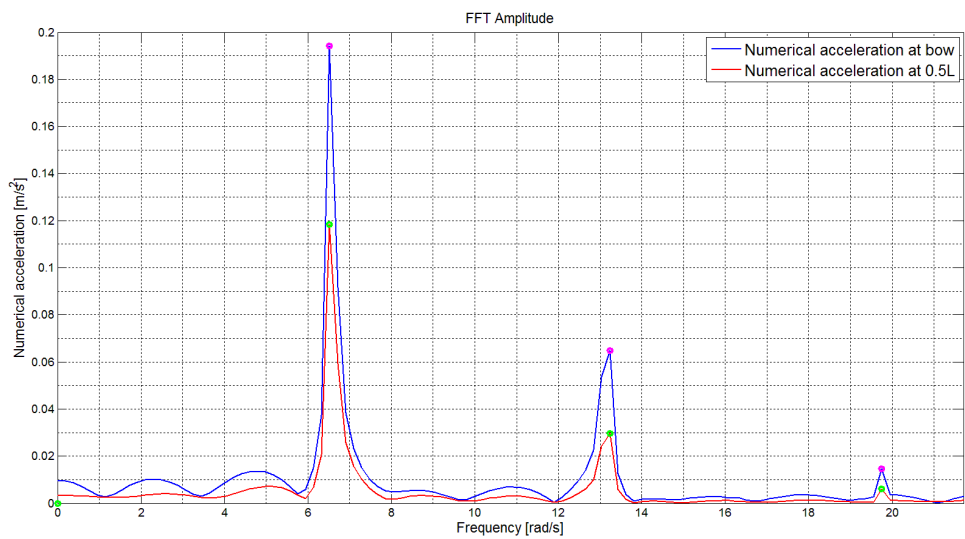


Figure 4.83. Accelerations FFT for monohedral hull at $v=4.6\text{ m/s}$, $f = 0.45\text{Hz}$

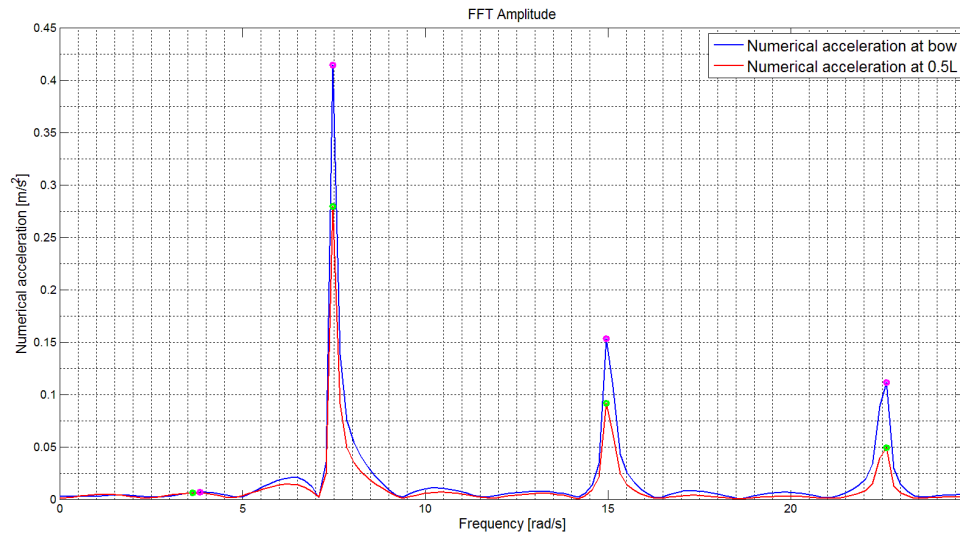


Figure 4.84 Accelerations FFT for monohedral hull at $v=5.75$ m/s, $f = 0.45$ Hz

Although the concept of warped hull is born with idea of decreasing impact accelerations at bow, from the experimental and numerical data it was observed that significant differences in hull forms, represented through deadrise angle variation, are not reflected proportionally in the motions results. Only difference has been found in acceleration responses, especially at high speed. The 1st harmonic of acceleration is similar for monohedral and warped models but the higher order harmonics for monohedral hull have higher values with respect to warped hulls. The results of the experimental tests, reported in Begovic et al. (2014), highlight that bottom warping reduces the influence of higher order harmonics; this effect is more evident in data measured at bow and at higher speeds.

To compare the numerical results with the experimental results, the numerical calculations were made under the same conditions of the experimental tests. This means that accelerations are calculated in the same longitudinal positions as in the experimental tests, which is different from longitudinal centre of gravity. However, it is worthy to note that the results are affected by the different LCG position of the models due to the constant static trim. WARP 2 have LCG position

almost 5% L_{OA} distant from the measuring point while for MONO this position is almost coincident with LCG. For this reason for WARP 2 accelerations are more affected by pitch. This involves that the difference in the 1st harmonic acceleration for monohedral and warped hull in favour of warped hull forms would be higher if the measurements would have been done at each CG position.

Two example of calculated FFT for monohedral and warped hull are shown in Figure 4.85 and Figure 4.86 at 5.75 m/s speed and for a frequency wave of 0.9Hz. The same results, considering only the first and the second harmonic, presented as monohedral vs warped hull bow accelerations harmonics, are given in Figure 4.87.

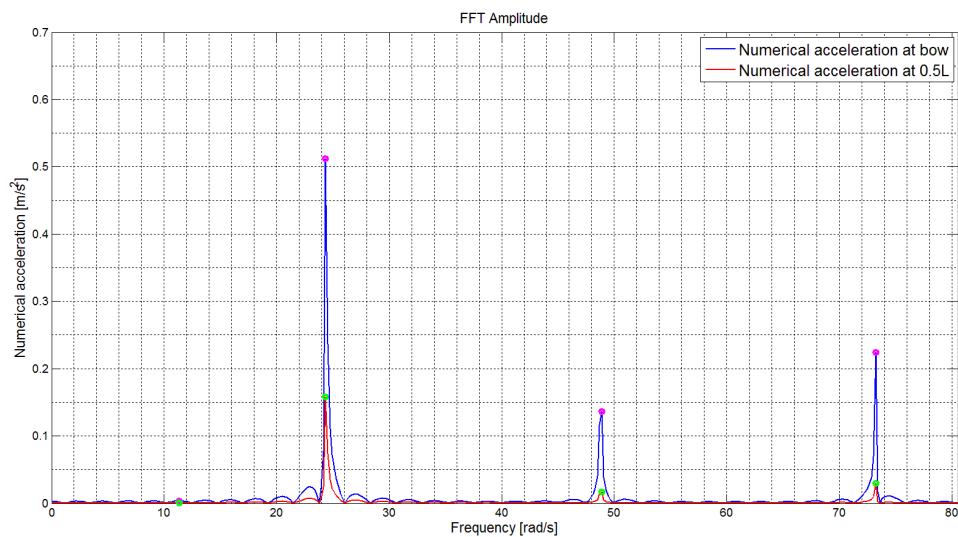


Figure 4.85. FFT for monohedral hull

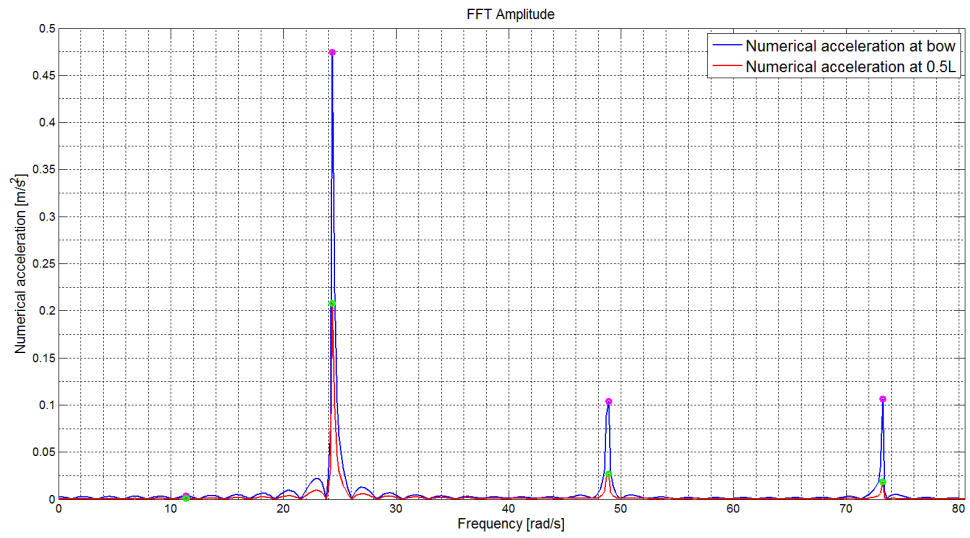


Figure 4.86. FFT for warped hull

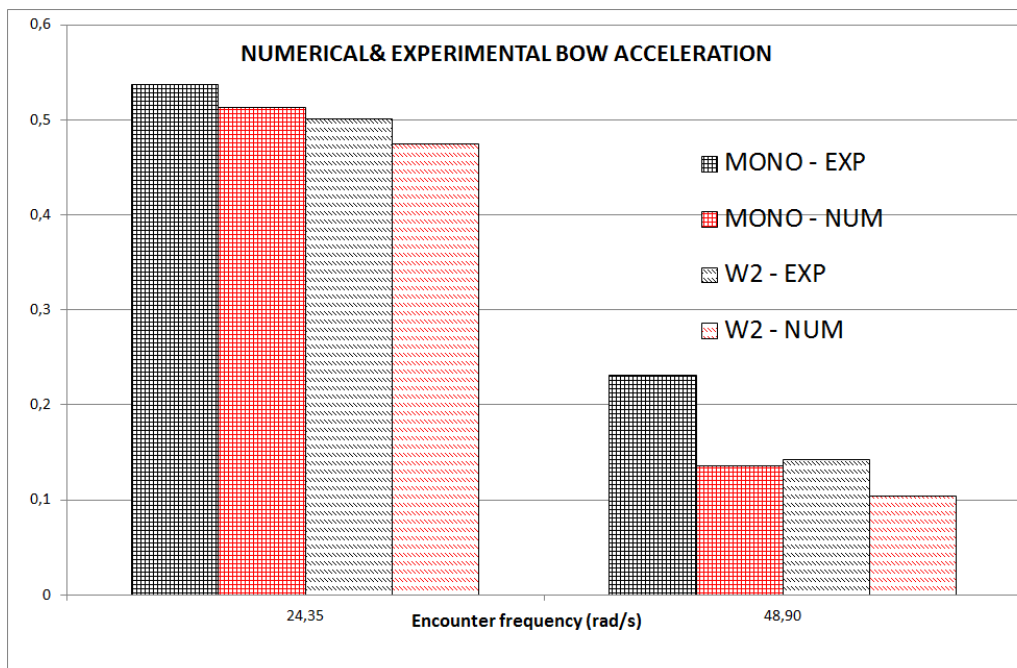


Figure 4.87. Numerical vs. experimental acceleration at bow for monohedral and warped hull at $v=5.75$ m/s and $f=0.9$ Hz

Chapter 5

5. CONCLUSIONS

5.1 Final remarks

Differences among numerical and experimental results for warped hull form obtained by first mathematical model have been attributed to mathematical model assumptions. First of all the pitch prediction was intended to improve and no hypothesis on small angle of pitch and horizontal velocity equal to advancing speed have been considered in second mathematical model. Further differences between the models are summarised in Table 4 and are regarding exciting force definition, hydrostatic force determination and effective immersion of section when the chine is wet. To compare effective improvements in motions prediction some comparisons between the experimental and the numerical values calculated by the first model and the second model are given. In Figure 5.1 and Figure 5.2 for monohedral hull's heave and pitch at the speed 5.75m/s are shown. For this speed with the first mathematical model the pitch was strongly underestimated and it is possible to note an improvement with the second mathematical model from the Figure 5.2.

Figure 5.7 show a comparison between the experimental values of first and second harmonic of the accelerations and the numerical calculated values with the first model and the second model at speed 5.75m/s. From the Figure 5.7 is possible to note an improvement in bow acceleration prediction by the second mathematical model. It is worth to note that bow accelerations should be analysed

by both time domain crest-trough analysis and spectral analysis of at least two harmonics.

As already said the first model gives satisfactory results for monohedral hull, in general, with the second model there is an improvement in the pitch and accelerations prediction but this improvement is not always appreciated. The significant improvement has been obtained for warped hull form. Examples of experimental and numerical results by 1st and 2nd model are given in the Figure 5.9 and Figure 5.10. This pitch prediction improvement, gives further improvement of bow accelerations. In the Figures Figure 5.11 and Figure 5.12 is reported a comparison between the time series obtained with the first and second model compared with the experimental ones, highlighting a good agreement between the numerical results, obtained with the second model, and the experimental results.

As with the first model, to validate accelerations calculations, in addition to the comparison of experimental and numerical time series, showed in Figure 4.44, Figure 4.45, Figure 4.48, Figure 4.49, Figure 4.52, Figure 4.53, Figure 4.56, Figure 4.57, Figure 4.60, Figure 4.61, Figure 4.64, Figure 4.65, Figure 4.68, Figure 4.69, Figure 4.72, Figure 4.73, Figure 4.76 and Figure 4.77, the comparison of the harmonics is done. The Figure 5.13 shows the 2nd model numerical results and the experimental ones for the highest speed and a wave's frequency of 0.9 Hz.

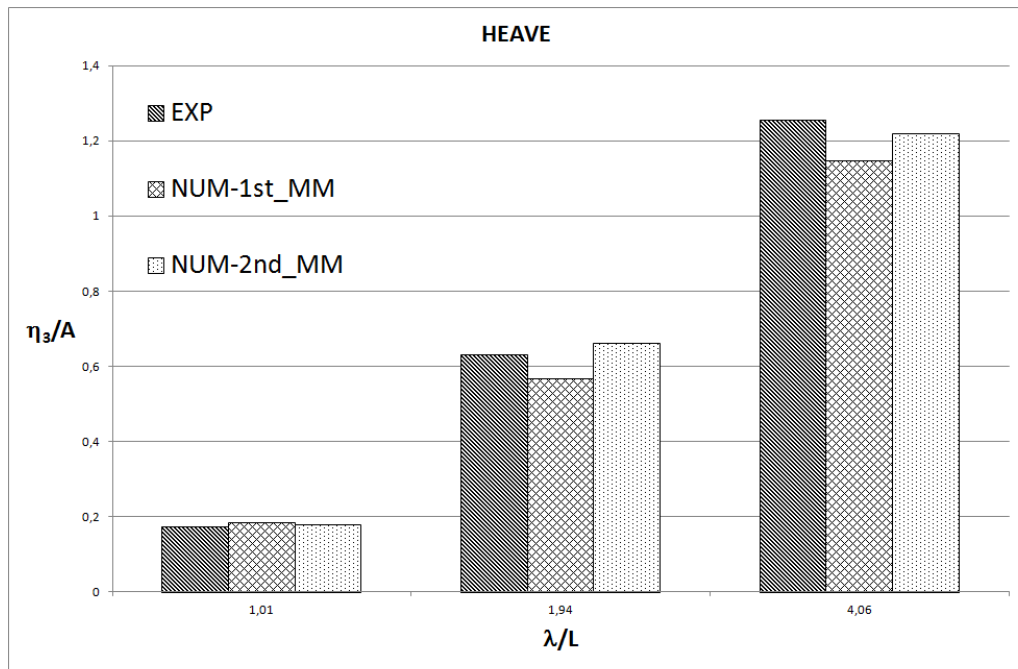


Figure 5.1. Numerical vs. experimental heave, $v= 5.75$ m/s

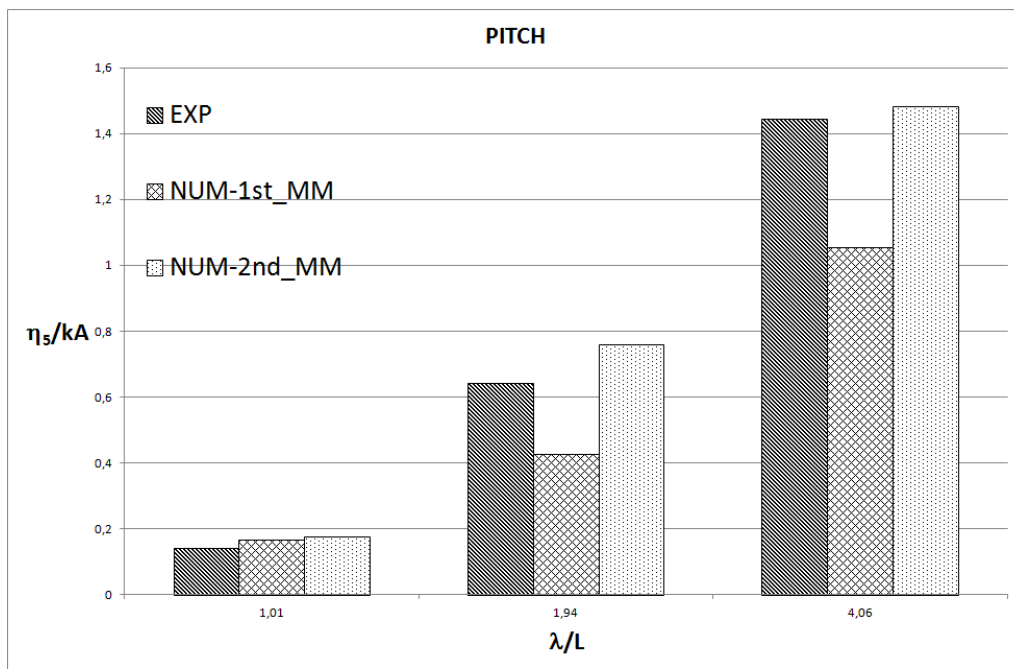


Figure 5.2. Numerical vs. experimental pitch, $v= 5.75$ m/s

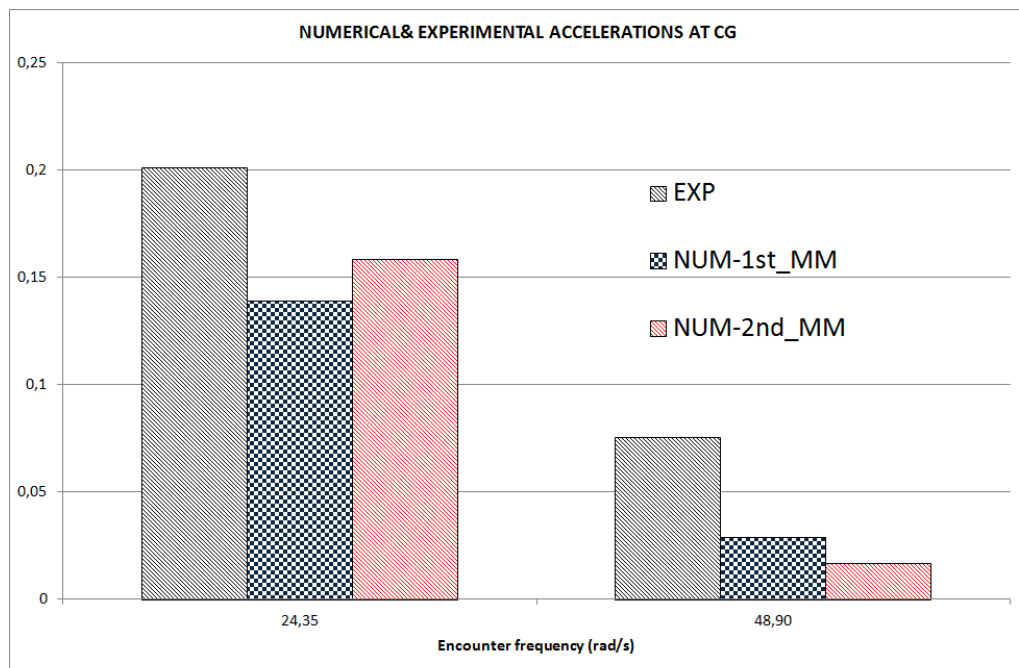


Figure 5.3. Numerical vs. experimental acceleration at CG (first and second harmonic), $v= 5.75$ m/s and $f=0.9$ Hz

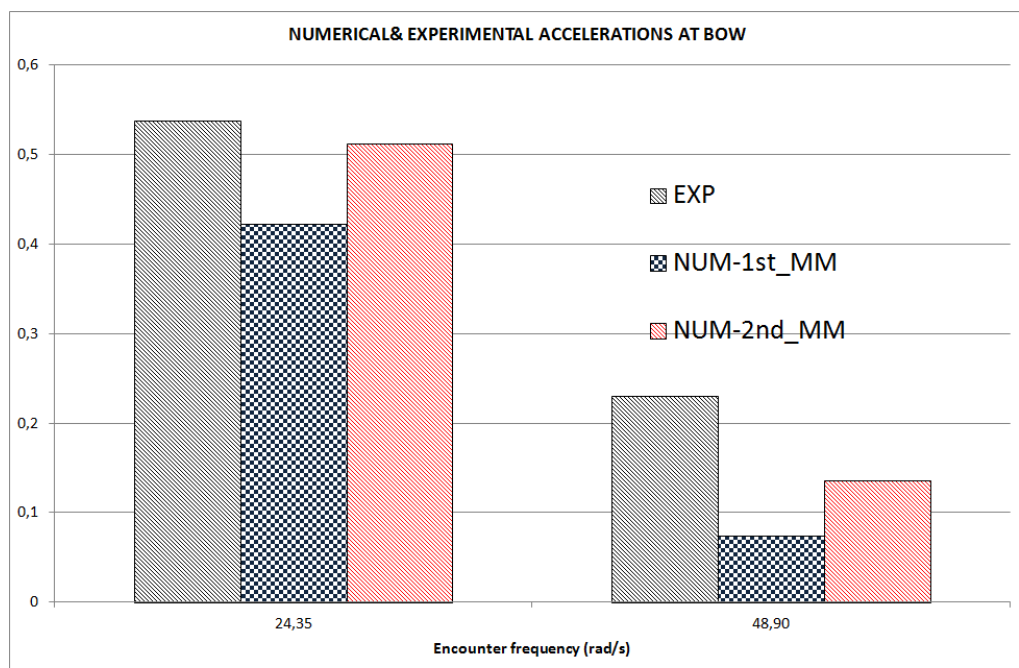


Figure 5.4. Numerical vs. experimental acceleration at bow (first and second harmonic), $v= 5.75$ m/s and $f=0.9$ Hz

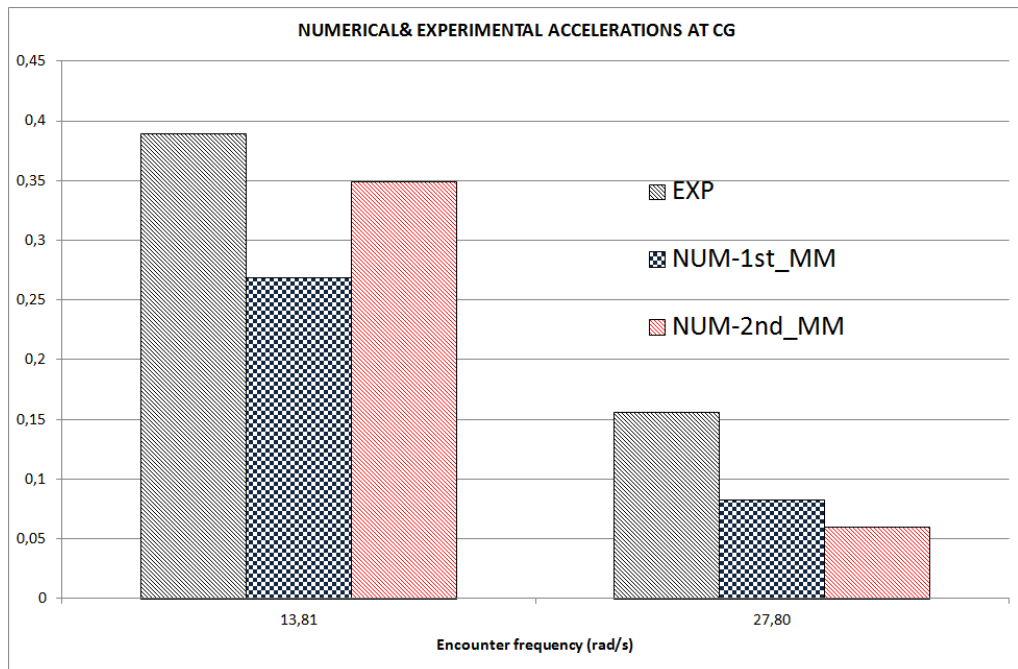


Figure 5.5. Numerical vs. experimental acceleration at CG (first and second harmonic), $v= 5.75$ m/s and $f=0.65$ Hz

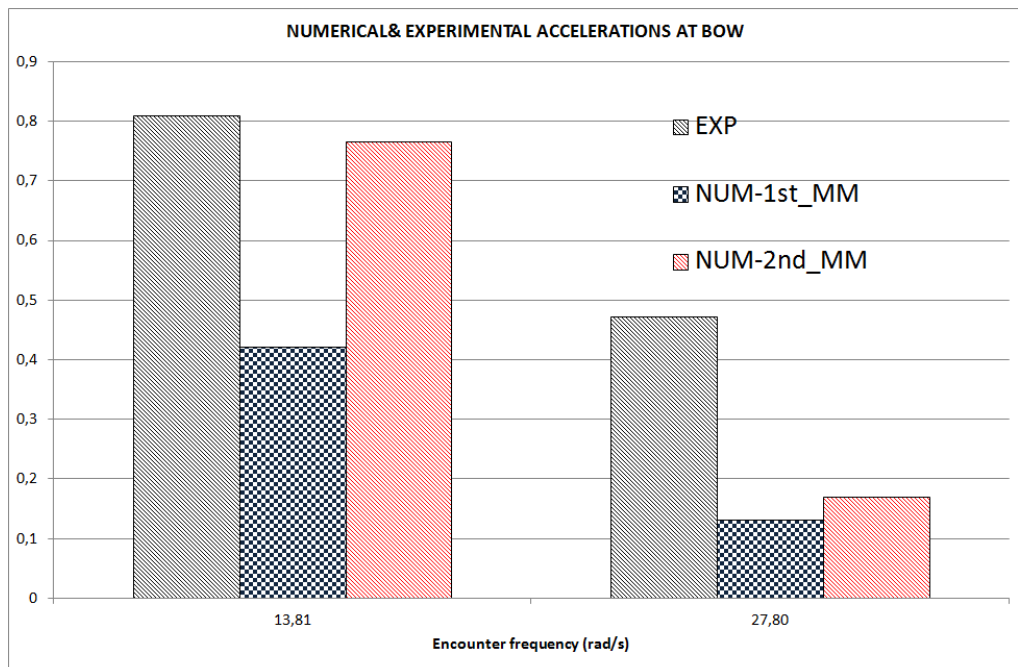


Figure 5.6. Numerical vs. experimental acceleration at bow (first and second harmonic), $v= 5.75$ m/s and $f=0.65$ Hz

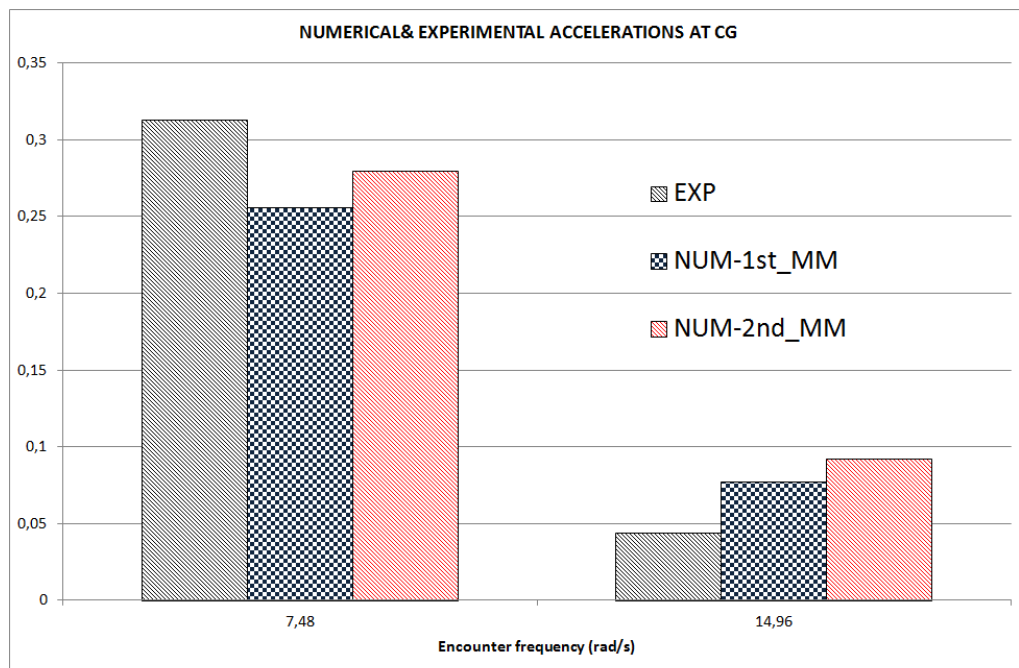


Figure 5.7. Numerical vs. experimental acceleration at CG (first and second harmonic), $v= 5.75 \text{ m/s}$ and $f=0.45 \text{ Hz}$

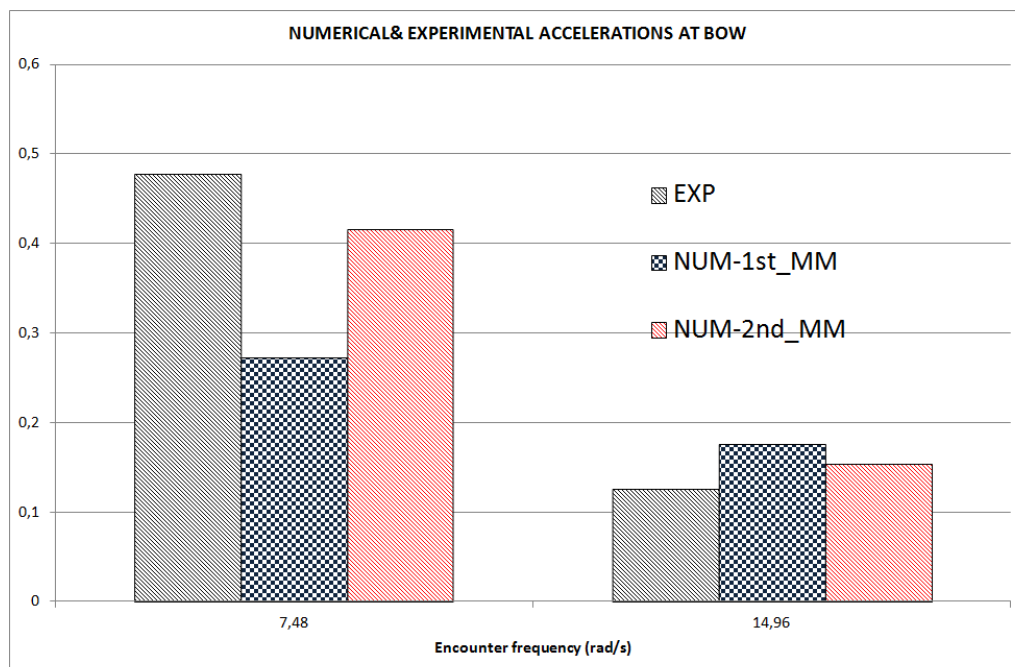


Figure 5.8. Numerical vs. experimental acceleration at bow (first and second harmonic), $v= 5.75 \text{ m/s}$ and $f=0.45 \text{ Hz}$

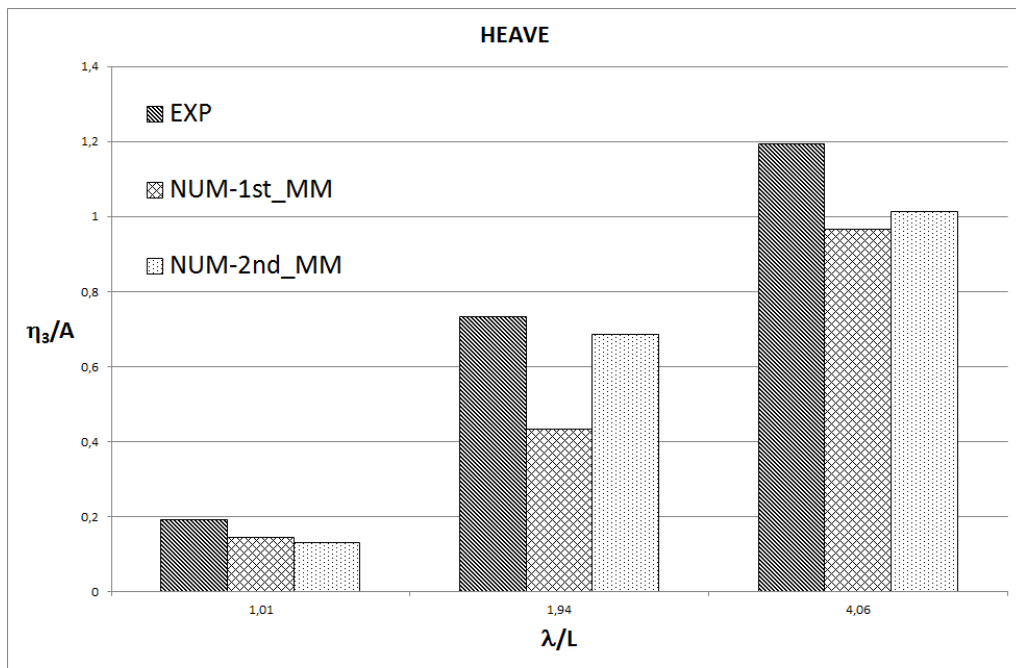


Figure 5.9. Numerical vs. experimental heave for warped hull, $v= 4.6$ m/s

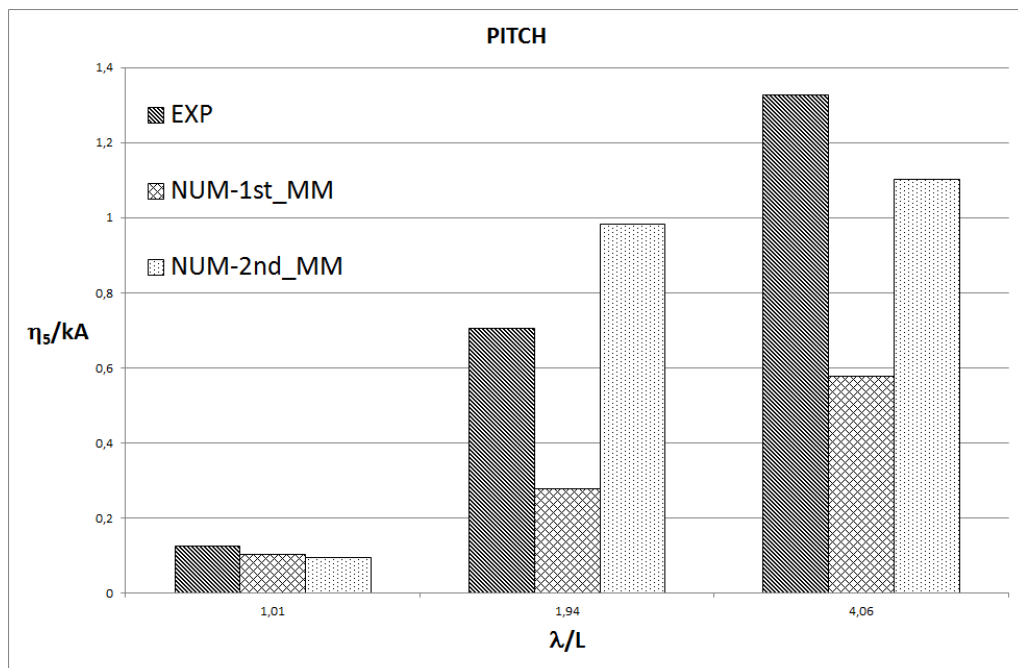


Figure 5.10. Numerical vs. experimental pitch for warped hull, $v= 4.6$ m/s

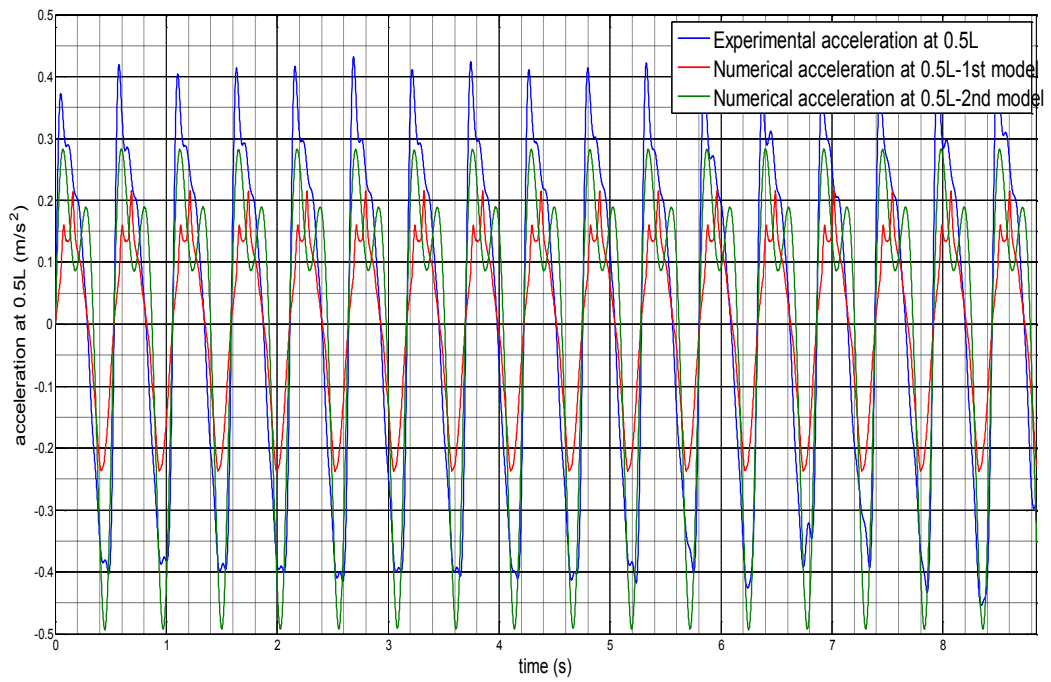


Figure 5.11. Numerical vs. experimental acceleration at LCG for warped hull, $v = 4.6$ m/s

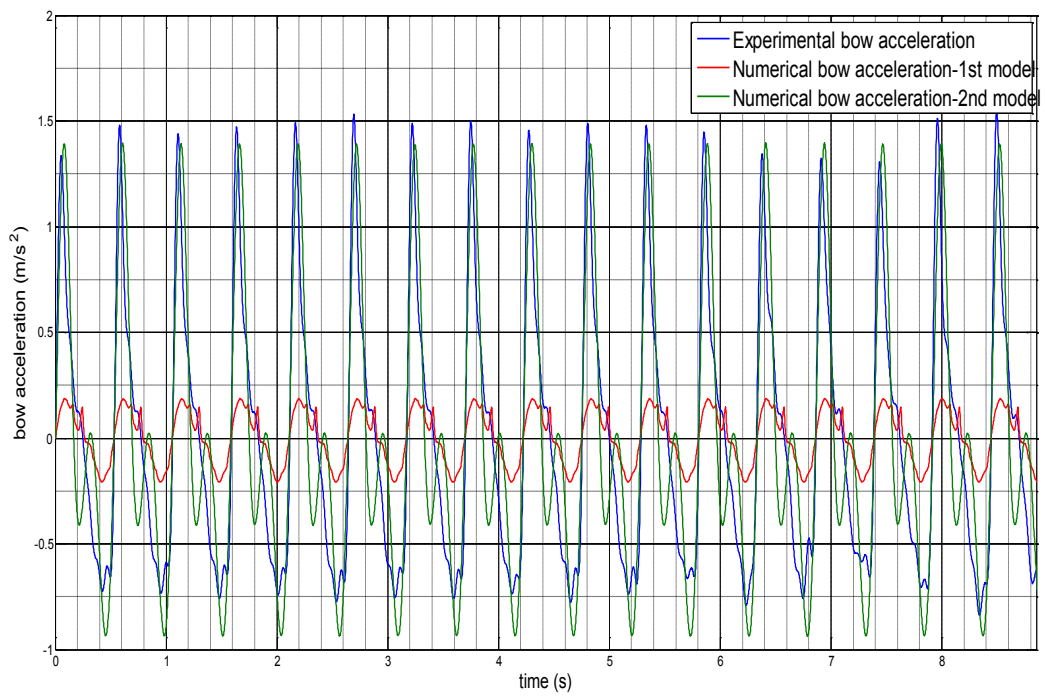


Figure 5.12. Numerical vs. experimental bow acceleration for warped hull, $v = 4.6$ m/s

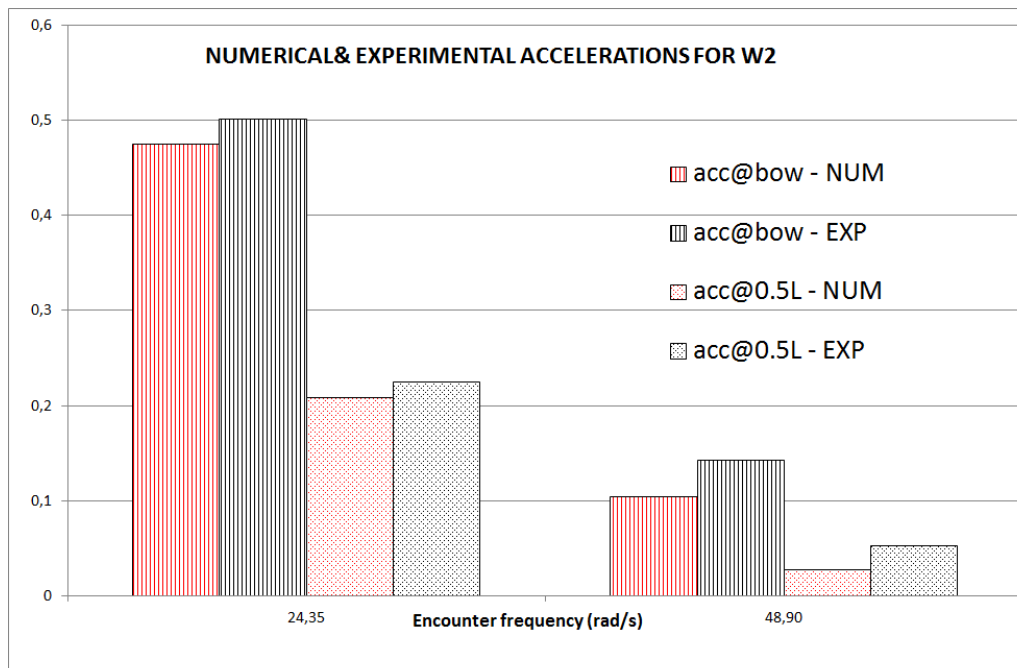


Figure 5.13. Numerical vs. experimental acceleration at bow for warped hull, $v = 5.75$ m/s and $f = 0.9$ Hz

5.2 Conclusions and future work developments

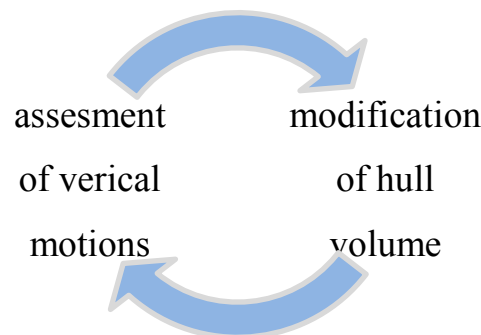
The aim of this Thesis was to develop numerical method, accurate, robust and fast to be used in design of fast small craft without excessive computational time necessity. Experimental program on warped planing hulls seakeeping, has been performed in Towing tank of Department of Industrial Engineering of University of Naples Federico II with aim to validate developed methodology. The availability of specific and dedicated experimental tests allowed to compare time series of experimental and numerical data results, not only typical values reported in literature, and furthermore to analyse them in the same manner. This synergy of numerical and experimental approaches resulted in accurate validation of developed methodology. Furthermore mathematical model is by its definition simplification of physical model, minor the number of assumption is, more realistic the model is. Again synergy of experimental and numerical approach

allowed to focus on phenomenon physics and to improve mathematical model accordingly.

The simplified mathematical model has been validated for measured accelerations and warped hull forms, showing some critical issues. The changes introduced in 1st mathematical model produces improvements in the assessment of heave, pitch and accelerations by the 2nd one. The 2D time domain fully non linear developed code is fast, robust and accurate.

Validation of the fully non linear code has been made with modern warped planing hull forms.

The more rigorous mathematical model allowed better assessment of vertical motions and consequently as the code output is the input for the successive time instant the immersed volume and wetted surface determination are more accurate. This more accurate wetted area for each section led to significant improvement for warped hull seakeeping assessment.



Nonlinearities in accelerations responses have been obtained by developed code with high accuracy in whole speed and wave frequencies range. Harmonics analysis is important step to determine the real response, very often, not appreciable only with crest-trough analysis in time domain. Differences experienced among physical (experimental) model of planing hull seakeeping and mathematical model and careful description of the importance of physical

quantities in mathematical formulation indicate possible improvements of mathematical model.

To increase the accuracy of the code the next step could be to have a more accurate investigation of the evaluation of the added mass. First of all, since Wagner's work, pile up coefficient $(1+k_p)$ is function only of deadrise angle and surely effect of forward speed should be taken into account. In addition, it might be interesting to do a more thorough investigation on the calculation of the coefficient of the incremental added mass due to chine immersion. As defined in 3.2.6 this coefficient is a function of an experimental coefficient, K , which is ≈ 2 for deadrise angle from 0 to 40 degrees, this implies a constant value with the angles that we find most commonly in modern hull shapes, and most importantly, the value does not change between the monohedral and warped hull.

Numerical code gives results for added mass, damping and forces components as a function of time; and this analysis will be performed to get better insight how they vary reciprocally in the case of planing hulls. Future developments are concerning pressure distribution along the hull and responses calculations in irregular sea.

REFERENCES

- [1] Ackers, R.H., 1999. Dynamic Analysis of Planing Hulls in the Vertical Plane. Meeting of New England Section of SNAME, 29 April 1999.
- [2] Barry, C.D., Ghosh, D., Akers, R., 2002. Implementation, Application and Validation of the Zarnick Strip Theory Analysis Technique for Planing Boats. High Performance Yacht Design Conference, Auckland, 4-6 December 2002.
- [3] Begovic, E., Bertorello, C., 2012. Resistance Assessment of Warped Hullform. *Ocean Engineering*, Vol 56 (2012), pp. 28–42, DOI: 10.1013/j.oceanengineering.2012.08.004.
- [4] Begovic, E., Bertorello, C., Pennino, S., 2014. Experimental seakeeping assessment of warped planing hull. *Ocean Engineering* 83C (2014), pp. 1-15, DOI: 10.1016/j.oceaneng.2014.03.012.
- [5] Begovic, E., Bertorello, C., Pennino, S., 2009. Experimental Assessment of Vertical Accelerations of Planing Hull. In: NAV 2009, 16th International Conference of Ship and Shipping Research, November 2009, Italy, ISBN 978-88-904394-0-7.
- [6] Begovic, E., Bertorello, C., 2009. Experimental Assessment of Seakeeping Characteristics for Non-Monohedral Planing Hulls. In: IMAM 2009, 13th International Conference Towards the Sustainable Marine Technology and Transportation, Istanbul, Turkey, October 2009, ISBN 978-975-561-355-0.
- [7] Bertorello, C., Oliviero, L., 2007. Hydrodynamic Resistance Assessment of Non-Monohedral Planing Hull Forms based on Savitsky's Method. *Australian Journal of Mechanical Engineering*, vol. 4, No.2, pp 209–224. Engineers Media, CROWS NEST, Australia. (ACN001311511).
- [8] De Jong, P., 2011. Seakeeping Behaviour of High Speed Ships- An experimental and numerical study, Ph.D. Thesis, ISBN 978-94-6190-263-4, Gildeprint drukkerijen, Enschede, The Netherlands.
- [9] Faltinsen, O., 1993. On Seakeeping of Conventional and High Speed Vessels. *Journal of Ship Research*. Vol. 37. No.2 : 87-101.

- [10] Faltinsen, O., 2005. *Hydrodynamics High Speed Marine Vehicles*. Cambridge University Press. ISBN0521845688. Cambridge/UK.
- [11] Faltinsen O., Zhao, R., 1993. Water Entry of a Two-dimensional Body, *Journal of Fluid Mechanics*, Volume 246 / January 1993, pp 593-612, DOI: <http://dx.doi.org/10.1017/S002211209300028X>.
- [12] Fridsma, G., 1969. “A Systematic Study of the Rough Water Performance of Planing Boats, Report 1275”, Stevens Institute of Technology, November 1969, Report 1275.
- [13] Fridsma, G., 1971. “A Systematic Study of the Rough Water Performance of Planing Boats. Irregular Waves – Part II”, Stevens Institute of Technology, March 1971, report SIT-DL-71-1495.
- [14] Garne, K., 2005. Improved time domain simulation of planing hulls in waves by correction of the near- transom lift. *International Shipbuilding Progress*, 52(3):201–230.
- [15] Garne, K., 2004. *Modelling of Planing Craft in Waves*, Ph.D. Thesis, ISBN 91-7283-861-2, KTH Stockholm.
- [16] Garne, K., Rosen, A., 2003. Time domain simulations and full scale trials on planing craft in waves. *International Shipbuilding Progress*, 50(3):177–208, 2003.
- [17] Ghadimi, P., Dashtimanesh, A., Reza, S., Yaser, D., Maghrebi, F., 2013. Development of a mathematical model for simultaneous heave, pitch and roll motions of planing vessel in regular waves, *International Journal of Scientific World*, 1(2) 2013, Science Publishing Corporation, www.sciencepubco.com/index.php/IJSW.
- [18] Hicks, J.D., Troesch, A.W., Jiang, C., 1995. Simulation and Nonlinear Dynamics Analysis of Planing Hulls, *Journal of Offshore Mechanics and Arctic Engineering*, Vol. 117, Feb. 1995, paged 38-45.
- [19] Keuning, J.A., Gerritsma, J., 1982. Resistance tests of a series of planing hull forms with a 25 degrees deadrise angle. *International Shipbuilding Progress*, 29(337):222–249, September 1982.

- [20] Kant, R., 1989. Tijdsdomein simulatie programma voor de bewegingen van planerende schepen in golven. Master's thesis, Delft University of Technology, Ship Hydromechanics Laboratory, May 1989.
- [21] Keuning, J.A., Gerritsma, J., van Terwisga, P.F., 1993. Resistance tests of a series of planing hull forms with a 30 degrees deadrise angle, and calculation model based on this similar systematic series. Technical Report MEMT 25, Delft University of Technology, Ship Hydromechanics Laboratory, June 1993.
- [22] Lewis, S.G, Hudson, D.A., Turnock, S.R., Blake, J.I.R., Ajit Sheno, R., 2006. Predicting Motions of High Speed RIBs: A Comparison of Non-linear Strip Theory with Experiments. 5 th International Conference on High Performance Marine Vehicles, 8-10 November, 2006, Australia.
- [23] Martin, M., 1976. Theoretical prediction of motions of high speed planing boats in waves. David W. Taylor Naval Ship Research and Development Center Report 76-0069.
- [24] Mei, X., Liu Y., Yue D. K.P., 1999. On the water impact of general two-dimensional sections, Applied Ocean Research 21 (1999) 1–15.
- [25] Metcalf, B.J., Faul L., Bumiller , E., Slutsky, J., 2005. Resistance tests of a systematic series of U.S. Coast Guard planing hulls, Carderock Division, Naval Surface Warfare Center, Report No. NSWCCD-50-TR-2005/063, December 2005.
- [26] Payne, P.R., 1988. Design of High-Speed Boats: Planing. Annapolis(USA): Fishergate Publishing Company Inc. ISBN 0942720067.
- [27] Payne, P.R., 1994. Recent developments in "added-mass" planing theory. Ocean Engineering 21.No.3, 257-309.
- [28] Payne, P.R., 1995 Contribution to planing theory. Ocean Engineering, Vol. 22.,No.7, 699-729.
- [29] Pierson, J.D., 1950. The Penetration of a Fluid Surface by a Wedge. Institute of the Aerospace Sciences, Incorporated New York, New York. July 1950.

- [30] Pierson, J.D., Dingee, D.A., Neidinger, J.,W., 1954. A Hydrodynamic Study of the Chines-Dry Planing Body. U.S. Navy, Office of Naval Research, Project No. NR062-012. Report No. 492. May 1954.
- [31] Royce, R.A., 2001. Impact Theory Extended to Planing Craft with Experimental Comparisons. Ph.D. Thesis, University of Michigan.
- [32] Ruscelli, D., 2009. Dynamics Of High Speed Craft, Ph.D. Thesis, University of Genova.
- [33] Savitsky, D., 1964. Hydrodynamic design of planing hulls. SNAME Mar. Technol. 1(1), Oct 1964.
- [34] Savitsky, D., Brown, W. P., 1976 Procedures for hydrodynamic evaluation of planing hulls in smooth and rough water. *Marine Technology*, 13, 381–400, Oct.
- [35] Savitsky, D., Koebel, J.G., 1993, Seakeeping of Hard Chine Planing Hulls. Technical Research Bulletin No. R-42, SNAME.
- [36] Savitsky D., De Lorme M.F., Datla R., 2006. Inclusion of “Whisker Spray” Drag in Performance Prediction Method For High-Speed Planing Hulls. Technical Report SIT-DL-06-9-2845, Presented at Meeting of New York Metropolitan Section The SNAME March 14, 2006.
- [37] Sebastiani, L., Ruscelli, D., Rambaldi, G., Viviani, M., 2008., A Momentum Theory Approach to the Seakeeping of Planing Crafts. HSMV2008.
- [38] Singleton, F.D., 2008. Technical Paper for BOAT3D, Planing Boat Time-Domain Simulation with Waves. Huston, Texas, Usa, www.DAofTX.com, 2008.
- [39] Soletic, L., 2010. Seakeeping of a Systematic Series of Planing Hulls. The 2nd Chesapeake Power Boat Symposium, Annapolis, Maryland, March 2010.
- [40] Sun, H., 2007. A Boundary Element Method Applied to Strongly Nonlinear Wave-Body Interaction Problems, Ph.D. Thesis, NTNU 2007, ISBN 978-82-471-3098-8.
- [41] Troesch, A., 2010. Dynamics and Hydrodynamics of High Speed Craft, PASI 2010 in Dynamics and Control of Manned and Unmanned Marine Vehicles, June 29, 2010, Barranquilla, Colombia.

- [42] Troesch, A.W., 1992. On the hydrodynamics of vertically oscillating planing hulls, *Journal of Ship Research* 36 (4), 317-331.
- [43] Taunton, D.J., Hudson, D.A., Sheno, R.A., 2010. Characteristics of a Series of High Speed Hard Chine Planing Hulls - Part I: Performance in Calm Water. *International Journal of Small Craft Technology*, Vol. 152, part B2, pp. 55 – 75.
- [44] Taunton, D.J., Hudson, D.A., Sheno, R.A., 2011. Characteristics of a Series of High Speed Hard Chine Planing Hulls - Part II: Performance in Waves. *International Journal of Small Craft Technology*, Vol. 153, pp B1-B22.
- [45] Van Deyzen, A., 2008. A Nonlinear Mathematical Model of Motions of a Planing Monohull in Head Seas. HIPER08, Naples, Italy.
- [46] Von Karman, Th., 1929. The Impact on seaplane Floats During Landing, national Advisory Committee for Aeronautics, Technical Note No. 321, Washington, 1929.
- [47] Wagner, H., 1932. Uber Stoss-und Gleitvorg-inge an der Oberfl~iche von Flfissig-keiten. *Zeitschrift fiir Angewandte Mathematik und Mechanik* (in English) 12. 193-251.
- [48] Wang, J., 2013. Theoretical modelling of free falling wedges entering the water surface: part I- wedge motions, *Proceedings of the ASME 2013 32nd International Conference OMAE2013*, June 9-14, 2013, Nantes, France, OMAE2013-10434
- [49] Yousefi, R., Rouzbeh, S., Shakeri, M., 2013. Hydrodynamic analysis techniques for high-speed planing hulls. *Applied Ocean Research* 42 (2013) 105–113.
- [50] Zarnick, E., 1978. A Nonlinear Mathematical Model of Motions of a Planing Boat in Regular Waves. DTNSRDC/SPD 0867-01.